FORMULATION AND IMPLEMENTATION OF A FRACTIONAL ORDER VISCOELASTIC MATERIAL MODEL INTO FINITE ELEMENT SOFTWARE AND MATERIAL MODEL PARAMETER IDENTIFICATION USING IN-VIVO INDENTER EXPERIMENTS FOR SOFT BIOLOGICAL TISSUES

A THESIS SUBMITTED TO
THE GRADUATE SCHOOL OF NATURAL AND APPLIED SCIENCES
OF
MIDDLE EAST TECHNICAL UNIVERSITY

BY

NAGEHAN DEMİRCİ

IN PARTIAL FULFILLMENT OF THE REQUIREMENTS
FOR
THE DEGREE OF MASTER OF SCIENCE
IN
MECHANICAL ENGINEERING

FEBRUARY 2012

Approval of the thesis:

FORMULATION AND IMPLEMENTATION OF A FRACTIONAL ORDER VISCOELASTIC MATERIAL MODEL INTO FINITE ELEMENT SOFTWARE AND MATERIAL MODEL PARAMETER IDENTIFICATION USING IN-VIVO INDENTER EXPERIMENTS FOR SOFT BIOLOGICAL TISSUES

submitted by **NAGEHAN DEMİRCİ** in partial fulfillment of the requirements for the degree of **Master of Science in Mechanical Engineering Department, Middle East Technical University** by,

Prof. Dr. Canan Özgen
Dean, Graduate School of **Natural and Applied Sciences** _____

Prof. Dr. Suha Oral
Head of Department, **Mechanical Engineering** _____

Assist. Prof. Dr. Ergin Tönük
Supervisor, **Mechanical Engineering Dept., METU** _____

Examining Committee Members

Prof. Dr. Turgut Tümer
Mechanical Engineering Dept., METU _____

Assist. Prof. Dr. Ergin Tönük
Mechanical Engineering Dept., METU _____

Prof. Dr. Suat Kadıoğlu
Mechanical Engineering Dept., METU _____

Assist. Prof. Dr. Cüneyt Sert
Mechanical Engineering Dept., METU _____

Prof. Dr. Nesrin Hasırcı
Chemistry Dept., METU _____

Date : 07.02.2012

I hereby declare that all information in this document has been obtained and presented in accordance with academic rules and ethical conduct. I also declare that, as required by these rules and conduct, I have fully cited and referenced all material and results that are not original to this work.

Name, Last name : Nagehan DEMİRCİ

Signature :

ABSTRACT

FORMULATION AND IMPLEMENTATION OF A FRACTIONAL ORDER VISCOELASTIC MATERIAL MODEL INTO FINITE ELEMENT SOFTWARE AND MATERIAL MODEL PARAMETER IDENTIFICATION USING IN-VIVO INDENTER EXPERIMENTS FOR SOFT BIOLOGICAL TISSUES

Demirci, Nagehan

M.Sc., Department of Mechanical Engineering
Supervisor: Assist. Prof. Dr. Ergin Tönük

February 2012, 237 pages

Soft biological tissue material models in the literature are frequently limited to integer order constitutive relations where the order of differentiation of stress and/or strain is integer-valued. However, it has been demonstrated that fractional calculus theory applied in soft tissue material model formulation yields more accurate and reliable soft tissue material models.

In this study, firstly a fractional order (where the order of differentation of stress in the constitutive relation is non-integer-valued) linear viscoelastic material model for soft tissues is fitted to force-displacement-time indentation test data and compared with two different integer order linear viscoelastic material models by using MATLAB® optimization toolbox.

After the superiority of the fractional order material model compared to integer order material models has been shown, the linear fractional order material model is extended to its nonlinear counterpart in finite deformation regime. The material model developed is assumed to be isotropic and homogeneous.

A user-subroutine is developed for the material model formulated to implement it into the commercial finite element software Msc.Marc 2010. The user-subroutine developed is verified by performing a small strain finite element analysis and comparing the results obtained with linear viscoelastic counterpart of the model on MATLAB®.

Finally, the unknown coefficients of the fractional order material model are identified by employing the inverse finite element method. A material parameter set with an amount of accuracy is determined and the material model with the parameters identified is capable of simulating the three different indentation test protocols, *i.e.*, “relaxation”, “creep” and “cyclic loading” protocols with a good accuracy.

Keywords: Fractional Calculus, Soft Biological Tissue, Viscoelasticity, Inverse Finite Element Method

ÖZ

YUMUŞAK BİYOLOJİK DOKULAR İÇİN KESİRLİ TÜREVLER YARDIMIYLA MALZEME MODELİ OLUŞTURULMASI VE SONLU ELEMANLAR ANALİZİ YAZILIMINA UYGULANARAK MALZEME PARAMETRELERİNİN YERİNDE CANLI İNDENTÖR DENEYLERİ KULLANILARAK ELDE EDİLMESİ

Demirci, Nagehan

Yüksek Lisans, Makina Mühendisliği Bölümü

Tez Yöneticisi: Yard. Doç. Dr. Ergin Tönük

Şubat 2012, 228 sayfa

Literatürde bulunan yumuşak biyolojik doku malzeme modelleri, çoğunlukla tam sayı türevler yardımıyla ifade edilirler ve malzeme modelinde bulunan gerilme ve/veya gerinmenin türev derecesi tam sayıdır. Bunun aksine, tam sayılı olmayan türevler yardımıyla oluşturulan yumuşak doku malzeme modellerinin daha doğru ve güvenilir malzeme modelleri olduğu gösterilmiştir.

Bu çalışmada, ilk olarak, yumuşak biyolojik dokular için kesirli (malzeme bağıntısındaki gerinmenin türev derecesi tam sayı olmayan) doğrusal viskoelastik malzeme modeli kuvvet-zaman-indentasyon deney verisine MATLAB® optimizasyon aracıyla uydurulmuş ve iki farklı tam sayı türevli malzeme modeliyle karşılaştırılmıştır.

Kesirli malzeme modelinin, tam sayı malzeme modellerine görece olan üstünlüğü gösterildikten sonra, doğrusal viskoelastik kesirli malzeme modeli, doğrusal olmayan eşdeğerine sonlu deformasyonlar altında genişletilmiştir. Geliştirilen malzeme modelinin eşyönsüz (izotropik) ve homojen olduğu varsayılmıştır.

Geliştirilen malzeme modeli için kullanıcı kodu oluşturularak, ticari sonlu elemanlar analizi programı Msc.Marc 2010'a uygulanması sağlanmıştır. Kullanıcı kodunun doğruluğu ise, küçük gerinme sonlu elemanlar analizi yapılarak, elde edilen sonuçlar doğrusal eşdeğer modelden elde edilen sonuçlarla karşılaştırılarak gösterilmiştir.

Son olarak, malzeme modelinin bilinmeyen sabitleri, evrik sonlu elemanlar metoduyla elde edilmiştir. Belli hassasiyetteki bir parametre setinin, üç farklı indentasyon test protolüne, başka bir ifadeyle, "gevşeme", "sünme" ve "devirli yükleme" protokollerine uyduğu gösterilmiştir.

Anahtar Kelimeler: Kesirli Analiz, Yumuşak Biyolojik Doku, Viskoelastisite, Evrik Sonlu Elemanlar Metodu

ACKNOWLEDGEMENTS

First of all i would like to express my deepest gratitude to my supervisor Assist. Prof. Dr. Ergin Tönük for his guidance, advice, criticism, encouragements and insight throughout the research.

Surely, I am grateful to my *family* for their invaluable support and endless love.

Additionally, I would like to thank my friends; *Ali Anıl Şahinci, Gözde Tanıl and Damla Hacıibrahimoğlu* for their friendship, technical assistance and support. This thesis would not have been possible without their never-ending encouragement, patience and support.

TABLE OF CONTENTS

ABSTRACT iv
ÖZ vi
CHAPTERS
INTRODUCTION 1
1.1 Soft Biological Tissue 2
1.2 Testing of Soft Tissue 2
1.3 Importance and Potential Usage of Soft Biological Tissue 3
Constitutive Equation 3
1.4 Application of Fractional Calculus Theory to Soft Tissue Material Modeling .. 5
1.5 Scope of the Thesis 6
1.6 Outline of the Thesis 6
2. LITERATURE SURVEY 8
2.1 Introduction to Fractional Calculus 8
2.1.1 Grünwald-Letnikov Fractional Definition 12
2.1.2 Riemann-Liouville Fractional Definition 14
2.1.3 Caputo Fractional Derivative Definition 17
2.2 Important Functions Related to the Fractional Calculus Theory 19
2.3 Numerical Evaluation of Mittag-Leffler Function 21
2.4 Applications of Fractional Calculus in Science and Engineering 23
2.5 Fractional Calculus in the Theory of Viscoelasticity 25
2.5.1 Finite Element Formulation of Fractional Constitutive Equations 31
2.5.2 Fractional Order Constitutive Equations Used for Modeling Soft Tissues 32
2.5.3 Hierarchical Analogies to the Fractional Element 35
2.6 Soft Tissue Behavior 44
2.7 Soft Tissue Indentation Experiments 46
2.8 Finite Element Analysis of Indentation 47
2.9 Inverse Finite Element Method for Extraction of Material Parameters 49

3. THE THEORY OF VISCOELASTICITY……51
3.1 Integer Order Spring-Dashpot Models 51
3.1.1 Creep and Relaxation Phenomena..... 56
3.2 Fractional Order Spring-Spring-pot Models 61
3.3 Curve-Fitting to Quasi-Static Experimental Data Using Fractional Order Constitutive Equations 72
3.4 Fractional Order Calculus Applied to Fung's Quasi-Linear Viscoelasticity Theory..... 83
4. THREE-DIMENSIONAL FRACTIONAL ORDER CONSTITUTIVE EQUATION FOR SOFT BIOLOGICAL TISSUES 93
4.1 Constitutive Equation 93
4.2 Implementation of the Material Model into Msc.Marc 2010 Software..... 102
4.3 User-Subroutine "*UELASTOMER*"..... 106
4.4 User-Subroutine Flow Chart..... 112
4.5 Verification of the User-Subroutine "*UELASTOMER*" 113
4.5.1 Matlab® Routine..... 113
4.5.2 Finite Element Analysis Routine 113
4.6 Verification of the User-Subroutine for Relaxation Response..... 116
4.7 Verification of the User-Subroutine for Creep Response..... 122
5. THREE-DIMENSIONAL FINITE ELEMENT MODEL OF THE INDENTATION EXPERIMENTS OF SOFT BIOLOGICAL TISSUE 126
5.1 Quarter Tissue Model 126
5.2 Finite Element Analysis Details 127
5.2.1 Material Properties 127
5.2.2 Element 127
5.2.3 Contact Properties 128
5.2.4 Solution 129
5.2.5 Loadcase Options 130
5.2.6 Solver 131
5.2.7 Finite Element Mesh 131
5.2.7.1 Node in Contact Criterion 132

5.2.7.2 Mean Strain Energy Criterion 137
5.2.7.3 Relative Equivalent Stress Criterion 139
5.2.7.4 Zienkiewicz-Zhu Criterion 140
5.2.8 Hexahedral Mesh Compared with Tetrahedral Mesh 141
5.3 First Simulation Results 144
5.4 Material Parameter Investigation 147
6. AXISYMMETRIC MODELING OF SOFT TISSUE 150
6.1 Mesh Optimization 150
6.2 Analyzing Experimental Data 154
6.3 Material Parameter Identification 158
6.3.1 Parameter Extraction for Experimental Relaxation Data 158
6.3.2 Parameter Extraction for Cyclic Loading Experiment Data 165
6.3.3 Simulation of Relaxation Experiment with Parameters Derived for Cyclic Loading Test 173
6.4 Effect of Indentation Rate on Preconditioning Behavior 188
6.5 Parameter Extraction for Creep Experiment Data 191
7. CONCLUSION AND RECOMMENDATIONS FOR FUTURE WORK 194
7.1 Summary 194
7.2 Results and Discussion 195
7.3 Future Work 197
REFERENCES……198
APPENDICES
A. FRACTIONAL DERIVATIVE OF SOME SIMPLE FUNCTIONS 213
B. INDENTATION EXPERIMENTS 215
B.1 Indentation Experiments 215
B.2 Experiment Protocols: 219
C. MATLAB CODES 222
C.1 Matlab Code for 1-D Fractional Viscoelastic Material Model 222
C.2 Matlab Code for 1-D Parameter Extraction 225
C.3 Matlab Code for Parameter Identification for Fung's QLV Theory 226
C.4 Matlab Code for Evaluation Approximate Mittag-Leffler Function 227

C.5 Matlab Code for FOV Model with Exact and Approximate M-L Function .. 229
C.6 UElastomer User-Subroutine Inputs and Outputs..... 231
C.7 User-Subroutine Developed for Implementation of the Material Model..... 233

LIST OF TABLES

TABLES

Table 3.1 Material Parameters Identified for Three Material Models 77
Table 3.2 Material Parameters Identified for Three Material Models 80
Table 3.3 Material Parameters Obtained for Fractional Zener Model 81
Table 4.1 Wall Time of the FE Solution……...121
Table 5.2 Mesh Refinement Level (Node in Contact)……..135
Table 5.3 Mesh Refinement Level and Wall Time (Mean Strain Energy) 139
Table 5.4 Time Step And Wall Time Relation (Hexahedral Mesh) 143
Table 5.4 Time Step And Wall Time Relation (Tetrahedral Mesh) 144
Table 6.1 Mesh Optimization Results (Axisymmetric Model)……153
Table 6.2 Parameter Set #1 159
Table 6.3 Parameter Set #2 161
Table 6.4 Parameter Set #3 162
Table 6.5 Parameter Set #4 163
Table 6.6 Parameter Set #5 164
Table 6.7 Parameter Set #6 165
Table 6.8 Parameter Set #7 168
Table 6.9 Parameter Set #8 169
Table 6.10 Parameter Set #9 170
Table 6.11 Parameter Set #10 171
Table 6.12 Parameter Set #11 172
Table 6.13 Parameter Set #12 174
Table 6.14 Parameter Set #13 175
Table 6.15 Parameter Set #14 176
Table 6.16 Parameter Set #15 179
Table 6.17 Parameter Set #1-6 181
Table 6.18 NSSE (%) Values 182
Table 6.19 Parameter Set #1-3 183
Table 6.20 NSSE (%) Values 184
Table 6.21 Parameters for the J-G-S Material Model 186

Table 6.22 Parameter Set #15 189
Table 6.23 Parameter Set #16 193
Table A.1 Fractional Derivative of Some Simple Functions……...213

LIST OF FIGURES

FIGURES

Figure 2.1 Left and right derivatives of a function 19
Figure 2.2 a) Elastic, b) Viscous, c) Fractional element 36
Figure 2.3 a) Maxwell model, b) Its fractional generalization..... 37
Figure 2.4 a) Kelvin-Voigt model b) Its fractional generalization..... 37
Figure 2.5 a) Zener model b) Its fractional generalization..... 37
Figure 2.6 a) Poynting-Thomson model b) Its fractional generalization 38
Figure 2.7 Fractance-type fractional model 38
Figure 2.8 Infinite Spring Dashpot Ladder 39
Figure 2.9 Generalized Maxwell Element with Infinite Ladder 40
Figure 2.10 Sierpinski-like network of springs and dashpots 41
Figure 2.11 The extra-cellular matrix at successive spatial scales..... 42
Figure 2.12 Continuous relaxation spectrum, hysteresis vs. logarithm of frequency 43
Figure 2.13 Fractal type tree model a) $\beta = 1$, b) $\beta = 0.7$ c) $\beta = 0.3$ 44
Figure 2.14 Preconditioning of tissue (n represents the number of cycles) 45
Figure 2.15 Schematic of the indentation problem 48
Figure 2.16 The finite element model of soft tissue and indenter..... 49
Figure 3.1 Elastic element, spring (left), viscous element, dashpot (right) 53
Figure 3.2 Maxwell Model (left), Voigt Model (or Kelvin model) (right)..... 54
Figure 3.3 Zener Model (The Standard Linear Solid) (Left), Kelvin Model (Right) 55
Figure 3.4 Anti-Zener Model (dashpot in series with Voigt - left)..... 59
Figure 3.5 Burger's Model (Creep Representation- Left)..... 60
Figure 3.6 The fractional Element, Spring-Pot 62
Figure 3.7 The relaxation modulus for a spring-pot element..... 64
Figure 3.8 The creep compliance for a spring-pot element 65
Figure 3.9 Fractional Maxwell (Left) and Voigt Model (Right)..... 66
Figure 3.10 Three-element fractional standard linear solid model 67
Figure 3.11 Creep compliance for three element fractional model..... 68
Figure 3.12 Relaxation modulus for three element fractional model..... 69
Figure 3.13 The three element fractional Zener model..... 70

Figure 3.14 Generalized Maxwell Model 74
Figure 3.15 Generalized Voigt Model 75
Figure 3.16 Curve-fit to Experimental Relaxation Data 76
Figure 3.17 Curve-fit to Creep Test Data..... 79
Figure 3.18 Curve-fit to Relaxation Test Data..... 82
Figure 3.19 Zener model connected in series..... 84
Figure 3.20 Fractal-type tree model representing FOV-QLV model..... 85
Figure 3.21 Ramp Strain Function 88
Figure 3.22 Raw Relaxation Experiment Data 90
Figure 3.23 Fractional Order QLV Model Fitted to Relaxation Test Data (1) 91
Figure 3.24 Fractional Order QLV Model Fitted to Relaxation Test Data (2) 92
Figure 4.1 Approximate vs. exact Mittag-Leffler function in the range $[0, 0.1]$ …..105
Figure 4.2 Approximate vs. exact Mittag-Leffler function in the range $(0.1, 15)$ …105
Figure 4.3 Approximate vs. exact Mittag-Leffler function in the range $[15, 100]$ ... 106
Figure 4.4 The User-Subroutine Flow Chart..... 112
Figure 4.5 Mentat interface for user-subroutine input 114
Figure 4.6 Inputted parameters via software interface. 114
Figure 4.7 The 8-Node Hexahedral Element with Applied Boundary Conditions .. 117
Figure 4.8 Relaxation curve obtained from FEA (Mentat interface) 118
Figure 4.9 User-subroutine Verification for Relaxation Response 119
Figure 4.10 User-subroutine Verification for Relaxation Response 120
Figure 4.11 Least square error graph for adaptive time stepping solution..... 121
Figure 4.12 Least square error graph for fixed time stepping solution 122
Figure 4.13 Creep curve obtained from FEA (Mentat interface)..... 124
Figure 4.14 Verification of the user-subroutine for the creep analysis 124
Figure 4.15 Least Square Error Plot Obtained for the Creep Analysis 125
Figure 5.1 Quarter Tissue Model with Indenter Tip……127
Figure 5.2 Hexahedral Herrmann Type Element 128
Figure 5.3 Domain Decomposition Method (DDM)..... 133
Figure 5.4 Adaptive Mesh Refinement 1 (Node in Contact) 135
Figure 5.5 Adaptive Mesh Refinement (Zoom in to Figure 5.4) 136
Figure 5.6 Cyclic Loading (Ten Cycles)..... 137
Figure 5.7 Adaptive Mesh Refinement (Mean Strain Energy) 138

Figure 5.8 Adaptive Mesh Refinement (Zoom in to Figure 5.7) 139
Figure 5.9 Accuracy of FE Solution (Hexahedral Mesh) 142
Figure 5.10 Accuracy of FE Solution (Tetrahedral Mesh) 143
Figure 5.11 Relaxation Simulation (Quarter Tissue Model)..... 145
Figure 5.12 Cyclic loading protocol (First cycle only) 146
Figure 5.13 Material Parameter Investigation (Trials 1-2-3-4)..... 148
Figure 5.14 Material Parameter Investigation (Trials 5-6-7) 149
Figure 6.1 Axisymmetric FEM of Soft Tissue and Rigid Body Indenter.....151
Figure 6.2 A Closer View of the Fine Mesh Region under the Indenter Tip..... 152
Figure 6.3 High Stress Concentration at the Edge of the Indenter Tip 152
Figure 6.4 View of the Whole Tissue Model after Indentation 153
Figure 6.5 Axisymmetric Mesh Optimization Result 154
Figure 6.6 First Cycle of the Cyclic Loading Experiment 155
Figure 6.7 Contact Start of the Indenter Tip with the Tissue..... 156
Figure 6.8 Contact End of the Indenter Tip with the Tissue 156
Figure 6.9 Stress Relaxation on Tissue During Cyclic Loading..... 157
Figure 6.10 Raw Relaxation Experiment Data 158
Figure 6.11 Relaxation Data Fit (Parameter Set 1) 159
Figure 6.12 Relaxation Data Fit (Parameter Set 2) 161
Figure 6.13 Relaxation Data Fit (Parameter Set 3) 162
Figure 6.14 Relaxation Data Fit (Parameter Set 4) 163
Figure 6.15 Relaxation Data Fit (Parameter Set 5) 164
Figure 6.16 Relaxation Data Fit (Parameter Set 6) 165
Figure 6.17 Comparison of FE Results 166
Figure 6.18 Raw Cyclic Loading Experiment Data 167
Figure 6.19 Raw Cyclic Loading Experiment Data (First Cycle)..... 167
Figure 6.20 Cyclic Loading Data Fit (Parameter Set 7)..... 168
Figure 6.21 Cyclic Loading Data Fit (Parameter Set 8)..... 169
Figure 6.22 Cyclic Loading Data Fit (Parameter Set 9)..... 170
Figure 6.23 Cyclic Loading Data Fit (Parameter Set 10)..... 171
Figure 6.24 Cyclic Loading Data Fit (Parameter Set 11)..... 172
Figure 6.25 Relaxation Data Fit (Parameter Set #11) 173
Figure 6.26 Relaxation Data Fit (Parameter Set 12) 174
Figure 6.27 Relaxation Data Fit (Parameter Set 13) 175

Figure 6.28 Relaxation Data Fit (Parameter Set 14) 176
Figure 6.29 Cyclic Loading Data Fit (Parameter Set 14)..... 177
Figure 6.30 Relaxation Data Fit After Three Cycles of Loading and Unloading 178
Figure 6.31 Cyclic Loading Response (Set of Parameters #15) 179
Figure 6.32 Relaxation Response (Set of Parameters #15)..... 180
Figure 6.33 Relaxation Response (Set of Parameters #1-6) 181
Figure 6.34 Relaxation Response (Set of Parameter #6) 182
Figure 6.35 Relaxation Response (Set of Parameter #1-3)..... 183
Figure 6.36 Cyclic Loading Response (Set of Parameter #6)..... 184
Figure 6.37 Parameter Set # 6 185
Figure 6.38 Relaxation data fit (NSSE: 0.0145 (1.45%)) 186
Figure 6.39 Loading and unloading for J-G-S Material Model 187
Figure 6.40 Preconditioning (Mullin's) Effect (Parameter Set 15)..... 189
Figure 6.41 Preconditioning (Mullin's) Effect (Parameter Set 15)..... 190
Figure 6.42 Raw Creep Experiment Data 191
Figure 6.43 Creep Behavior Simulation (1)..... 192
Figure 6.44 Creep Behavior Simulation (2)..... 192
Figure 6.45 Creep Data Fit (Parameter Set 16)..... 193

Figure B.1 Just before the tissue is indented (1), after the tissue is indented (2)….215
Figure B.2 Indenter device. Control box (1), test unit (2), portable computer (3)... 216
Figure B.3 Different type of indenter tips ((Petekkaya, 2008)) 217
Figure B.4 Indenter test device 218
Figure B.5 Ellipsoidal tips with different dimensions. 218
Figure B.6 Alignment Element 219

CHAPTER 1

INTRODUCTION

Human body has been a great challenge to understand since ancient times. The complicated mechanisms constructing the whole body are analyzed separately to ease the understanding. When the skeletal system is considered for instance, a further distinction can be made considering the functionalities of the sub-systems, such as, bones, cartilage, skeletal muscles, tendons and brain. Each sub-system has a unique mechanical behavior (behavior of the system under the action of forces, resulting motion and/or deformation) and should be analyzed independently. Their respective mechanical behavior may be expected to be related to their specific composition, structure, location and diverse function of the organism.

The healthy or pathological condition of the tissue is highly dependent on the structure, e.g. *stiffness* of the tissue. The identification of tissue properties under normal and pathological living conditions is highly important in diagnosing and treating disease or injury. It is a well-known example that cancerous tissues have higher stiffness compared to normal tissues. With this knowledge on hand the diagnosis of the "cancer" can be improved and expedited. Another well-known example can be the "diabetic foot syndrome" which can cause the loss of the feeling of foot due to diabetes and can even require the amputation of the foot. "Bedsores" also known as decubitus (or pressure) ulcer lesions is another example for soft tissue diseases. Bedsores are fairly dangerous on wheelchair users and paralyzed people. Those diseases mentioned above reveal several important characteristics of soft tissue behavior. Those important characteristics can only be understood with a deep mechanical knowledge. Interdisciplinary work involving the clinicians and the mechanical people is necessary to enlighten the unknowns of the human soft tissue behavior.

1.1 Soft Biological Tissue

Soft tissues in a human body are defined as tissues which are capable to go into finite deformations. They are differentiated from hard tissues, such as bones in the human body, with this capability they possess. Soft tissues also behave highly different from traditional engineering materials, such as steel or aluminum. Although, the linear elastic theory for infinitesimal strains applies well for most of the engineering materials and hard tissues, this theory could not be applied for soft biological tissues which can undergo large deformations. For soft tissues undergoing large deformations, nonlinear elastic (large/finite strain) theory should be applied to analyze their stress-strain behavior.

Almost all of the soft tissues are composed of a mixture of solid and liquid medium, e.g. *cells and extracellular matrix*. Therefore, they are classified as viscoelastic materials. In this regard, the nonlinear elastic theory which is suggested for soft biological tissues under large deformations is necessary but not sufficient. To model the nonlinear elastic and the viscoelastic properties of soft tissues, nonlinear elastic theory and the viscoelasticity theory should be applied together. This methodology for modeling of soft tissues is one of the aims of this study. As we learn more about the characteristics of living materials the ideas about mathematical modeling broaden itself without a doubt.

1.2 Testing of Soft Tissue

The testing of soft biological tissues is usually similar to testing of traditional engineering materials. Simple tension and compression, biaxial testing, simple shear tests, fatigue or impact testing are also applicable to soft tissues. However the testing methods should include comprehensive testing protocols when complex nonlinear tissues are considered. Indentation testing of soft tissues involves comprehensive testing protocols, such as, “creep”, “relaxation” and “cyclic loading” test protocols. The most important point through experimentation is the condition and the state of the tissue.

There are three basic types of biological tissue mechanical testing according to the physiological state and condition of the tissue, which are;

- *Ex-vivo:* The tissue is experimented in an artificial controlled environment, outside the living organism with minimal changes to its natural environment, and up to 24 hours after the tissue taken apart.
- *In-vitro:* Being similar to ex-vivo, the tissue is taken away from its natural living condition however; the living tissue is dead now and the environment can be a controlled environment too.
- *In-vivo:* In in-vivo experimentation, the tissue is alive and in its normal living conditions, however, the testing can be a tough procedure, because of the complicated test set-up it would require. This type of experimentation however provides the most accurate information about the mechanical behavior of the tissue.

1.3 Importance and Potential Usage of Soft Biological Tissue Constitutive Equation

Much of the biomechanics study first focuses on the formulation of reliable constitutive equations and then the solution of initial and boundary value problems. Therefore the formulation of appropriate constitutive relations is highly crucial in biomechanics. As Fung (1993) states, the most serious frustration to a biomechanician is the lack of reliable information regarding the living tissue constitutive equations. Without an appropriate constitutive equation, analyses cannot be done and boundary and initial value problems cannot be solved. Therefore a hypothetical material model formulated should be demonstrated to agree well with the experimental findings.

For almost a century, researchers tried to curve-fit the theoretical and subjective material models to the experimental outcomes. However these works were just simple curve-fits and the models were a close approximation rather than exactly representing the real tissue behavior. Still, the search for an objective material model for soft tissues is under research. This is due mostly to the complexity of the tissue behavior and not obtaining sensitive and accurate experimental results. The tissue

mechanical behavior is highly dependent on the tissue being tested or modeled, the age, gender and physiological condition of the individual and finally the time the tissue is being tested. The micro-structure of the soft tissue is dependent on several factors as listed, and one experiment result obtained on one day, cannot always correlate with another data obtained at another day. These difficulties in obtaining experimental data, further complicates the modeling procedure. As a result, the development of constitutive equation for soft tissues requires more sensitive experimental data.

The question of choosing the appropriate model to fit the experimental data is an important one. The models were created to correlate with the experimental data. A developed model shall fit *all* the experiment data including, relaxation, creep, hysteresis…etc. However, a model may not fit all the experiment data and fit only one type of data and the same material model with the same material constants produce a totally different response than the experimentally observed behavior for another type of experiment. This means, the material model is barely a curve fit to a specific experimental data and is not a real material model predicting the mechanical response of the material within a reasonable accuracy at least within some reasonable range.

One of the most important outcomes of development of a reliable living material model is the implementation of the material model to a finite element code. The finite element method which was introduced in 1956 is a valuable and very powerful tool in studying numerical solution of soft tissue problems and with the advance of computer technology, real-world problems involving soft tissues can be simulated and solved.

The mechanical interaction of soft tissues with devices such as prosthesis, orthesis and implants can be mechanically analyzed and simulated with the aid of reliable constitutive equation of soft tissue. Surgical planning and clinician education (simulation of surgery for training purposes), haptic technology, medical simulation of minimally invasive procedures, rehabilitation robotics, tissue engineering, remodeling, artificial tissue substitutes can be the possible applications of living tissue material modeling. The idea behind these researches can be explained with an

analogy. “Just as the pilots train themselves in flight simulators, the surgeons can be able to train themselves without actually cutting anyone” (Scilingo, Sgambelluri, & Bicchi).

1.4 Application of Fractional Calculus Theory to Soft Tissue Material Modeling

The classical viscoelastic models often require several parameters to adequately represent the living material behavior. The experimental set-ups needed to identify those parameters are not always available and usually limited data is available. Therefore, there is a need for accurate models involving as few unknown parameters as possible. In that respect, constitutive equations using fractional derivatives has the advantage of being representative of the material behavior with fewer parameters. The fractional derivative parameter which is the order of time derivative of stress and/or strain in the constitutive equation is an extra parameter to be identified, which can replace many other parameters in regular integer order models by simplifying the material model; however the identification of this parameter usually requires dealing with cumbersome mathematics compared to integer order models. In the literature, several numerical algorithms are suggested for dealing with the fractional order differentiation and integration for soft tissue material models. As one of the goals of this thesis was the identification of parameters of the material model developed via curve-fitting to experimental data by using the inverse finite element method, a good agreement between the model and the experimental data is needed to be obtained with small but adequate number of parameters. Another goal was to model different experiments (*i.e.* cyclic indentation at different rates, relaxation and creep**)** with a single set of material parameters with certain accuracy.

Another advantage of dealing with fractional order derivatives in viscoelasticity theory is the inclusion of the memory behavior by definition in fractional operations which is peculiar to viscoelastic materials. Viscoelastic materials have memory and fractional calculus applied in the viscoelasticity theory is the mimicry of the memory (Schiessel H. , Metzler, Blumen, & Nonnenmacher, 1995). Fractional derivatives depend on the material past, evidencing a memory mechanism, and include inherently the history of a process. Further the fractional order parameter provides a

smooth transition from elastic to a nearly classic viscoelastic material when the order of time derivative is bounded by $[0,1]$.

In addition, fractional relations of viscoelastic materials can be realized physically through hierarchical arrangements of springs and dashpots which is a strong support for the idea that, fractional order viscoelastic material models are better candidates for material models of soft biological tissues. The soft tissues are composed of several similar structures (representing self-similarity on many scales) bounded together and the hierarchical models are the theoretical representations of this real tissue structure.

The points that are mentioned above are the main motivation in utilizing the fractional calculus in characterizing the viscoelastic behavior of soft tissues.

1.5 Scope of the Thesis

Nearly all available commercial finite element package programs offer classical integer order elastic material models, such as Mooney-Rivlin, Neo-Hookean, Yeoh, Ogden, Arruda-Boyce and viscoelastic material models such as Prony series…etc. The scope of this thesis is the formulation of a fractional order viscoelastic material model for soft tissues and implementing it into the commercial finite element software Msc.Marc 2010 by developing a material model user-subroutine. With the material model implemented into finite element software, the soft-tissue unknown material parameters are identified by fitting the force-displacement-time data of the finite element model to the experimental data obtained from experiments performed on in-vivo human fore-arm in a previous work (Petekkaya, 2008).

1.6 Outline of the Thesis

Chapter 2 begins with the introduction to fractional calculus theory in pure mathematics and continues with the applications of fractional calculus theory to science and engineering and especially to viscoelasticity theory. Several works from the literature are presented. In Chapter 3, fractional order, nonlinear, viscoelastic

material model is presented and the user-subroutine developed for the material model implemented is analyzed. In Chapter 4, a three-dimensional, quarter tissue model with ellipsoid indenter tip is introduced and finite element analyses techniques are explained. In Chapter 5, an axisymmetric model of the soft tissue and cylindrical indenter tip is introduced and solutions of several finite element simulations are presented. Further, the parameter sets tried and the final parameter set determined is found.

Finally in Chapter 6, a brief summary of the work is presented and the results obtained are discussed. Further, recommendations for future work are presented.

CHAPTER 2

LITERATURE SURVEY

2.1 Introduction to Fractional Calculus

Fractional calculus where the integrals and derivatives are of "fractional" order is defined and studied, as old as integer order calculus. In the early discovery of calculus, Leibniz (1646-1716) introduced the notation $d^n y/dx^n = D^n y$ for differentiation where n represents a non-negative integer. The question about the meaning of non-integer operations in integral and differential calculus were raised early in mathematics history. In 1695, L'Hospital in a letter to Leibniz asked what happens if the order of derivative is $1/2$? Leibniz replied: "It is a paradox but some day useful consequences will be drawn". The non-integer order differential and integral calculus includes not only the fractional numbers, but it comprises any arbitrary number, rational-irrational and even complex numbers. Therefore the term "fractional calculus" is a misnomer and might be better labeled generalized integration and differentiation of arbitrary order. However for historical reasons, the word "fractional" is used instead of the word "arbitrary" (Ross, 1977).

The "*fractional calculus*" is the name for the theory of integrals and derivatives of arbitrary order, which unify and generalize the notions of integer-order differentiation and n-fold integration (Podlubny I. , 2009).

For any natural number n, the derivative of a function $f(x)$ can be expressed as;

$$D^n f(x) = \lim_{h \to 0} h^{-n} \sum_{m=0}^{n} (-1)^m \binom{n}{m} f(x - mh) \tag{2.1}$$

where the binomial is,

$$\binom{n}{m} = \frac{n!}{m!(n-m)!} = \frac{\Gamma(n+1)}{\Gamma(m+1)\Gamma(n-m+1)}, \quad 0 \le m \le n \tag{2.2}$$

which is also valid for non-integer values. (The full derivation of the generalized differentiation expression is explained at the web-page xuru.org (Xuru, 2008)).

In the formulation above $\Gamma(n) = (n-1)!$ is called the Euler's gamma function which is a special and basic function of the fractional calculus. The importance comes from the eligibility of the function to generalize the factorial $n!$ and allowing n taking non-integer and even complex values. After some derivations and by using the displacement operator of the differentiation $\left(d_h^{\alpha} f(x)\right) = f(x+\alpha h)$, the generalized differentiation expression is shown as follows;

$$D^{\alpha} f(x) = \lim_{h \to 0} h^{-\alpha} \sum_{n=0}^{\infty} (-1)^n \frac{\Gamma(\alpha+1)}{n!\Gamma(\alpha-n+1)} f(x-nh) \tag{2.3}$$

Although integer order derivatives and integrals have a clear understanding and physical and geometrical interpretation (the slope at a point and the area under a curve within limits of integration), fractional order differentiation and integration do not have a clear physical interpretation. Since the appearance of the idea of arbitrary (not necessary integer) order there was not any acceptable geometric and physical interpretation of those operations for more than 300 years (Dalir & Bashour, 2010).

A single expression for integration and differentiation of arbitrary order is provided by Bayin (2010),

For N successive derivatives,

$$\frac{d^n f}{dx^n} = \lim_{N \to \infty} \left\{ \left[\frac{x-a}{N} \right]^{-n} \sum_{j=0}^{N-1} [-1]^j \binom{n}{j} f\left(x - j\left[\frac{x-a}{N} \right] \right) \right\} \tag{2.4}$$

For N successive integrals,

$$\frac{d^{-n}f}{d\left(x-a\right)^{-n}}=\lim_{N\to\infty}\left\{\left[\frac{x-a}{N}\right]^{n}\sum_{j=0}^{N-1}\binom{j+n-1}{j}f\left(x-j\left[\frac{x-a}{N}\right]\right)\right\} \tag{2.5}$$

Note that,

$$\left[-1\right]^{j}\binom{n}{j}=\binom{j+n-1}{j}=\frac{\Gamma\left(j-n\right)}{\Gamma\left(-n\right)\Gamma\left(j+1\right)} \tag{2.6}$$

and

$$\left[dx\right]^{n}=\left[d\left(x-a\right)\right]^{n} \tag{2.7}$$

Finally, the two expressions (equations 2.4 and 2.5) can be unified and for this expression the n value takes integer values of both signs.

$$\frac{d^{n}f}{\left[d\left(x-a\right)^{n}\right]}=\lim_{N\to\infty}\left\{\frac{\left[\frac{x-a}{N}\right]^{-n}}{\Gamma\left(-n\right)}\sum_{j=0}^{N-1}\frac{\Gamma\left(j-n\right)}{\Gamma\left(j+1\right)}f\left(x-j\frac{\left[x-a\right]}{N}\right)\right\} \tag{2.8}$$

This definition can be further modified to include the non-integer values of n.

The most important contributors to the field of fractional calculus are, Euler (1730), Lagrange (1772), Laplace (1812), Lacroix (1819), Fourier (1820), Abel (1823), Liouville (1832), Riemann (1847), Grünwald (1867) and Letkinov (1872), so that a satisfactory expression for the generalization of integration and differentiation to fractional orders has been developed (Oldham & Spanier, 1974).

Euler, in 1730 developed the generalization of the formula (Dalir & Bashour, 2010),

$$\frac{d^{n}x^{m}}{dx^{n}}=m\left(m-1\right)...\left(m-n+1\right)x^{m-n} \tag{2.9}$$

by the property of the Gamma function,

$\Gamma(m+1) = m(m-1)...(m-n+1)\Gamma(m-n+1)$ (Greenberg, 1998), (pg. 218) to obtain,

$$\frac{d^n x^m}{dx^n} = \frac{\Gamma(m+1)}{\Gamma(m-n+1)} x^{m-n} \tag{2.10}$$

The Gamma function plays a central role in finding the inverse Laplace transforms of fractional powers (Magin R. , 2004, pg. 33).This function is intrinsically tied to fractional calculus by definition.

Lacroix in 1819 in his long book called "Calculus" obtained a formula for the fractional derivative of powers,

$$D^\alpha x^\beta = \frac{\Gamma(\beta+1)}{\Gamma(\beta-\alpha+1)} x^{\beta-\alpha} \tag{2.11}$$

where α and β are fractional numbers.

Then by replacing α with $1/2$ and letting $\beta = 1$, he achieved the half derivative of the function $y = f(x) = x$ (Ross, 1977).

$$\frac{d^{1/2} y}{dx^{1/2}} = \frac{\Gamma(2)}{\Gamma(3/2)} x^{1/2} = \frac{2}{\sqrt{\pi}} \sqrt{x} \tag{2.12}$$

On the other hand, Joseph Liouville's (1809-1882) second definition of fractional derivative is,

$$D^\alpha x^{-\beta} = (-1)^\alpha \frac{\Gamma(\alpha+\beta)}{\Gamma(\beta)} x^{-\alpha-\beta} \tag{2.13}$$

Some mathematicians preferred Liouville's definition; on the other hand some other mathematicians preferred Lacroix's formula. This caused discrepancies between the

two definitions. However, William Center, in 1850 realized that the fractional derivative of a constant is not zero for Lacroix's definition whereas it becomes zero for Liouville's definition while $\Gamma(0)=\infty$ and $1/\Gamma(\infty)\cong 0$.

At the present time there are several notations in use which denote a fractional operator. A convenient notation proposed by Harold T. Dewis (1936) is as follows,

If β is an arbitrary positive real number, ${}_aD_t^{-\beta}$ denotes integration of order β (integral or anti-derivative operator), whereas ${}_aD_t^{\beta}$ denotes differentiation of order β (derivative operator). The subscripts a and t denote limits, called the "terminals", since in fractional calculus there is no geometric interpretation of integration and differentiation of arbitrary order, the term "terminal" is preferred instead of the term "limit" (Ross, 1977).

There are several definitions and approaches to the fractional derivative. The most popular of them are summarized in the following sections.

2.1.1 Grünwald-Letnikov Fractional Definition

The Grünwald-Letnikov (G-L) approach starts from the fundamental definition of differentiation,

$$f'(x)=\frac{df}{dt}=\lim_{h\to 0}\frac{f(x+h)-f(x)}{h} \tag{2.14}$$

and continues to the nth order differentiation and a final step is including the non-integer values of n which is provided by the gamma function instead of the factorial in binomial coefficient definition (Loverro, 2004),

$$d^n f(x) = \lim_{h\to 0} \frac{1}{h^n} \sum_{m=0}^{n} (-1)^m \binom{n}{m} f(x-mh)$$

$$ {}_aD_x^{\beta} f(x) = \lim_{h\to 0} h^{-\beta} \sum_{m=0}^{\left[\frac{x-a}{h}\right]} (-1)^m \frac{\Gamma(\beta+1)}{m!\Gamma(\beta-m+1)} f(x-mh) \tag{2.15}$$

and for negative values of β,

$$d^{-n} f(x) = \lim_{h\to 0} h^n \sum_{m=0}^{n} (-1)^m \binom{-n}{m} f(x-mh)$$

$$ {}_aD_x^{-\beta} f(x) = \lim_{h\to 0} h^{\beta} \sum_{m=0}^{\frac{x-a}{h}} \frac{\Gamma(\beta+m)}{m!\Gamma(\beta)} f(x-mh) \tag{2.16}$$

$$= \frac{1}{(\beta-1)!} \int_a^x (x-\tau)^{\beta-1} f(\tau)\, d\tau$$

The equation above is adoped from (Podlubny I. , 1999), (pg. 46) which is equivalent to the Riemann-Liouville fractional definition represented in the next section while

$$\binom{-\beta}{m} = (-1)^m \frac{\Gamma(\beta+m)}{\Gamma(\beta)m!} \tag{2.17}$$

The G-L definition of fractional derivatives is mainly used today for the numerical approximations of fractional derivatives. It is expressed by the gamma function (Podlubny I. , 1999),

$$ {}_aD_x^{\beta} f(x) = \frac{1}{\Gamma(-\beta)} \int_a^x (x-\tau)^{-\beta-1} f(\tau)\, d\tau \tag{2.18}$$

The definition for the fractional integration is,

$$ {}_aD_x^{-\beta} f(x) = \frac{1}{(\beta-1)!} \int_a^x (x-\tau)^{\beta-1} f(\tau) d\tau \tag{2.19}$$

where $\Gamma(\beta)=(\beta-1)!$.

Also,

$$ {}_aD_x^{-\beta-1} f(x)=\frac{1}{\beta!}\int_a^x (x-\tau)^{\beta} f(\tau)d\tau \tag{2.20} $$

The commutative relationships and restrictions of these definitions are explained in detail in (Podlubny I. , 1999). A geometric interpretation for the Grünwald "differ-integral" is provided also in (Lorenzo & Hartley, 1998) and a numerical treatment of fractional differential equations based on the Grünwald-Letkinov definition is discussed in (Scherer, Kalla, Tang, & Huang, 2011).

2.1.2 Riemann-Liouville Fractional Definition

Unlike the G-L approach which derives its definition from differentiation, Riemann-Liouville (R-L) derivative approach derives its definition from integration and is based on Cauchy's formula for calculating iterated integrals (n-fold integration).

$$ D^{-1} f(x)=\int_0^x f(t)dt \tag{2.21} $$

$$ D^{-2} f(x)=\int_0^x\int_0^{t_2} f(t_1)dt_1dt_2=\int_0^x\int_{t_1}^x f(t_1)dt_2dt_1=\int_0^x f(t_1)\int_{t_1}^x dt_2dt_1=\int_0^x f(t)(x-t)dt \tag{2.22} $$

Continuation with this method yields the formula of iterated integrals,

$$ D^{-n} f(x)=\frac{1}{(n-1)!}\int_0^x f(t)(x-t)^{n-1}dt \tag{2.23} $$

Generalization to non-integer values provides the popular definition of "*fractional integral*",

$$ {}_aD_x^{-\beta} f(x)=\frac{1}{\Gamma(\beta)}\int_a^x (x-t)^{\beta-1} f(t)dt,\ \mathrm{Re}(\beta)>0 \tag{2.24} $$

Also,

$$ {}_{a}J_{x}^{\beta} f(x) = \frac{1}{\Gamma(\beta)} \int_{a}^{x} (x-t)^{\beta-1} f(t)\,dt \tag{2.25} $$

and

$$ D^{\beta} J^{\beta} = I \tag{2.26} $$

where I is the identity operator, therefore D^{β} is defined as the left inverse of J^{β} (Debnath, 2003).

Although the notation of fractional integration and differentiation differ only according to the sign of the parameter β, the change of fractional integration to differentiation do not differ by only changing sign of the parameter β on the right hand side of the equation. By analytical continuation with the assumption that the function $f(x)$ is n times continuously differentiable, it can be shown that,

$$ {}_{a}D_{x}^{\beta} f(x) = {}_{a}D_{x}^{n-\alpha} f(x) = {}_{a}D_{x}^{n}\, {}_{a}D_{x}^{-\alpha} f(x) = \frac{d^{n}}{dx^{n}} \left(\frac{1}{\Gamma(\alpha)} \int_{a}^{x} (x-t)^{\alpha-1} f(t)\,dt \right) \tag{2.27} $$

which gives the definition of the R-L fractional derivative and is also named the "*integro-differential*" expression. The important property of fractional derivative is the non-locality of the operator, which means that the derivative is not only dependent on the value at the point considered but the value of the function on the whole interval. In ordinary differential equations, the problem's derivative is known at a particular time if the values of the problem at that time are known. However for fractional differential equations, previous values of the solution and the derivatives are required for the solution to be obtained. This "memory" effect of the convolution allows modeling of various physical phenomena, such as, viscoelasticity, diffusion, viscoplasticity. Therefore unlike ordinary derivatives, which are point functionals, fractional derivatives are hereditary functionals, possessing a total memory of the past states (Diethelm, Ford, Freed, & Luchko, 2005).

Riemann-Liouville (R-L) fractional derivative with the lower limit being negative infinity yields the Weyl derivative which is a popular definition as well. There are computational advantages of selecting in Equation 2.27, $a=-\infty$ (Magin R. , 2004).

$$ {}_{-\infty}D_x^{\beta} f(x) = \frac{1}{\Gamma(-\alpha)} \int_{-\infty}^{x} \frac{f(t)}{(x-t)^{\beta+1}} dt \tag{2.28} $$

Fractional derivatives are therefore non-local operators. However when the derivative is defined in the following way, the limit assures locality,

$$ D^{\beta} f(x) = \lim_{a \to x} {}_{a}D_x^{\beta} f(x) \tag{2.29} $$

The most important property of R-L fractional definition is,

$$ {}_{a}D_x^{\beta}\left({}_{a}D_x^{-\beta} f(x)\right) = f(x) \tag{2.30} $$

which means that the R-L fractional differentiation operator is a left inverse to the *R-L* fractional integration operator of the same order β.

There is a link between R-L and G-L approaches to the differentiation of arbitrary order. If the function $f(x)$ is continuously differentiable in the interval $[a,x]$ and that $f^{n}(x)$ is integrable in $[a,x]$, then for every β $(0<\beta<n)$ the R-L derivative $\left({}_{a}D_x^{\beta} f(x)\right)$ exists and coincides with the *G-L* derivative $\left({}_{a}D_x^{\beta} f(x)\right)$. While R-L approach is useful in calculating derivatives of simple functions such as $\left(x^{a}, e^{x}, \sin(x)\right)$, G-L approach is more useful in utilization of numerical evaluation due to the summation form of the function.

One of the contemporary problems of fractional calculus is the requirement that the function $f(x)$ and its derivatives to be identically zero for $x=a$ (the time of the initialization). This property assures that,

$$ {}_aD_x^{\alpha}\,{}_aD_x^{\beta} f(x) = {}_aD_x^{\beta}\,{}_aD_x^{\alpha} f(x) = {}_aD_x^{\alpha+\beta} f(x) \tag{2.31} $$

2.1.3 Caputo Fractional Derivative Definition

Caputo derivative ${}^{C}D^{\beta} = J^{n-\beta} D^{n} f(x)$ with $n-1 < \beta \le n$ is defined as,

$$ {}_a^{C}D_x^{\beta} f(x) = \frac{1}{\Gamma(\beta-n)} \int_a^x \frac{f^{(n)}(\tau)\,d\tau}{(x-\tau)^{\beta+1-n}}, \ (n-1 \le \beta < n) \tag{2.32} $$

Another definition is,

$$ \lim_{\beta \to n} {}_a^{C}D_x^{\beta} f(x) = f^{(n)}(x), \ n = 1, 2... \tag{2.33} $$

which gives the conventional n^{th} order derivative where β is the parameter describing the order of the fractional derivative.

The importance of Caputo's fractional order integration and differentiation is; while formulating the initial values for initial value problems of fractional order differential equations, the Laplace transform of the Caputo derivative allows utilization of initial values of classical integer-order derivatives with known physical interpretations. Whereas R-L fractional order differential equations has initial conditions which cannot be physically interpreted. Therefore the Caputo fractional derivative is more suitable to be treated by the Laplace transform technique in that it requires the knowledge of the initial values of the functions (Gorenflo & Mainardi, 1997). Mathematical modeling based on advanced rheological models naturally leads to differential equations of fractional order and the necessity of the formulation of initial conditions arises. The initial conditions for fractional differential equations of Caputo derivatives take the same form as integer order derivatives with known physical interpretations (Podlubny I. , 1999).

Another important property of Caputo's fractional derivative is that the Caputo's fractional derivative of a constant is zero.

$$ {}_{0}^{C}D_{x}^{\beta} A = 0, \quad f(x) = A = \text{constant} \tag{2.34} $$

It is known that for zero initial conditions R-L, G-L and Caputo fractional derivatives coincide. A summary of the criterions that must be satisfied with the generalized calculus is provided in several papers (Ross, 1974b), (Ross, 1977), (Lorenzo & Hartley, 1998).

There are also two different definitions of a fractional derivative, which are the left fractional derivative and the right fractional derivative. Suppose a function $f(x)$ defined in the interval $[a,b]$ where a and b can be infinite as well. For the left fractional derivative, the lower terminal is at the left end of the interval. It can be expressed as,

$$ {}_{a}D_{x}^{\beta} f(x) = \begin{cases} \dfrac{d^n}{dx^n}\left[\dfrac{1}{\Gamma(n-\beta)}\displaystyle\int_a^x \dfrac{f(\tau)}{(x-\tau)^{\beta+1-n}}\right], n-1<\beta<n \\ \dfrac{d^n}{dx^n} f(x), \beta = n \end{cases} \tag{2.35} $$

The right definition attempts to arrive at the same result in a reverse order,

$$ {}_{x}D_{b}^{\beta} f(x) = \begin{cases} \dfrac{d^n}{dx^n}\left[\dfrac{1}{\Gamma(n-\beta)}\displaystyle\int_x^b \dfrac{f^n(\tau)}{(x-\tau)^{\beta+1-n}}\right], n-1<\beta<n \\ \dfrac{d^n}{dx^n} f(x), \beta = n \end{cases} \tag{2.36} $$

The left fractional derivative represents the past of $f(x)$; on the other hand the right fractional derivative represents the future of $f(x)$. The notions of left and right fractional derivatives can be considered from the physical and mathematical viewpoints.

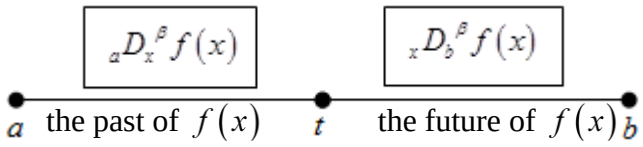

Figure 2.1 Left and right derivatives of a function

The physical "causality principle" means that the present state of the process started at the instant $\tau = a$, the current value of $f(x)$ depends on all its previous (past) states $f(\tau)$ $(a \le \tau < x)$. Since we are not aware of the present state of any process on the results of its development in the future, only left derivatives should be considered for modeling physical problems. This principle resembles the "*Boltzmann superposition principle*" in the theory of viscoelasticity. In superposition principle the stress at time t is the summation of the stress effects of each of the strain pulses in the strain history. The principle of causality is invoked and only the pulses prior to or up to the present time are included. Pulses in the future are considered to have no effect in the present. In the limit as the pulse width $\Delta\tau$ becomes infinitesimal the summation converges to an integral as presented in Equation 2.37 (Lakes, 1999),

$$\sigma(t) = \int_0^t E(t-\tau)\frac{d\varepsilon(\tau)}{d\tau}d\tau \tag{2.37}$$

or

$$\varepsilon(t) = \int_0^t J(t-\tau)\frac{d\sigma(\tau)}{d\tau}d\tau \tag{2.38}$$

2.2 Important Functions Related to the Fractional Calculus Theory

One of the important functions related to fractional calculus other than the gamma function is the Mittag-Leffler function (1903, 1905) which is introduced by G. M. Mittag Leffler (1846-1927). It can be thought of as the "generalized" (natural

expansions) of the exponential function and it is seen on the solution of fractional order differential equations as in similarity that exponential functions are seen on the solution of ordinary differential equations (Hanneken, Vaught, & Achar, 2007). Although exponential functions are easy to grasp (a repeated multiplication of a numerical value; $x^3 = x \cdot x \cdot x$), the generalization of an exponential function may be complicated to understand ($x^{\pi} = ?$).

Mittag-Leffler (M-L) function is a special completely monotonic function which depends on two the parameters α and β as is seen in Equation 2.39 in power series representation and the parameters α and β appear only in the gamma function.

$$E_{\alpha,\beta}(z) = \sum_{k=0}^{\infty} \frac{z^k}{\Gamma(\alpha k + \beta)}, \ (\alpha > 0, \beta > 0) \tag{2.39}$$

When letting α and β to be equal to one, the M-L function turns out to be the simple exponential function, which is a particular case of M-L function. Letting the parameter β equal to one gives the one parameter M-L function, which is,

$$E_{\beta}(z) = \sum_{k=0}^{\infty} \frac{z^k}{\Gamma(\beta k + 1)} = E_{\beta,1}(z) \tag{2.40}$$

Some special M-L functions reduce to (Podlubny I. , 1999),

$$E_{\alpha,\beta}(0) = \frac{1}{\Gamma(\beta)} \tag{2.41}$$

$$E_{1,1}(z) = \exp(z) \tag{2.42}$$

$$E_{1/2,1}(z) = e^{z^2} erfc(-z) \tag{2.43}$$

$$E_{1,2}(z) = \frac{e^z - 1}{z} \tag{2.44}$$

$$E_{0,1}(z) = \frac{1}{1-z} \tag{2.45}$$

The M-L function is a completely monotonic function for $\beta \in (0,1]$, $z > 0$, while it satisfies the Equation 2.46 (Bateman, 1955),

$$(-1)^n \frac{d^n}{dt^n}\left[E_\beta(-z)\right] \geq 0, \;\; n = 1, 2, 3... \tag{2.46}$$

An important characteristic of the M-L function is its asymptotic behavior. When the argument $z \leq 0$, the M-L function decreases monotonically. Further, it is well known that, M-L function interpolates between the stretched exponential (at small values of its argument) and the power law (at large values), while both functions decay quite differently from the exponential function (Magin, et al., 2011).

Asymptotic expansion of the M-L function for especially long relaxation times (Bateman, 1955), (Annin, 1961) is described and used in several papers (Koeller, 1984), (Enelund, Maehler, Runesson, & Joseffson, 1999), (Erdelyi, Magnus, Oberheltinger, & Tricomi, 1954).

$$E_\beta(z) = -\sum_{n=1}^{\infty} \frac{z^{-n}}{\Gamma(1-\beta n)} \tag{2.47}$$

A detailed explanation for the asymptotic expansion of the M-L function and a vast number of references related to the M-L function can be found in (Haubold, Mathai, & Saxena, 2009).

2.3 Numerical Evaluation of Mittag-Leffler Function

Numerical approximations of fractional differential equations can be computationally expensive. An efficient algorithm should be developed in order to reduce the computational cost. A collection of numerical algorithms for the solution of various problems (fractional order integrals, derivatives of Caputo-type, differential equations of Caputo type) can be found in (Diethelm, Ford, Freed, & Luchko, 2005).

Analytical solutions of fractional differential equations are often expressed in terms of M-L functions. Therefore a numerical algorithm is usually required for the evaluation of the M-L function. When considering the M-L function, when the argument z of the M-L function is too large, the series expression of the M-L function converges very slowly. In order to avoid this disadvantage a practical way is suggested by (Hanneken, Vaught, & Achar, 2007).

For the special case of $\beta = 1$,

$$E_{\alpha,1}(-x) = g_{\alpha,1}(-x) + f_{\alpha,1}(-x) \tag{2.48}$$

$$g_{\alpha,1}(-x) = \frac{2}{\alpha}\exp\left[x^{1/\alpha}\cos(\pi/\alpha)\right]\cos\left[x^{1/\alpha}\sin(\pi/\alpha)\right] \tag{2.49}$$

$$f_{\alpha,1}(-x) = \frac{1}{\pi}\int_0^\infty \left\{\frac{\exp\left(-x^{1/\alpha}r\right)r^{\alpha-1}\sin(\pi\alpha)}{r^{2\alpha}+2r^{\alpha}\cos(\pi\alpha)+1}\right\}dr \tag{2.50}$$

A computation algorithm for the two parameter M-L function and its derivative and a fast computation scheme for the one parameter M-L function were developed in the work of Diethelm et al. (2005). The fast computation scheme for evaluating the M-L function is especially efficient for finite element implementations, while Padé approximates were developed in this scheme. The defining series, its asymptotic expansion and a Padé approximate is applied for different intervals. The scheme is presented in Equation 2.51.

$$E_\beta\left(-x^\beta\right) \approx \begin{cases} -\sum_{k=0}^{4}\frac{(-x)^{\beta k}}{\Gamma(1+\beta k)}, & 0 \le x \le 0.1 \\ \frac{a_0 + a_1 x + a_2 x^2}{1 + b_1 x + b_2 x^2 + b_3 x^3}, & 0.1 < x < 15 \\ -\sum_{k=0}^{4}\frac{(x)^{-\beta k}}{\Gamma(1-\beta k)}, & x \ge 15 \end{cases} \tag{2.51}$$

A simple algorithm for evaluating the M-L function with a criterion to select either the exact series or the asymptotic representation is developed by (Welch, Rorrer, Duren, & JR., 1999). Fractional derivatives of some simple functions can be found in Appendix A.

2.4 Applications of Fractional Calculus in Science and Engineering

In every mathematical investigation a question arises *whether the mathematical result formulated could be applied in the real world*.

Abel, in 1823 was the first to apply fractional calculus to a solution of the "tautochrone" problem (to find the shape of a frictionless wire lying in a vertical plane such that the time required for a bead placed on the wire to slide to the lowest point of the wire (under the action of gravity) is the same regardless of where the bead is first placed (Ross, 1977)) and showed that the solution is a "cycloid". As also pointed out in the book of Samko et, al. (1993) Abel not only solved the "tautochrone" problem but also gave a general solution for the integral equation,

$$k(x)=\int_a^x \frac{f(t)}{(x-t)^{\alpha}}dt,\ \ x>a,\ \ 0<\alpha<1 \tag{2.52}$$

He multiplied the Equation 2.52 with $\frac{1}{\Gamma(0.5)}$ to obtain the half integration of function $f(x)$,

$$\frac{k}{\Gamma(0.5)}=\frac{1}{\Gamma(0.5)}\int_0^x (x-t)^{-1/2}\ f(t)dt={}_0D_x^{-1/2}f(x) \tag{2.53}$$

On the other hand Liouville was one of the first persons who attempted to solve differential equations by means of fractional operations.

Fractional calculus is rarely applied in engineering and science up to now mainly because it is more complicated than the ordinary calculus and there are

contradictions among the mathematicians and mathematical axioms they presented. The absence of a unique definition for fractional integration and differentiation caused many difficulties which slowed the acceptance and application of fractional calculus in science and engineering. On the contrary, it will become apparent that just as the fractional exponents such as the square root find their way into numerous equations and applications, the integrations and derivatives of "arbitrary" order can find practical use in many modern applications.

The fields that fractional calculus has found attention can be listed as,

- Diffusion processes
- Electrical science (signal processing)
- Electrochemistry
- Electromagnetic theory
- Probability
- Rheology (viscoelasticity)
- Material creep
- Dynamics
- Control theory
- Fluid mechanics
- Mathematical biology
- Economics
- Finance
- Earthquake sciences

Although the domain of applications and potential applications of fractional calculus are very broad, with the exception of rheology (and in particular viscoelasticity) the

depth of research and application serves to be quite limited in other fields. Viscoelasticity seems to be the field of the most extensive applications of fractional differential and integral operators (Podlubny I. , 1999).

2.5 Fractional Calculus in the Theory of Viscoelasticity

The early history of fractional calculus in the theory of viscoelasticity begins with Nutting (1921), where at this time it has been shown that the stress relaxation phenomenon could be described by fractional powers of time which contradicts with the traditional approach that stress relaxation is best described by decaying exponentials. Scott-Blair (1944) and Scott-Blair, et.al (1944) used fractional calculus approach to model these early observations of Nutting. Scott-Blair in his papers, argued the importance of studying the rheological properties of non-traditional materials such as rubber and plastics, as they differ in rheological sense considerably from Newtonian or Hookean behavior. In 1939, Scott-Blair and Coppen suggested that the "firmness" or elasticity of a material which are neither true fluids nor perfectly elastic solids (therefore an intermediate material) can be described by an equation $S = \psi \sigma t^{-k}$ where ψ is a measure of "firmness" and k becomes zero for an elastic solid and unity for a Newtonian fluid. In 1944, Scott-Blair actually, obtained a fractional order differential expression for these "intermediate" materials, such that,

$$\chi = S \Big/ \frac{\partial^m \sigma}{\partial t^m} \tag{2.54}$$

He admitted that, these types of functions can be solved in terms of the gamma function; however, no one has attempted to solve these equations up until that year.

He also adds "*I gave up the work eventually, because I could not find a definition of a fractional differential that would satisfy the mathematicians.*" (Mainardi, 2010)

The M-L function is first appeared as a relaxation function in the paper of Gross (1947). However Gross did not connect the M-L relaxation kernel with the fractional calculus approach.

In 1936, Gemant has shown that time derivatives of fractional order could model the viscoelastic behavior. Gemant was the first to propose a viscoelastic model of fractional order. In his model, the first order ordinary derivative of stress of "Maxwell fluid model" has been replaced by a semi-derivative. To clarify the problem definite deviation between the quantitative experimental results obtained from elasto-viscous (now termed as viscoelastic) bodies and the theoretical Maxwell equation. He applied semi-differentiation to the Maxwell equation of viscoelastic bodies,

$$S = F/\eta + 1/(\eta E)^{1/2}\left(d^{1/2}F/dt^{1/2}\right) \tag{2.55}$$

where S is the strain, F is the stress, η is the viscosity, E is the shear modulus of elasticity and t is time.

Further Gemant, gave a physical justification to the semi-derivative differential equation. Gemant has also shown that the stiffness and damping properties of viscoelastic materials are well represented by fractional powers of frequency.

$$V = \left(1 - i(\omega\tau)^{0.5} / (1 + \omega\tau)\right) \tag{2.56}$$

He also discussed the physical meaning of half-derivative and emphasized that the fractional derivative in a differential equation hardly controls the behavior of a real medium.

Later in 1980, Rabotnov in his book translated the early papers of Gerasimov (1948) and Rabotnov (1948) which was originally written in Russian. Gerasimov used explicitly fractional order derivative written in the form of Caputo derivative to define his viscoelastic model, whereas Rabotnov preferred to use Volterra integral operators with weakly singular kernels which can be interpreted in terms of fractional integrals and derivatives (Mainardi, 2010). In his book, Rabotnov emphasizes that the term "*hereditary elasticity*" which is usually replaced by the word "*viscoelasticity*". In addition the author argues that, the phenomenon of

heredity should not be considered as a combination of Hookean elasticity and Newtonian viscosity, rather it should be taken as a primary element of itself. Therefore the author rejects the model representations in rheology. In his book fractional exponential operators are defined in terms of Abel operator $\left(I_{\alpha}^{*}\right)$ which fulfills the "fading memory principle" and whose kernel is,

$$I_{\alpha} = \frac{t^{\alpha}}{\Gamma\left(1+\alpha\right)} \tag{2.57}$$

In addition, the relation between the fractional exponential operator and the Mittag-Leffler function is provided. Friedrich (1991), states that the asymptotic expansion Rabotnov has provided, is incorrect.

Koeller, in 1984 generalized some of the concepts of Rabotnov's theory as well as demonstrated the connection of fractional calculus to the theory of linear viscoelasticity. It has been shown that Rabotnov's theory of hereditary solid mechanics is equivalent to requiring that the stress in the dashpot is proportional to fractional derivative of strain in dashpot. In general Rabotnov's notation is used and fractional calculus is related to the theory of Abel's integral equation. The fractional integral is related to the Abel operator is,

$$D^{-\beta} f\left(t\right) = I_{\alpha}^{*} f\left(t\right) \tag{2.58}$$

and from the equation above,

$$D^{\beta} I_{\alpha}^{*} f\left(t\right) = f\left(t\right) \tag{2.59}$$

The term "spring-pot" has arisen for the fractional element and the use of springs and dashpots for viscoelastic models is generalized to include fractional derivatives and integrals. The dashpot element in the ordinary Maxwell and Kelvin-Voigt elements is replaced by this spring-pot element. The creep and relaxation functions for the fractional Maxwell, Kelvin-Voigt and three-element models are derived by employing the Rabotnov's theory of Hereditary Solid Mechanics. Creep and

relaxation functions in terms of the M-L function which depends on the fractional derivative parameter β are obtained. It is also shown that when the "*memory parameter β "* varies from zero to one, the fractional order constitutive equation represents a transition from elastic solid behavior to Newtonian viscous fluid behavior. Unless the β parameter is equal to unity, it has been stated that the creep and relaxation times do not have any physical meaning.

Actually almost 10 years before, Caputo and Mainardi (1971a, 1971b) also obtained the creep and relaxation functions by the Laplace transform method for a fractional differential equation of the form $\left(D^{\beta}+\frac{1}{t_1^{\beta}}\right)\sigma(t)=E_0\left(D^{\beta}+\frac{1}{\tau_1^{\beta}}\right)\varepsilon(t)$. The fractional order viscoelastic solid, which is a spring in parallel with Maxwell element, is represented in (Caputo & Mainardi, 1971b). The material model is introduced and has the constitutive relation,

$$\left(1+\tau^{\beta}D_*^{\beta}\right)\sigma(t)=E\left(1+\rho^{\beta}D_*^{\beta}\right)\varepsilon(t),\ \ \sigma_0=E\left(\frac{\rho}{\tau}\right)^{\beta}\varepsilon_0 \tag{2.60}$$

It has been suggested that the derivatives of fractional order of Caputo type (Caputo, 1967) can be successfully used to model the dissipation in seismology and in metallurgy. Meanwhile, Rabotnov in 1974 in his CISM Lecture Notes pointed out that (Mainardi, 2010),

"That's why it was of great interest for me to know the paper of Caputo and Mainardi from the University of Bologna published in 1971. These authors have obtained similar results independently without knowing the corresponding Russian publications…"

In 1991, Friedrich formulated a four parameter (fractional order derivatives are different for stress and strain) Maxwell model and the relaxation and retardation functions are derived analytically by employing the Laplace transformation methods. The relaxation function is defined in terms of a power law term and the M-L function and the retardation function is defined in terms of solely the power law term. In

addition, the asymptotic behavior of the relaxation function for short and long times is investigated. It has been shown that the generalized M-L function is not of fractional exponential type but of a power-law type. For thermodynamical compatibility of the fractional Maxwell model, the restrictions should be $\beta \geq \alpha > 0,\ \lambda > 0$ which are less restrictive compared to the work of (Bagley & Torvik, 1986).

In the same year, T. F. Nonnenmacher (1991) indicated a close relation between the power law representation of viscoelastic behavior and fractional derivatives. The similarities and the differences between the power law approach and the fractional calculus approach in viscoelasticity is discussed in the paper (Bagley R. L., 1989). It is demonstrated that the two models have mathematically similar relaxation spectra. This similarity produces an asymptotic equivalence of the models at long relaxation times.

In the same year, Bagley and Torvik (1984) gave a physical justification to the description of constitutive equations of fractional order through describing certain motions of a Newtonian fluid for particular geometries. A fractional derivative, where the order of differentiation is ½ has been shown to describe the behavior of a real, physical system (rigid plate bounded by a Newtonian fluid). A year before, Bagley and Torvik (1983) has also provided physical justification to the fractional calculus in viscoelasticity theory, such that, fractional derivatives of order ½ appears in stress-strain relations of polymer solutions and polymer solids with no cross-linking which is adapted from Rouse's theory (Rouse, 1953) (Equation 2.61).

$$\sigma(t) = \mu_s D\varepsilon(t) + \left[\frac{3}{2}(\mu_0 - \mu_s)nkT\right]^{1/2} D^{1/2}\left[\varepsilon(t)\right] \tag{2.61}$$

Fractional order models are consistent with the predictions of the molecular theory of polymer solids and provide a link between accepted microscopic theories of ideal viscoelastic media. Bagley in 1979 (under supervision of Prof. Torvik) offered a general three dimensional constitutive equation with fractional derivatives for homogeneous and isotropic materials. Later In 1986, again Bagley and Torvik

concluded that, the fractional orders of stress and strain in constitutive equations must be the same in order to ensure the second law of thermodynamics which satisfies the non-negative rate of mechanical energy dissipation and internal work whenever cyclic loading histories are imposed on a material. Also the parameters of the model should be restricted to the conditions $\tau > 0,\ E_0 > E_\infty > 0,\ \beta \in (0,1)$ where τ is the time constant, E_0 is the instantaneous (glassy) modulus, E_∞ is the long term (rubbery) modulus and β is the order of time derivative.

A three element, four parameter (previously five parameters) fractional viscoelastic model has been studied for the requirements of thermodynamics. The constraint $\alpha = \beta$ predicts positive mechanical energy dissipation for all frequencies. The five parameter model is fitted to nitrile rubber and other 130 different materials. The five parameter model reduces to the four-parameter model eventually (Equations 2.62 & 2.63).

$$\sigma(t) + bD^{\beta}\left[\sigma(t)\right] = E_0\epsilon(t) + E_1 D^{\alpha}\left[\epsilon(t)\right] \text{ : Five-parameter model} \tag{2.62}$$

$$\sigma(t) + bD^{\alpha}\left[\sigma(t)\right] = E_0\epsilon(t) + E_1 D^{\alpha}\left[\epsilon(t)\right] \text{ : Four-parameter model} \tag{2.63}$$

They also found out that the five-parameter model presented in Equation 2.62 is consistent with the thermodynamic principles (thermodynamically admissible) and robust in describing materials exhibiting short relaxation time phenomena and the constraints of the parameters predict realistic relaxation and creep responses.

Lion, in 1997 has also considered the thermodynamic admissibility of the fractional element and the fractional Zener model by deriving the free energy functionals and concluded that the Clausius Duhem inequality is satisfied for arbitrary deformation histories in the uniaxial and three dimensional cases for the fractional Zener model.

Drozdov in 1997 was the first to construct a fractional order constitutive model suitable for nonlinear mechanics of continua with finite strains in 3-D. The 1-D

linear fractional viscoelastic models (Kelvin-Voigt and the Maxwell model), is extended to finite viscoelastic models in 3-D.

2.5.1 Finite Element Formulation of Fractional Constitutive Equations

In 1987, Padovan developed numerical algorithms for the Grünwald-Riemann-Liuoville fractional differentiation formulation to reduce the mathematical complexity of fractional operators for finite element simulations of models involving viscoelastic materials.

From 1995 to 2005, Mikael Enelund and Klas Adolfsson published several papers related to the fractional viscoelastic models for finite element simulations.

In 1999, in the paper (Enelund, Maehler, Runesson, & Joseffson, 1999), the three dimensional, anisotropic, standard linear viscoelastic solid (N-Maxwell chains coupled in parallel) with fractional order internal variables is presented and a numerical algorithm for fractional differentiation and integration of the constitutive response is developed. Padovan (1987) has also established a numerical algorithm for solving fractional constitutive equations but without employing internal variables. Only the history of the internal variables needs to be stored in this formulation. The greatest effort in this paper is the implementation of the algorithm and the viscoelastic model into the commercial finite element software Abaqus. Asymptotic expansion of the Mittag-Leffler function is employed when displaying the stress relaxation for larger times (Bateman, 1955).

In 2003, Adolfsson and Enelund developed the numerical algorithm and the constitutive response for the nonlinear domain by splitting the deformation gradient into isochoric and volumetric parts. The generalization to large deformations is based on the approach by Simo and Hughes (1989). Numerical algorithm involves approximating the fractional differentiation by using convolution quadrature and the integration of the constitutive response is based on the generalized midpoint rule. The elastic part is modeled using a modified Neo-Hookean model and the viscoelastic part is two Maxwell chains, with one of the relaxation time constant being infinite. The numerical formulation and the constitutive response are

implemented into a finite element code and the analytical and numerical results are compared for the fractional order of 0.5 and shown that they agree well. It has been concluded that a classical model with a large number of internal variables can be reduced to a fractional order model with a single internal variable (Adolfsson, Enelund, & Olsson, 2005). In the thesis of Adolfsson (2003) it has been found out that for the fractional order of $\beta = 0.67$, 10000 Maxwell Model chain, (MM) elements are necessary to predict the normalized relaxation function with less than 1% error and 100 MM elements to predict the normalized relaxation with error being around 5%. It can be concluded that fractional order Voigt model is the correct model for the given material.

A three dimensional constitutive law is described by Wei and Shimizu, (2001) and the finite element formulation is studied. The numerical algorithm in combination with the well-known Newmark algorithm, for the solution of fractional integration is adopted to formulate the FE analysis. Schmidt and Gaul, in 2002, implemented a three-dimensional fractional constitutive equation by employing Grünwald definition of fractional derivative, into a finite element code and compared it with an integer order derivative constitutive equation by parameter identification in the time domain and demonstrated the better performance of fractional constitutive equations in curve-fitting the model to experimental data.

2.5.2 Fractional Order Constitutive Equations Used for Modeling Soft Tissues

In 1994, Suki et al., employed fractional order procedures to describe the pressure/volume response of the whole lung. Stress relaxation in lung tissue is well-defined by the power law $t^{-\beta}$ and fractional time derivatives in the constitutive equation lead naturally to power law relaxation function. The description of observed viscoelastic behavior is superior for fractional order models compared to integer order models while fractional elements naturally contain a continuous distribution of time constants. Fung (1993) demonstrated that, for a distribution of time constants (range of frequency), the observed phenomena for the tissues is satisfied that the hysteresis of the stress-strain curve is independent of the frequency.

Power law behavior is also observed for muscle cells. Djordjevic et al., (2003) employed fractional calculus methods to define the smooth muscle cell rheological behavior and showed that fractional calculus offers a unifying mathematical approach to various problems in bioengineering.

In 2006, Kohandel et al., and Davis et al., compared the constitutive equation of brain in separate papers. The former paper employs an integer order constitutive equation (hyper-elastic Ogden model for the elastic part and Prony series for the viscoelastic part) and in the second part of the study fractional order Zener model is employed to define the material behavior of the brain parenchyma. The two papers are not cross correlated and not compared. The investigations are analyzed separately. In part 1 of the study, the integer order model is fitted to experimental data and also the finite element simulations have been performed. In the second part, where the four parameter fractional order Zener model is employed, there is not any finite element simulation of the experiments and the four parameter Zener model is compared to the non-fractional Zener model and four parameter integer order Burgers model. It has been shown that the four parameter fractional order Zener model fits better to the experimental data (creep and relaxation) than the three parameter integer order Zener model and the four parameter Burgers model.

In 2006, Craiem and Armentano analyzed the arterial wall mechanics in-vivo by using a four parameter fractional order material model. In 2008, Craiem et al. investigated the arterial wall mechanics by applying the Fung's quasi-linear viscoelasticity (QLV) theory and a three parameter fractional order relaxation function based on modified Voigt model is offered. An interesting result is, the fractional order is found to be in the range $[0.1, 0.3]$ similar to the other results as well (Doehring, Freed, Carew, & Vesely, 2005), (Suki, Barabasi, & Lutchen, 1994), (Craiem D. O., Rojo, Atienza, Guinea, & Armentano, 2008). These values support the idea of fractal-like structures (Magin R. , 2004) and the model shows viscoelastic behavior. In those researches the main idea in using fractional models is that the response includes a combination of power law function represented by M-L summation and the aortic tissue relaxation is well represented by power law relations

naturally. In 2010, Craiem and Magin analyzed the red blood cell mechanical behavior by fractional order rheological models.

In 2002 NASA published a report for the constitutive development of fractional order viscoelasticity using the fractional calculus (Freed, Diethelm, & Luchko, 2002). This first annual report is a three year project "Advanced Soft Tissue Modeling for Telemedicine and Surgical Simulation" and the objective of the report is the extension of 1-D fractional viscoelastic models to their 3-D equivalents and developing numerical algorithms for the solution. Although it has been stated that there will be a second annual report for the representation of material models for soft tissues, the second annual report is either not published or restricted to the academia.

In 2006, NASA had a need to understand how much force is transmitted to the load-bearing bones of the body during exercise to reduce the bone lose in astronauts during space mission. This requires material models for the soft tissue constituents of the heel-pad. Freed and Diethelm (2006) introduced a K-BKZ viscoelastic model (Bernstein, A, & Zapas, 1963) which employs an elastic strain energy function. Four elastic and five viscoelastic kernels (generalized Maxwell model (GMM), the stretched exponential of Kohlrausch-William-Watts (KWW), QLV, FOV, regularized fractional derivative model) are introduced as the candidate models. The best model is chosen to be the power-law for the elastic part of the response and a regularized fractional derivative for the viscoelastic kernel. A regularization parameter is applied to push the singularity outside the interval of integration therefore a fractional derivative is regularized. In 2007, Freed and Diethelm extended the elastic law of Fung, which describes the nonlinear stress-strain behavior of soft biological tissues, to a viscoelastic material model which includes fractional derivatives of Caputo type. Then a 3-D constitutive model is developed from this 1-D material model of continuation of the model of Caputo and Mainardi (1971a, b) where finite deformations and/or rotations are permitted. Polar configuration is applied in the formulation of the model. The fractional differential equation for material model formulation is

$$\left(1+\tau^{\alpha}D_{*}^{\alpha}\right)s(t)=\frac{E}{\beta}\left(\exp\left(\beta\varepsilon(t)-1\right)\right)+\rho^{\alpha}\left(E+\beta s(t)\right)D_{*}^{\alpha}\varepsilon(t) \tag{2.64}$$

where the parameters are,

E: rubbery modulus

$E(\rho/\tau)^{\alpha}$: glassy modulus are strictly greater than zero.

$s(t)$ is the dynamic stress response and $\varepsilon(t)$ is the strain function.

When the strain is taken as $\varepsilon(t)=\dfrac{t^{\alpha}}{\rho^{\alpha}\beta\Gamma(1+\alpha)}$ a special case occurs while the solution of the differential equation yields $\varepsilon(t)=\dfrac{1}{\beta}\ln\left(\dfrac{\beta\tau^{\alpha}}{E}D_{*}^{\alpha}s(t)\right)$ which indicates that strain can be interpreted as a function of stress and its history. Tension, stress relaxation and cyclic tests are simulated with this model and it has been shown that the model compares very nicely with the experimental data.

Wilkie et. al, (2011) formulated a hyperelastic, fractional viscoelastic model to describe the infant brain tissue. Brain tissue is represented by a Kelvin-Voigt viscoelastic solid and a hyperelastic spring is coupled in parallel to a fractional viscoelastic dashpot. By employing fractional derivatives the material deformation history is incorporated into the stress-strain relation. Further Chang et. al, (2011) analyzed the impact response of human frontal bone, where the soft tissues surrounding the human frontal bone are modeled as a fractional viscoelastic solid model. Grahovac and Zigic, in 2010 employed fractional derivatives when modeling the hamstring muscle group in ramp-and-hold stress relaxation. It has been shown that, the model fits well to the experimental data with a restricted number of experimental points.

2.5.3 Hierarchical Analogies to the Fractional Element

In 1995, Schiessel et. al., presented that the fractional constitutive equations are physically meaningful. Starting from the Boltzmann (Ludwig Boltzmann 1844-1906) superposition integral $\left(\sigma(t)=\int_{-\infty}^{t}G(t-\tau)\dfrac{d\varepsilon(\tau)}{d\tau}d\tau\right)$ and Weyl expression of a fractional integral and employing a relaxation modulus such as

$G(t) = \frac{E}{\Gamma(1-\beta)}\left(\frac{t}{\tau}\right)^{-\beta}$, the constitutive relation for the fractional element has been derived $\left(\sigma(t) = E\tau^{\beta}\frac{d^{\beta}\varepsilon(t)}{dt^{\beta}}\right)$ and symbolized by a triangle.

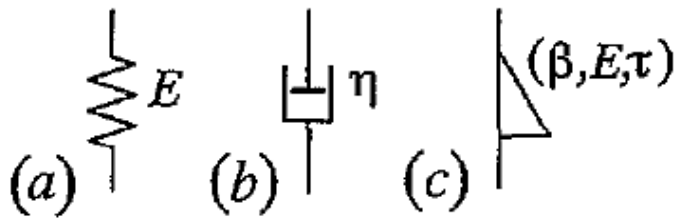

Figure 2.2 a) Elastic, b) Viscous, c) Fractional element
(Adopted from (Schiessel H. , Metzler, Blumen, & Nonnenmacher, 1995))

The question here arises is that, "What *combination of springs and dashpots give rise to a fractional element?*"

Recent studies demonstrated that the fractional relation can be realized physically through "ladder", "tree" or "fractal network" structures. For the generalizations of the simplest viscoelastic models (Maxwell, Kelvin-Voigt, Zener and Poynting-Thomson model) both of the elements (spring and dashpot) are replaced by the fractional element by setting $0 \le \beta < \alpha \le 1$. Actually, there are three possibilities in constructing a fractional rheological model, either combining more than one fractional element, or using only one fractional element since it contains the properties of both the Hookean (spring) and Newtonian (viscous) elements, or combining fractional and integer order elements together. In the work of Schiessel et. al., (1995) all four basic classical elements are generalized by replacing all the elements with the fractional element (Figures 2.3-2.6).

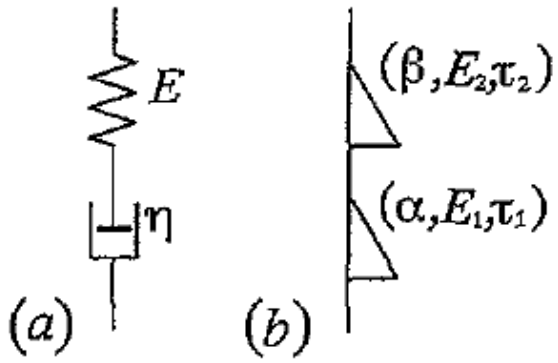

Figure 2.3 a) Maxwell model, b) Its fractional generalization
(Adopted from (Schiessel H. , Metzler, Blumen, & Nonnenmacher, 1995))

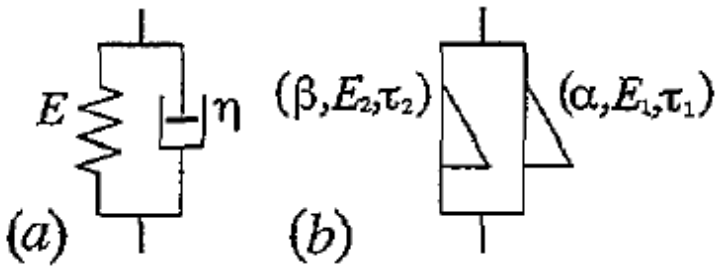

Figure 2.4 a) Kelvin-Voigt model b) Its fractional generalization
(Adopted from (Schiessel H. , Metzler, Blumen, & Nonnenmacher, 1995))

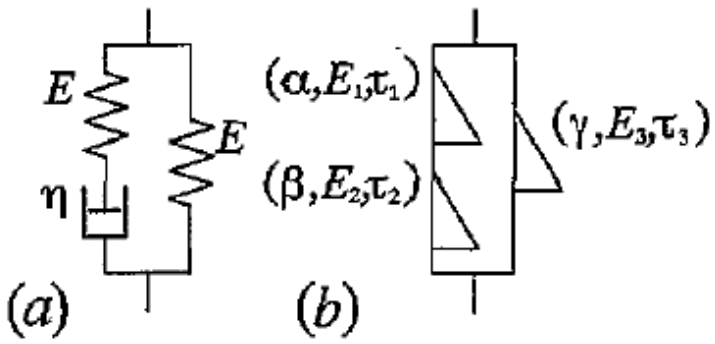

Figure 2.5 a) Zener model b) Its fractional generalization
(Adopted from (Schiessel H. , Metzler, Blumen, & Nonnenmacher, 1995)

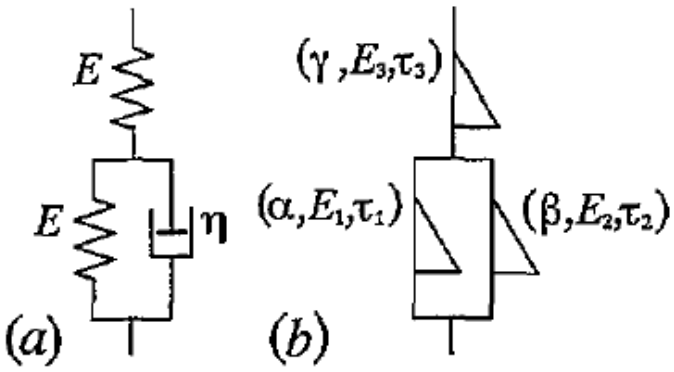

Figure 2.6 a) Poynting-Thomson model b) Its fractional generalization
(Adopted from (Schiessel H. , Metzler, Blumen, & Nonnenmacher, 1995))

The creep and relaxation functions for those generalized models are defined in terms of Fox H-functions. A multi element model, which consists of an infinite number of classical springs and dashpots ordered hierarchically in a self-similar structure, is suggested also by (Schiessel H. , Metzler, Blumen, & Nonnenmacher, 1995). Those types of models are called a "*fractance*" (Podlubny I. , 1999) (Figure 2.7).

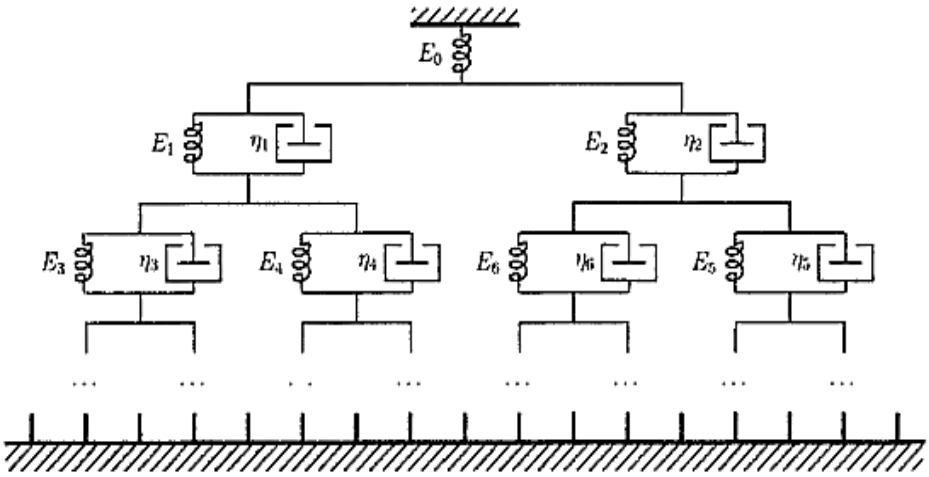

Figure 2.7 Fractance-type fractional model
(Adopted from (Podlubny I. , 1999) originally in (Heymans & Bauwens, 1994))

In the work of Schiessel and Blumen (1993) it is shown that fractional order derivatives of stress and strain have hierarchical (mechanical) analogues which consist of springs and dashpots. A mechanical arrangement for generalized dashpot element (fractional element) and generalized (fractional) Maxwell element (serial arrangement of two hierarchical systems) are presented and called the "*ladder model*" representation. Therefore it can be concluded that, a single spring-pot can be decomposed into an infinite spring-dashpot ladder (Magin R. L., 2006). The connection between observed fractional order viscoelastic behavior is replicated across the cellular to bulk tissue scales (Craiem & Magin, 2010).

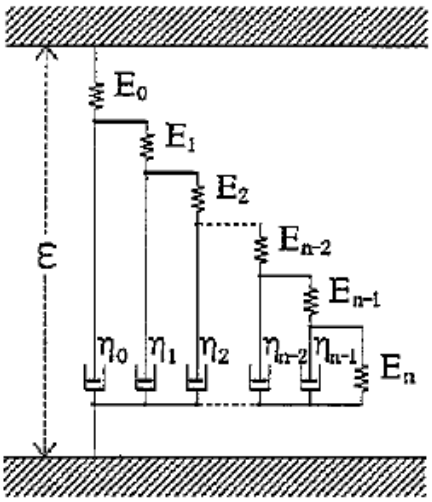

Figure 2.8 Infinite Spring Dashpot Ladder
(Adopted from (Schiessel and Blumen, 1993))

After a sudden strain jump, only the first spring E_0 is deformed. The stress set up in the spring will gradually relax and fade away as the piston of the dashpot η_0 overcomes the resistance of the damping fluid. Simultaneously, the spring in parallel E_1 is deformed. In this way the deformation moves continuously into the ladder. When the fractional order gets higher, the deformation penetrates the ladder faster (Figures 2.8-2.9). A mechanical ladder which consists of infinite number of springs and dashpots whose stress strain relation obeys the gel equation with order ½ is also

offered by Schiessel and Blumen, (1995). A Serpinski- like network is shown in Figure 2.10. This network structure is seen to provide a link between fractal models of materials and the underlying fractional order constitutive equations describing the stress-strain behavior (Magin R. , 2004) (Figure 2.10).

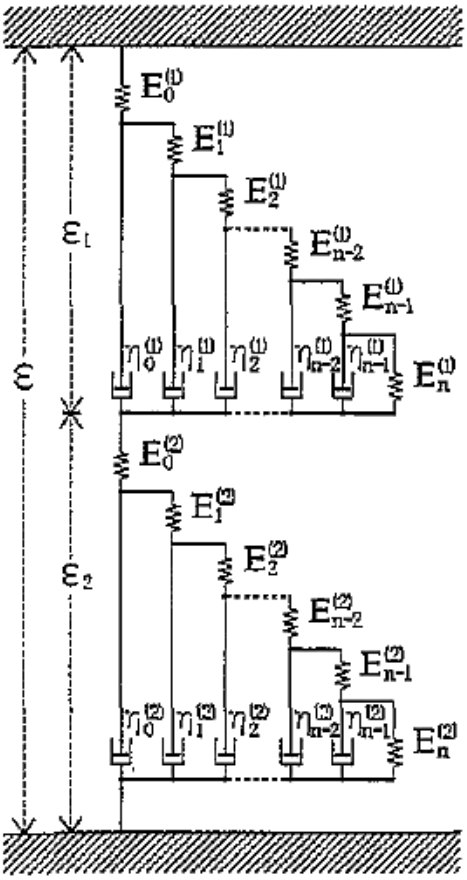

Figure 2.9 Generalized Maxwell Element with Infinite Ladder
(Adopted from Schiessel & Blumen (1993))

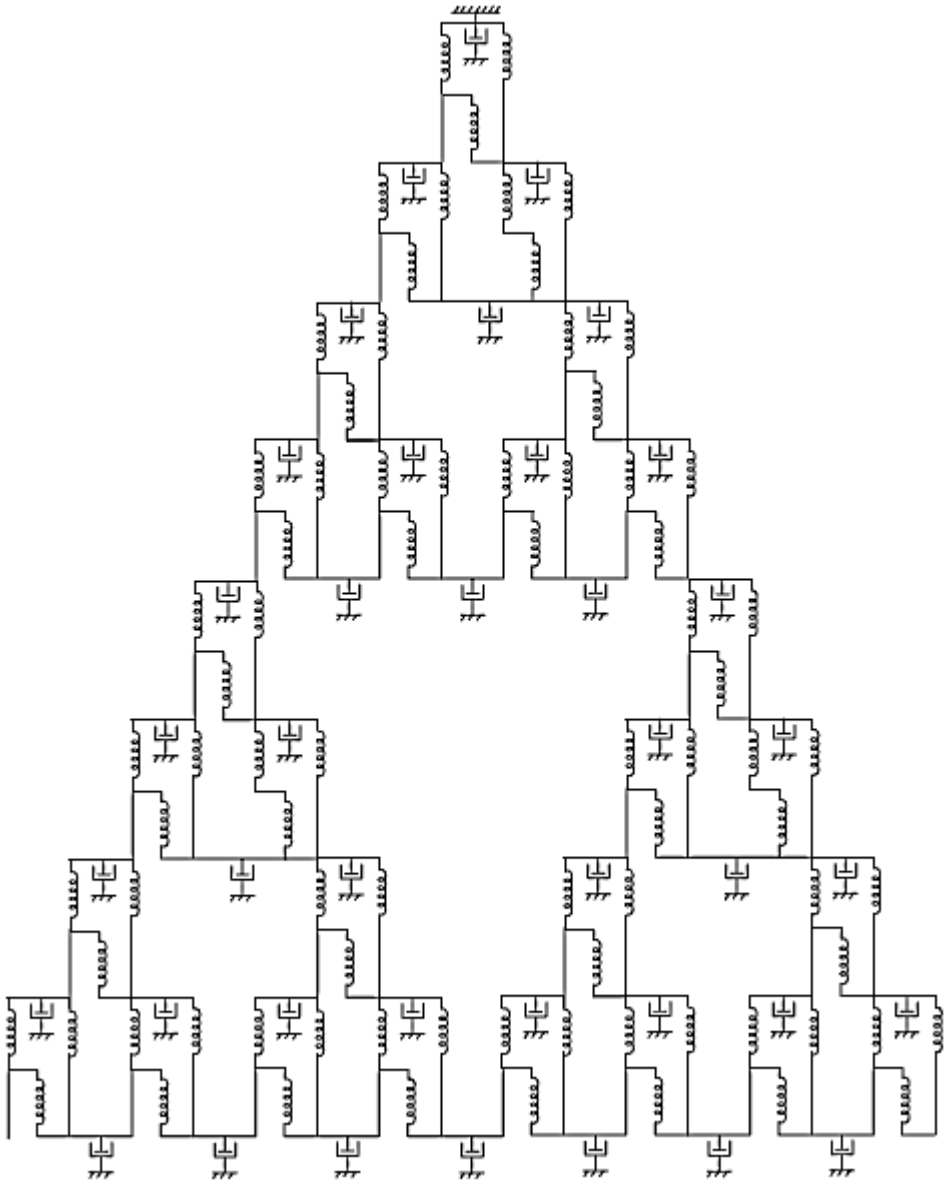

Figure 2.10 Sierpinski-like network of springs and dashpots
(Adopted from (Schiessel and Blumen, 1995))

Another fractional ladder mechanical model is suggested for soft tissues to describe the power law behavior observed in soft tissues where the ultrasonic attenuation coefficient in mammalian tissue is approximated by a frequency dependent power law (Kelly & McGough, 2009). The viscoelastic and self-similar properties of the tissue is captured by this infinite-ladder model. The ladder model can be considered as a fundamental mechanical component (a spring-pot). It has been hypothesized that the order of the fractional derivative is a function of the fractal dimension of the

underlying geometry. Soft tissue consists of hierarchical arrangements of elastic and fluid-like components. Self-similarity pattern is observed in soft tissues where every soft tissue is composed of elastic substrates in a fluid medium under different spatial scales (Figure 2.11). This behavior forms the basis for the fractal structure. Based on the structure shown below, the viscoelastic, self-similar or fractal properties of the tissue are seen clearly which motivates a hierarchical mathematical model. Further research is the relationship between fractional calculus and fractals, where a fractal is defined as a rough or fragmented geometric shape and when split into parts it is a copy of the whole-as an example “lung tissue”. Microscopically observing the lung tissue reveals the fact that, the smaller we observe the tissue, self-similarity exists meaning the tissue repeats itself under several levels of magnification.

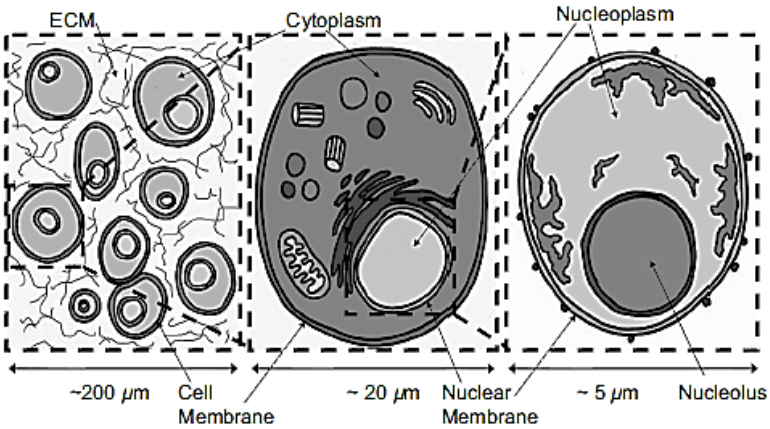

Figure 2.11 The extra-cellular matrix at successive spatial scales
(Adopted from (Kelly & McGough, 2009)

The biological structures vary at successive spatial scales; however the essential features are the same, fluid media with elastic bodies. This self-similar pattern forms the basis for the fractal structure. The springs of the model correspond to elastic structures of the tissue and the dampers of the model correspond to the inter- and intra-cellular fluids such as cytoplasm.

Fractal type tree model is suggested in Doehring, Freed, Carew, and Vesely, (2005) for fractional order quasi linear models. Fung's quasi-linear viscoelasticity model involves continuous spectrum reduced relaxation function, which implies infinite series of Zener elements connected in series. Integration of the responses of the Zener model produces a wide and flat frequency response (Figure 2.12). The fractal tree model is a *hierarchical* arrangement of Zener bodies, where the depth and branching of the tree depends on the fractional order (Figure 2.13). The corresponding hysteresis diagram shows an infinite number of bell shaped curves, which add up to a continuous curve of nearly constant height over a very wide range of frequencies (Butchal & Kaiser, 1951). In this model (Figure 2.12 - top row), the springs are nonlinear and each Zener unit contributes to a small bell-shaped curve. The material response obtained from the continuous relaxation spectrum converges to the response of the simplest fractional order model. This result is proved both numerically and analytically by (Adolfsson, Enelund, & Olsson, 2005).

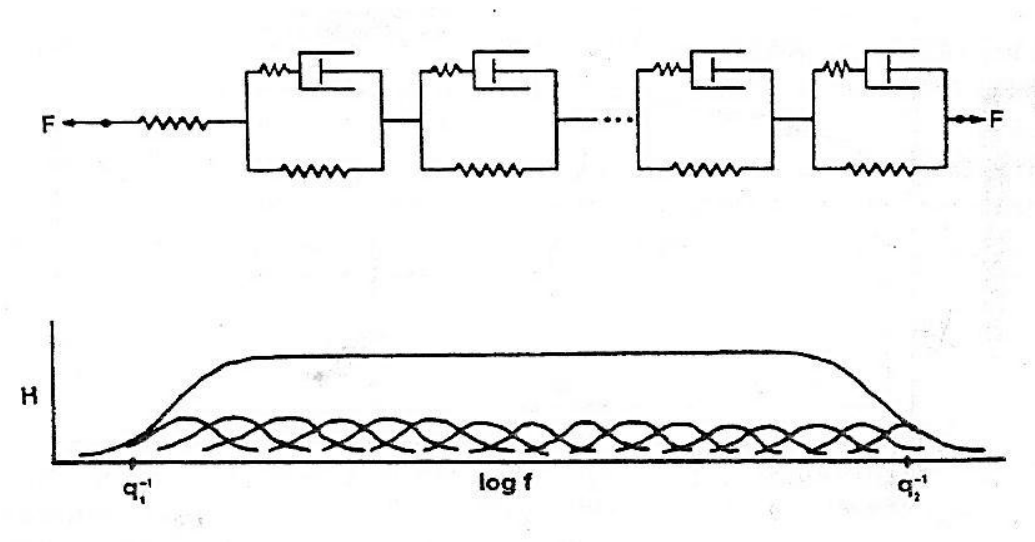

Figure 2.12 Continuous relaxation spectrum, hysteresis vs. logarithm of frequency (Adopted from (Maurel, Wu, Thalmann, & Thalmann, 1998) reprinted from (Fung, 1993))

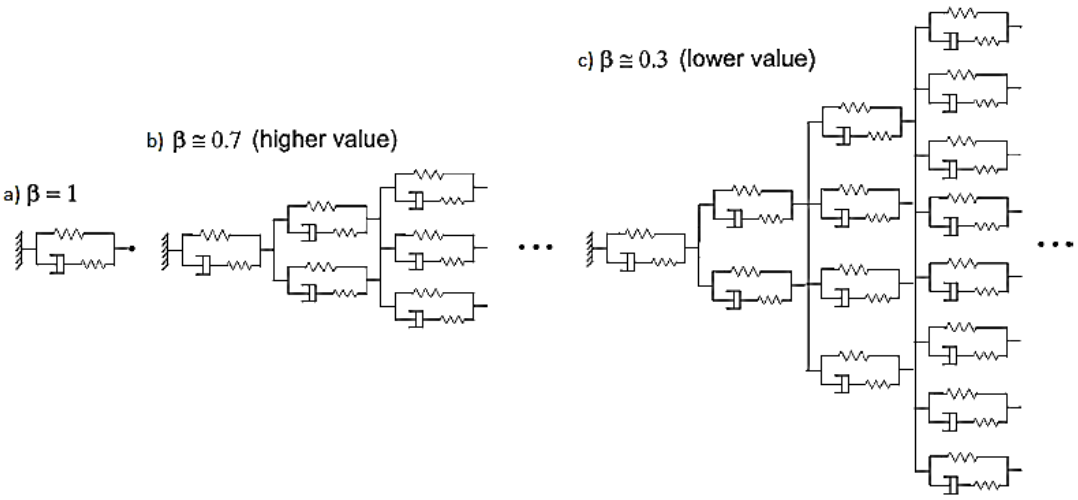

Figure 2.13 Fractal type tree model a) $\beta = 1$, b) $\beta = 0.7$ c) $\beta = 0.3$
(Adopted from (Doehring, Freed, Carew, & Vesely, 2005))

2.6 Soft Tissue Behavior

Although each biological soft tissue exhibits unique behavior, general characteristic behaviors are common to many tissues. Soft tissues exhibit a nonlinear, inelastic and anisotropic behavior over finite strains. Nonlinear stress-strain relationship, a hysteresis loop in cyclic loading, stress relaxation at constant strain, creep at constant stress, and preconditioning in repeated cycles are common to connective tissues such as ligaments, skin and mesentery and also to blood vessels and muscles (Fung, 1993), (Sun & Sacks, 2005).

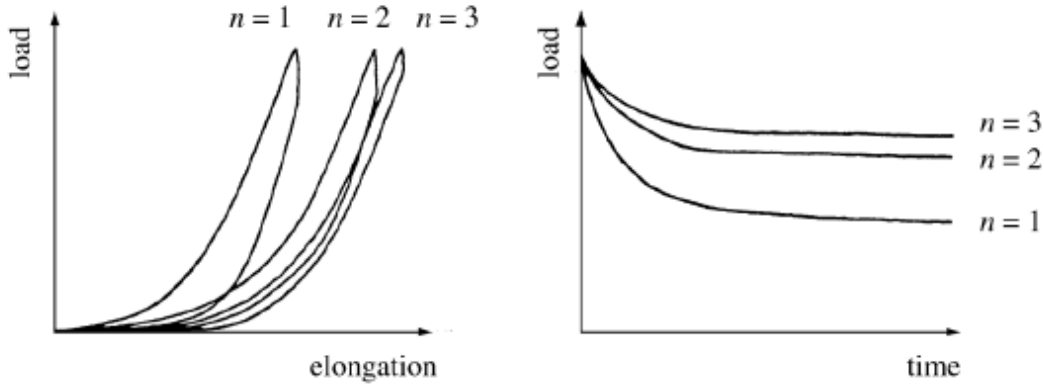

Figure 2.14 Preconditioning of tissue (n represents the number of cycles)
(Adopted from (Fung, 1993))

When loading and unloading of the tissue repeats itself, then a curve shift is present as can be seen in Figure 2.14 at the left. When the curve shift is no further seen, the tissue shows a steady, repeatable behavior and is said to be "*preconditioned*". During preconditioning period, a curve shift is also present for the relaxation curve shown in Figure 2.14 at the right. This behavior is dependent on the tissue morphology and structure, while its microstructure changes under force and/or deformation.

Earlier in 1970s, soft tissues were assumed as linear elastic materials to predict their elastic modulus for an assumed value of Poisson's ratio. Such approaches are also used to calculate the modulus of tissues at a particular time during their time-dependent response. However the tissue is known to behave highly non-linear.

Finite deformation nonlinear tissue behavior is usually modeled by the strain energy function of the form

$$W = \sum_{i+j=1}^{N} C_{ij} \left(I_1 - 3\right)^i \left(I_2 - 3\right)^j \tag{2.65}$$

where I_1 & I_2 are the first and second principal strain invariants and $i, j = 1, 2, 3$. Miller and Chinzei, (1997) employed this formulation in the form of convolution

integral to model the *in-vitro*, uniaxial unconfined compression of swain brain tissue and the corresponding material constants are determined.

2.7 Soft Tissue Indentation Experiments

Identification of mechanical properties of soft biological tissues is an active research area while it can be utilized in surgical planning and better treatment procedures by simulating the surgical operations on computer platform (Miller K. , Chinzei, Orssengo, & Bednarz, 2000). The mechanical characterization of the soft tissue behavior can further be utilized in the education of clinical people, diagnosing the clinical pathologies, better medical device design and understanding of mechanical tissue damage. It has been known that under pathological conditions, the stiffness, nonlinear and viscoelastic structure of soft tissues change. Therefore the determination of mechanical behavior of soft tissues under physiologically living and *in-vivo* conditions is highly important (Silver-Thorn, 1999). In in–vitro experiments, the morphology of the tissue changes while the tissue loses its vividness (Gefen & Margulies, 2008). Therefore it has been thought that in-vivo experiments are more appropriate for soft tissue mechanical behavior identification (Ottensmeyer, Kerdok, Howe, & Dawson, 2004). In the literature there exist several soft tissue identification experiment set-up designs for specific purposes. Indentation experiments have been commonly used in the testing of the mechanical properties of biological soft tissues. Indentation device is mainly composed of a cylindrical or elliptical indenter tip which is used to indent the tissue, a load cell to measure the tissue reaction force and the indentation force, a sensor to measure the displacement on the tissue and a linear actuator to initiate the motion with a high sensitivity control of velocity. Indentation devices usually work with step motors in order to induce the motion. Some other indentation devices work under the principle of human control which causes experimental subjectivity. However, by step motors, the human control or human sourced biases in the experiments are minimized which results in more objective test results.

Apart from indentation devices, there are several order types of test devices for specific purposes. Dhar et al., (2007) developed the resonator system, Nava et al., (2003) and Mazza et. al., (2006) developed the measurement method with aspiration,

Samur et. al., (2007) developed a minimally invasive indentation device with robot arm, Ahn and Kim (2009) developed an indentation system which works with a DC motor, Lu et al., (2009) and Han et al., (2002) developed a hand-held load and position controlled indentation device, Zheng et al., (1996) developed an indentation device which involves an ultrasonic measurement device. It is known that hand-held indentation systems are less reliable compared to computer controlled devices (Kawchuk, Liddle, Fauvel, & Johnston, 2006). It is important that the indentation devices should be totally computer controlled, accurate and reliable in order to eliminate subjectiveness of test results.

It has been reported by several authors that soft tissues show hysteresis under cyclic loading, relaxation under constant displacement and creep under constant force. The mechanical behavior is complex, nonlinear and involves anisotropy (Tay, Kim, & Srinivasan, 2006), (Fung, 1993), (Arıtan, Oyadiji, & Bartlett, 2008). It should also be noted that, the soft tissue mechanical behavior also depends on the indentation rate and time, the individual and for the same individual the testing place.

The complex mechanical behavior of soft tissues is examined by indentation devices and force-time and displacement-time graphs for material modeling can be obtained. The details of the indentation experiments are presented in Appendix B.

2.8 Finite Element Analysis of Indentation

The finite element method provides an efficient numerical tool for large scale computations of time-dependent materials.

Finite element analysis of indentation experiments are widely studied in the literature. In 1992, Spilker et al., investigated the indentation problem on a thin layer of soft tissue such as cartilage with a circular plane-ended indenter. The bone is modeled by attaching a layer of soft tissue to the bone. Indentation problem is solved by axisymmetric approximation. The effect of friction at the tissue-indenter interface is investigated. In the indentation test a plane-ended cylindrical indenter is positioned normal to the tissue surface and subjected to an instantaneously prescribed load

(creep) or a ramp displacement (stress relaxation) (Spilker, 1992) (Figure 2.15). Indenter permeability and interface adhesion are investigated.

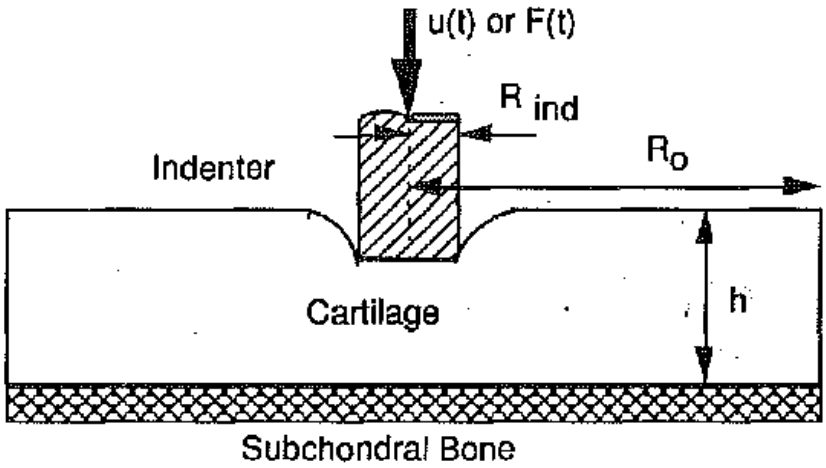

Figure 2.15 Schematic of the indentation problem
(Adopted from (Spilker, 1992))

Choi and Zheng (2005), investigated the finite element of indentation with two different-sized indenters by employing an axisymmetric finite element model of the tissue with rigid-cylindrical flat ended indenters. The tissue is assumed to be linearly elastic and Young's modulus and Poisson's ratio is obtained by the simulation of the several force-deformation pairs.

Liu, Kerdok, and Howe (2004), developed a finite element model of the indentation problem for determining material properties of soft tissue by employing the Arruda-Boyce constitutive model for large indentations and including material nonlinearities (Figure 2.16).

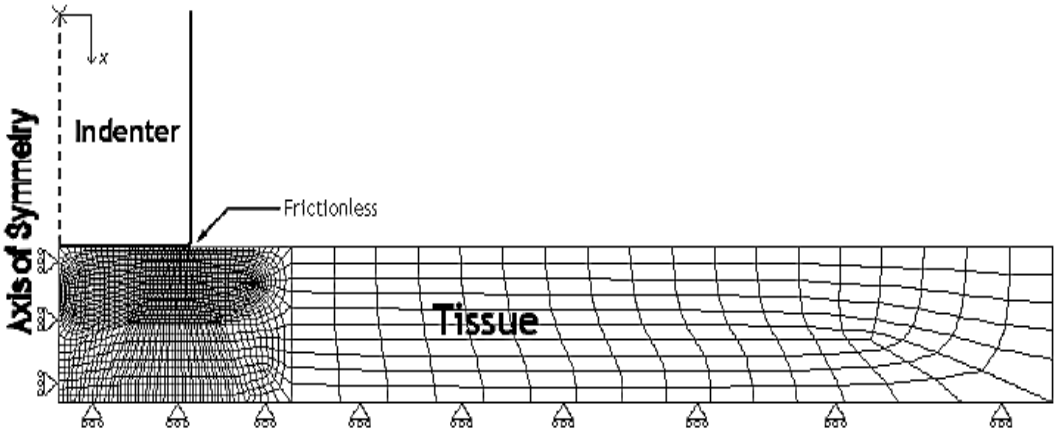

Figure 2.16 The finite element model of soft tissue and indenter
(Adopted from (Liu, Kerdok, & Howe, 2004))

Spherical indenter tips are also employed in the literature especially for articular cartilage (Korhonen, Saarakkala, Töyras, Laasanen, Kiviranta, & Jurvelin, 2003). Petekkaya et al. (2010) introduced ellipsoid indenter tips to determine the in-plane anisotropy of soft tissues via indenter experiments.

2.9 Inverse Finite Element Method for Extraction of Material Parameters

Several authors have demonstrated the power of inverse finite element method for material model parameter identification (Lei & Szeri, 2007), (Liu, Kerdok, & Howe, 2004). Inverse finite element modeling is used to fit the mathematical formulation in the form of constitutive equation to the experimental data. Determining the most suitable constitutive response and using the finite element methodology allows one to simulate different modes of deformation that are not possible with experimentation. One can either search for the parameters by trial-and-error method on the other hand; algorithms can also be available for the most sensitive parameter extraction. The algorithm or procedure in either case, aims to minimize the error between experimental data and the theoretical model prediction by employing least-squares method which is frequently used to curve-fit experimental data. Determining the most sensitive parameters by trial and error involves some difficulties; however the built-in curve-fitting capabilities of finite element software are limited to standard test protocols. Therefore one should either construct an optimization algorithm and

finite element formulation as a user-subroutine for parameter searching for complicated problems or use trial and error methodology. In order to develop an optimization algorithm for commercial FE software, Matlab; which provides an excellent platform for nonlinear least squares, could be executed sequentially with the FE software to initiate the parameter search routine. This procedure is not one of the aims of this thesis study and trial and error methodology is preferred for material parameter identification.

CHAPTER 3

THE THEORY OF VISCOELASTICITY

3.1 Integer Order Spring-Dashpot Models

To predict the response of a material to any history of stress or strain (as a function of time) constitutive equations are developed. At sufficiently small (theoretically infinitesimal) strains, the behavior of a viscoelastic material is well described by the linear theory of viscoelasticity.

The simplest form of a constitutive law is a functional relation,

$$v = f(u) \tag{3.1}$$

where $v(t)$ and $u(t)$ are functions of time.

The quantity v at a given time t is determined by the value of u at the same time t. However, when the value of the quantity $v(t)$ at a time t is determined not only by the quantity $u(t)$ at the same time t, but also by the whole history of the variation of the function $u(\tau)$, $\tau \in (-\infty, t)$ then the relation is represented as,

$$v = F_{-\infty}^{t}(u) \tag{3.2}$$

This functional can be of any type, linear or nonlinear, or in the form of Volterra integral operators. Such a constitutive equation can be defined as (Rabotnov, 1980),

$$v(t) = u(t) + \int_{-\infty}^{t} K(t,\tau)u(\tau)\,d\tau \tag{3.3}$$

Equation 3.3 is a general constitutive equation which satisfies the history principle.

In 1909, Osborne and Sutherland, found out from experimental data that inflated balloons representing the urinary bladder exhibit viscoelasticity as evidenced by hysteresis, stress relaxation and stress-strain relation that does not obey the linear elastic law. In addition, as a consequence of the previous statement, the modulus of elasticity is shown to be a function of the strain, but not a constant, under large strains.

Therefore, since then, the foremost problem of rheology (science of the deformation and flow of matter) is to express the behavior of complex materials in terms of stress strain and time. Flügge in 1967 stated that,

"*No mathematical theory can completely describe the complex world around us. Every theory is aimed at certain class of phenomena, formulates their essential features and disregards what is of minor importance.*"

For a long time, mechanics of deformable bodies has been based upon Hooke's law, which is based on the assumption of linear elasticity. However, in reality all materials especially most of the engineering materials such as, metals, concrete, wood, soil etc. and rubber-like materials deviate from Hooke's Law and display viscous-like and elastic characteristics. Viscoelastic materials are those for which the stress-strain relationship depends on time (Lakes, 1999). Some phenomena in viscoelastic materials are, "*creep*", "*relaxation*" and "*hysteresis*".

In the viscoelastic approach the behavior of complex materials is expressed as a physical mixture of ideal Hookean solid and ideal Newtonian fluid. Hookean solid is an ideal linear elastic element-which is a "*spring*" that only stores elastic mechanical energy and an ideal linear viscous element-which is a "*dashpot*" that dissipates mechanical energy into other forms (mainly heat). Therefore a "*viscoelastic"* material combines elastic and viscous characteristics together. Energy is stored in springs as elastic strain energy and mechanical energy is dissipated in dashpots as heat. No energy is dissipated in a spring and no energy is stored in a dashpot.

Figure 3.1 Elastic element, spring (left), viscous element, dashpot (right)

The constitutive equation (the relation between stress and strain) for a Hookean solid is,

$$\sigma(t) = E\epsilon(t) \tag{3.4}$$

and for Newtonian fluids,

$$\sigma(t) = \eta \frac{d\epsilon(t)}{dt} \tag{3.5}$$

where E and η are the material constants. For a viscous material the stress is proportional to the strain rate and for an elastic material stress is proportional to the strain itself.

Real materials combine properties of these two limit cases and lie in between ideal elastic solids and ideal viscous (Newtonian) fluids.

When the elements are combined in series the combination is known as the Maxwell element and when the elements are combined in parallel the combination is known as the Voigt element (Figure 3.2). The deformation on those models are assumed "*quasi-static*", therefore inertia effects are neglected.

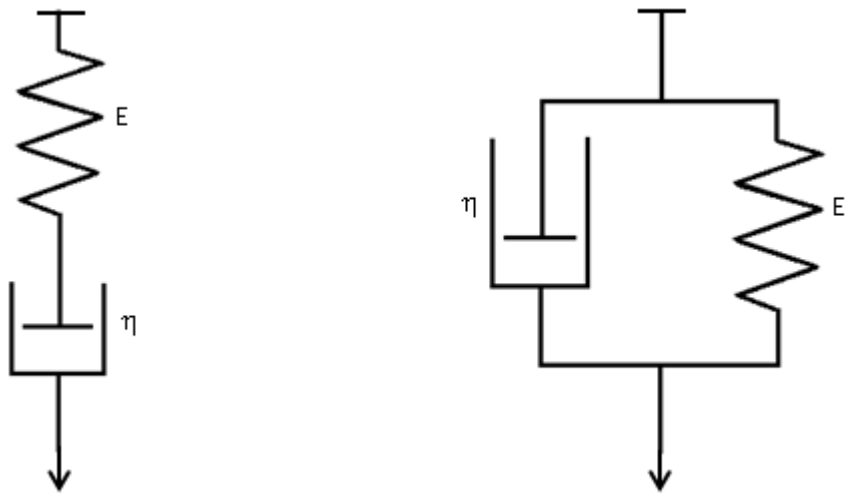

Figure 3.2 Maxwell Model (left), Voigt Model (or Kelvin model) (right)

The constitutive equation related to Maxwell model is,

$$\frac{d\epsilon}{dt} = \frac{1}{E}\frac{d\sigma}{dt} + \frac{\sigma}{\eta} \tag{3.6}$$

and for the Voigt model, the constitutive relation is given as,

$$\sigma = E\epsilon + \eta\frac{d\epsilon}{dt} \tag{3.7}$$

The ratio $\tau = \eta/E$ gives the relaxation time for the Maxwell model and the retardation time for the Voigt model. Retardation time controls the rate of growth of strain following the step imposition of the stress and relaxation time controls the rate of decay of stress following the step imposition of strain. Maxwell material is a type of simplest viscous fluid and also called the relaxation element while it can represent stress relaxation and exhibits a non-reversible strain creep and capable of unlimited deformation under finite stress whereas the Voigt material shows the simplest behavior of an elastic solid where there is no instantaneous deformation and no stress relaxation but it can represent creep. While Maxwell model represents a simple

viscoelastic fluid with no preferred initial shape Voigt model has no physical counterpart since all real viscoelastic solids have an instantaneous elastic response. More complicated models involve the combination of Maxwell element parallel with a spring (Zener model) and Voigt element in series with a spring (Kelvin model) (Figure 3.3).

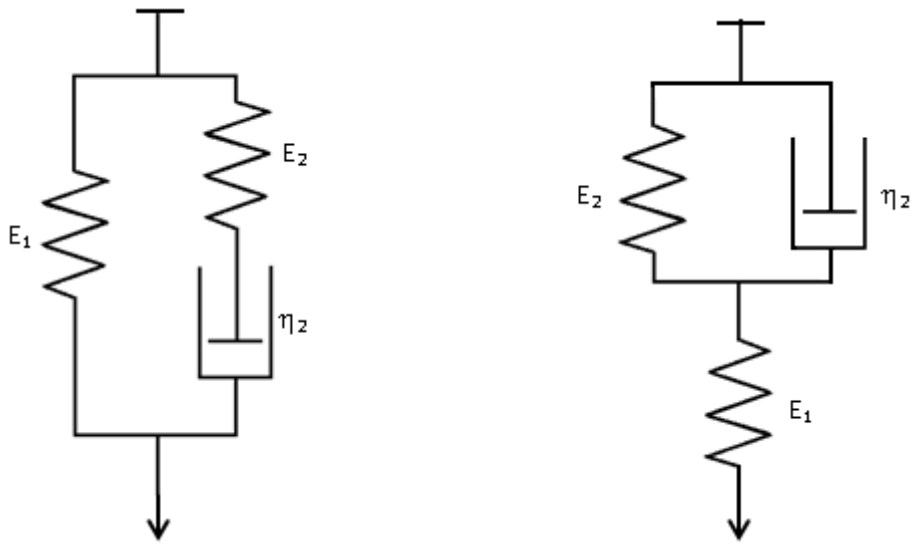

Figure 3.3 Zener Model (The Standard Linear Solid) (Left), Kelvin Model (Right)

The constitutive equation related to Zener model (also called the standard viscoelastic solid) can be given as,

$$\frac{d\sigma}{dt}+\frac{E_2}{\eta_2}\sigma=\left(E_1+E_2\right)\frac{d\epsilon}{dt}+\frac{E_1E_2}{\eta_2}\epsilon \tag{3.8}$$

and the constitutive equation related to Kelvin model is given as,

$$\frac{d\sigma}{dt}+\frac{E_1+E_2}{\eta_2}\sigma=E_1\frac{d\epsilon}{dt}+\frac{E_1E_2}{\eta_2}\epsilon \tag{3.9}$$

Actually the models presented above represent the same material behavior and also in the textbook of Francesco Mainardi (Mainardi F, 2010), they are both named as the "Zener Model". The limiting values of the material functions for $t \to 0^+$ and $t \to \infty$ are the instantaneous (glassy) and equilibrium (rubbery) modulus of elasticity respectively. The glassy modulus for this model is $E_0 = E_1 + E_2$ and the rubbery modulus is $E_\infty = E_1$. Then the constitutive relation in terms of the glassy and rubbery modulus becomes,

$$\tau_r \frac{d\sigma}{dt} + \sigma = E_0 \tau_r \frac{d\varepsilon}{dt} + E_\infty \varepsilon \tag{3.10}$$

where $\tau_r = \dfrac{\eta_2}{E_2}$ is the relaxation time.

Under constant stress, the model instantaneously deforms and then reaches an asymptotic value which is the viscous part of the model where permanent deformation occurs.

3.1.1 Creep and Relaxation Phenomena

A creep test consists of applying a force to a model previously unloaded and then maintaining this force constant. On the other hand a relaxation test consists of imposing a constant extension on a model and measuring the force required to do so as a function of time (Bland, 1960). An increase in strain with time is called "*creep*" and a decrease in stress in time is called "*relaxation*" (Lakes, 1999).

Creep and relaxation can occur in shear or in volumetric deformation. $G(t)$ is called the relaxation modulus, and $J(t)$ is the creep compliance in shear deformation. For volumetric deformation, elastic bulk modulus is defined. The creep process is characterized either by the "creep strain" ϵ_c which is defined as the difference between the strain ϵ and the initial elastic strain ϵ_0 or by the creep compliance $J(t)$

which equals to the ratio of the creep strain to the applied stress. In linearly viscoelastic materials, the creep compliance is independent of the stress level.

On the other hand the stress relaxation phenomenon is defined as the decrease of stress in time for a fixed strain and the stress relaxation modulus $G(t)$ is the ratio of stress to the initial strain (Drozdov A D, 1996). In linear materials, it is independent of the strain level so it is a function of time alone.

Usually, $J(t)$ is denoted as the strain response to the unit step of stress according to the creep test and $G(t)$ is the stress response to a unit step of strain according to the relaxation test, where the unit step function is known as the Heaviside unit-step function (Mainardi F, 2010),

$$\begin{aligned} &H(t)=\begin{cases}0, t<0\\ 1, t>0\end{cases}\\ &\sigma(t)=H(t)\Rightarrow\epsilon(t)=J(t)\\ &\epsilon(t)=H(t)\Rightarrow\sigma(t)=G(t)\end{aligned} \tag{3.11}$$

There is a basic relation between $J(t)$ and $G(t)$ for the linear models presented above is called the "*reciprocity relation",*

$$J=\frac{1}{G} \tag{3.12}$$

where J and G are the constants.

$J(t)$ and $G(t)$ are both monotonic functions $\left(\frac{dG(t)}{dt}\leq 0\right)$, $\left(\frac{dJ(t)}{dt}\leq 0\right)$ where the former is related to the physical phenomena of stress relaxation and the latter is related to strain creep. In linearly viscoelastic materials, the creep compliance is independent of the stress level and relaxation modulus is independent of the strain level applied.

The creep compliance $J(t)$ and the relaxation modulus $G(t)$ related to the standard linear solid model (Zener model) are,

$$J(t)=\left(\frac{1}{E_2}-\frac{E_1}{E_2(E_1+E_2)}\right)\left(e^{(-t/\tau_c)}\right) , \tag{3.13}$$

$$G(t)=E_1+E_2e^{-t/\tau_r} , \tag{3.14}$$

where $\tau_c=\frac{(E_1+E_2)\eta_2}{E_1E_2}=\tau_r\frac{(E_1+E_2)}{E_2}$.

The retardation time is larger than the relaxation time.

Differential constitutive equations can also be represented by integral type constitutive equations. Standard viscoelastic solid constitutive equation can also be written in the integral form. With a new variable $\sigma(t)=z(t)\exp\left(-\frac{A_0}{A_1}t\right)$ integrating the constitutive equation provided above for S.L.S, the stress-strain relation written in integral form becomes (Drozdov A. D., 1996),

$$\sigma(t)=(E_2+E_1)\left\{\epsilon(t)-\frac{E_2^2}{\eta_2(E_2+E_1)}\right\}\int_0^t\epsilon(s)\exp\left[-\frac{E_2}{\eta_2}(t-s)\right]ds \tag{3.15}$$

Equation 3.15 is a typical "*Volterra equation*" and at current time, t, the history of strains up to time t sum up.

As a remark, fractional derivative is the Volterra integral operator with a kernel of a special form (Abel's kernel) which depends on an arbitrary parameter β where $(0\le\beta\le1)$. Abel's kernel definition is,

$$J_\beta(t)=\frac{t^\beta}{\Gamma(1+\beta)},\ -1\le\beta\le0 \tag{3.16}$$

and the fractional derivative is,

$$\frac{d^{\beta} f(t)}{dt^{\beta}} = \int_{0}^{t} J_{-\beta-1}(s)\, f(t-s)\, ds \tag{3.17}$$

When a dashpot is added either in series to a Voigt model or in parallel to a Maxwell model, the newly formed model is named as the anti-Zener model. The two similar representations of the anti-Zener model are shown in Figure 3.4 (Mainardi F. , 2010), which does not possess a definite undeformed state due to damper therefore is a fluid model,

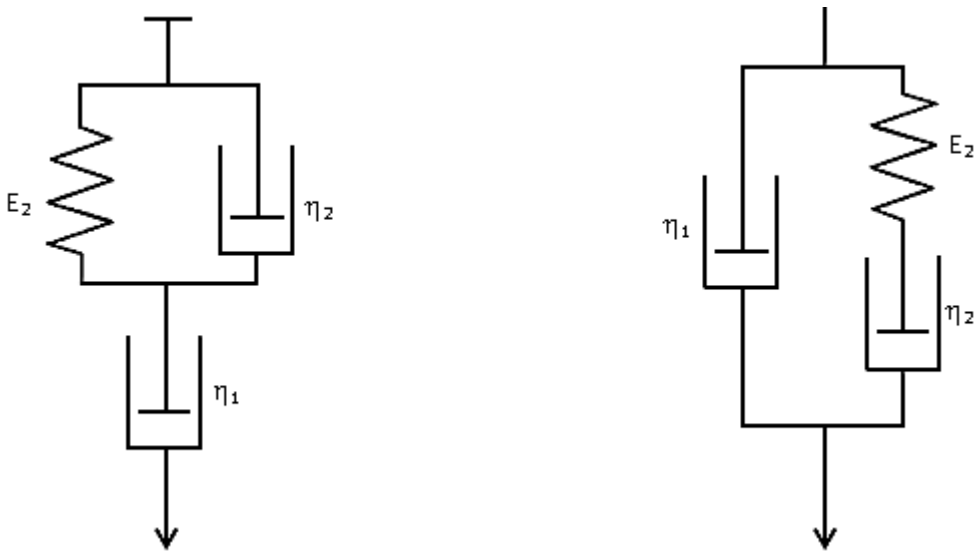

Figure 3.4 Anti-Zener Model (dashpot in series with Voigt - left)
Anti-Zener Model (dashpot in parallel with Maxwell- right)

On the contrary of the Zener model, for the anti-Zener model the relaxation time must be greater than the retardation time. Because of their characteristics, Zener model is also called as the "*three-element elastic model*" and anti-Zener model is called as the "*three-element viscous model*".

Another important viscoelastic model is the "*Burger's model*" where a spring and a dashpot in series (Maxwell element) are added to the Voigt model (Figure 3.5).

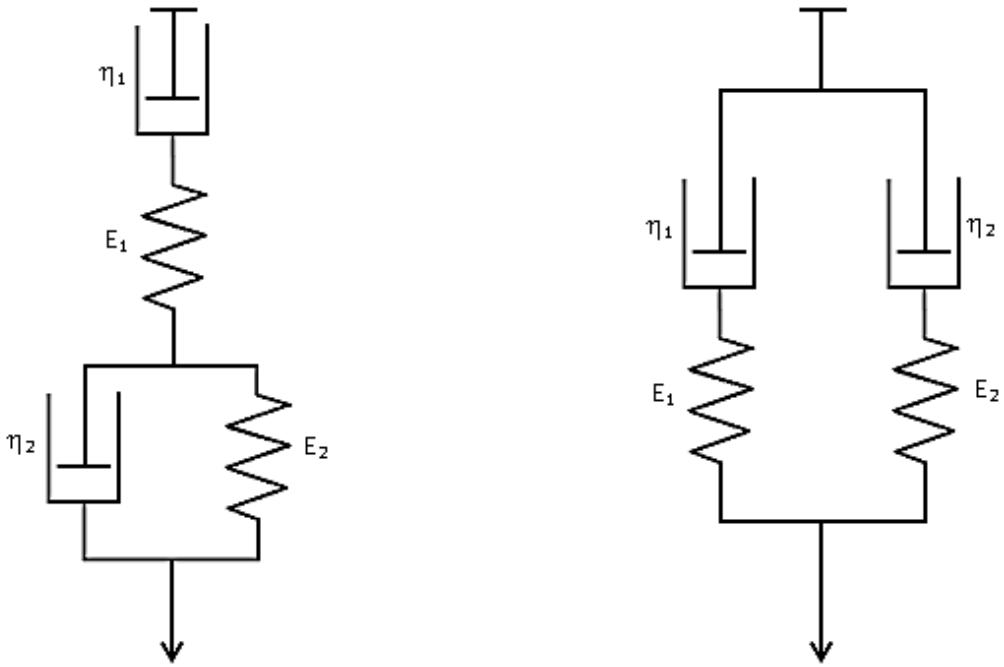

Figure 3.5 Burger's Model (Creep Representation- Left)
(Relaxation Representation - Right)

The constitutive equation for the Burger's model is,

$$\frac{d^2\sigma}{dt^2}+\left(\frac{E_1}{\eta_2}+\frac{E_2}{\eta_2}+\frac{E_1}{\eta_1}\right)\frac{d\sigma}{dt}+\frac{E_2E_1}{\eta_2\eta_1}\sigma=E_1\frac{d^2\epsilon}{dt^2}+\frac{E_2E_1}{\eta_2}\frac{d\epsilon}{dt} \tag{3.18}$$

For a linearly viscoelastic material, the slope of the stress-strain curve is nonlinear even though the material is assumed to be linearly viscoelastic. The reason is that even though the stress and strain are linearly related at a particular time, viscoelastic material behavior depends heavily on time.

Another important point about viscoelastic materials is that they dissipate mechanical energy unlike the purely elastic materials which do not dissipate mechanical energy as heat when the load is applied and then the load is removed (Üsü, 2008). This property is known as "*hysteresis*", when a cyclic loading is applied to the material a phase lag (hysteresis) occurs, leading to dissipation of mechanical energy.

Although the models presented above are assumed to behave linear under infinitesimal strains, the majority of viscoelastic media behave physically nonlinear. Therefore it becomes a necessity to analyze the viscoelastic behavior in the framework of nonlinear mechanics of continua accounting for both physical and geometrical nonlinearity. In nonlinear viscoelasticity, the pseudo-elastic material coefficients are time-dependent.

3.2 Fractional Order Spring-Spring-pot Models

Fractional calculus is broadly applied into the theory of linear viscoelasticity and particularly to the linear viscoelastic models. Representation of linear viscoelastic constitutive equations in terms of fractional derivatives allows definition of models as they are "transient" between differential and integral constitutive equations while fractional calculus deals with integro-differential equations.

The applications of fractional calculus on the "observed" viscoelastic phenomena of soft biological tissues are useful while it includes the natural incorporation of power law behavior and system memory where arbitrary fractional order is defined as the "memory parameter". Whereas, an integer order derivative is a local operator, fractional derivatives depend on material past, evidencing a memory mechanism that can be adjusted using the fractional order β (Magin R., 2004). In addition, the advantage of fractional derivatives in the theory of viscoelasticity affords the identification of fewer experimental parameters while the arbitrary differentiation order serves as one parameter to be identified.

Fractional calculus applied in the viscoelastic models comes from the idea that for "intermediate" materials (in between fluid and solid) there should be a non-integer order derivative relation between stress and strain. As spring element represents a

Hookean elastic solid and a dashpot element Newtonian viscous fluid, a new element called "*spring-pot*" represents an intermediate material between an elastic solid and a viscous fluid. The name "*spring-pot"* is used in Koeller's paper (1984). This new element *spring-pot* is symbolized by a diamond (suggested by Bagley and Torvik (1979) (Figure 3.6).

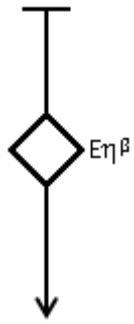

Figure 3.6 The fractional Element, Spring-Pot

The constitutive equation related to the fractional element is, (Scott-Blair, M.A., Sc., & C., 1944), (Scott-Blair G. W., 1974),

$$\sigma(t) = E\eta^{\beta}\frac{d^{\beta}\epsilon}{dt^{\beta}},\ 0 < \beta \leq 1 \tag{3.19}$$

The arbitrary fractional order β which varies from zero to one is defined as the "non-dimensional *memory* parameter" and the variation of this memory parameter allows the constitutive equation to shift from a representation of a solid state to fluid state. To be clear when $\beta = 0$ the material has perfect memory and represents a solid state $\left(\sigma(t) = E\epsilon(t)\right)$ and when $\beta = 1$ the material has no memory defining the fluid state $\left(\sigma(t) = E\eta\frac{d^{\beta}\epsilon(t)}{dt^{\beta}}\right)$. ($\eta = F/E$) represents the characteristic relaxation time or retardation time depending on the model specified where F is the viscosity for a dashpot element and E is the modulus of elasticity for the spring element. Fractional

order derivative β characterizes the power law response which is observed on most of the soft tissues. The relaxation data usually do not follow a simple exponential; however it is described by a power law expression of the form,

$$G(t) = \frac{E}{\Gamma(1-\beta)}\left(\frac{t}{\tau}\right)^{\beta} \tag{3.20}$$

which is the relaxation modulus for the fractional element and τ is the time constant.

For all values of β that lie in between zero and one, the fractional element provides a smooth monotone transition from elastic to viscous response.

Creep and relaxation behavior of soft biological tissues may be described and analyzed using the methods of fractional calculus. Koeller (1984) applied fractional calculus to the theory of viscoelasticity and obtained creep and relaxation functions in terms of Mittag-Leffler function. To find the relaxation modulus, strain in the constitutive equation is replaced by the Heaviside unit-step function. The output is the stress relaxation modulus,

$$G(t)/E = \frac{1}{\Gamma(1-\beta)}\left(\frac{t}{\eta}\right)^{-\beta}, \ 0 < \beta \le 1 \tag{3.21}$$

When $\sigma(t) = H(t)$, the output is the creep compliance,

$$EJ(t) = \frac{1}{\Gamma(1+\beta)}\left(\frac{t}{\eta}\right)^{\beta}, \ 0 < \beta \le 1 \tag{3.22}$$

The reduced relaxation function is a monotonic non-increasing function and the retardation function is a monotonic non-decreasing function.

For various values of the memory parameter β, the plot of the relaxation modulus and creep compliance versus non-dimensional time for the fractional element, spring-

pot is provided in Figures 3.6 and 3.7 respectively. For smaller times, a much faster decay is obvious, and for large times a much slower decay is present.

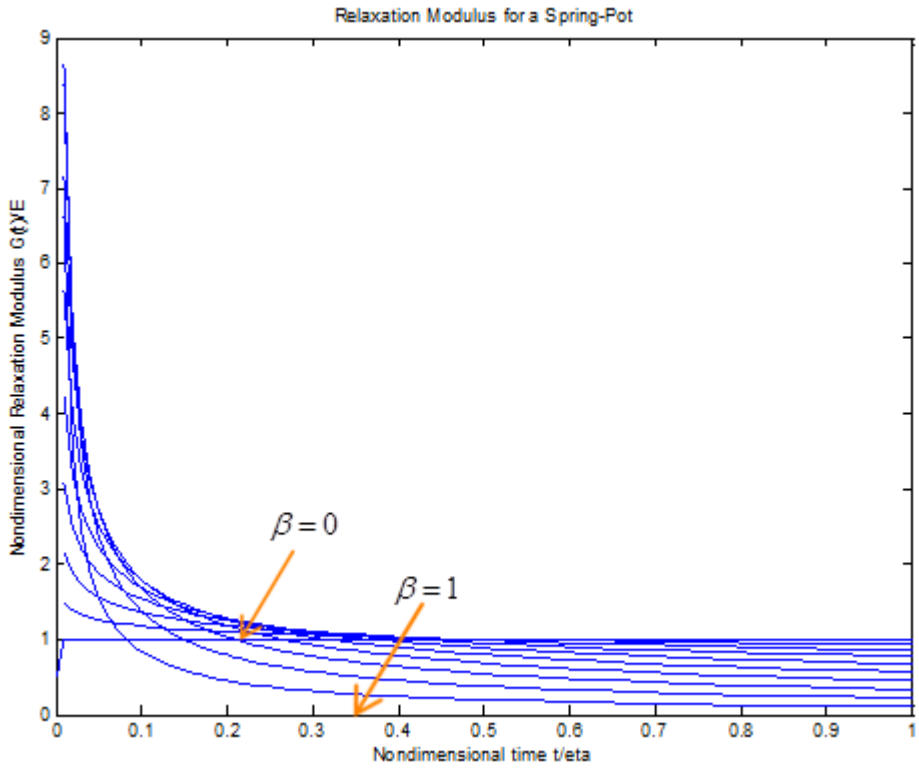

Figure 3.7 The relaxation modulus for a spring-pot element for fractional orders $(0 \le \beta \le 1)$ in increments of 0.1

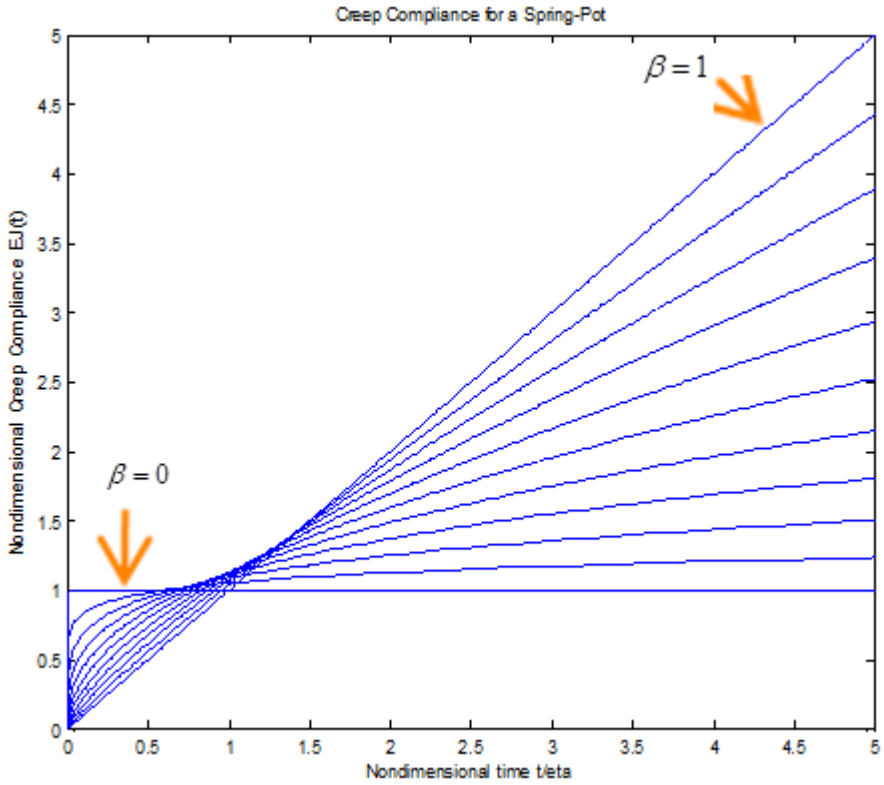

Figure 3.8 The creep compliance for a spring-pot element for various fractional orders $(0 \le \beta \le 1)$ in increments of 0.1

For the linear fractional order viscoelastic model representations, the dashpot in the linear integer order viscoelastic models is replaced with the "*spring-pot*" element. From Figures 3.7 and 3.8, it can be stated that a wide variety of responses can be obtained when a spring-pot is used in the classical linear viscoelastic models. For the two element Maxwell and Voigt models, generalizations of the models can be made with the fractional element named spring-pot.

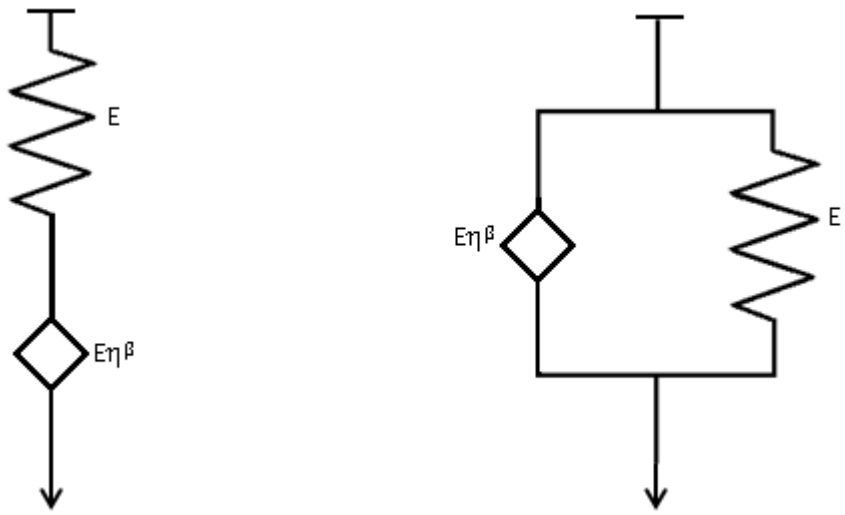

Figure 3.9 Fractional Maxwell (Left) and Voigt Model (Right)

The constitutive relation for the fractional Voigt-model is,

$$\sigma(t) = E\epsilon(t) + E\eta^{\beta}\frac{d^{\beta}\epsilon(t)}{dt^{\beta}} \tag{3.23}$$

The creep compliance and relaxation modulus are,

$$J(t) = \frac{1}{E}\left\{1 - E_{\beta}\left[-\left(\frac{t}{\eta}\right)^{\beta}\right]\right\} \tag{3.24}$$

$$G(t) = E + E\eta^{\beta}\frac{t^{-\beta}}{\Gamma(1-\beta)} \tag{3.25}$$

where $\eta = F/E$ and $E_{\beta}[\bullet]$ is the Mittag-Leffler function. F and E are the coefficients of the spring-pot for its limiting values of β.

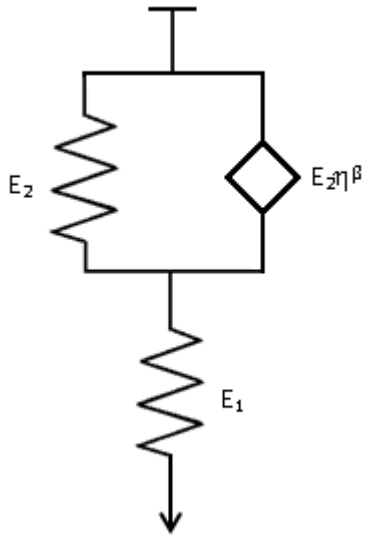

Figure 3.10 Three-element fractional standard linear solid model

For the three element fractional elastic solid element (Figure 3.10), Caputo and Mainardi, (1971a) generalized the integer order derivatives in the standard linear solid model to fractional order. The constitutive equation, creep compliance and the relaxation modulus related to the fractional standard linear solid model are (Welch, Rorrer, Duren, & JR., 1999),

$$\left(\frac{d^{\beta}}{dt^{\beta}}+\frac{\left(E_2+E_1\right)}{E_2\eta^{\beta}}\right)\sigma\left(t\right)=E_1\left(\frac{d^{\beta}}{dt^{\beta}}+\frac{1}{\eta^{\beta}}\right)\epsilon\left(t\right) \tag{3.26}$$

$$J\left(t\right)=\frac{1}{E_1}\left\{1+\frac{E_1}{E_2}\left\{1-E_{\beta}\left[-\left(\frac{t}{\eta}\right)^{\beta}\right]\right\}\right\} \tag{3.27}$$

$$G\left(t\right)=E_1\left\{1-\frac{E_1/E_2}{1+E_1/E_2}\left\{1-E_{\beta}\left[-\left(\frac{t}{\tau}\right)^{\beta}\right]\right\}\right\} \tag{3.28}$$

where $\tau=\frac{\eta}{\sqrt[\beta]{1+E_1/E_2}}$.

The model reduces to the integer order three parameter viscoelastic solid model when $\beta \to 1$ and to a solid spring model when $\beta \to 0$.

Plot of the creep compliance and relaxation modulus versus non-dimensional time regarding fractional solid model is presented in Figures 3.11 and 3.12. The figures illustrate that the parameter β determines the time duration of the transition from glassy to rubbery behavior. The parameters η and τ determine the time at which the transition is centered for creep compliance and relaxation modulus, respectively. The remaining parameters simply determine the magnitude of the initial and terminal plateaus. In practice, the stress relaxation function should first jump to the value of the glassy modulus and then monotonically decrease to a lower asymptote of the rubbery modulus. Similarly for creep, it first jumps to the value of the reciprocal of the glassy modulus and then monotonically increases to an upper asymptote which again should be the reciprocal of the rubbery modulus.

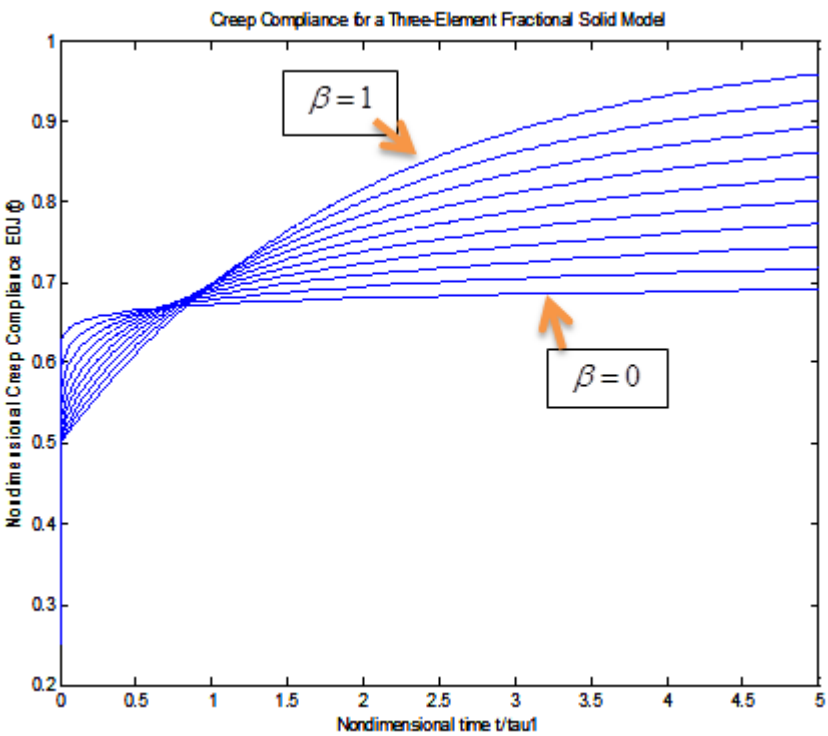

Figure 3.11 Creep compliance for three element fractional model for various fractional orders $(0 \le \beta \le 1)$ in increments of 0.1

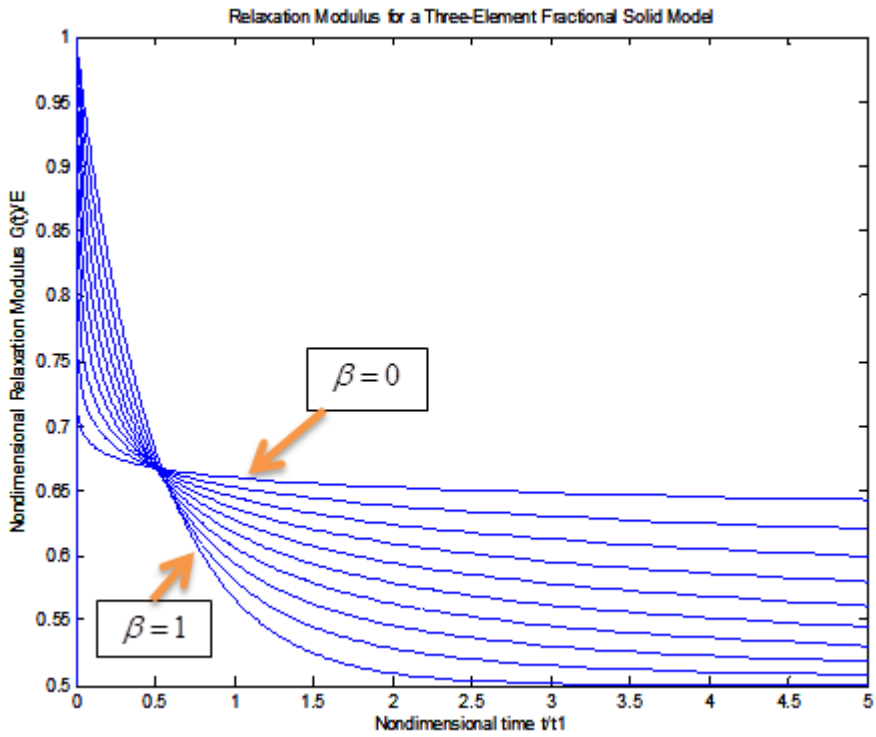

Figure 3.12 Relaxation modulus for three element fractional model for various fractional orders $(0 \le \beta \le 1)$ in increments of 0.1

The "memory" of the viscoelastic material becomes dominant with lower values of β. Initial non-dimensional times (*i.e.* $(t/\tau) < 1$) stress relaxation (steep decay) and creep increase is most significant with decreasing order of the fractional derivative.

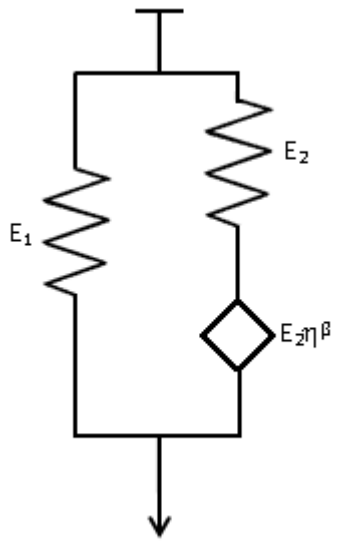

Figure 3.13 The three element fractional Zener model

For the other representation of the three-element fractional order viscoelastic (FOV) model (fractional Zener model) (Maxwell model is parallel to the spring element – Fig. 3.13) the relaxation modulus is (Craiem D. O., Rojo, Atienza, Guinea, & Armentano, 2008),

$$G(t) = E_1 + E_2 \left\{ E_\beta \left[-\frac{t^\beta}{\tau} \right] \right\} \tag{3.29}$$

where $\tau = \left(\frac{\eta}{E_2} \right)^{1/\beta}$.

When employing $E_0 = E_1 + E_2$ and $E_\infty = E_1$ the relaxation function becomes,

$$G(t) = E_\infty + (E_0 - E_1) \left\{ E_\beta \left[-\frac{t^\beta}{\tau} \right] \right\} \tag{3.30}$$

where $\tau = \left(\frac{\eta}{E_2} \right)^{1/\beta}$.

In this formulation, the relaxation time constant gives the transition from short time glassy behavior to the long time rubbery behavior and the fractional order β gives the slope of the relaxation curve between the two regions.

The creep compliance is (Davis, Kohandel, Sivaloganathan, & Tenti, 2006),

$$J(t) = \frac{1}{E_\infty} + \left(\frac{1}{E_0} - \frac{1}{E_\infty}\right)\left\{E_\beta\left[-\frac{E_\infty}{E_0}\left(\frac{t}{\tau}\right)^\beta\right]\right\} \tag{3.31}$$

where $E_0 = E_1 + E_2,\ E_\infty = E_1,\ \tau = \left(\frac{\eta}{E_2}\right)^{1/\beta}$.

FOV models represent the "*fading memory*" principle because the memory kernels are monotonically decreasing functions of time. Also as the fractional derivatives result in non-local operators, they implicitly provide the "fading memory" property. Fading memory under the concept of stress-strain relation is defined as; the strain that produces a stress that does not only depend on the current strain but also on the previous strain history in such a manner that the current stress depends stronger on the recent strain history than on the distant strain history. Integer-order derivative is a local operator whereas fractional derivatives depend on the material past, evidencing a memory mechanism that can be adjusted using the fractional parameter β (Magin R. , 2004).

The constitutive equation for the three element fractional solid model involves four material parameters to be extracted by experimental data. With fewer elements more parameters are available for curve-fitting to experimental data in means of least-squares. One advantage and usage of fractional viscoelastic models comes from this idea. The efficacy of fractional calculus models is dependent upon their ability to adequately fit the experimental data with fewer parameters (Welch, Rorrer, Duren, & JR., 1999). Experimental results suggest that rheological properties that give rise to viscoelasticity have behavior based on fractional instead of integer calculus (Bagley & Torvik, 1983). On the contrary, one disadvantage of using fractional models may be the increased complexity due to cumbersome mathematics.

Considering FOV models applied to biological soft tissues, Craiem and Armentano (2006), applied 4-parameter fractional order derivative model on arterial wall tissue of sheep whose experimental data is gathered on anaesthetized sheep in-vivo. Later in 2008 Craiem et al., applied the same model (FOV- standard linear solid model) on human arterial tissue where the experimentation is performed in-vitro. Their results show that fractional models should be considered as a plausible alternative to describe arterial viscoelasticity while it represents the power-law relaxation behavior better compared to standard linear solid model which is predicting by exponential decays.

3.3 Curve-Fitting to Quasi-Static Experimental Data Using Fractional Order Constitutive Equations

The question is: "What should be the minimum number of parameters that is required for an accurate description of the observed material behavior?"

It has been observed that employing fractional calculus principles to the linear viscoelasticity theory, the parameters necessary to describe the observed material behavior are significantly reduced compared to the integer order viscoelastic models (Enelund, Maehler, Runesson, & Joseffson, 1999), (Bagley & Torvik, 1983), (Schmidt & Gaul, 2002), (Wei & Shimizu, 2001) (Craiem & Armentano, 2006) (Welch, Rorrer, Duren, & JR., 1999).

In order to extract the parameters for the chosen material model, experimentation must be done. Considering the fractional order material model parameters, when one knows the creep compliance and relaxation modulus expressible in terms of the Mittag-Leffler function and when one evaluates the Mittag-Leffler function numerically it is possible to fit the fractional order model to the experimental data by means of classical curve-fitting techniques, like least squares.

As a part of this thesis, while it has been proposed that fractional order material models are more appropriate to curve-fitting than simple integer order viscoelastic models, it has been thought to verify this hypothesis for one dimensional linear viscoelastic case by comparing the curve-fitting capabilities of a one-term (two

parameters) and two-term (five parameters) integer order material models and a three element (four parameters) fractional order material model. Fractional order (four parameters) Zener model and one-term and two-term Prony series representations are chosen as the material model candidates to be compared among their curve-fitting sensitivities to in-vivo force-displacement-time data of soft biological tissues. The experimental data to be fitted is obtained from the creep and relaxation tests performed on soft biological tissues (the bulk soft tissues of the human forearm) (Petekkaya 2008) and used directly.

For curve fitting, nonlinear least squares algorithm is selected through the efficient optimization toolbox of the package program MATLAB®. By minimizing the least squares error measure between the measured data and the model, the model parameters are identified optimally.

Prony series is of the form $\sum_{i=1}^{N} \alpha_i \cdot e^{-t/\tau_i}$ where N represents the number of terms in the Prony series and α_i are the coefficients to be determined. When the material is modeled as "generalized Maxwell solid", the relaxation function is typically modeled as Prony series representation (Figure 3.14),

$$G(t) = E_0 \left(1 - \sum_{i=1}^{N} \alpha_i \left(1 - e^{-t/\tau_i} \right) \right) \tag{3.32}$$

where α_i is the i 'th Prony relaxation constant

$\tau_i = \eta_i / E_i$ is the i 'th Prony relaxation time constant

E_0 is the instantaneous (glassy) modulus of the material.

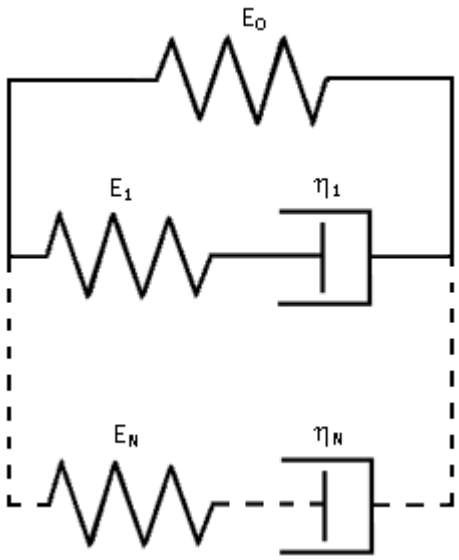

Figure 3.14 Generalized Maxwell Model

When the material model is the "generalized Voigt model", the creep compliance is typically modeled as (Figure 3.15),

$$J(t) = D_0\left(1 + \sum_{i=1}^{N} \alpha_i'\left(1 - e^{-t/\tau_i'}\right)\right) \tag{3.33}$$

where α_i' is the i 'th Prony retardation constant

$\tau_i' = \eta_i'/E_i'$ is the i 'th Prony retardation time constant

D_0 is the instantaneous compliance of the material.

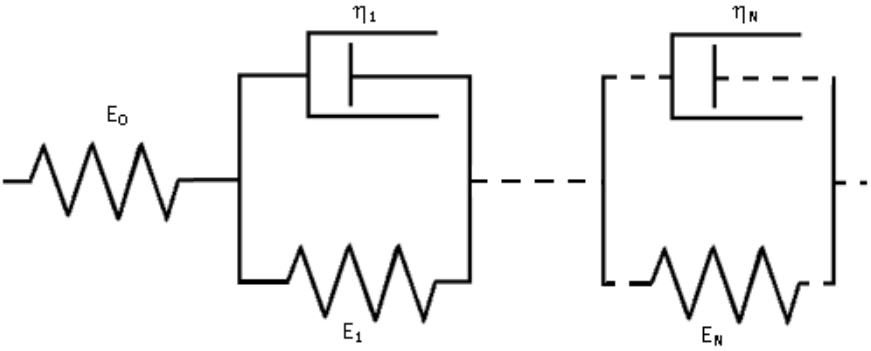

Figure 3.15 Generalized Voigt Model

By using MATLAB® optimization toolbox and "*lsqnonlin*" command, in nonlinear least squares sense with Levenberg-Marquardt algorithm the one-term and two-term Prony series and three-element (four parameter) fractional order viscoelastic model (Zener model) are fitted to the experimental relaxation data as shown in Figure 3.16. FOV-Zener model has weak singularity at $t = 0$ while M-L function contains a weak singularity at $t = 0$; therefore the values are computed for the smallest time possible which is $10^{-9} s$. The exact value of the M-L function is calculated by a Matlab *m*-file supplied by Igor Podlubny (2009). Initial guesses for the parameters to be identified were adopted from (Craiem D. O., Rojo, Atienza, Guinea, & Armentano, 2008),

$E_1 = 0.5$,

$E_2 = 0.5$,

$\eta = 1$,

$\beta = 0.5$.

Least squares error was calculated by the formulation given in Equation 3.34 to evaluate the quality of fitting and all LSE values calculated were found to be below 1%.

$$LSE = \sqrt{\frac{\sum_{i=1}^{n}\left[\sigma_{measured}(i) - \sigma_{model}(i)\right]^2}{\sum_{i=1}^{n}\sigma_{measured}(i)^2}} x100 \tag{3.34}$$

In order to represent the better curve-fitting properties of fractional order model compared to integer order model the three plots are shown together in Figure 3.16.

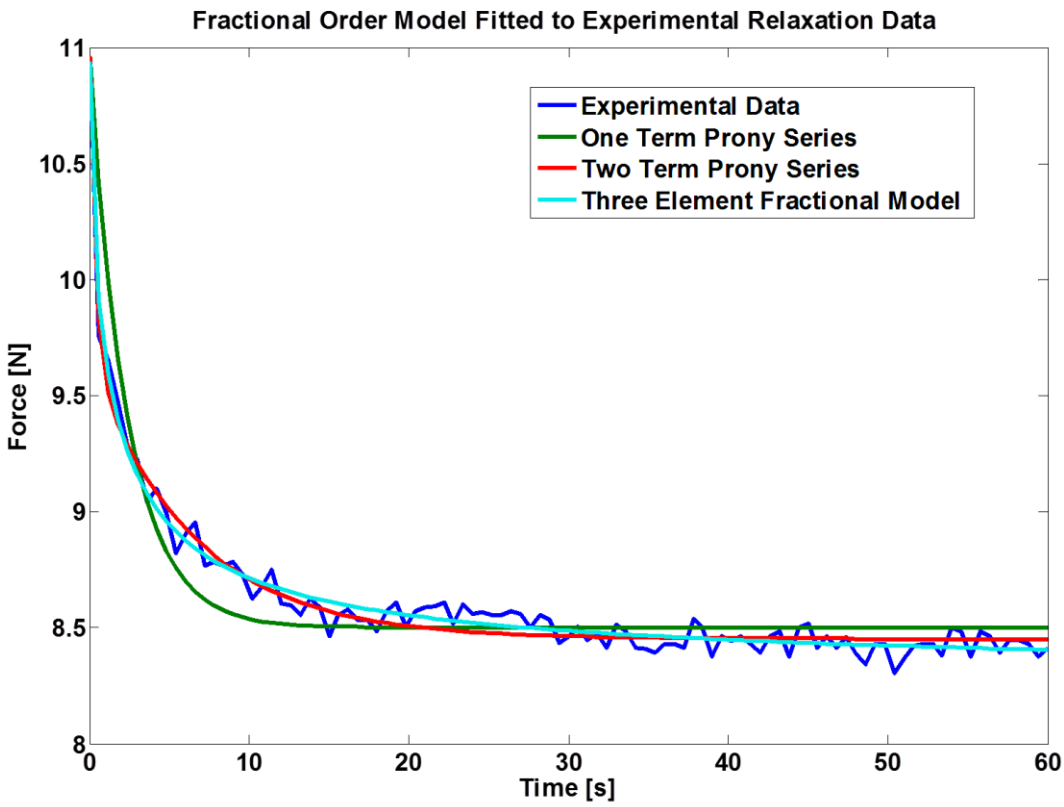

Figure 3.16 Curve-fit to Experimental Relaxation Data

The one-term Prony series representation has three elements and therefore needs three parameters to be identified and the two-term Prony series has five elements and needs five parameters to be identified. In contrast, the fractional Zener model has only three elements and four parameters to be identified.

One term Prony series representation relaxation modulus is,

$$G(t) = E_0\left(1-\alpha_1\left(1-e^{-t/\tau_1}\right)\right) \tag{3.35}$$

Two-term Prony series representation relaxation modulus is,

$$G(t) = E_0\left(1-\alpha_1\left(1-e^{-t/\tau_1}\right)-\alpha_2\left(1-e^{-t/\tau_2}\right)\right) \tag{3.36}$$

And finally the three-element fractional order Zener model relaxation modulus is,

$$G(t) = E_1\left\{1-\frac{E_1/E_2}{1+E_1/E_2}\left\{1-E_\beta\left[-\left(\frac{t}{\tau}\right)^\beta\right]\right\}\right\},\ \tau = \frac{\eta}{\sqrt[\beta]{1+E_1/E_2}} \tag{3.37}$$

The relaxation modulus of the Zener model is similar in form to the one-term Prony series representation, where the exponential function is replaced with the generalized exponential function, Mittag-Leffler function for the fractional case, which adds one extra parameter to the model, although the element number is the same, this extra fractional order parameter enables better curve-fitting.

The parameters of the three material models identified for the relaxation data by curve-fit are presented in Table 3.1.

Table 3.1 Material Parameters Identified for The Three Material Models

FOV ZenerModel Parameters	**Value**	**Unit**	**One & Two-Term Prony Series Parameters**	**Value**	**Value**	**Unit**
E_1	8.2623	MPa	α_1	0.1096	0.2246	-
E_2	2.6777	MPa	τ_1	6.4926	2.3872	s
η	3.4435	$MPa \cdot s$	α_2	0.1194	-	-
β	0.6186	-	τ_2	0.3892	-	s
LSE	0.0344	%	LSE	0.0510	0.0832	%

It can clearly be seen from Figure 3.16, although the number of parameters for the three-element FOV model (four parameter Zener model) necessary to fit the data is less than two-term Prony series representation, the curve-fitting sensitivity is much better. As it is observed, one-term Prony series is far from fitting the data properly.

The same result is reached in the work of Welch et al. (1999), where the four-parameter FOV model and a higher order Prony series representation is fitted to relaxation test data of polyurethane where FOV model is capable of representing the relaxation data with fewer parameters. The success of curve fitting of fractional order models compared to integer order models is also investigated somewhere else (Davis, Kohandel, Sivaloganathan, & Tenti, 2006). The point is that, the curve-fit superior capability of the fractional order model does not come from the increased number of parameter (as when it is compared with the integer order Burgers model), but rather it is inherit to non-integer order derivative. Integer order Burgers model has the same number of parameters with the fractional Zener model, however the fractional model fits better to the experimental data (Davis, Kohandel, Sivaloganathan, & Tenti, 2006). By this curve-fit, particular property of relaxation, as the initial steep decay and the slow asymptotic descent until stability is correctly demonstrated.

The same procedure was applied to the creep test data, and the result obtained was very similar to the relaxation test data. The experimental data together with three model fits are presented in Figure 3.17.

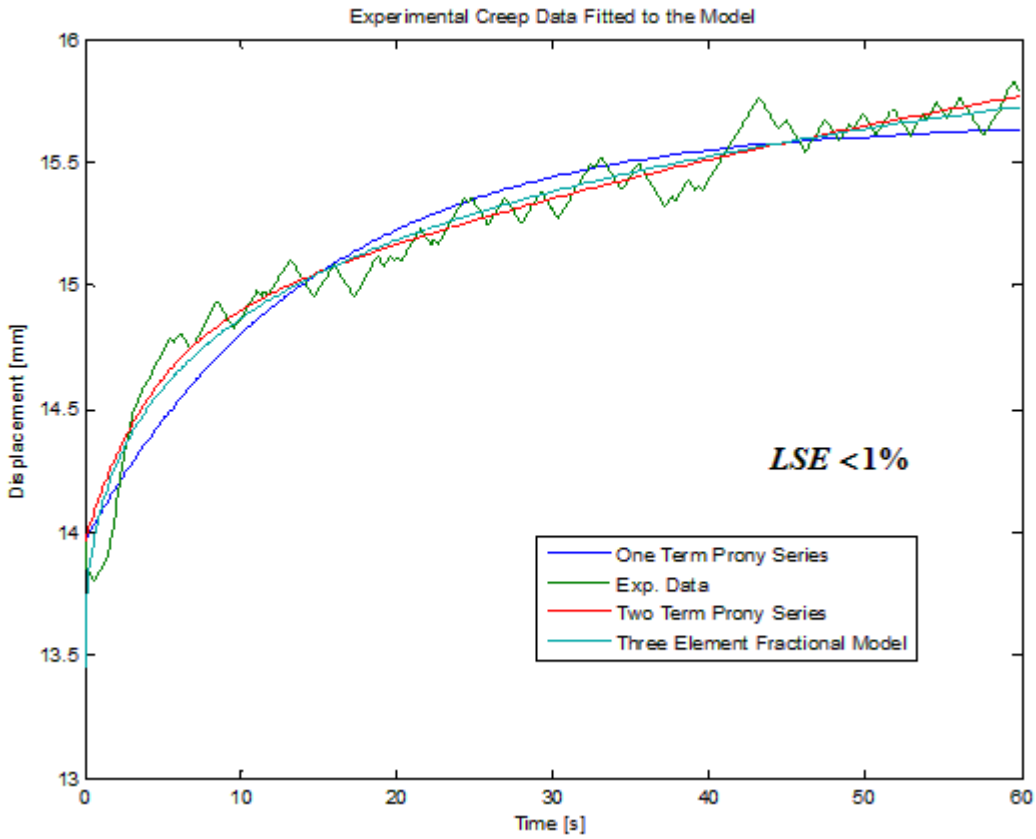

Figure 3.17 Curve-fit to Creep Test Data

The parameters for the three material models identified for the creep data curve-fit are presented in Table 3.2.

Table 3.2 Material Parameters Identified for The Material Models

FOV Zener Model Parameters	**Value**	**Unit**	**One & Two-Term Prony Series Parameters**	**Value**	**Value**	**Unit**
E_1	0.0566	MPa	α_1	0.1335	0.1215	-
E_2	0.0177	MPa	τ_1	18.7864	14.6465	s
η	4.9661	$MPa \cdot s$	α_2	0.0552		-
β	0.4392	-	τ_2	4.1610		s
LSE	0.0195	%	LSE	0.0290	0.0312	%

While carrying on the comparison between the Prony series representation and FOV model fit, increasing the number of terms in the Prony series representation yields more accuracy, increasing the number of elements or parameters in FOV models could possibly cause raised mathematical complexity due to the Mittag-Leffler function which is cumbersome to deal with. This comes out as the pay-off related to the FOV models.

To fit the material model formulated to the relaxation experiment data needs the parameters of the model to be extracted. The three-element fractional order Zener model has two different representations. The parameters extracted are according to the viscoelastic spring-dashpot model where a spring is in parallel with the Maxwell element. However for the one-term Prony series representation the viscoelastic spring-dashpot model is in the form of a spring in series with a Kelvin-Voigt element. Therefore new parameters should be obtained to fit the fractional order viscoelastic material model to the same relaxation experiment data. This parameter extraction procedure was performed manually by modifying the parameters. The two graphs representing the two configurations of the spring-dashpot material model should overlap, which means the models formulated with the idenfied parameters fit the experimental data. A new MATLAB® code is prepared for this purpose which

can also be found in the Appendix C. The extracted parameters are presented in Table 3.3.

Table 3.3 Material Parameters Obtained for Fractional Zener Model

Parameter	**Value**	**Unit**
E_1	10.9634	MPa
E_2	32.8377	MPa
η	2.1947	$MPa \cdot s$
β	0.5800	-
LSE	0.0353	%

After the parameters are extracted for two representations, the graph was plotted for both representations of the fractional Zener model with the experimental data as well. The same graph with different parameters fitted to the relaxation experimental data was obtained is presented in Figure 3.18. The two graphs perfectly fit the experimental data with the LSE being less than 1%.

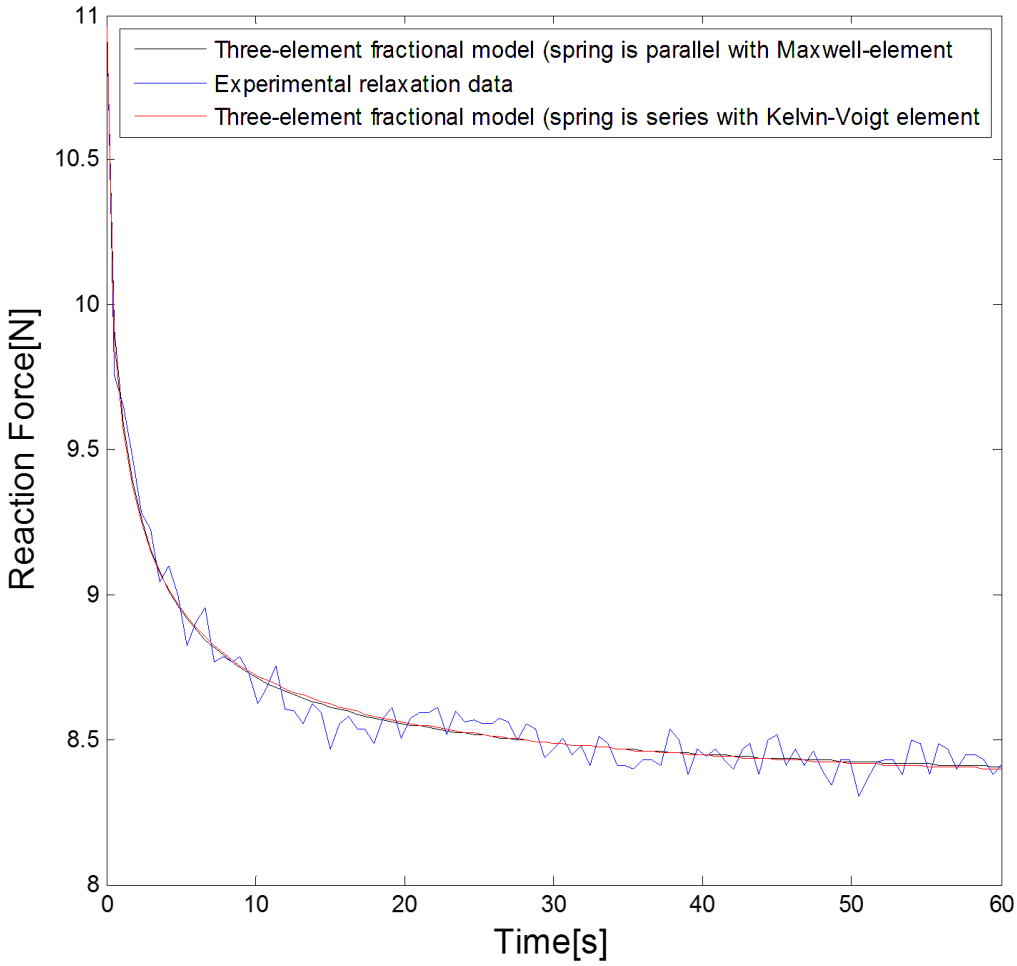

Figure 3.18 Curve-fit to Relaxation Test Data
(for Two Configurations of the Model)

To sum-up, the advantages of generalization to any real-order derivative allows one to,

- describe the complex material models accurately with less number of parameters
- improve the curve-fitting sensitivity
- provide physical justification in rheological situations and
- represent hierarchical, fractal-like structures.

M-files written in MATLAB® related to this curve-fit are provided in Appendix C.

3.4 Fractional Order Calculus Applied to Fung's Quasi-Linear Viscoelasticity Theory

For small deformations, linear theory of viscoelasticity applies well on soft biological tissues. However for finite deformations, the nonlinear stress-strain characteristics and time and history dependent viscoelastic behavior of living tissues are given by a special theory of Fung called the quasi-linear viscoelastic approach. In quasi-linear viscoelasticity (QLV) theory (Fung, 1993) the relaxation function is defined as the product of a reduced relaxation function and a nonlinear elastic response, where the reduced relaxation function is a function of only time, and the elastic response is a function of strain only. Therefore a separable non-linear viscoelasticity kernel exists and by using the superposition principle, stress function is formulated due to the strain applied. The separable stress function is given as the convolution of reduced relaxation function and instantaneous elastic response,

$$\sigma\left(\varepsilon(t),t\right)=G(t)*\sigma^{(e)}(\varepsilon) \tag{3.38}$$

and by applying the superposition principle at time t where $t>\tau$,

$$\sigma\left(\varepsilon(t),t\right)=\int_{-\infty}^{t} G(t-\tau)\frac{\partial\sigma^{e}\left[\varepsilon(t)\right]}{\partial\varepsilon}\frac{\partial\varepsilon}{\partial\tau}d\tau \tag{3.39}$$

When the motion starts at $t=0$, the relaxation function becomes,

$$\sigma\left(\varepsilon(t),t\right)=\int_{0}^{t} G(t-\tau)\frac{\partial\sigma^{(e)}\left[\varepsilon(t-\tau)\right]}{\partial\varepsilon}\frac{\partial\varepsilon}{\partial\tau}d\tau \tag{3.40}$$

where $\varepsilon(t)$ is the time-dependent strain, $\sigma^{(e)}\left[\varepsilon(t)\right]$ is the instantaneous nonlinear elastic response, $\frac{\partial\varepsilon}{\partial\tau}$ is the strain history and $G(t)$ is the monotonically decreasing reduced relaxation function.

Thus the stress at any time t is equal to the instantaneous stress response decreased by an amount depending on the past history and the stress at time t is the sum of the contributions of all the past changes, each governed by the same reduced relaxation function. This equation represents a "hereditary integral" and the stress at any time depends on all that has happened before, on the entire stress history. The lower limit of integration is written as $-\infty$ which means that the integration is taken before the very beginning of the motion. One can assume that t starts at 0 instead of negative infinity to represent the experimental situation which is stress and strain free at $t = 0$. QLV model uses a continuous spectrum reduced relaxation function, implying an infinite number of Zener models connected in series as in Figure 3.19.

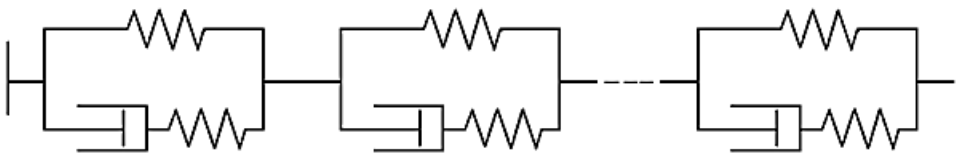

Figure 3.19 Zener model connected in series

Fung (1993) has suggested applying a reduced relaxation function in the form below,

$$G(t) = \frac{1 + c\left[E\left(\frac{t}{\tau_2}\right) - E\left(\frac{t}{\tau_1}\right)\right]}{1 + c\ln\left(\frac{\tau_2}{\tau_1}\right)} \tag{3.41}$$

where $E(y_1) = \int_{y_1}^{\infty} \frac{e^{-y}}{y} dy \begin{cases} y = \frac{t}{\tau} \\ y_1 = \frac{t}{\tau_1} \end{cases}$ is the first exponential integral, c is the dimensionless positive constant which determines the degree of the viscoelasticity of

the material, τ_1 and τ_2 are the short and long term viscoelastic time constants, respectively. Taking the partial derivative of reduced relaxation function yields,

$$\frac{\partial G(t)}{\partial t} = \frac{c}{t}\left(\frac{e^{-t/\tau_2} - e^{-t/\tau_1}}{1 + c\ln(\tau_2/\tau_1)}\right) \tag{3.42}$$

The parameters of this reduced relaxation function can be difficult to estimate and show low sensitivity during the adaptation processes (D. Craiem et al., 2008), (Craiem D. , Rojo, Atienza, Armentano, & Guinea, 2008).

It is emphasized that the QLV model can be represented by a number of Zener solids connected in series, while FOV-QLV can be represented by a fractal-type tree model where depth and branching of the tree depends on the so-called "*order of evolution*" β (Doehring, Freed, Carew, & Vesely, 2005) as presented in Figure 3.20.

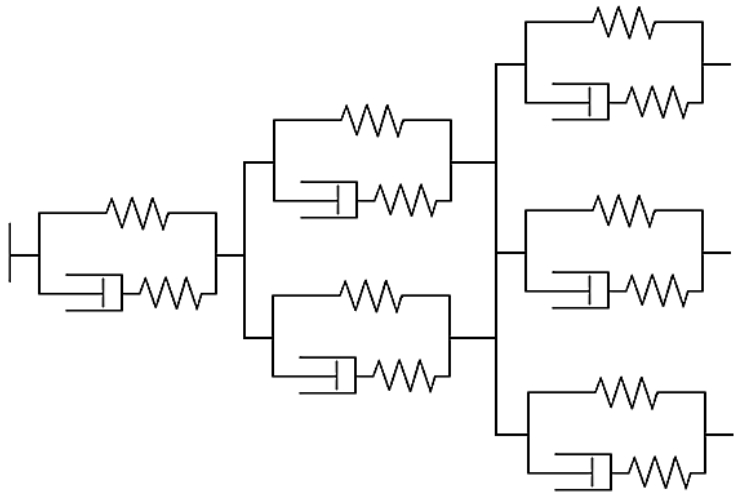

Figure 3.20 Fractal-type tree model representing FOV-QLV model
(Adopted from (Doehring, Freed, Carew, & Vesely, 2005)

An exponential approximation or a power law can be chosen to describe the instantaneous nonlinear elastic response. The exponential approximation might be,

$$\sigma^{(e)}(\varepsilon) = A\left(e^{B\varepsilon} - 1\right) \tag{3.43}$$

and the constants A and B are to be found by fitting the experimental data. A power law equation which is offered by (Doehring, Freed, Carew, & Vesely, 2005) might be,

$$\sigma^{(e)}(\varepsilon) = A\varepsilon^{B} \tag{3.44}$$

where the constants A and B are to be determined by fitting to the experimental data as well.

In FOV formulation of the QLV theory, the reduced relaxation function suggested by Fung is replaced by a function containing the Mittag-Leffler function (Doehring, Freed, Carew, & Vesely, 2005), (Craiem D. , Rojo, Atienza, Armentano, & Guinea, 2008). The relaxation function defined for the FOV solid (FOV-SLS) in Doehring et al., (2005) is,

$$G(t) = \left(\frac{\tau}{\rho}\right)^{\beta} + \left(1 - \left(\frac{\tau}{\rho}\right)^{\beta}\right) E_{\beta,1}\left(-\left[\frac{t}{\tau}\right]^{\beta}\right) \tag{3.45}$$

where τ and ρ are the characteristic short-term relaxation and long-term creep time constants. Its partial derivative is,

$$\frac{\partial G(t)}{\partial t} = \frac{-1}{\tau}\left(1 - \left(\frac{\tau}{\rho}\right)^{\beta}\right) E_{\beta,0}\left(-\left[\frac{t}{\tau}\right]^{\beta}\right) \tag{3.46}$$

The derivative in Equation 3.46 can also be verified in (Podlubny I. , 1999, pg. 22).

In the work of Craiem et al., (2008) a reduced relaxation function based on fractional order modified Voigt model is defined to replace the Fung's reduced relaxation function. The relaxation function must be a continuously varying decreasing function.

Considering the fractional order Voigt model (1st case), the reduced relaxation function becomes,

$$G(t) = E + F\frac{t^{-\beta}}{\Gamma(1-\beta)} \tag{3.47}$$

and considering the fractional order Zener model (2nd case) the reduced relaxation function in notation of this work becomes,

$$G(t) = E_1 + E_2\left\{E_\beta\left(-\left[\frac{t}{\rho}\right]^\beta\right)\right\} \tag{3.48}$$

where $\rho = E_2/\eta$.

The power law relation for simulating the instantaneous elastic response and the Kelvin-Voigt fractional viscoelastic model for the reduced relaxation function are to be substituted into the stress-strain relation of Fung in this part. After, the unknown material parameters are to be identified by curve-fitting to the experimental data.

FOV-QLV theory is implemented for a ramp strain function which means, strain increases linearly up to a specified time, t_0 , and then strain remains constant until the end of the total time as in Figure 3.21.

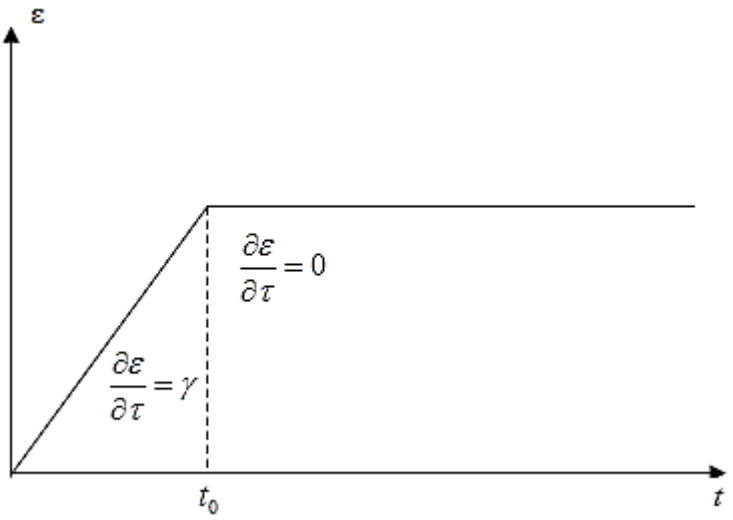

Figure 3.21 Ramp Strain Function

Therefore, the stress relaxation function has two phases: first one is the ramp phase, the other one is the step phase. Curve-fitting is performed separately for these two phases. The stress relaxation function for the ramp phase is defined as (here t indicates the time before t_0),

$$\sigma\left(0 \le t < t_0\right) = \int_0^t G\left(t-\tau\right) AB\left(\gamma\tau\right)^{B-1} \gamma d\tau \tag{3.49}$$

and the stress response from t_0 to the end of the experiment involves stress history from zero to t_0 plus the stress history from t_0 to the end of the experiment as shown as an integral below,

$$\sigma\left(t \ge t_0\right) = \int_0^{t_0} G\left(t-\tau\right) AB\left(\gamma\tau\right)^{B-1} \gamma d\tau + \int_{t_0}^{t} G\left(t-\tau\right) AB\left(\gamma\tau\right)^{B-1} \left(0\right) d\tau \tag{3.50}$$

where the second integral term drops due to zero slope (constant strain state). Here γ is the strain rate chosen during the experimentation and t_0 is also specified by observing the experiment data.

For the first case the relaxation function for the specified time intervals is,

$$\sigma\left(0 \le t < t_0\right) = \int_0^t \left(E + F \frac{\left(t-\tau\right)^{-\beta}}{\Gamma\left(1-\beta\right)} \right) AB\left(\gamma\tau\right)^{B-1} \gamma d\tau \tag{3.51}$$

$$\sigma\left(t \ge t_0\right) = \int_0^{t_0} \left(E + F \frac{\left(t-\tau\right)^{-\beta}}{\Gamma\left(1-\beta\right)} \right) AB\left(\gamma\tau\right)^{B-1} \gamma d\tau \tag{3.52}$$

and the unknown parameters are $A, B, E, F, \beta, \gamma$.

For the second case the relaxation function for the specified time intervals is,

$$\sigma\left(0 \le t < t_0\right) = \int_0^t \left(E_1 + E_2 \left\{ E_\beta \left(-\left[\frac{t-\tau}{\rho} \right]^\beta \right) \right\} \right) AB\left(\gamma\tau\right)^{B-1} \gamma d\tau \tag{3.53}$$

$$\sigma\left(t \ge t_0\right) = \int_0^t \left(E_1 + E_2 \left\{ E_\beta \left(-\left[\frac{t-\tau}{\rho} \right]^\beta \right) \right\} \right) AB\left(\gamma\tau\right)^{B-1} \gamma d\tau \tag{3.54}$$

and the unknown parameters are $A, B, E_1, E_2, \rho, \beta, \gamma$.

Experimental data for parameter identification was obtained from (Petekkaya, 2008). The actual relaxation experiment data is shown below. This data was obtained by 4 mm/s indentation rate and approximately 14 mm of indentation of the tissue.

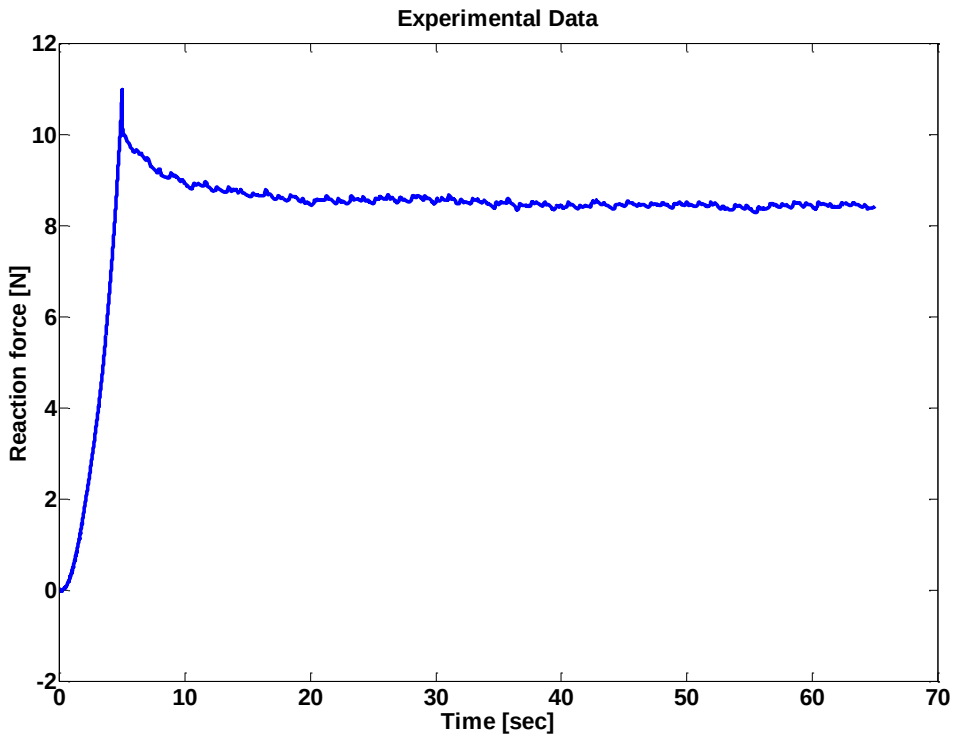

Figure 3.22 Raw Relaxation Experiment Data

A manual parameter search was done. One result is shown in Figure 3.23. The parameters identified were,

$$A = 1,\ B = 2,\ E = 1.1,\ F = 1.05,\ \beta = 0.24,\ \gamma = 0.47\,.$$

The Matlab code is provided in the Appendix C.

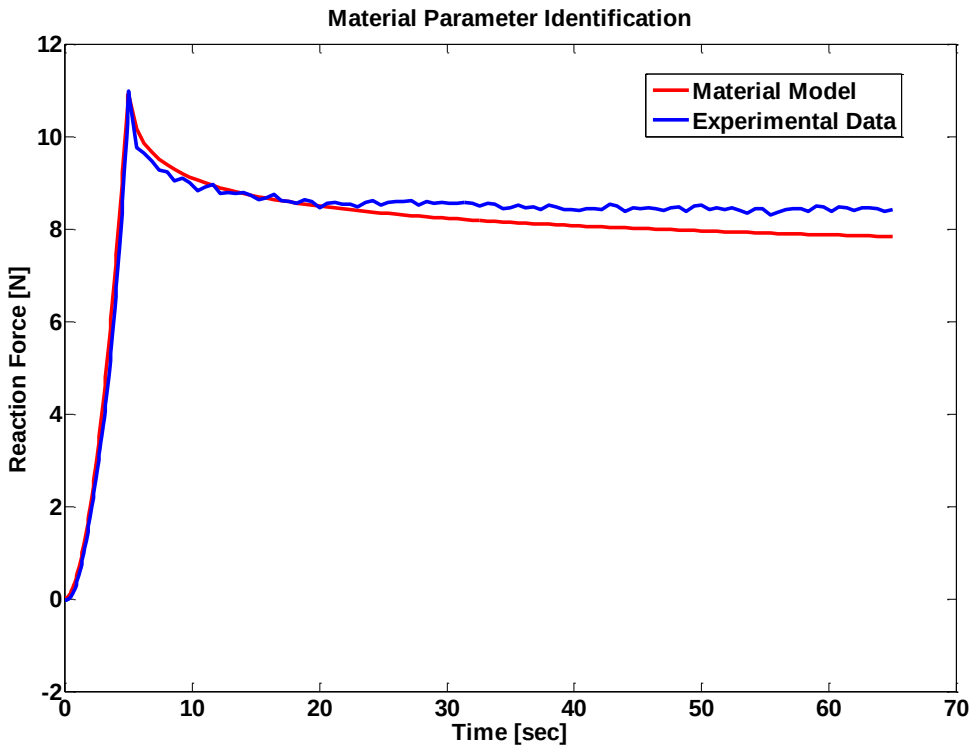

Figure 3.23 Fractional Order QLV Model Fitted to Relaxation Test Data (1)

However, Matlab® optimization toolbox can also be used to determine the material parameters that fit to the experimental data. For this purpose Matlab® "*lsqcurvefit*" function is employed. The parameters obtained are,

$$A = 1.3331,\ B = 2.0543,\ E = 1.0720,\ F = 0.9881,\ \beta = 0.1325,\ \gamma = 0.3875$$

and the fit is presented in Figure 3.24.

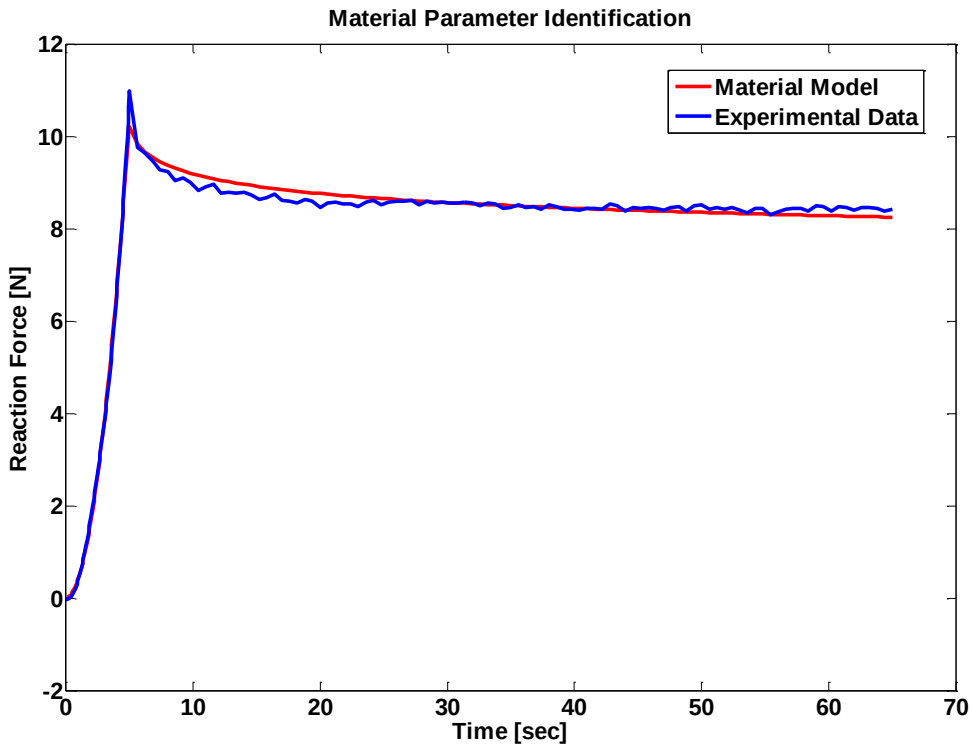

Figure 3.24 Fractional Order QLV Model Fitted to Relaxation Test Data (2)

CHAPTER 4

THREE-DIMENSIONAL FRACTIONAL ORDER CONSTITUTIVE EQUATION FOR SOFT BIOLOGICAL TISSUES

4.1 Constitutive Equation

The aim of this section is to extend the one-dimensional fractional order viscoelastic (FOV) material models introduced into their three-dimensional equivalents for a finite deformation regime in time domain.

In the work of Tönük and Silver-Thorn (2004), an extended James-Green-Simpson material formulation is used to characterize the bulk soft tissue creep and relaxation behavior. An appropriate set of nonlinear viscoelastic material coefficients is obtained by using inverse finite element techniques. The material formulation chosen (James-Green-Simpson instantaneous elastic and two terms Prony series time dependent) is type of a phenomenological formulation where the tissue is assumed as bulk tissue and the structural and microscopic effects related to the tissue behavior are underestimated. The parameters to be obtained from the material formulation give clues related to physical interpretation at the macroscopic level. Estimation of structural and micro-structural parameters require more extensive experimental set-up designs therefore phenomenological material modeling requiring less complicated experimental set-up is preferred for soft bulk tissue behavior simulation.

One of the best known approaches to the elasticity of bodies capable of finite deformation is to postulate the form of an elastic potential, or strain energy function W (the work that must be done on unit volume of the material in the reference state to deform it to the current state) (Fung, 1993).

In the paper of James-Green and Simpson (1975) two analytic forms of the strain energy function for isotropic and incompressible materials are suggested which involve five or nine material constants. Strain energy function which is also called as

the elastic potential energy function is a measure of the energy stored in volume of the material as a result of deformation (Ogden R. W., 1984).

Treloar, (1949) points out that the process of modifying or correcting a strain energy function to suit a set of data is nothing more than the "*three-dimensional analogue of simple curve-fitting*". Any phenomenological strain energy function is a convenient mathematical representation and no meaning should be attached to the numerical constants over and above that of simple regression coefficients (James, Green, & Simpson, 1975).

If a body is for example elastically isotropic, the strain energy function must be a function of the strain invariants of either left or right Cauchy deformation tensors. Well known examples are Mooney (1940), Rivlin (1947) and Rivlin (1965) material models.

The general mathematical theory of large deformation isotropic elasticity was developed by Rivlin in a series of papers (Rivlin R. S., 1948). Sahay in 1984 examined the suitability of various strain energy functions reported in the literature. The strain energy functions which are widely discussed and quoted in the literature are tabulated in the paper.

When a body is perfectly elastic, an elastic potential or strain energy function W exists, measured per unit volume of the undeformed body and the material is called "*hyperelastic"* or *"Green Elastic"* when there exists a strain-energy function for the material, which is a scalar function of one of the strain and deformation tensors whose derivative with respect to a strain component determines the corresponding stress component (Malvern, 1969) such that,

$$S_{ij} = \frac{\partial W(E)}{\partial E_{ij}} = 2\frac{\partial W(C)}{\partial C_{ij}} \tag{4.1}$$

where

$W(E)$ is the strain energy per unit undeformed volume

E is the Green-Lagrange finite strain tensor

C is the symmetric right Cauchy-Green deformation tensor

S is the symmetric second Piola-Kirchoff stress tensor

$i, j = 1, 2, 3$ for a three dimensional problem

The general constitutive equation for incompressible hyperelastic materials is (Holzapfel, 2000),

$$W = W(F) - p(J - 1) \tag{4.2}$$

where $J = \det(F)$ and F is the deformation gradient tensor. p serves as an indeterminate *Lagrange multiplier* which can be identified as "hydrostatic pressure". Differentiating with respect to the deformation gradient yields the general constitutive equation for the first Piola-Kirchoff stress tensor P which in general is not symmetric,

$$P = -pF^{-T} + \frac{\partial W(F)}{\partial F} \tag{4.3}$$

Premultiplying with F^{-1} provides the second Piola-Kirchoff stress tensor S which is a symmetric tensor,

$$S = -pF^{-1}F^{T} + F^{-1}\frac{\partial W(F)}{\partial F} = -pC^{-1} + 2\frac{\partial W(C)}{\partial C} \tag{4.4}$$

When a body is deformed, the elastic strain energy W may be expressed in terms of the strain invariants of Green-Lagrange finite strain tensor I_1, I_2 and I_3 for isotropic materials (James, Green, and Simpson, 1975),

$$W = \sum_{i,j,k=0}^{\infty} C_{ijk}(I_1 - 3)^i (I_2 - 3)^j (I_3 - 1)^k \tag{4.5}$$

where

$I_1 = \lambda_i^2 + \lambda_j^2 + \lambda_k^2$ (Trace of the strain tensor, C_{ii})

$I_2 = \lambda_i^2\lambda_j^2 + \lambda_j^2\lambda_k^2 + \lambda_k^2\lambda_i^2 \ldots$ (Cofactor trace of the strain tensor, $\frac{1}{2}\left(I_1^2 - C_{ij}C_{ij}\right)$)

$I_3 = \lambda_i^2\lambda_j^2\lambda_k^2$ (Determinant of the strain tensor, $det(C)$)

and C_{ijk} are material parameter constants and $i, j, k = 1, 2, 3$.

The finite strain tensor in terms of the principal stretches for general homogeneous deformation is defined as,

$$\gamma = \begin{bmatrix} \lambda_i^2 & 0 & 0 \\ 0 & \lambda_j^2 & 0 \\ 0 & 0 & \lambda_k^2 \end{bmatrix} \tag{4.6}$$

The incompressibility condition requires $\lambda_1\lambda_2\lambda_3 = 1$ and $I_3 = 1$. For incompressible materials the strain energy density function defined above reduces to,

$$W = \sum_{i,j=0}^{\infty} C_{ij}\left(I_1 - 3\right)^i\left(I_2 - 3\right)^j \ldots \tag{4.7}$$

which expands as,

$$W = C_{10}\left(I_1 - 3\right) + C_{01}\left(I_2 - 3\right) + C_{11}\left(I_1 - 3\right)\left(I_2 - 3\right) + C_{20}\left(I_1 - 3\right)^2 + C_{02}\left(I_2 - 3\right)^2 \ldots \text{etc.}$$

(The term C_{00} is always taken to be zero while for the stress free reference configuration strain energy is zero.)

Third order (including up to third order terms in $\left(I_1 - 3\right)$ and $\left(I_2 - 3\right)$) strain energy density function per unit volume which gives us the nine-parameter James-Green-Simpson material formulation is,

$$
\begin{aligned}
W &= C_{10}\left(I_1-3\right)+C_{01}\left(I_2-3\right)+C_{11}\left(I_1-3\right)\left(I_2-3\right) \\
&+C_{20}\left(I_1-3\right)^2+C_{02}\left(I_2-3\right)^2+C_{21}\left(I_1-3\right)^2\left(I_2-3\right)+C_{12}\left(I_1-3\right)\left(I_2-3\right)^2 \\
&+C_{30}\left(I_1-3\right)^3+C_{03}\left(I_2-3\right)^3
\end{aligned}
\tag{4.8}
$$

It is also possible to choose terms out of the expansion of W such that only certain orders of deformation are included (deformation approximation). Then the third order (five parameters) expansion becomes,

$$
\begin{aligned}
W &= C_{10}\left(I_1-3\right)+C_{01}\left(I_2-3\right)+C_{11}\left(I_1-3\right)\left(I_2-3\right) \\
&+C_{20}\left(I_1-3\right)^2+C_{30}\left(I_1-3\right)^3
\end{aligned}
\tag{4.9}
$$

The equation above represents an incompressible, isotropic (in undeformed configuration), homogeneous, hyperelastic material where the strain energy density function is defined in terms of the strain invariants. The strain invariants in terms of principal stretch ratios are,

$$
\begin{aligned}
I_1 &= \lambda_1^2+\lambda_2^2+\lambda_3^2 \\
I_2 &= \lambda_1^2\lambda_3^2+\lambda_2^2\lambda_3^2+\lambda_1^2\lambda_2^2 \equiv \frac{1}{\lambda_1^2}+\frac{1}{\lambda_2^2}+\frac{1}{\lambda_3^2} \\
I_3 &= \lambda_1^2\lambda_2^2\lambda_3^2
\end{aligned}
\tag{4.10}
$$

Then the strain energy density function in terms of principal stretch ratios becomes,

$$
\begin{aligned}
W &= C_{10}\left(\lambda_1^2+\lambda_2^2+\lambda_3^2-3\right)+C_{01}\left(\lambda_1^2\lambda_3^2+\lambda_2^2\lambda_3^2+\lambda_1^2\lambda_2^2-3\right) \\
&+C_{11}\left(\lambda_1^2+\lambda_2^2+\lambda_3^2-3\right)\left(\lambda_1^2\lambda_3^2+\lambda_2^2\lambda_3^2+\lambda_1^2\lambda_2^2-3\right) \\
&+C_{20}\left(\lambda_1^2+\lambda_2^2+\lambda_3^2-3\right)^2+C_{30}\left(\lambda_1^2+\lambda_2^2+\lambda_3^2-3\right)^3
\end{aligned}
\tag{4.11}
$$

Introduction of a large number of material constants into the model to describe soft biological tissues does make the model more sophisticated and also it makes the model validation more and more difficult especially in the case of soft tissues (Sahay, 1984).

Throughout these formulations, it is supposed that the temperature remains constant (isothermal mechanical behavior) and the strain energy function depends only on the terminal states of strain and not on the history of straining (Ogden R. W., 1972).

Because of the high resistance to the volume changes compared to the resistance to the shear distortions in the rubber-like materials, it is more convenient in numerical simulations to split the strain energy function defined into a volumetric and a deviatoric part for incompressible and nearly incompressible materials (Liu & Choudhry, 2004).

The elastic and inelastic properties of a certain material often exhibit different behavior with respect to volumetric and deviatoric deformations. This requires the additive split of the strain energy function in terms of principal strain invariants,

$$\Psi = U\left(J\right) + W\left(\bar{I}_1, \bar{I}_2\right) \tag{4.12}$$

and in terms of the principal stretch ratios,

$$\Psi = U\left(J\right) + W\left(\bar{\lambda}_1, \bar{\lambda}_2, \bar{\lambda}_3\right) \tag{4.13}$$

The deviatoric parts of the invariants and principal stretches are defined in terms of the determinant of the deformation gradient tensor $J = \det\left(F\right)$. The determinant of the deformation gradient tensor is equal to unity for totally incompressible materials. However, for nearly incompressible materials, it depends on the Jacobian (determinant of the deformation gradient tensor). The deviatoric strain and stretches in terms of the Jacobian are defined as

$\bar{I}_1 = J^{-2/3} I_1,\ \bar{I}_2 = J^{-4/3} I_2$ and $\bar{\lambda}_i = J^{-1/3} \lambda_i,\ \left(i = 1, 2, 3\right)$ respectively.

Therefore, it is the user's decision, whether assuming the tissue model as nearly incompressible or totally incompressible. In this sense, it was decided to take model soft biological tissues as nearly incompressible, while the bulk modulus taken a finite

(but rather large) value and does not tend to infinity as it is the case for totally incompressible materials. For infinitesimal strain conditions the sum of the material constants C_{01} and C_{10} has a physical meaning as the one half of the shear modulus.

The bulk modulus was taken as 5000 times the initial shear modulus and is calculated with the simple relation,

$$K = 5000 * \mu = 5000 * 2 * \left(C_{01} + C_{10} \right) \tag{4.14}$$

where

K : bulk modulus

μ : shear modulus

C_{01} & C_{10} : instantaneous nonlinear elastic material parameters (tangent modulus around zero strain)

The bulk modulus is assumed to be independent of the material deformation and is set as a constant. As the bulk modulus is set constant throughout the deformation and the stiffness of the material increases with the deformation, a deformation dependent volume preserving behavior is observed for nearly incompressible tissues.

As linear elastic material formulations are not able to simulate the observed nonlinear material behavior of soft tissues, nonlinear elastic material formulations are also not able to simulate the time-dependent viscoelastic phenomena such as creep, relaxation and hysteresis during cyclic-loading. Therefore the same nonlinear material formulation should be extended in a form such that the viscoelastic properties are included in the formulation.

In the paper Vannah, S. et. al. (1996), in order to estimate the material stiffness, indentations were modeled using the James-Green-Simpson strain energy function. The James-Green-Simpson potential function is written in terms of the principal stretch ratios (deformed length/original length) and the stress is obtained. By employing a “multiple regression” method material parameters are obtained by

curve-fitting to the experimental data. The same procedure will be applied here in order to extract the material parameters.

A time-dependent strain energy function could be defined as a nonlinear elastic strain energy function multiplied with a time-dependent stress relaxation function (as stress is obtained from strain) or a time dependent creep compliance (when strain is obtained from stress). This is given as,

$$W(C,t) = \widehat{W}(C)G(t) \tag{4.15}$$

Tönük and Silver-Thorn (2004), proposed a time-dependent strain energy density $W(t)$ in relaxation form such that,

$$W(t) = W_0\left[1-\delta_1\left(1-e^{(-t/\tau_1)}\right)-\delta_2\left(1-e^{(-t/\tau_2)}\right)\right] \tag{4.16}$$

where the term in brackets is the constitutive equation of the generalized Kelvin-Voigt linear viscoelastic material model (two terms Prony series representation) and W_0 is the instantaneous (glassy) strain energy density. δ_1 is the short-term relaxation magnitude and τ_1 is the corresponding time constant, δ_2 is the long-term relaxation magnitude and τ_2 is the corresponding time constant.

It was shown in the previous section that one-dimensional fractional order constitutive equations with less parameters fit better to the experimental data compared to integer-order constitutive equations. It has been showed that, three-element fractional order viscoelastic model (fractional order Zener model) fits to the experimental data better compared to two term Prony series representation. Therefore a modification to the above formulation is suggested such that, three- element fractional order relaxation function should be used instead of two term Prony series representation.

Therefore the proposed time-dependent strain energy density formulation becomes,

$$W(t) = W_0 E_1 \left\{ 1 - \frac{E_1/E_2}{1+E_1/E_2} \left\{ 1 - E_\beta \left[-\left(\frac{t}{\tau} \right)^\beta \right] \right\} \right\} \tag{4.17}$$

where

$$W_0 = C_{10}(I_1 - 3) + C_{01}(I_2 - 3) + C_{11}(I_1 - 3)(I_2 - 3) + C_{20}(I_1 - 3)^2 + C_{30}(I_1 - 3)^3$$

and

$$\tau = \frac{\eta}{\sqrt[\beta]{1 + E_1/E_2}}.$$

Under axisymmetric loading conditions the two independent invariants of the strain tensor are dependent for an incompressible material. As $I_1 = I_2$, the five parameter James-Green-Simpson material model can be simplified to three parameter equivalent formulation for axisymmetry such that,

$$W_0 = C_1(I - 3) + C_2(I - 3)^2 + C_3(I - 3)^3 \tag{4.18}$$

where

$$C_1 = C_{10} + C_{01}$$
$$C_2 = C_{11} + C_{20}$$
$$C_3 = C_{30}.$$

W_0 represents the nonlinear-elastic response of the tissue due to instantaneous loading. In an elastic material, under purely mechanical theory, deformation is not accompanied by any dissipation of mechanical energy and all energy expended in deformation is stored in the body and can be recovered upon unloading (Belytschko, Liu, & Moran, 2001). Other behaviors of elastic materials are path independence and reversibility. However, for viscoelastic materials, mechanical energy dissipation occurs under loading and unloading.

The final material formulation developed is the nonlinear, 3-D generalization of the 1-D fractional order three-element linear viscoelastic Zener material model and named as extended generalized fractional order James-Green-Simpson material model.

Simplifying the material parameters and making the equation resemble the one-term Prony series representation yields,

$$W(t) = W_0 \left\{ 1 - \delta \left\{ 1 - E_\beta \left[-\left(\frac{t}{\tau} \right)^\beta \right] \right\} \right\} \tag{4.19}$$

where

$$\delta = \frac{\mathrm{E}_1/\mathrm{E}_2}{1+\mathrm{E}_1/\mathrm{E}_2}, \tau = \frac{\eta}{\sqrt[\beta]{1+E_1/E_2}} \text{ and}$$

$$W_0 = C_{10}(I_1-3) + C_{01}(I_2-3) + C_{11}(I_1-3)(I_2-3) + C_{20}(I_1-3)^2 + C_{30}(I_1-3)^3$$

The total number of parameters becomes nine (5 nonlinear elastic parameters and 4 viscoelastic parameters for three elements) which is less than the number of parameters used in the two-term Prony representation which has ten parameters (five nonlinear elastic parameters and five viscoelastic parameters for every element). One can therefore conclude that by introducing fractional order derivative operators in constitutive relations the number parameters to be extracted are reduced.

4.2 Implementation of the Material Model into Msc.Marc 2010 Software

The capability to model viscoelastic material governed by fractional order constitutive equations in FEA software is so far very limited. Few examples can be, (Padovan, 1987), (Enelund, Maehler, Runesson, & Joseffson, 1999) and (Schmidt & Gaul, 2002). Although Padovan presented a 2-D and a simpler constitutive equation and Enelund et al., (1999) presented a more detailed solution algorithm.

After formulating the fractional order material model theoretically, it is to be implemented in the Msc.Marc software for practical applications and finite element simulations of real world problems of soft biological tissues. Implementation of a hyperelastic material model into the Msc.Marc 2010 software is rather easy and has examples in the literature. Liu and Choudhry in 2004 established a framework to implement generalized isotropic hyperelastic material models into MSC.Marc software. The model is implemented into the program by specifying the derivatives of the strain energy function in terms of either strain invariants or principal stretches.

Definition of the user's own hyperelastic material model into the program is a very useful and efficient procedure while most of the strain energy functions are of polynomial, logarithmic or exponential type. In addition, the rather complicated part, which is the derivation of second and fourth order unit tensors, is taken into account by the program.

A user-subroutine has to be written for the finite element implementation of this material model (Equation 4.19) into Msc. Marc 2010 software. Therefore a suitable numerical method should be provided for the finite element implementation of the Mittag-Leffler function appearing in the material model formulated.

For this purpose Freed and Diethelm (2002) proposed a scheme for fast computations of the Mittag-Leffler function which is especially suitable for finite element applications.

Specifically, it is defined in series when the argument is defined between the limits $[0, 0.1]$ and $[15, \infty]$ and in between these ranges a Padè approximate (or rational polynomial) is applied which is a simple optimization procedure to extract the coefficients of the polynomial. An order $[n/m]$ Padè approximant to a function is a ratio of two polynomials of degrees n and m that approximates the function. The well-known definition of the M-L function is employed for small time periods and the asymptotic expansion of the series is employed whenever the argument (normalized time) is greater than $x > 15$. The scheme for calculating the approximate M-L function is given in Equation 4.20.

$$E_{\beta}\left(-x^{\beta}\right) \approx \begin{cases} -\sum_{k=0}^{4} \frac{(-x)^{\beta k}}{\Gamma(1+\beta k)}, & 0 \le x \le 0.1 \\ \frac{a_0 + a_1 x + a_2 x^2}{1 + b_1 x + b_2 x^2 + b_3 x^3}, & 0.1 < x < 15 \\ -\sum_{k=0}^{4} \frac{(x)^{-\beta k}}{\Gamma(1-\beta k)}, & x \ge 15 \end{cases} \tag{4.20}$$

The coefficients $\left[a_o, a_1, a_2, b_1, b_2, b_3\right]$ are listed in the table given in the reference paper. The argument x is $\left[-\left(\frac{t}{\tau}\right)\right]$ which represents normalized time.

This approximate scheme is compared for each interval, to the exact value of the M-L function. The Matlab® code which is used for computing the exact value of the M-L function is written by Podlubny, I. (2009).

The approximation scheme for the Mittag-Leffler function is almost the same with the exact value of the function (Figures 4.1 to 4.3). Therefore it can be deduced that this approximation scheme could be employed in the user-subroutine.

The Matlab® code for the comparison of the approximate and exact Mittag-Leffler function is presented in Appendix C.

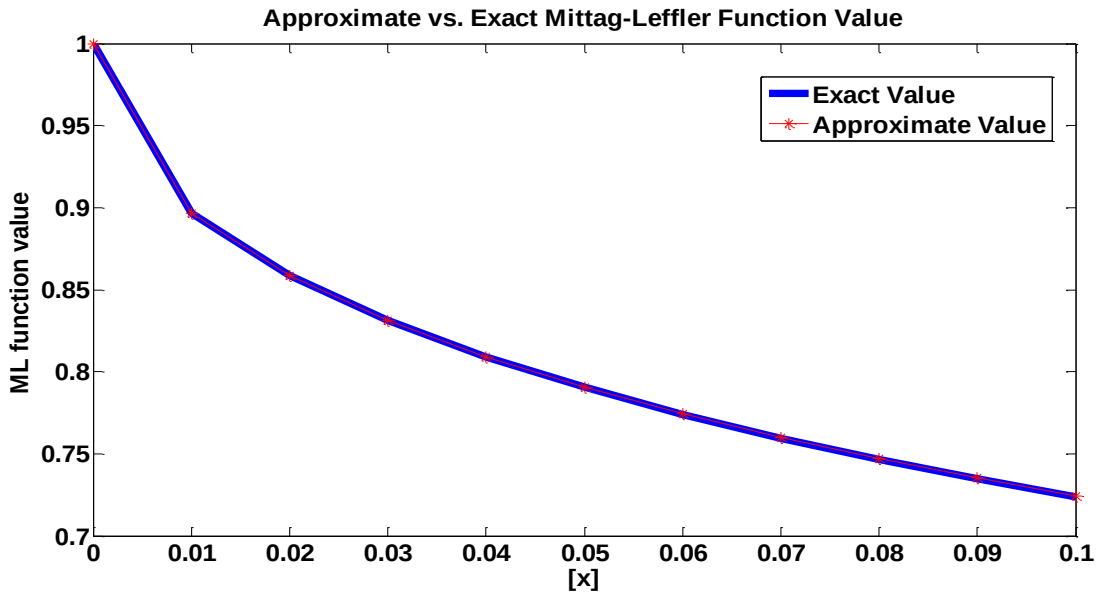

Figure 4.1 Approximate vs. exact Mittag-Leffler function in the range $[0, 0.1]$

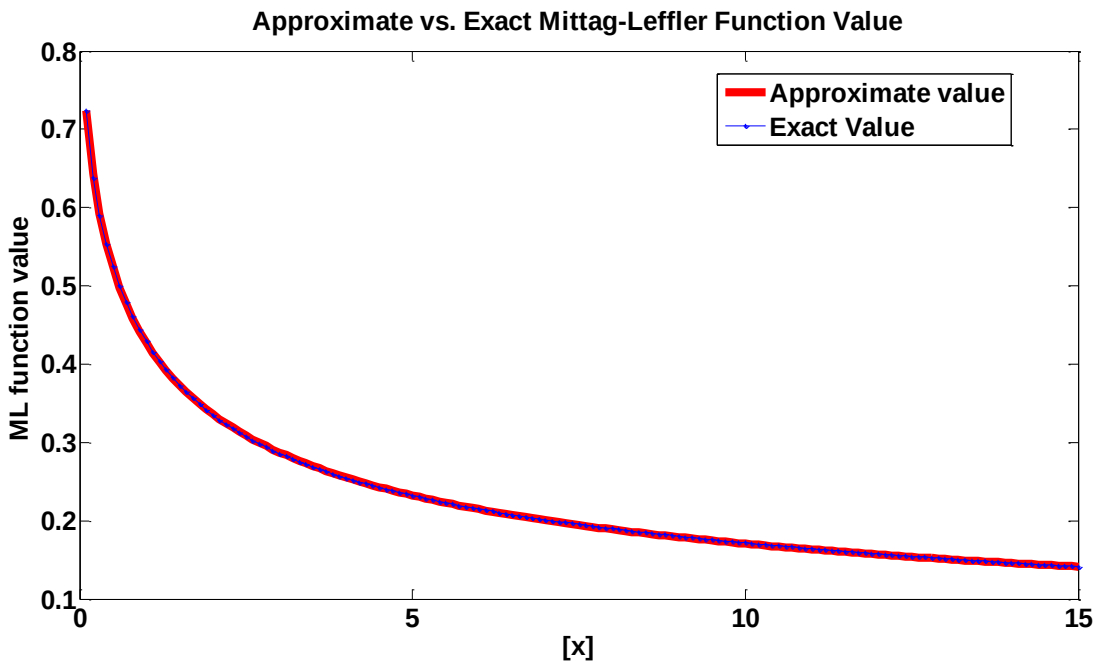

Figure 4.2 Approximate vs. exact Mittag-Leffler function in the range $(0.1, 15)$

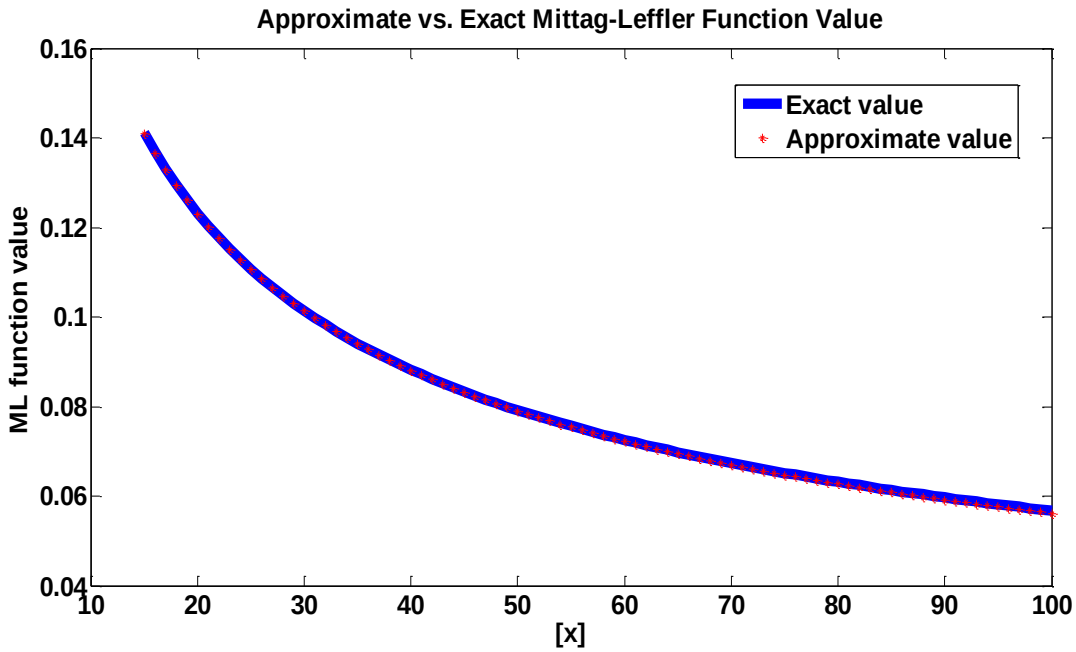

Figure 4.3 Approximate vs. exact Mittag-Leffler function in the range $[15,100]$

4.3 User-Subroutine "*UELASTOMER*"

The "*UELASTOMER*" user-subroutine available in Msc.MARC 2010 user-subroutine list was used to implement the material model formulated into finite element code.

This user-subroutine allows the user to define his/her own material model. For this user-subroutine only the deviatoric part of the strain energy function needs to be defined for rubber-like materials, as rubber-like materials are considered as nearly incompressible. The format of the user-subroutine is provided in Volume D of the Msc.Software documentation and can be found in the Appendix C as well.

The user-subroutine was written in Fortran 95 language.

According to the format of the user-subroutine, for the OGDEN model, only the strain energy function in terms of the principal stretches must be defined (deviatoric

part only). The bulk modulus however has to be defined through the interface under "material properties" Ogden model option.

The Ogden material model formulation is defined with respect to the eigenvalues of the right or left Cauchy-Green strain tensor. As the user-subroutine (*uelastomer*) developed was activated through Ogden model, the material model is to be re-defined to be compatible with the Ogden material model.

For this purpose, the strain energy function must be defined in terms of principal stretches (deviatoric part only). The principal strain invariants when defined in terms of the principal stretches are written as (deviatoric part only),

$$\begin{aligned} \bar{I}_1 &= \bar{\lambda}_1^2 + \bar{\lambda}_2^2 + \bar{\lambda}_3^2 \\ \bar{I}_2 &= \bar{\lambda}_1^2 \lambda_2^2 + \bar{\lambda}_2^2 \bar{\lambda}_3^2 + \bar{\lambda}_1^2 \bar{\lambda}_3^2 \\ \bar{I}_3 &= \bar{\lambda}_1^2 \bar{\lambda}_2^2 \bar{\lambda}_3^2 \end{aligned} \tag{4.21}$$

As the material is assumed to be nearly incompressible the third principal strain invariant is not needed.

The *uelastomer* user-subroutine (Msc.Marc/Mentat 2010 help Volume D, pg. 303) requires the first and second derivatives of the strain energy density function with respect to principal stretches (deviatoric part) as outputs in terms of the input variables.

The material model in terms of the principal stretches (deviatoric part only) becomes,

$$W(t) = W_0 \cdot G(t) \tag{4.22}$$

where

$$W_0 = C_{10}\left(\bar{\lambda}_1^2 + \bar{\lambda}_2^2 + \bar{\lambda}_3^2 - 3\right) + C_{01}\left(\bar{\lambda}_1^2\bar{\lambda}_2^2 + \bar{\lambda}_2^2\bar{\lambda}_3^2 + \bar{\lambda}_1^2\bar{\lambda}_3^2 - 3\right)$$
$$+C_{11}\left(\bar{\lambda}_1^2 + \bar{\lambda}_2^2 + \bar{\lambda}_3^2 - 3\right)\left(\bar{\lambda}_1^2\bar{\lambda}_2^2 + \bar{\lambda}_2^2\bar{\lambda}_3^2 + \bar{\lambda}_1^2\bar{\lambda}_3^2 - 3\right)$$
$$+C_{20}\left(\bar{\lambda}_1^2 + \bar{\lambda}_2^2 + \bar{\lambda}_3^2 - 3\right)^2 + C_{30}\left(\bar{\lambda}_1^2 + \bar{\lambda}_2^2 + \bar{\lambda}_3^2 - 3\right)^3$$

And

$$G(t) = \left\{1 - \delta\left(1 - E_\beta\left[-\left(\frac{t}{\tau}\right)^\beta\right]\right)\right\}$$

The necessary output relations that must be defined in the user-subroutine are; the first derivative of the strain energy function with respect to $\bar{\lambda}_1$, $\bar{\lambda}_2$ and $\bar{\lambda}_3$, the second derivative of the strain energy function with respect to $\bar{\lambda}_1$, $\bar{\lambda}_2$ and $\bar{\lambda}_3$, and finally the derivative of the strain energy function with respect to $\left(\bar{\lambda}_1\bar{\lambda}_2\right)$, $\left(\bar{\lambda}_2\bar{\lambda}_3\right)$ and $\left(\bar{\lambda}_1\bar{\lambda}_3\right)$.

The nomenclature for the user-subroutine variables is,

w0: Instantaneous strain energy function $\left(W_0\right)$

enerd: Time dependent material model $\left(W(t)\right)$

gt: Relaxation function $\left(G(t)\right)$

w1: Derivative of the time dependent material model with respect to the first deviatoric principal stretch $\left(\partial \mathrm{W}(\mathrm{t})/\partial\bar{\lambda}_1\right)$

w2: Derivative of the time dependent material model with respect to the second deviatoric principal stretch $\left(\partial \mathrm{W}(\mathrm{t})/\partial\bar{\lambda}_2\right)$

w3: Derivative of the time dependent material model with respect to the third deviatoric principal stretch $\left(\partial \mathrm{W}(\mathrm{t})/\partial\bar{\lambda}_3\right)$

w11: Second derivative of the time dependent material model with respect to the first deviatoric principal stretch $\left(\partial^2 \mathrm{W}(\mathrm{t})/\partial\bar{\lambda}_1^2\right)$

w22: Second derivative of the time dependent material model with respect to the

second deviatoric principal stretch $\left(\partial^2 \mathrm{W}(\mathrm{t})/\partial\bar{\lambda}_2^2\right)$

w33: Second derivative of the time dependent material model with respect to the third deviatoric principal stretch $\left(\partial^2 \mathrm{W}(\mathrm{t})/\partial\bar{\lambda}_3^2\right)$

w12: Second derivative of the time dependent material model with respect to the first and second deviatoric principal stretch $\left(\partial^2 \mathrm{W}(\mathrm{t})/\partial\bar{\lambda}_1\partial\bar{\lambda}_2\right)$

w23: Second derivative of the time dependent material model with respect to the second and third deviatoric principal stretch $\left(\partial^2 \mathrm{W}(\mathrm{t})/\partial\bar{\lambda}_2\partial\bar{\lambda}_3\right)$

w13: Second derivative of the time dependent material model with respect to the first and third deviatoric principal stretch $\left(\partial^2 \mathrm{W}(\mathrm{t})/\partial\bar{\lambda}_1\partial\bar{\lambda}_3\right)$

x1: First principal stretch ratio (deviatoric) $\left(\bar{\lambda}_1\right)$

x2: Second principal stretch ratio (deviatoric) $\left(\bar{\lambda}_2\right)$

x3: Third principal stretch ratio (deviatoric) $\left(\bar{\lambda}_3\right)$

detft: Jacobian, determinant of the deformation gradient $\left(J = \det\left(F\right)\right)$

h1: First principal strain invariant $\left(I_1\right)$

h2: Second principal strain invariant $\left(I_2\right)$

h3: Third principal strain invariant $\left(I_3\right)$

delta: Viscoelastic material parameter $\left(\delta = \left(E_1/E_2\right)/\left(1+E_1/E_2\right)\right)$

tau: Viscoelastic material parameter $\left(\tau = \left(\eta\right)/\left(\sqrt[\beta]{1+E_1/E_2}\right)\right)$

c01: Nonlinear elastic material parameter $\left(C_{01}\right)$

c10: Nonlinear elastic material parameter $\left(C_{10}\right)$

c11: Nonlinear elastic material parameter $\left(C_{11}\right)$

c20: Nonlinear elastic material parameter $\left(C_{20}\right)$

c30: Nonlinear elastic material parameter $\left(C_{30}\right)$

beta: Fractional order $\left(\beta\right)$

fml: The Mittag-Leffler function $\left(E_\beta\left[-\left(t/\tau\right)^\beta\right]\right)$

ga: The Gamma function $\left(\Gamma\left(\bullet\right)\right)$

cptim: Current time of the solution (t)

The user-subroutine is presented in Appendix C.

The coefficients of the Padè approximation formula depending on the β parameter (fractional order derivative) is provided to the main user-subroutine via an input file. The input file created is named as "data1.dat". This file includes the value of the β parameter and the coefficients of the polynomial.

A sub-function is developed for the calculation of the gamma function which appears in the approximate M-L function. The code for the calculation of the simple gamma function is taken from (Nan, 2009). The code is tested and compared with the known values of the gamma function in Matlab® function library. The code provides accuracy up to six digits.

All the variables used in the user-subroutine are real constants in double precision format.

Two "common blocks" are included in the user-subroutine, which are "*creeps*" and "*concom*". The variables "*cptim*" and "*timinc*" comes via "*creeps*" common block description and the variables "*inc*" and "*incsub*" comes through the "*concom*" common block description. The variable "*cptim*" is necessary to define the time at the beginning of the current increment. The number of increments, where the variable is "*inc*", can be predefined by the user (fixed time stepping) or the program itself can define the number of increments and the time step at each increment (adaptive time stepping).

In each case, the time at the current time step is necessary for the iterative solution of the nonlinear problem. The variable "*timinc*" can be the same for each increment (fixed time stepping) or could change at each increment (adaptive time stepping). Although the variable "*cptim*" is used as a variable in the user-subroutine, the variable "*timinc*" is not used as a variable in the user-subroutine, since it is not necessary.

In order to check the numerical values obtained from the user-subroutine at each increment, the variables "*timinc, cptim, inc, ga, fml,* and *gt*" are written to an output file named "datanew.dat" at each time increment. By this new file, the programmer was able to observe the numerical output values, and if any discrepancies occur in the numerical results (eg. imaginary number), one can understand that there is a mistake in the user-subroutine and the user-subroutine needs to be debugged. The user-subroutine is presented in Appendix C. The flow chart for the user-subroutine is provided in Section 4.4.

4.4 User-Subroutine Flow Chart

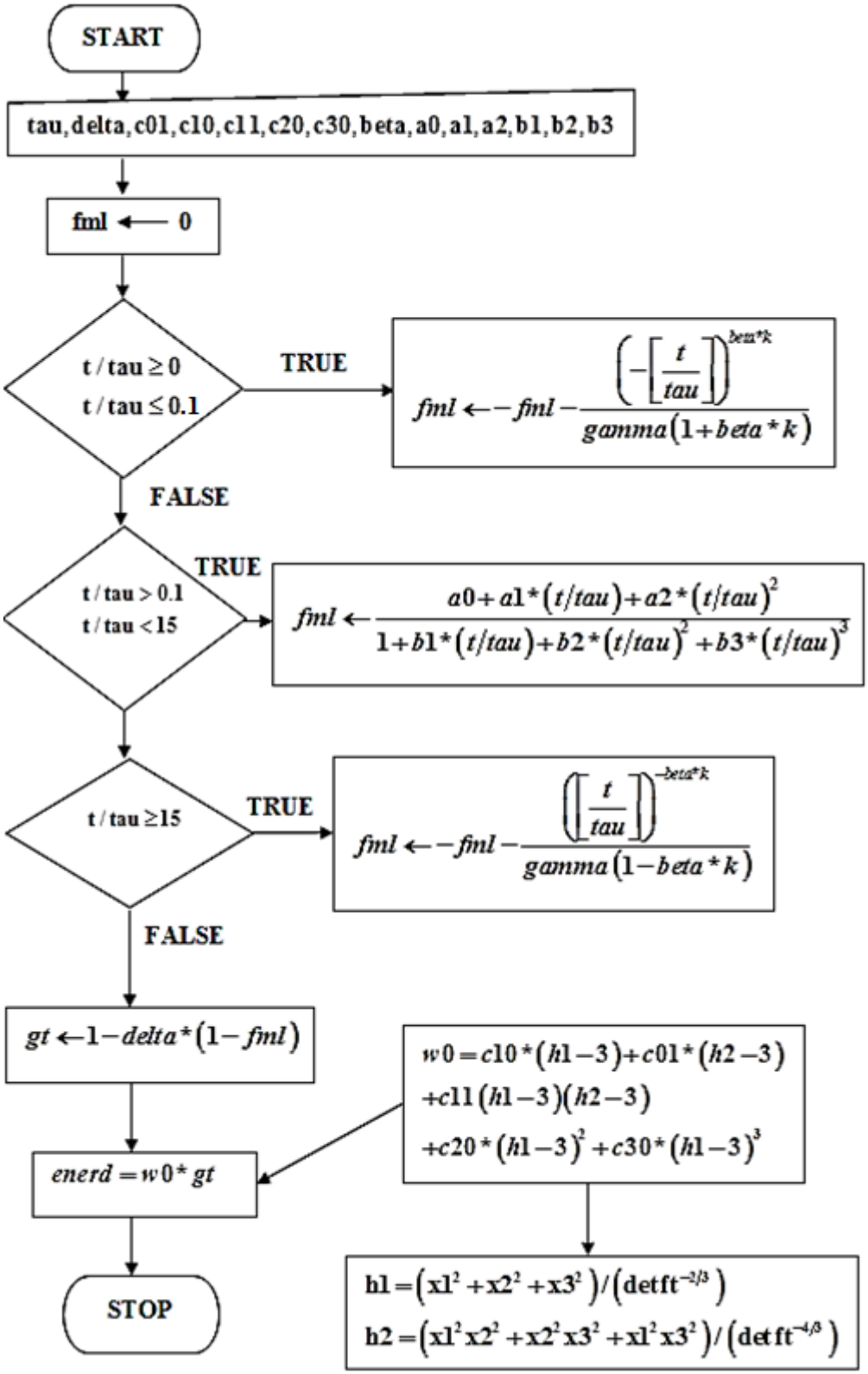

Figure 4.4 The User-Subroutine Flow Chart

4.5 Verification of the User-Subroutine "*UELASTOMER*"

In order to verify the user-subroutine developed, it must be shown that the "normalized reaction force" vs. "time" graph obtained from the small strain finite element analysis on Msc.Marc overlaps the graph obtained from MATLAB® for the same applied boundary conditions and given parameters. For small strain boundary conditions the nonlinearity of the response can be assumed as linear. Therefore the nonlinear material model can be reduced to a linear material model. The user-subroutine is verified for creep and relaxation response.

4.5.1 Matlab® Routine

In Matlab® *m*-file, unit step displacement (Heaviside-step function) is applied to obtain the reaction force via the relaxation modulus.

Later the normalized relaxation function involving the M-L function is calculated with the numerical approximation formulation of the M-L function to be compared with the normalized reaction force results obtained from the finite element analysis (Matlab® code is presented in Appendix C).

4.5.2 Finite Element Analysis Routine

As the user-subroutine developed defines the fractional order material model formulated, it is entered to the software through "*material properties*" section. Under "*material properties*" section on Msc.MARC 2010® interface, Ogden material model is selected with the user-subroutine "*uelastomer*" (Figure 4.5).

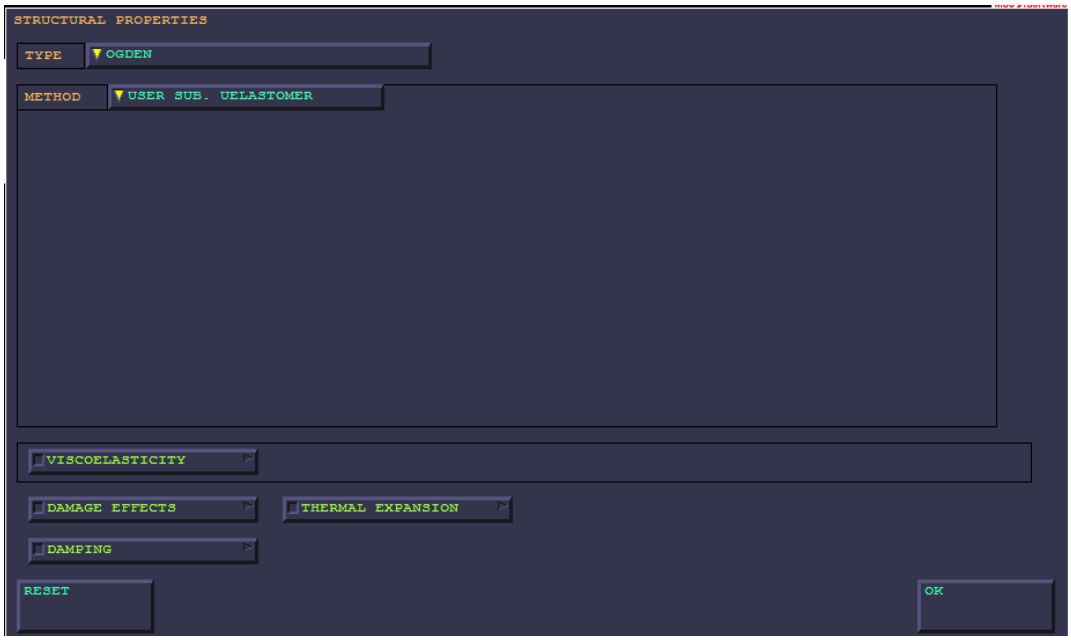

Figure 4.5 Mentat interface for user-subroutine input

Although the material type is selected as Ogden and the user-subroutine is entered through this material model type, the coefficients for the Mooney-type material model $\left(C_{01}, C_{10}, C_{11}, C_{20}, C_{30}\right)$ must be entered as "0" under Mooney model definition option (Figure 4.6).

Figure 4.6 Inputted parameters via software interface.

The material properties are supplied via the user-subroutine. However, bulk modulus must be supplied via the Mentat interface. Under material properties, either under Ogden type, the bulk modulus is entered through "*entered values*" or under Mooney type the bulk modulus is entered according to the Equation 4.14 (see Figure 4.5).

For this analysis, the value of the bulk modulus is entered by the user as "20000 MPa" while the non-linear elastic material coefficients are taken as unity (*i.e.* 1 MPa) for simplicity.

An eight-node hexahedral element with "*Herrmann formulation"* is employed. Elements with "*Herrmann formulation*" in MSC.Marc 2010 software are suitable for nearly incompressible or incompressible materials like soft tissue, rubber, polymers.

Also "*Large Strain*", "*Updated Lagrange*", "*Multiplicative Hyperelasticity*" and "*3 - D Analysis*" options were selected. The iterative numerical solution is chosen as "*Full Newton-Raphson Method*".

As a note, "*Updated Lagrange"* framework is especially useful for large deformation analysis, since typically excessive element distortion in rubbery materials leads to premature termination of the analysis. For "*Updated Lagrange*" elasticity, both conventional elements, as well as "*Herrmann elements"* can be used for plane strain, axisymmetric and 3-D problems.

Selecting a proper time step increment is an important aspect for a nonlinear solution. Large steps size often leads to many cycles per increment and if the step size is too large it can lead to inaccuracies and non-convergence. On the other hand, using too small step size is inefficient and increases the time consumption.

"Adaptive time stepping scheme" is employed for the finite element analysis to optimizing the time step constraint of the solution. For the adaptive time-stepping scheme, the time step changes from one increment to the other and also within an increment depending on the selected convergence criteria.

Different relative force tolerance (convergence) ratios affect the accuracy of the solution. The word "*accuracy*" refers to the difference between the exact solution and the finite-element solution and the word "*convergence* (monotonically decreasing error)" refers to the accuracy as the number of elements in the mesh is increased (Reddy, 1985).

The "*convergence testing criteria"* is chosen as "*relative residual force*". The tolerance value is provided by the user. The formulation for the convergence criteria is,

$$Relative: \frac{\|F_{residual}\|_{max}}{\|F_{reaction}\|_{max}} < Tol$$

where

$\|F_{residual}\|_{max}$ = maximum residual force

$\|F_{reaction}\|_{max}$ = maximum reaction force and

Tol = tolerance value specified by the user.

This value should be taken 1% or smaller for heavily nonlinear problems to obtain a good accuracy.

4.6 Verification of the User-Subroutine for Relaxation Response

For small deformations, soft tissues, rubbers... etc. are assumed to behave as linear viscoelastic materials. For levels of strain exceeding some critical value, the viscoelastic behavior becomes measurably nonlinear. Therefore small displacement boundary condition is applied onto the four planar nodes of the element (Figure 4.7) which would result in small strain in the material. As each side of our element is only 1 mm thick, the displacement boundary condition applied is 1% of the length of the side of the element which is "0.01 mm". Figure 4.7 presents the 8-noded hexahedral element with applied boundary conditions.

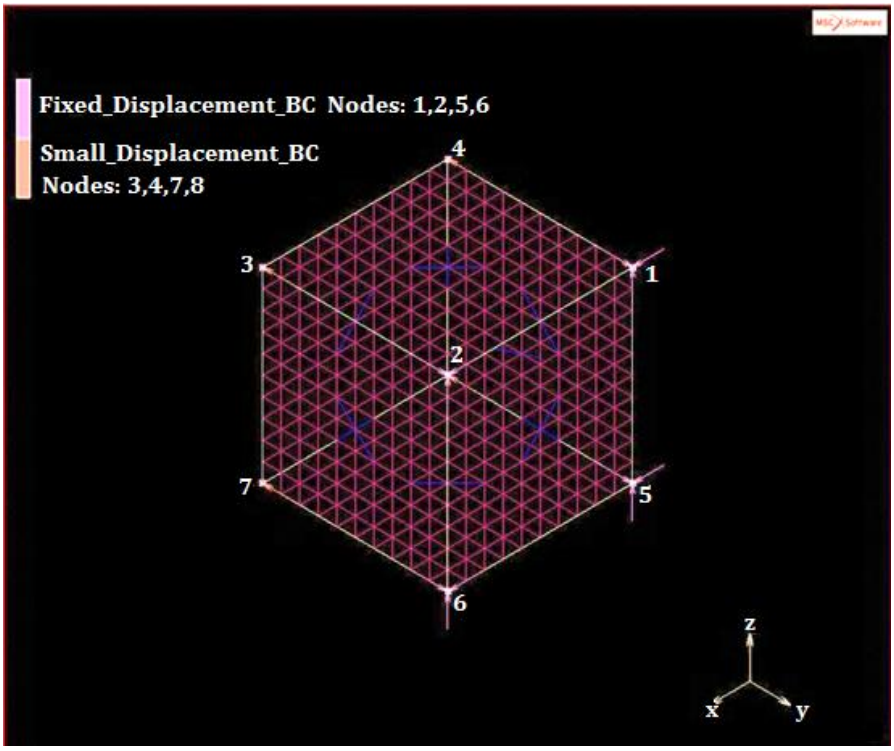

Figure 4.7 The 8-Node Hexahedral Element with Applied Boundary Conditions

Initially, for a small period of time (0.01 seconds) ramp displacement is applied to observe the instantaneous elastic response and after $t = 0.01$the displacement is held constant to observe the relaxation response for 100 seconds. The initial ramping period is held relatively small in order to approximate unit step function.

The parameters of the material model (nonlinear elastic) for the finite element analysis are equal to unity for simplification,

$$C_{01}, C_{10}, C_{11}, C_{20}, C_{30} = 1 \text{ MPa}$$

and the fractional order is

$$\beta = 0.5 .$$

The relaxation modulus is,

$$G(t)=\left\{1-\delta\left(1-E_{\beta}\left[-\left(\frac{t}{\tau}\right)^{\beta}\right]\right)\right\}$$

where

$$\delta=\frac{E_1/E_2}{1+E_1/E_2} \text{ and } \tau=\frac{\eta}{\sqrt[\beta]{1+E_1/E_2}}$$

And the viscoelastic parameters δ and τ are chosen arbitrarily as,

$\delta=0.2$ and $\tau=2s$.

The finite element analysis result obtained for adaptive time stepping scheme is illustrated in Figure 4.8.

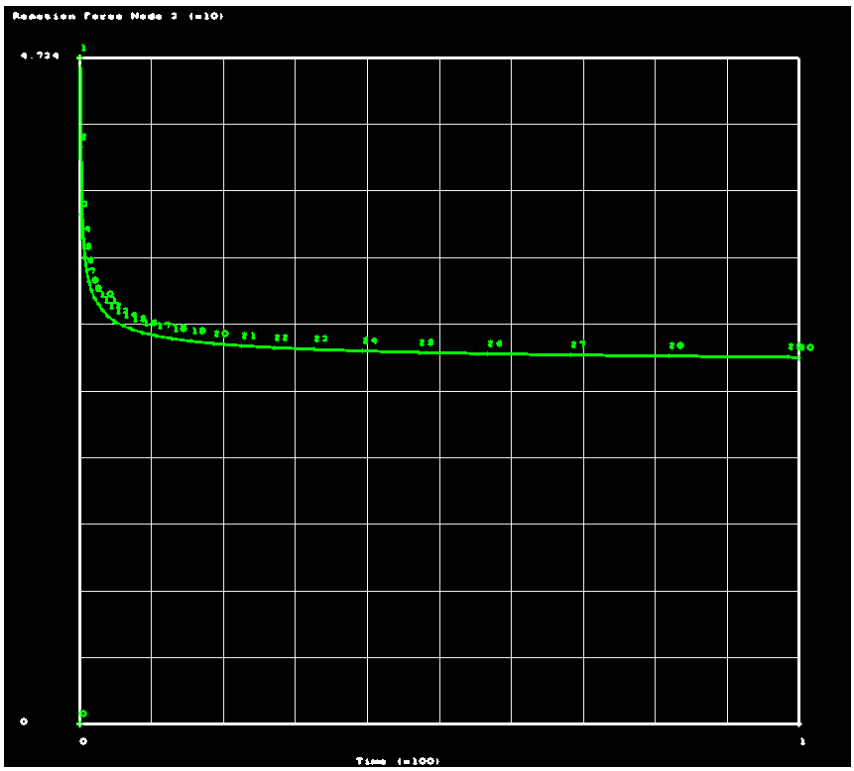

Figure 4.8 Relaxation curve obtained from FEA (Mentat interface)

The analytical result obtained from Matlab®, is compared with the finite element, numerical result obtained and plotted together (Figure 4.9). The reaction force obtained from Matlab® for one dimensional fractional linear viscoelastic material model becomes equal to the normalized reaction force data (the reaction force is normalized with the nonlinear instantaneous elastic response) obtained from the finite element analysis performed on Msc.Marc 2010 with a sum of least square error of order 10^{-9} (Refer to Figures 4.11 and 4.12). As the deformation is small enough (1% of the thickness of the model (small strain)) both of the curves overlap. We conclude that the numerical results agree very well with the analytical results and the user-subroutine works correctly.

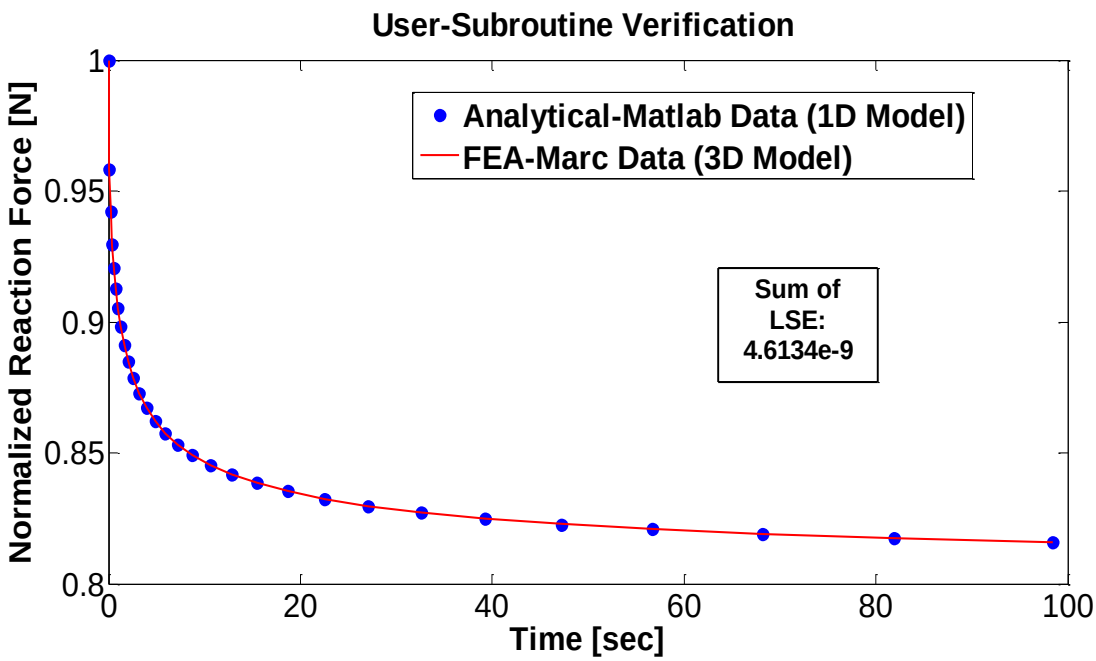

Figure 4.9 User-subroutine Verification for Relaxation Response (Adaptive Time Stepping)

Finite element analysis has been performed for fixed time stepping scheme as well. The result obtained is illustrated in Figure 4.10.

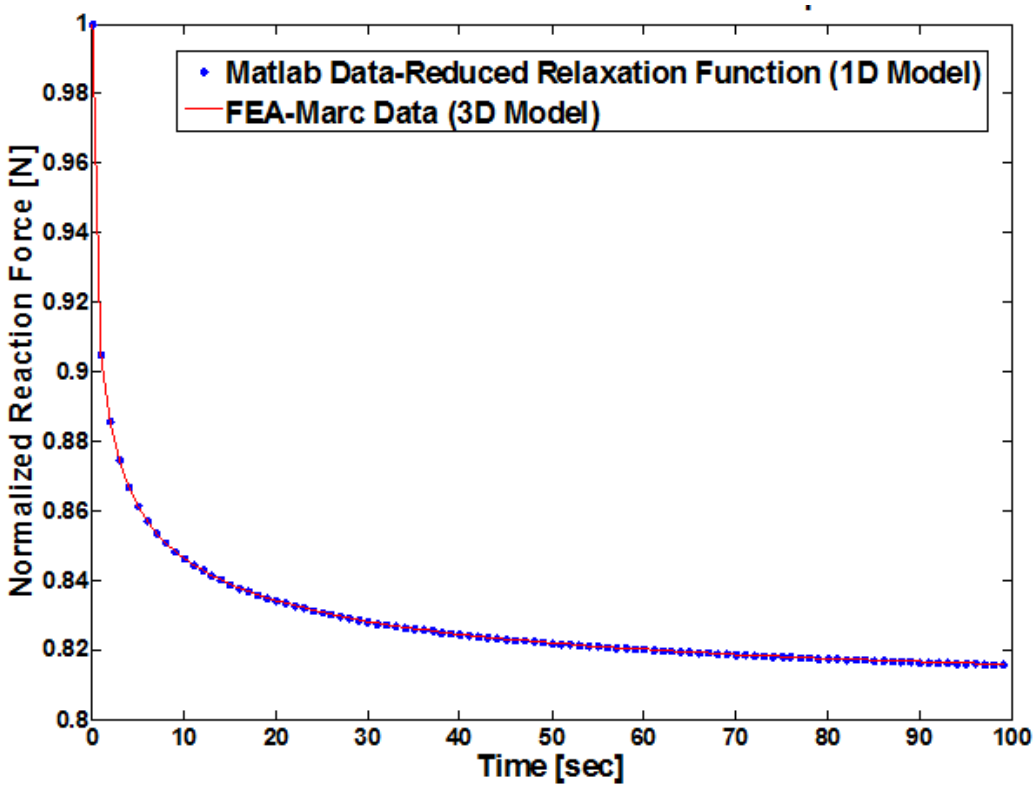

Figure 4.10 User-subroutine Verification for Relaxation Response
(Fixed Time Stepping)

It is well known that, for severe nonlinearities adaptive time stepping scheme is able to capture the nonlinearity of the problem. It is also seen that, adaptive time stepping scheme is very efficient in capturing the nonlinearity of the problem and obtains accurate results with least CPU time possible. Fixed time stepping is good when the nonlinearity is mild or the response is smooth. On the other hand adaptive time stepping is useful when the problem involves sudden nonlinearities; therefore adaptive time stepping scheme automatically locates and handles the sudden nonlinearities. When fixed time stepping scheme is preferred, CPU time increases drastically (Table 4.1).

Table 4.1 Wall Time of the FE Solution

Parameter	Fixed Time Stepping Scheme	Adaptive Time Stepping Scheme
Number of Increments	100	30
Wall Time [sec]	**122400**	100

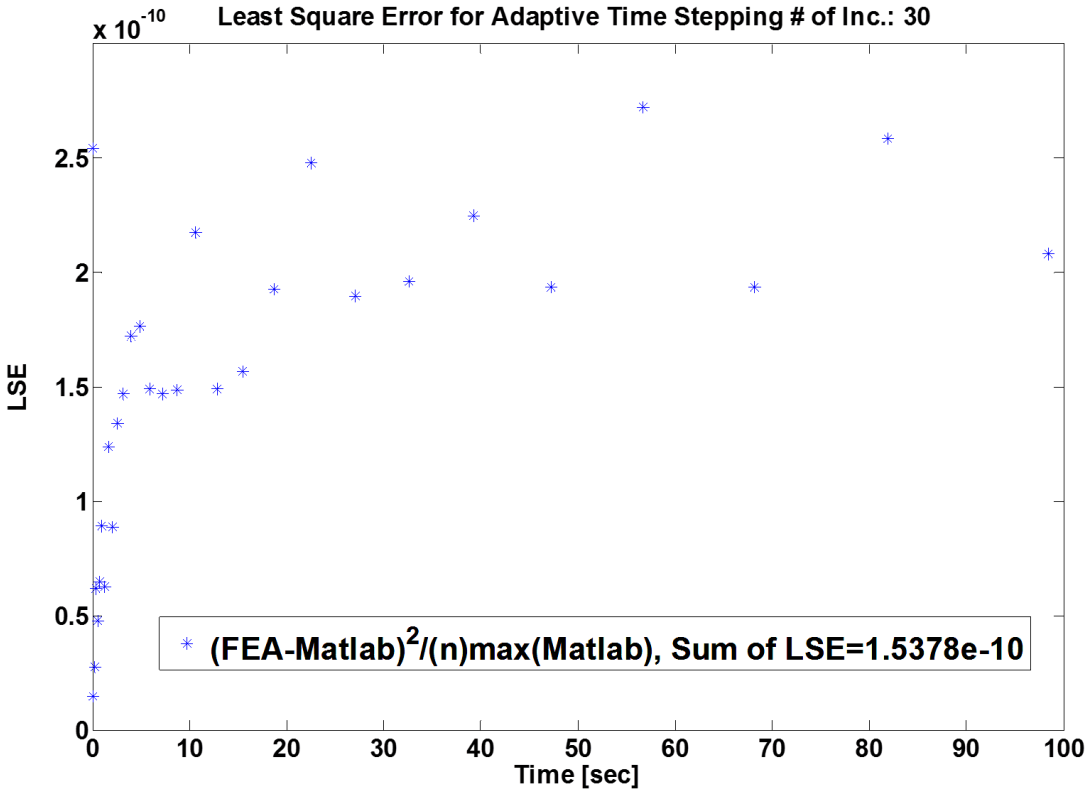

Figure 4.11 Least square error graph for adaptive time stepping solution

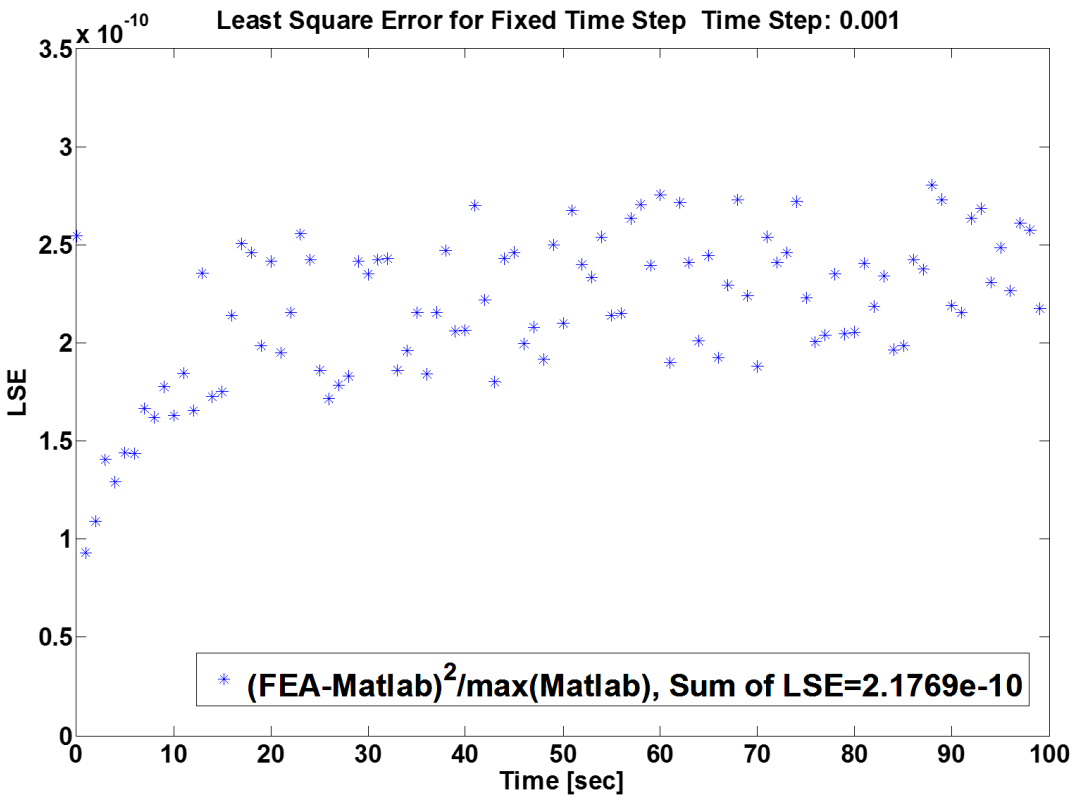

Figure 4.12 Least square error graph for fixed time stepping solution

4.7 Verification of the User-Subroutine for Creep Response

The same method is employed for the verification of the user-subroutine for the creep behavior. Creep analysis result obtained from the finite element analysis is shown in Figure 4.13.

In order to obtain this data, force boundary condition is applied to the nodes where a displacement boundary condition was applied before, for the analysis of relaxation behavior. The force is held constant for 100 s to observe the creep behavior. The most important point for the creep analysis is the magnitude of the applied force boundary condition. In simulating the relaxation behavior, 1% displacement was applied to the one-element model and the resulting peak force is noted. When simulating the creep behavior, this peak force is applied in order to create a 1% displacement on the model. The number of significant figures is critical, while the magnitude of the force developed is very low.

In order to verify the user-subroutine for the creep behavior, the parameters employed for the finite element analysis must be converted for utilizing for the analytical formulation.

Rewriting the creep compliance for the fractional viscoelastic Zener material model,

$$J(t) = \frac{1}{E_1}\left\{1 + \frac{E_1}{E_2}\left\{1 - E_\beta\left[-\left(\frac{t}{\eta}\right)^\beta\right]\right\}\right\} \tag{4.23}$$

Msc.Marc software utilizes the user-defined constitutive equation in relaxation form, therefore the creep parameters must be written in the relaxation form.

For the relaxation formulation, the parameters for δ and τ were 0.2 and $2s$ respectively. The creep parameters in the relaxation form are calculated to be as,

$$\delta' = \frac{E_1}{E_2} = 0.25$$

and

$$\tau' = \eta = (\tau)\left(\sqrt[\beta]{1 + E_1/E_2}\right) = 2.2361s$$

As to sum up, the parameters for the finite element analysis are,

$C_{01} = C_{10} = C_{11} = C_{20} = C_{30} = 1$ and $\delta = 0.2,\ \tau = 2s$ and the parameters employed in Matlab® code are, $\delta = 0.25,\ \tau = 2.2361s$.

By employing this methodology, the user-subroutine developed is verified for the creep analysis as well.

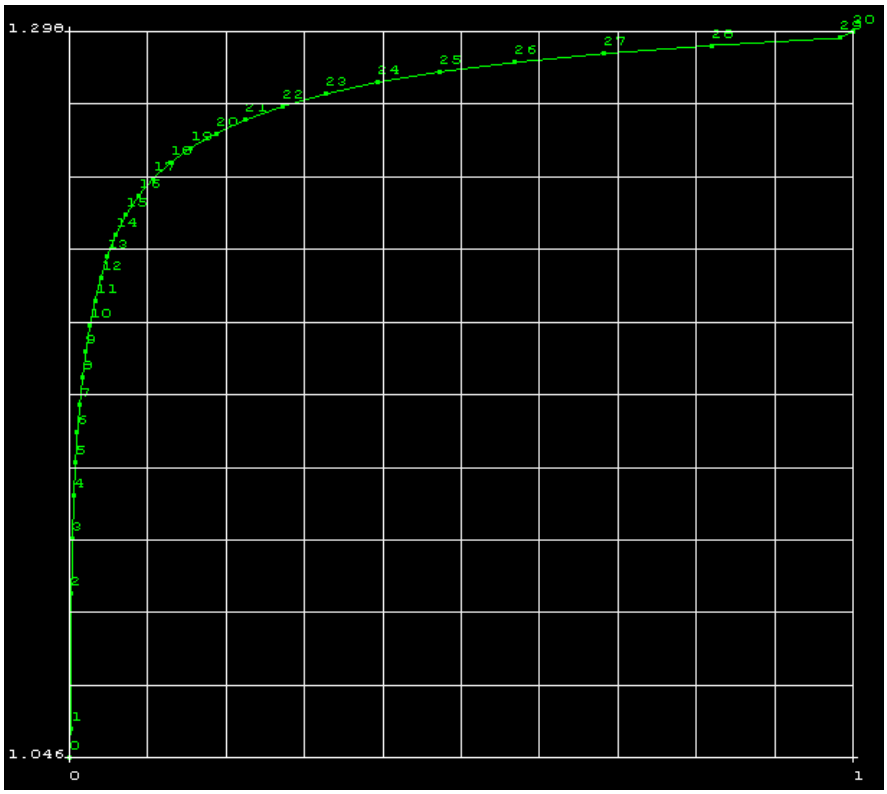

Figure 4.13 Creep curve obtained from FEA (Mentat interface)

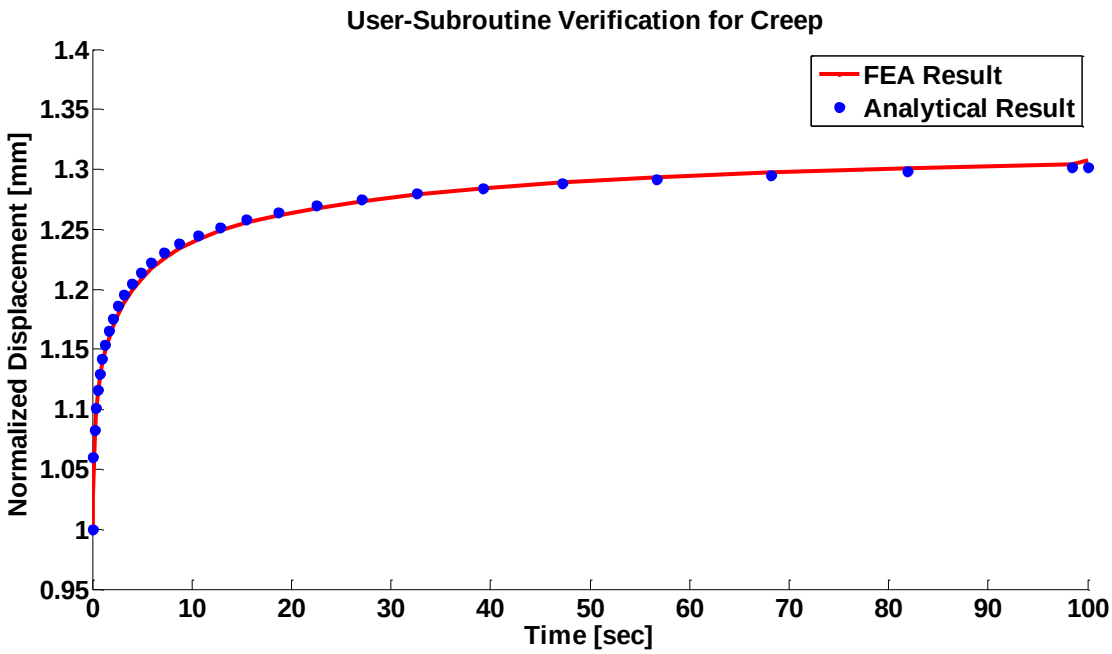

Figure 4.14 Verification of the user-subroutine for the creep analysis

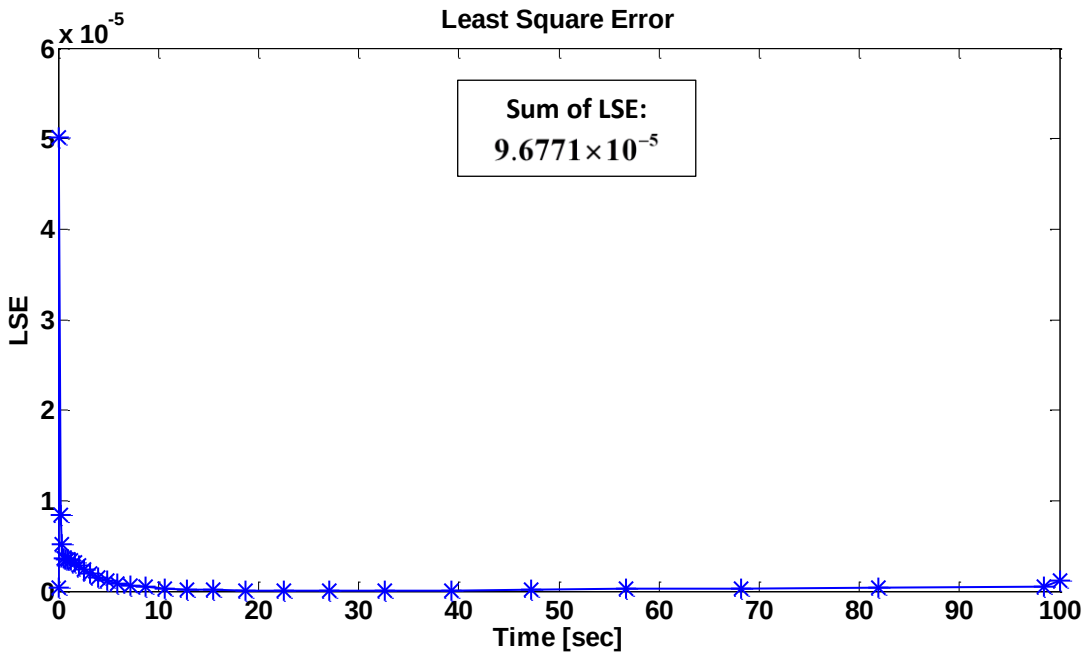

Figure 4.15 Least Square Error Plot Obtained for the Creep Analysis

CHAPTER 5

THREE-DIMENSIONAL FINITE ELEMENT MODEL OF THE INDENTATION EXPERIMENTS OF SOFT BIOLOGICAL TISSUE

Three-dimensional (quarter) and axisymmetric soft tissue models are developed. Three dimensional finite element model of the soft tissue in the vicinity of the indenter was developed to simulate the mechanical indentation experiments performed on the soft tissue. By employing the inverse finite element method, unknown material parameters of the material model are extracted.

5.1 Quarter Tissue Model

A 3-dimensional model of the soft biological tissue is developed. As the model includes symmetry with respect to the x and z axis, a quarter model of the tissue is applicable. Model dimensions are $(200 \times 36.9 \times 200)\,mm$. Three dimensional view of the tissue with the ellipsoid indenter tip is shown in Figure 5.1.

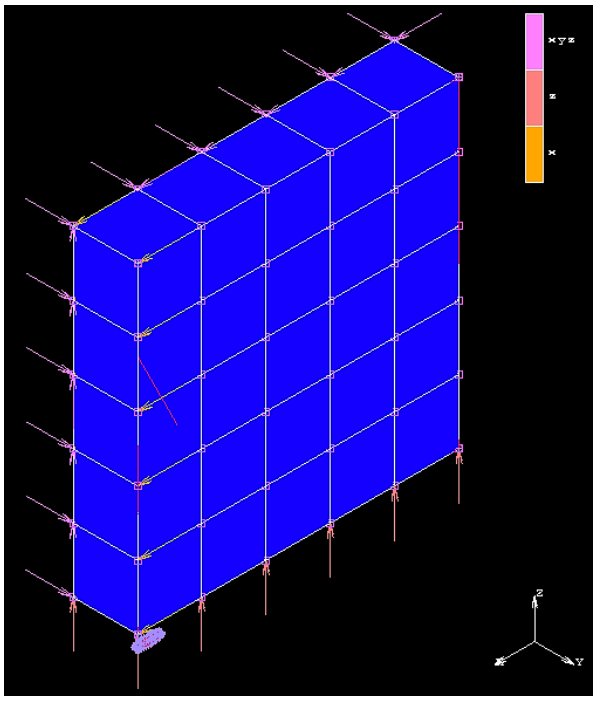

Figure 5.1 Quarter Tissue Model with Indenter Tip

Adaptive mesh refinement technique was applied to this model; therefore a coarse mesh with initial 25 elements was constructed. Displacement boundary conditions were applied to symmetry planes, normal to those planes, and, the bone was assumed to be bonded to the tissue. Boundary conditions are presented in Figure 5.1.

5.2 Finite Element Analysis Details

5.2.1 Material Properties

Under material properties, Ogden material model with the use subroutine "*uelastomer*" option was selected in Marc user-interface menu and bulk modulus was entered from this menu.

5.2.2 Element

As near incompressibility is assumed through the material model formulated, a suitable element needs to be chosen. The use of standard displacement elements

leads to “locking” behavior (Liu & Choudhry, 2004). Marc 2010 offers special elements with Herrmann formulation which allows the study of compressible and nearly incompressible materials in both axisymmetric and three-dimensional cases. An eight-noded, isoparametric, three dimensional brick element with Hermann formulation was employed (Element 84). For element 84, there is also one extra node for the pressure variable which is a negative hydrostatic pressure for Mooney or Ogden material formulation (see Figure 5.2).

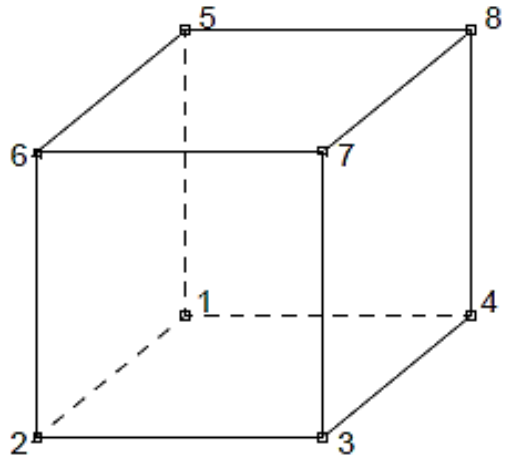

Figure 5.2 Hexahedral Herrmann Type Element

5.2.3 Contact Properties

The tissue was regarded as “deformable contact body” and the indenter tip was regarded as “rigid contact body” (compared to soft tissue) with velocity or position control. Velocity control enables the user to apply several indentation rates. The complicated motion of the rigid body (indenter) enables the user to simulate different experiment protocols; cyclic loading, relaxation or creep. Contact type was chosen as “*touching*” for the rigid body and “*no contact*” option is chosen for the deformable body (soft tissue).

5.2.4 Solution

A nonlinear, iterative solution was performed. For nonlinear problems, the stiffness matrix is dependent on both the current displacement and the force vector unlike the linear systems.

$$F = K\left(F, u\right) \times u \tag{5.1}$$

Where u is the nodal displacement vector, F is the nodal force vector and K is the stiffness matrix.

"Large strain" and "*Nonlinear"* procedures are activated by allowing "*Updated Lagrange* and "*Multiplicative Decomposition"* options. For large strain formulation, updated Lagrange procedure is necessary to be activated by default. From the two natural classes of large deformation problems, large displacement and small strain or large displacement and large strain, the analysis that was performed involves, large displacement and large strain together. In addition to geometric nonlinearities due to large displacement and contact, material nonlinearities are present in the model.

In the "*Lagrangian"* formulation, the finite element mesh is attached to the material and moves through space along with the material. The "*Lagrangian"* approach naturally describes the deformation of structural elements, such as the indentation problem. In the "*Total Lagrangian"* approach the equilibrium is expressed with the original undeformed state as the reference, and in the "*Updated Lagrangian"* approach, the current configuration acts as the reference state. Theoretically and numerically, the two formulations yield the same result, however for certain material behavior, the usage of "*Total Lagrangian"* formulation is inconvenient. For deformations involving excess distortions, "*Updated Lagrangian"* formulation is favored. The "*uelastomer*" user-subroutine is used to define a strain energy function in the "*Updated Lagrange*" framework. Also "*Multiplicative Decomposition*" method is selected while; it is suitable for *Herrmann* type elements.

5.2.5 Loadcase Options

Important parameters for the loadcase options are the "*stepping procedure*" (adaptive or fixed time stepping), "*convergence testing*" parameters and "*solution control*". For fixed time stepping, the total loadcase time and the number of steps are entered by the user. For multi-criteria time stepping procedure, only the total loadcase time is entered by the user. Important parameters for adaptive time stepping are; the initial fraction of the total loadcase time and desired number of recycles. With the initial fraction of the loadcase time, the initial time step of the solution is determined. The accuracy of the numerical result is mainly dependent on the time step chosen. Therefore lower initial fraction of loadcase time provides more accurate solutions, however increases the computational time significantly.

On the other hand, desired number of recycles is a controlling parameter for the time step. When the desired number of recycles is not reached through the solution of the increment, then the current time step is increased with the time step increase factor provided by the user (default value is 1.2). On the other hand, when the desired number of recycles is exceeded, then the current time step is decreased by the same factor.

When using adaptive time stepping scheme, it is necessary to be careful at the important peaks of the loading history, so that those important peaks are not missed due to adaptive stepping.

For convergence testing, relative residual force criterion is used. For this criterion, the maximum residual force divided by the maximum reaction force is checked and compared to the tolerance value provided by the user.

The solution procedure was an iterative procedure which is the full Newton-Raphson method. For this procedure, the tangent stiffness matrix is reformulated for each iteration (recycle). However, in the modified Newton-Raphson method, the stiffness matrix is formulated only once per increment. This leads to lower cost, but a slow convergence can be a consequence. The modified Newton-Raphson method is effective for large, mildly nonlinear problems but without material nonlinearities.

It is possible to define as much loadcases as desired with different convergence options and convergence ratios, loadcase times or stepping procedures. All these parameters affect the nonlinear analysis accuracy and solution time. Important parameters when dealing with such nonlinear problems are,

- Convergence tolerance
- Maximum number of recycles
- Initial fraction of loadcase time
- Desired number of recycles/increments
- The solution method

5.2.6 Solver

When direct solvers are used with the Newton-Raphson method, it leads to computational inefficiencies for 3D, nonlinear problems. Therefore iterative solver techniques of the Marc software should be used. CASI iterative solver option is selected. The convergence capability of the solution is related to the singularity ratio. An error criterion is defined in this option which is based on the ratio of the residuals in the solution and the reaction force. A tolerance value is specified in the solver option. The CASI iterative solver is not used with higher order Herrmann elements. For this with strong material and contact nonlinearity, the efficiency in using the modified Newton-Raphson method can be deprived by increased number of iterations and nonconvergence. Iterative solvers should not be used with modified Newton-Raphson technique. Although an iterative solver is more appropriate to the nature of nonlinear problems, a direct solver (multifrontal sparse) is rather selected, while it allows parallelization and therefore the time cost of the solution is reduced significantly.

5.2.7 Finite Element Mesh

Adaptive meshing procedures are applied to the model while this routine gives the user an idea about the fineness (or coarseness) of the mesh which must be taken into consideration for optimizing the mesh. A very fine mesh increases the time cost of

solution non-essentially and a very coarse mesh on the other hand, although reducing the time cost of the solution significantly, gives inaccurate results. Therefore the main goal in developing an appropriate, optimal mesh for the finite element analysis is dependent on the mesh quality, time of solution and accuracy of the obtained results.

The adaptive mesh generation capability increases the number of elements and nodes according to the criteria selected to improve the accuracy of the solution. When the local adaptivity criterion is used with nonlinear analysis, the mesh is adjusted at each increment when necessary, to satisfy the adaptivity criterion. Local adaptivity is available in a parallel analysis. The adaptive meshing procedure divides the elements and ties the nodes to assure compatibility.

The automatic global remeshing technique was not employed, while it does not allow solution with hexahedral elements, only lower order tetrahedral elements are supported. Also with global remeshing technique, parallel processing is not supported.

Criteria tried for adaptive meshing procedure are treated in sections 5.2.7.1 through 5.2.7.4.

5.2.7.1 Node in Contact Criterion

With this criterion, an element is subdivided if one of its nodes comes into contact with the rigid body. This criterion should provide an initial estimate to the degree of fineness of the mesh. Local adaptivity criterion is applied to all the elements initially, rather than only on the element that comes into contact with the rigid body. Number of levels determines the coarseness of the mesh. By changing the number of levels from 1 to 8, as the mesh gets finer, the solution times increase significantly.

3 mm indentation with 1mm/s indentation rate was applied on the tissue. Then the indenter was retracted back with the same rate. In this study the numerical values of the nonlinear and viscoelastic parameters were insignificant while this study gives an idea about the number of levels necessary to be applied in order to get accurate

results. All the analyses were performed on a Windows 7 Professional, Intel Core i7 CPU, and 3.07 GHz, 6 GB RAM and 64-bit operating system desktop computer. Although, the material parameters were insignificant at this moment, the nonlinear material coefficients were taken as unity, the relaxation time constant was 2 s and the relaxation magnitude was taken as 0.2.

$C_{01} = 1$

$C_{10} = 1$

$C_{11} = 1$

$C_{20} = 1$

$C_{30} = 1$

$\delta = 0.2$

$\tau = 2s$

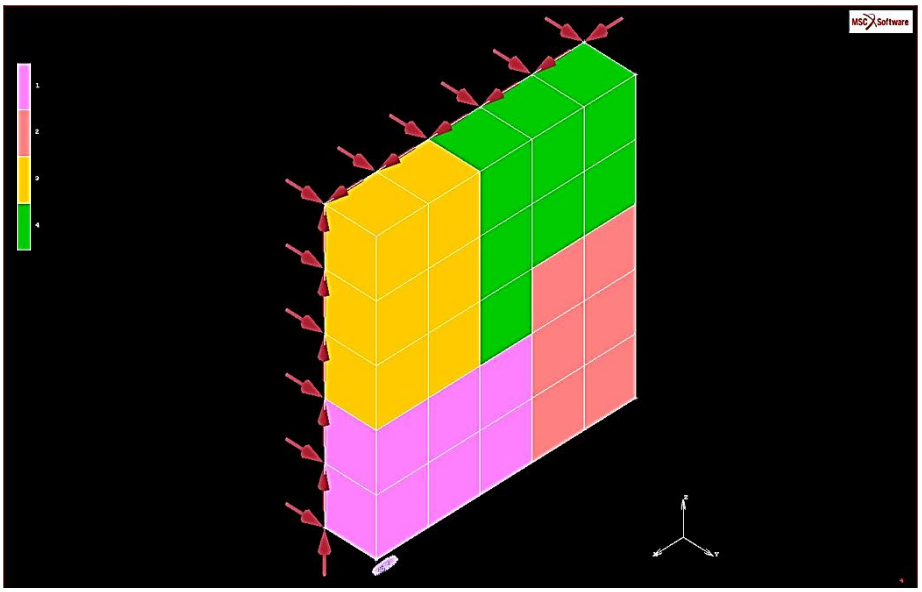

Figure 5.3 Domain Decomposition Method (DDM)

In order to observe the parallelization performance of the Marc solver, domain decomposition method, DDM, was applied. In this solution method, the model is decomposed into domain of elements. Although the total numbers of elements are the

same, each domain may have different number of elements depending on the number of domains. 4 domains are generated for the soft tissue model as presented in Figure 5.3. “Metis best” automatic decomposition method was applied. It can be clearly observed from Table 5.1 that, applying DDM reduces the wall time of the solution significantly.

Table 5.1 Mesh Refinement Level and Wall Time (Node in Contact)

Number of Levels	**Total Solution Time [s] (Without Parallelization)**	**Total Solution Time – Wall Time [s] (With Parallelization – 4 Processors)**
4	45	(-)
5	72	(-)
6	145	(-)
7	598	165.56
8	1797	460.39
9	6601	(-)

From Table 5.2 and Figure 5.4, it can be seen that until level 4 mesh refinement, the results vary considerable. Therefore at least level 4 mesh refinement must be employed. From number of refinement levels 6 to 9, we should zoom into the peak values of the graph (see Figure 5.5). To make a valid assumption of the accuracy of the solutions, relative error values obtained from different mesh refinement levels are compared. In addition, the total time of the solution needs to be considered for an optimal finite element analysis solution.

Table 5.2 Mesh Refinement Level (Node in Contact)

Number of Levels	Absolute Error [N]	Relative Error [%]
4 - 5	0.649	39.64
5 - 6	0.012	0.525
6 - 7	0.023	1.001
7 - 8	0.005	0.215
8 - 9	0.004	0.172

As a conclusion, it can be stated that level 6 mesh refinement is appropriate according to accuracy and CPU time constraints for the solution of the indentation problem.

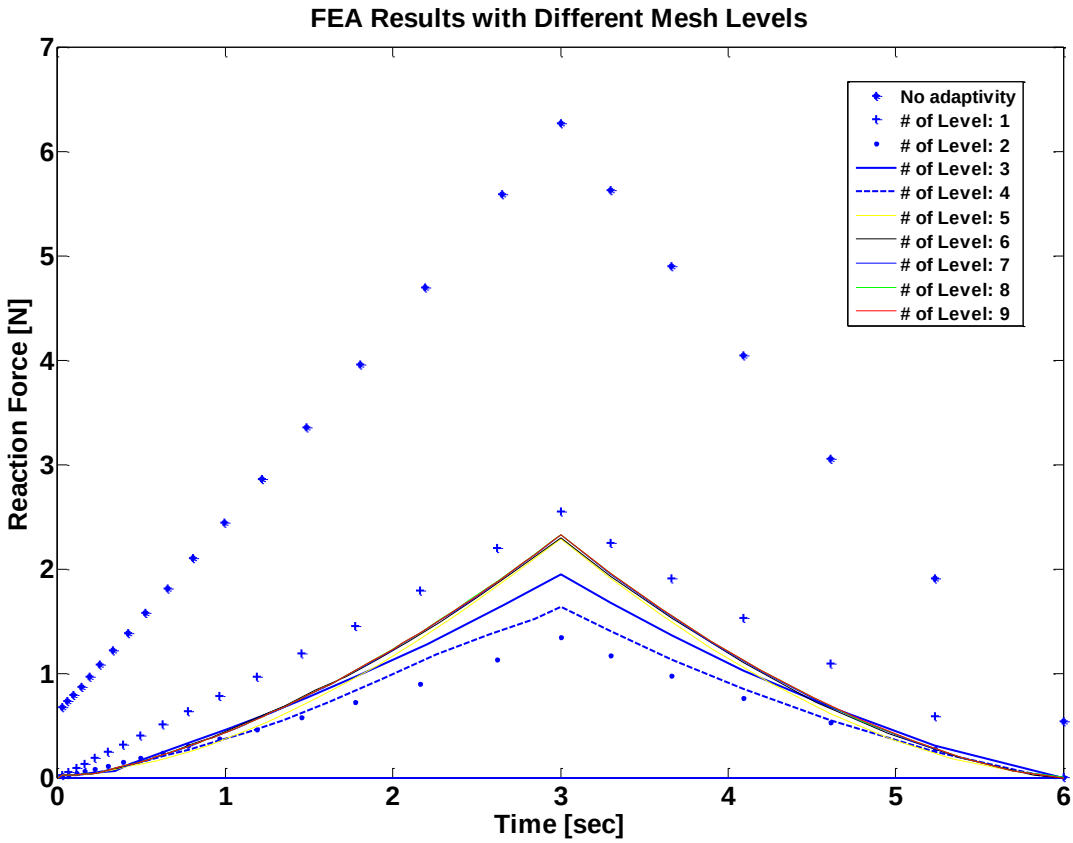

Figure 5.4 Adaptive Mesh Refinement 1 (Node in Contact)

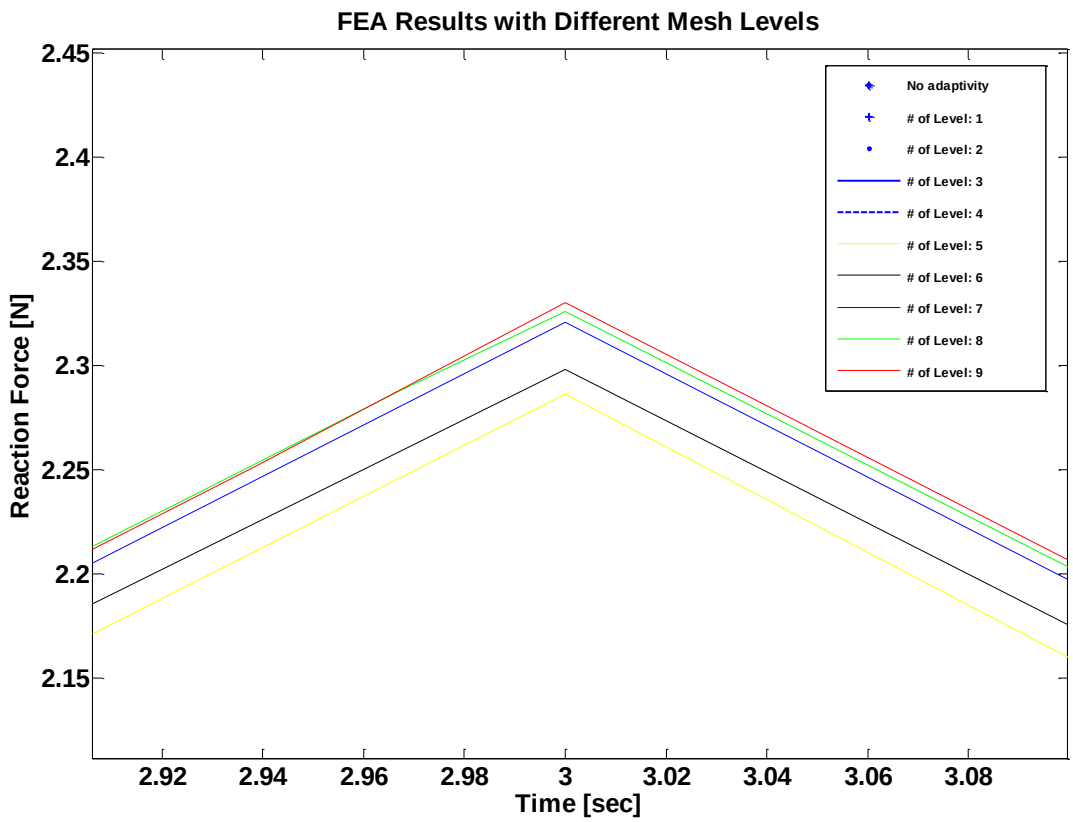

Figure 5.5 Adaptive Mesh Refinement (Zoom in to Figure 5.4)

Cyclic loading experiment protocol is simulated via finite element analysis with 2 mm indentation and 1 mm/s indentation rate for 10 cycles. DDM is employed and the program is run through command monitor display (cmd). Preconditioning behavior is clearly observed at the end of the ten cycles (Figure 5.6).

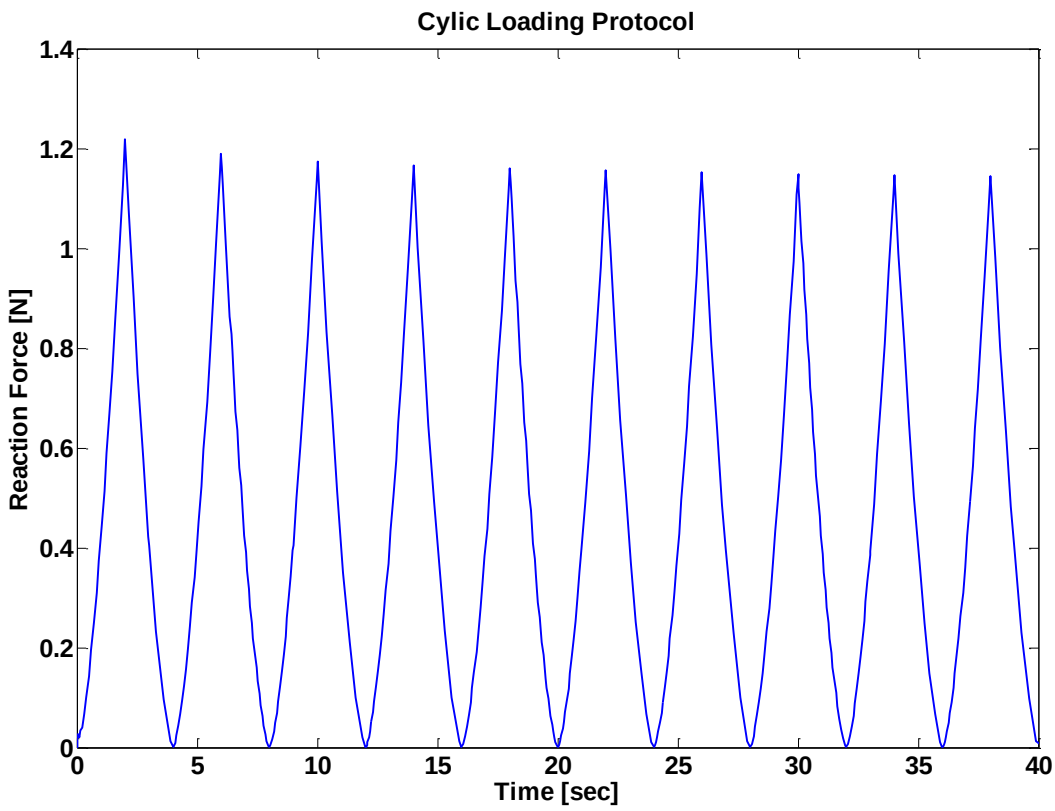

Figure 5.6 Cyclic Loading (Ten Cycles)

5.2.7.2 Mean Strain Energy Criterion

Regarding this criterion, an element is refined if the strain energy of the element is greater than the average strain energy in a chosen set of elements, times a given numerical value. Mathematically representing,

$$element\ \ strain\ energy > \frac{total\ \ strain\ energy}{\#\ \ of\ \ elements} * VALUE \tag{5.2}$$

The numerical value and the refinement level are entered to the program. Results obtained are presented in Figures 5.7 and 5.8. As it can be seen clearly from Figure 5.7 that, number of refinement level affects the result the most, on the other hand changing the numerical value has minimum effect on the results.

Wall time depending on the mesh refinement level is also compared and shown in Table 5.3. As it can be seen as the refinement level increases, the wall time of the finite element analysis increases drastically. This criterion is less preferable compared to the "*node in contact*" criterion regarding time constraints.

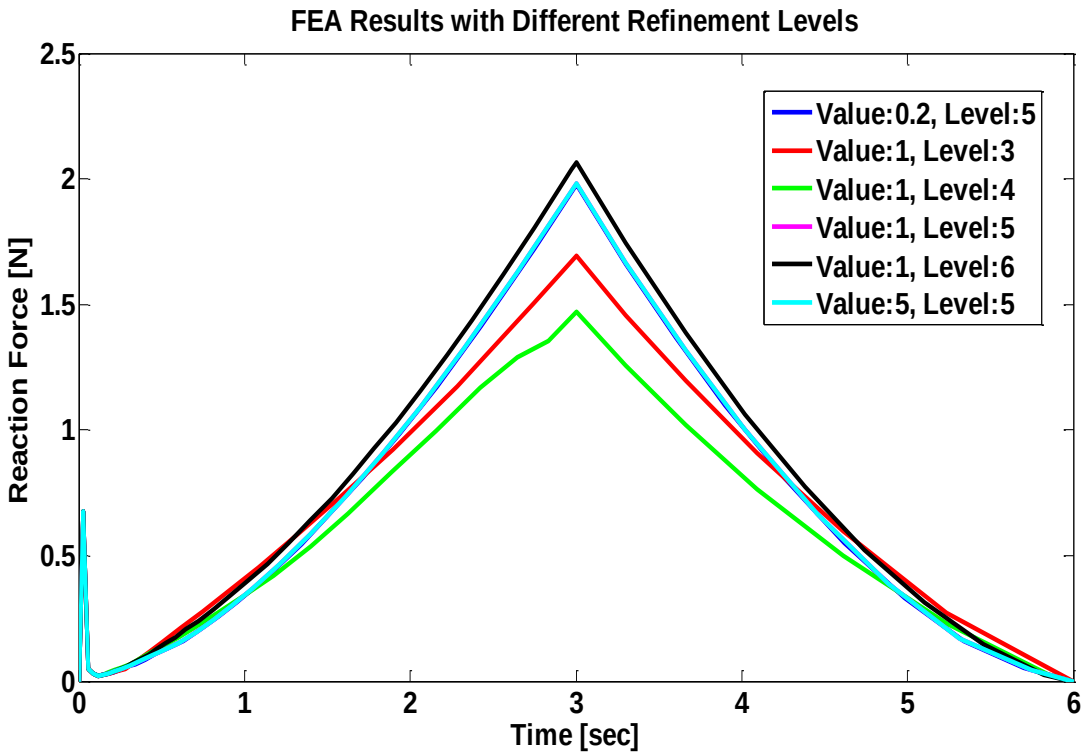

Figure 5.7 Adaptive Mesh Refinement (Mean Strain Energy)

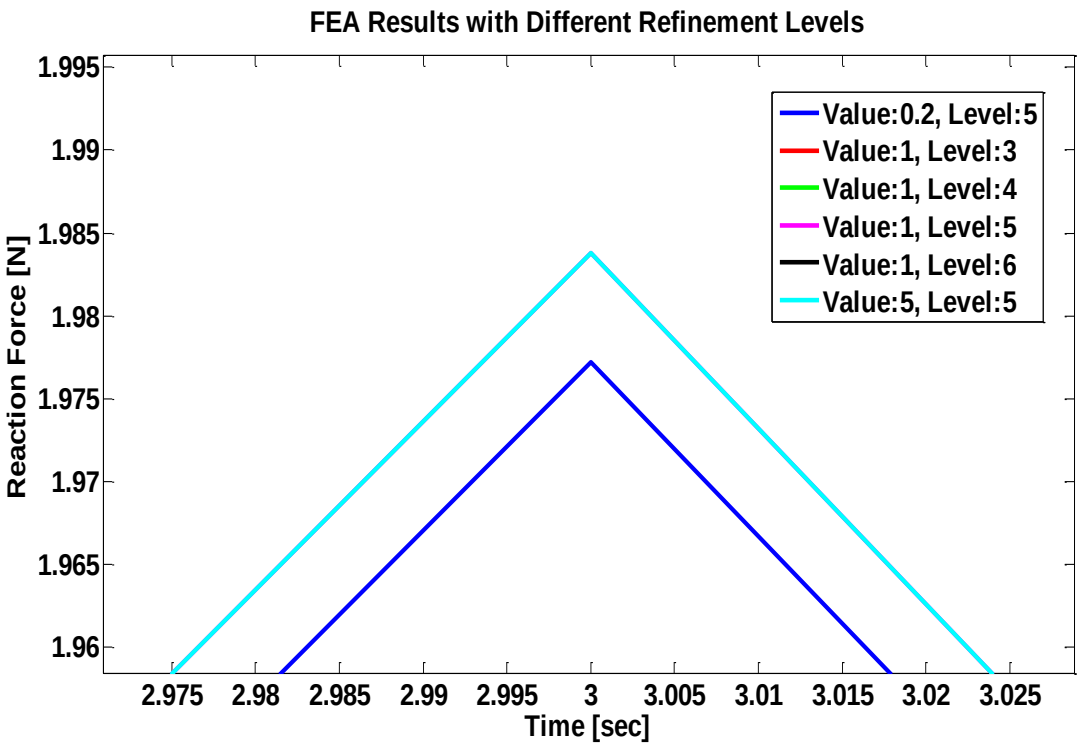

Figure 5.8 Adaptive Mesh Refinement (Zoom in to Figure 5.7)

Table 5.3 Mesh Refinement Level and Wall Time (Mean Strain Energy)

Mean Strain Energy Criterion	**Wall Time of FEA [s]**
Value: 1, Level: 3	60
Value: 1, Level: 4	270
Value: 5, Level: 5	1674
Value: 1, Level: 5	1676
Value: 0.2, Level: 5	9986
Value: 1, Level: 6	22665

5.2.7.3 Relative Equivalent Stress Criterion

Within this criterion, an element is subdivided if the current element stress value is a given fraction of the maximum relative value. This criterion is not efficient due to

time constraints. As "*wall time*" of the solution is a priority constraint in optimizing the mesh, it must be taken into consideration while material model parameter identification requires several consecutive runs of the finite element model.

5.2.7.4 Zienkiewicz-Zhu Criterion

In this criterion an error norm is defined, such that,

$$\pi^2 = \frac{\int \left(\sigma^* - \sigma\right)^2 dV}{\int \sigma^2 dV + \int \left(\sigma^* - \sigma\right)^2 dV} \gamma^2 \tag{5.3}$$

where σ^* is the smoothed stress and σ is the calculated stress. The stress error is defined as $X = \int \left(\sigma^* - \sigma\right)^2 dV$. Zienkiewicz-Zhu error estimator tries to estimate the error due to the finite element discretization. An element is subdivided if the error calculated exceeds user defined numerical values, f_1, f_2 and f_3, such that,

$$\pi > f_1 \text{ and } X_{el} > f_2 * X / NUMEL + f_3 * X * f_1 / \pi / NUMEL$$

where "*NUMEL"* is the number of elements in the mesh.

The mesh refinement apart from the Zienkiewicz-Zhu criterion, gives satisfactory results for indentation depth of 3 mm. However, the tissue model should be indented at most the half of the tissue thickness, and those criterions do not enable accurate simulation results. Only the Zienkiewicz-Zhu criterion provides accurate finite element simulation results when indentation depths are 10 to 14 mm. The final refined mesh of the tissue model after indentation is demonstrated in Figure 5.9.

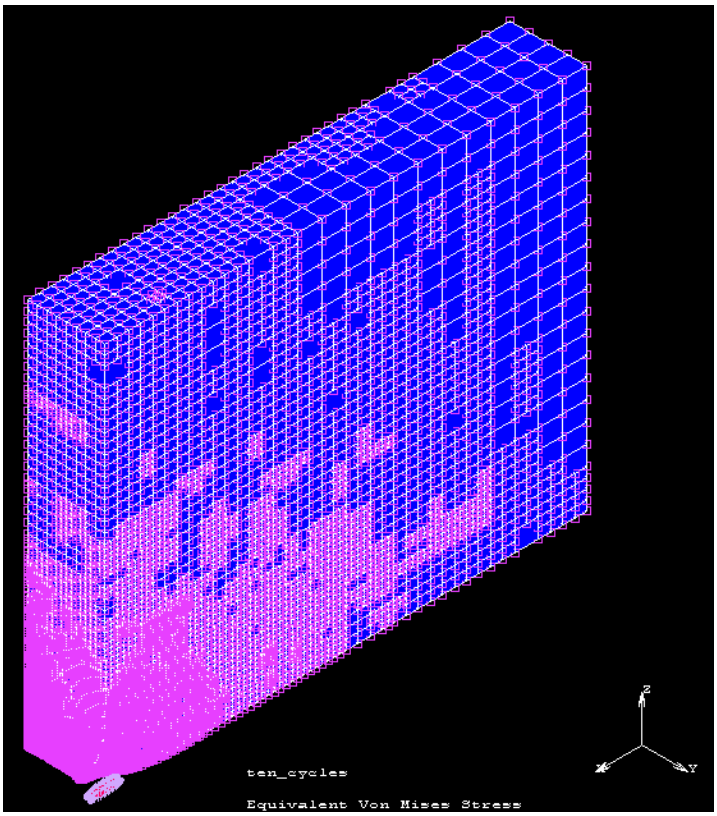

Figure 5.9 Zienkiewicz-Zhu Criterion Mesh Refinement

5.2.8 Hexahedral Mesh Compared with Tetrahedral Mesh

In this part, hexahedral mesh with mesh refinement technique and Zienkiewicz-Zhu criterion is compared with a manual tetrahedral mesh with same material properties and simulation parameters. 3 mm indentation with 1 mm/s indentation rate is applied to the tissue model with hexahedral mesh and tetrahedral mesh.

Different mesh types (hexahedral and tetrahedral) were compared by employing the adaptive time stepping procedure. It is known that, the accuracy of the solution depends significantly on the time step value chosen. In order to increase the accuracy of the solution time step size should be sufficiently low, however decreasing the time step size unnecessarily increases the solution time drastically. For adaptive time stepping procedure, the time step size is correlated with the initial fraction of the load-case time which is an important parameter that controls the accuracy of the solution. The accuracy of the hexahedral mesh apart from the refinement level and the refinement value depends on the initial fraction of the load-case time. Initial

fraction of the load-case time determines the initial time step of the solution. For our case, the total load-case time is 3 seconds and therefore when the initial fraction of the load-case time is 0.1; initial time step of the solution becomes 0.3 seconds. Figure 5.10 demonstrates the power of the initial load-case time value chosen on the solution performance and accuracy. The simulations were performed with the same material parameters defined in previous section. The indenter is assumed to indent and then retract immediately. From Figure 5.10 it is observed that the solution convergence is dependent to the initial fraction of the load-case time parameter defined by the user. Table 5.4 also demonstrates the wall time versus initial fraction of the load-case time.

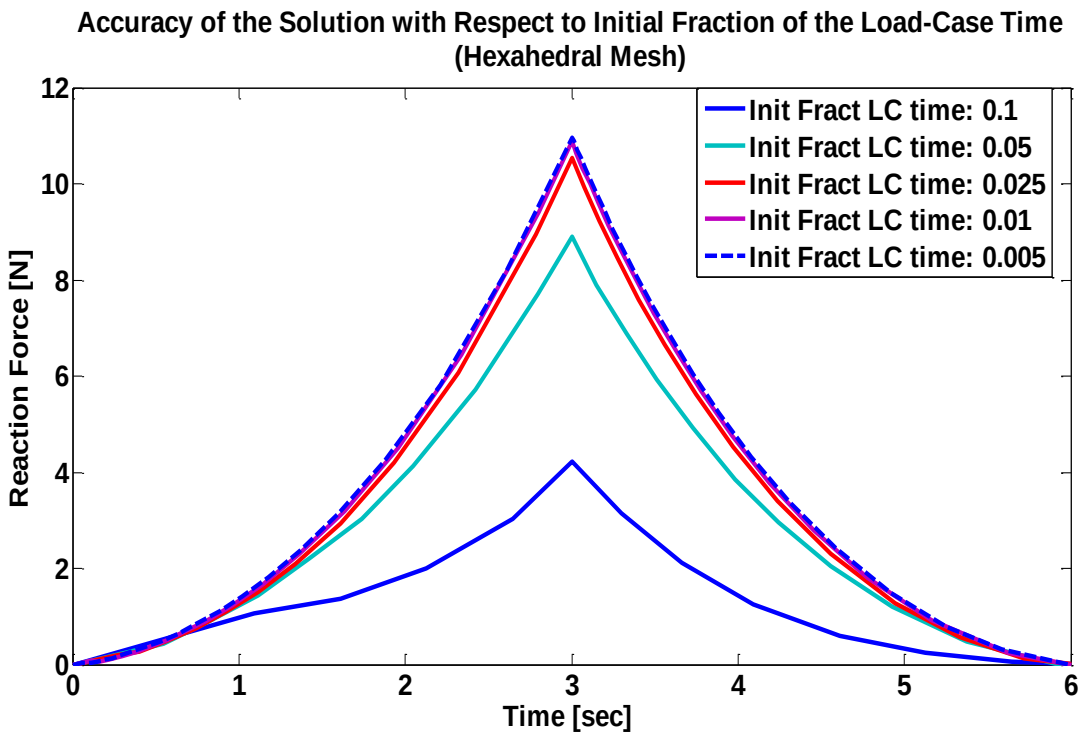

Figure 5.10 Accuracy of FE Solution (Hexahedral Mesh)

Table 5.4 Time Step And Wall Time Relation (Hexahedral Mesh)

Initial Fraction of the Load-Case Time (Hexahedral Mesh)	**Wall Time (s)**
0.1	625
0.05	2191
0.025	3703
0.01	11210
0.005	12814

For tetrahedral mesh, the initial fraction of the load-case time does not have any significant effect on the accuracy of the solution. This is due, either the mesh is constructed manually or the mesh is accurate enough.

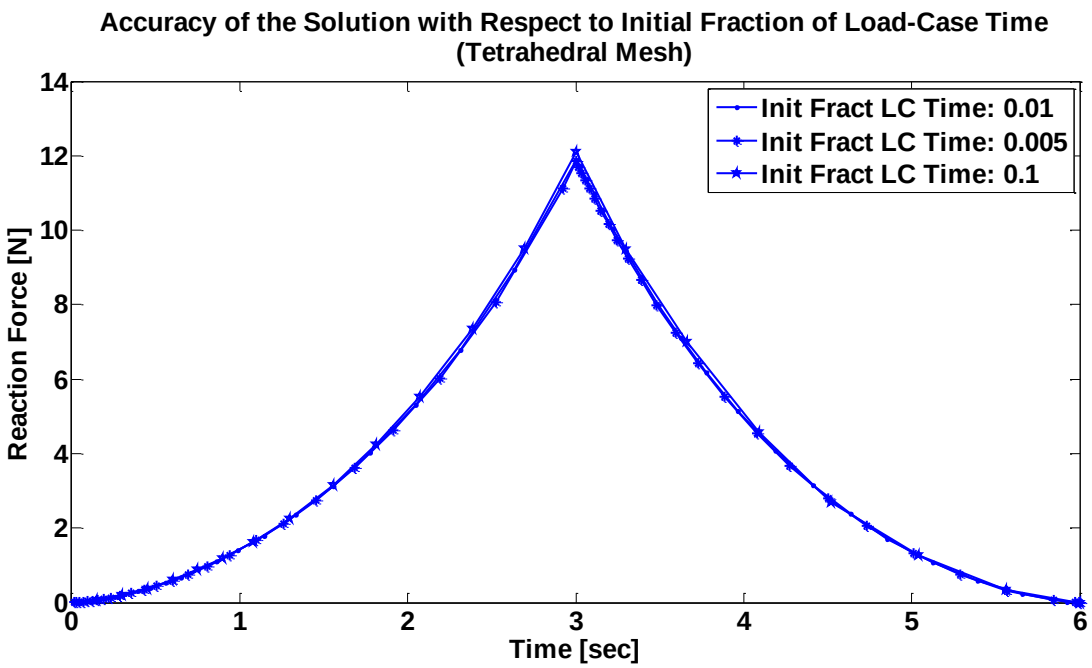

Figure 5.11 Accuracy of FE Solution (Tetrahedral Mesh)

Table 5.5 Time Step And Wall Time Relation (Tetrahedral Mesh)

Initial Fraction of the Load-Case Time (Tetrahedral Mesh)	**Wall Time (sec)**
0.1	3196
0.01	3805
0.005	4464

The hexahedral mesh with mesh refinement in Msc.Marc 2010 provides more user control on the solution and therefore becomes more efficient and accurate compared to the tetrahedral mesh when the solution parameters are chosen properly. When using automatic time stepping scheme, the finite element program reduces the time step if it is too large to converge. However when the initial fraction of the load-case time is set too large at the beginning of the solution, then the program is unable to reduce the time step below the user defined criteria and then terminates prematurely. Therefore it is very important to input the initial fraction of the load-case time as lowest, for the solution to work out. However, this option increases the wall time drastically; even the program increases the time step where available.

5.3 First Simulation Results

Large deformation simulations are done where the nonlinear elastic and viscoelastic material parameters are taken as unity $C_{01}, C_{10}, C_{11}, C_{20}, C_{30}, E_1, E_2, \eta = 1$ and the fractional order is $\beta = 0.5$. The tissue model is indented 50% of its thickness similar to experiments done by Petekkaya (2008) with 1 mm/s velocity and relaxation and hysteresis behaviors are observed. The relaxation curve obtained is demonstrated in Figure 5.12.

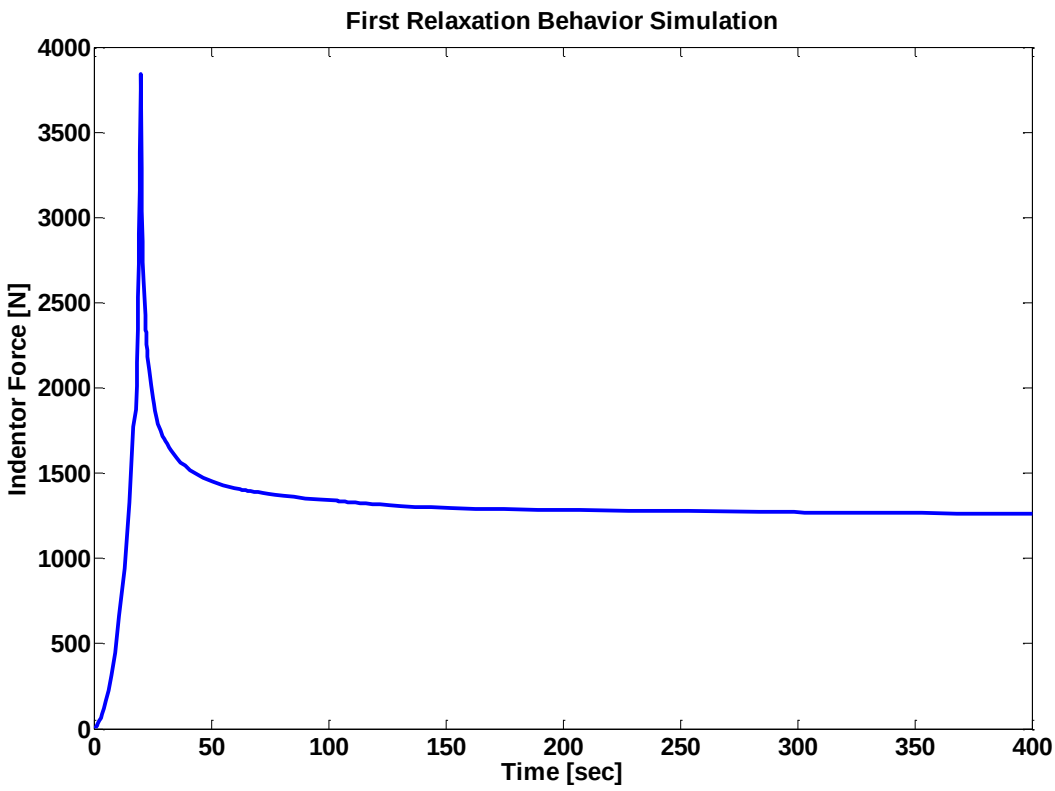

Figure 5.12 Relaxation Simulation (Quarter Tissue Model)

Wall time for the relaxation analysis is approximately 100000 seconds which is approximately more than 1 day.

Cyclic loading protocol (first cycle only) was also simulated. The tissue reaction force –time behavior is presented in Figure 5.13.

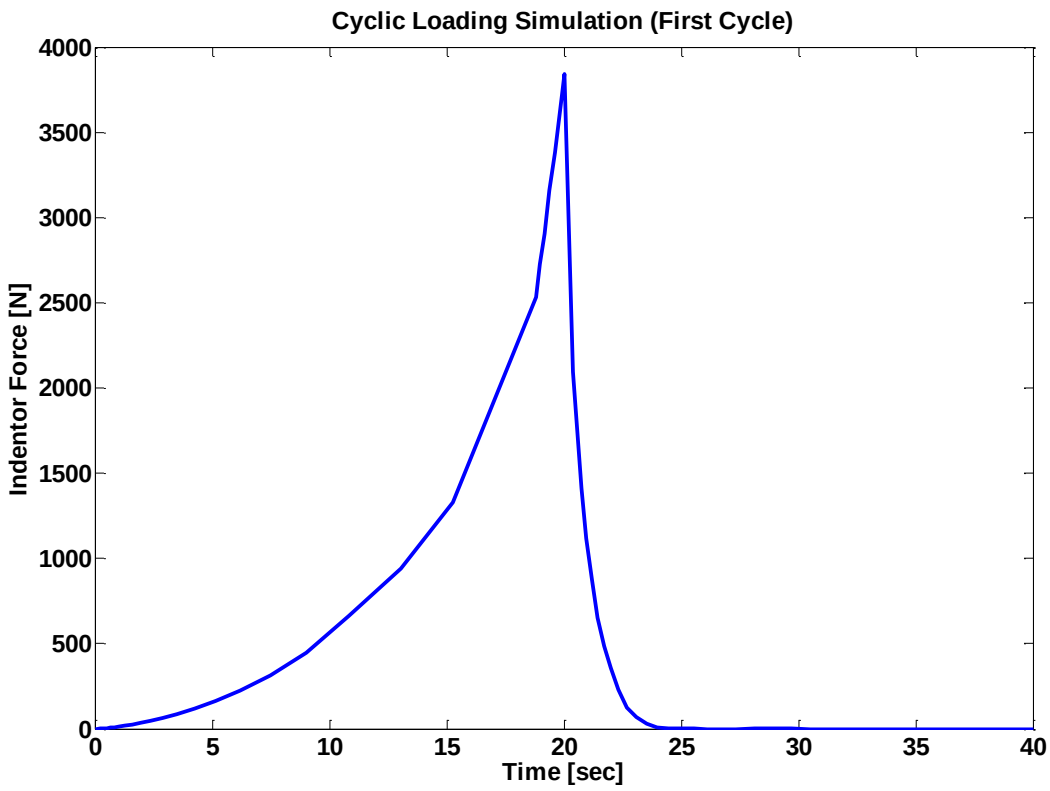

Figure 5.13 Cyclic loading protocol (First cycle only)

A permanent deformation is present on the tissue model as it can be seen from Figure 5.13, which represents the viscous property of the tissue. Again the wall time for the solution of this simulation is approximately 1 day, which is too long for iterative material property determination.

As stated in the thesis of Potvin (2001), although the classical integer order models yield generally poor representation of the experimental data, the fractional model yields a satisfactory representation but with a much higher CPU time due to the hereditary nature of the fractional derivatives. It is recommended in the thesis, to use Prony series models, unless the data to perform the parameter identification is limited. In that case, the fractional order model can be interesting despite the higher demands of solution time. For our work, axisymmetric model of the soft tissue is preferred due to time constraints.

5.4 Material Parameter Investigation

In order to fit the fractional order material model to the experimental data by curve-fitting of the material parameters, the effect of each material parameter to soft tissue mechanical behavior has to be analyzed separately. For this reason, several different finite element simulations with different material parameters were performed with cyclic loading simulation protocol. 4 mm/s indentation rate and approximately 18 mm of indentation to the soft tissue model is simulated for one cycle (indenting and retracting back). The indenter tip is modeled as ellipsoidal with dimensions of 16x4 mm. The tissue model has dimensions of 200x36.9x200mm while the tissue thickness at the day of experiment data gathered is measured as 36.9 mm from the ultrasound imaging (Petekkaya, 2008). For this simulation, two load cases have been defined. The convergence tolerance is taken relatively small for indenting load case (0.003) and taken relatively high for retracting load case (0.1), in order to get accurate and fast simulation results.

In cyclic loading nonlinear elastic parameters are more dominant on soft tissue response therefore time dependent parameters were kept constant at values,

$$\beta = 0.2,\ \ \tau = 5s,\ \ \delta = 0.2$$

The nonlinear elastic material parameters were altered for each simulation to observe the characteristic behavior of each parameter.

Trial 1: $C_{01} = 2.5e-4,\ C_{10} = 2.5e-4\ , C_{11} = 5e-3\ , C_{20} = 5e-3,\ C_{30} = 5e-3\ MPa$

Trial 2: $C_{01} = 2.5e-4,\ C_{10} = 2.5e-4\ , C_{11} = 5e-3\ , C_{20} = 5e-3,\ C_{30} = 2.5e-3\ MPa$

Trial 3: $C_{01} = 8e-4,\ C_{10} = 8e-4\ , C_{11} = 5e-3\ , C_{20} = 5e-3,\ C_{30} = 1e-4\ MPa$

Trial 4: $C_{01} = 1e-4,\ C_{10} = 1e-4\ , C_{11} = 1e-3\ , C_{20} = 1e-3,\ C_{30} = 1e-4\ MPa$

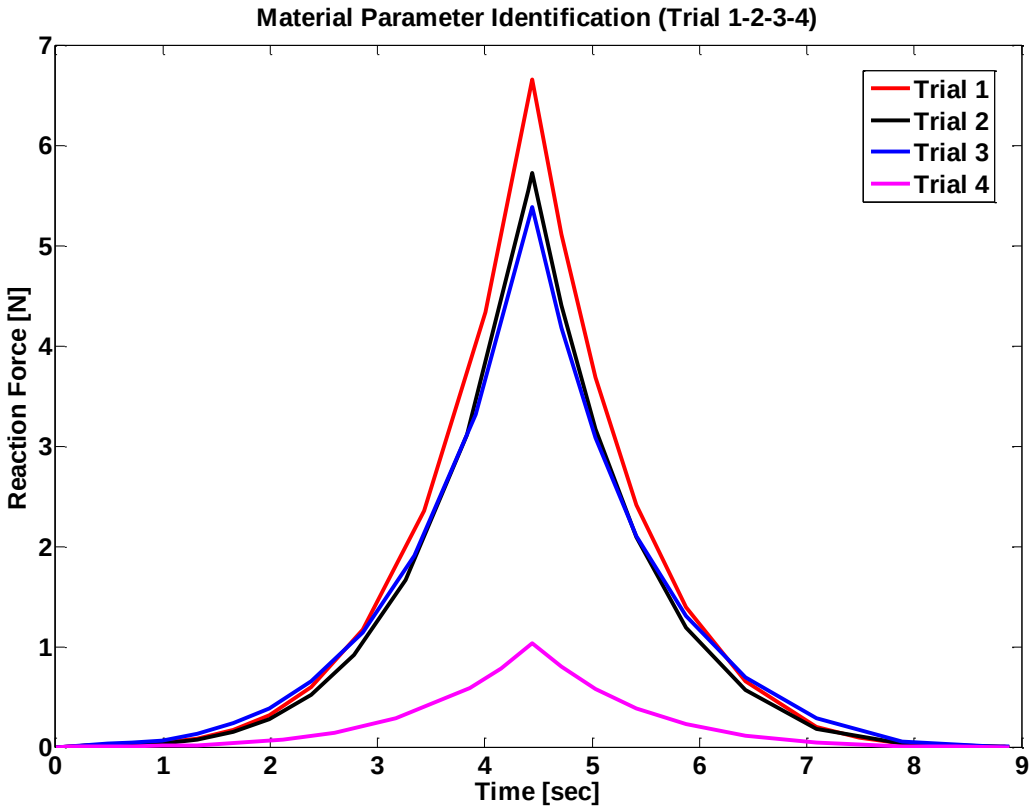

Figure 5.14 Material Parameter Investigation (Trials 1-2-3-4)

Trial 5: $C_{01} = 6.25e-3,\ C_{10} = 6.25e-3\ , C_{11} = 1e-3\ , C_{20} = 1e-3,\ C_{30} = 1e-4\ MPa$

Trial 6: $C_{01} = 6e-3,\ C_{10} = 6e-3\ , C_{11} = 5e-4\ , C_{20} = 1e-3,\ C_{30} = 1e-4\ MPa$

Trial 7: $C_{01} = 6e-3,\ C_{10} = 6e-3\ , C_{11} = 2.5e-4\ , C_{20} = 2.5e-4,\ C_{30} = 5e-5\ MPa$

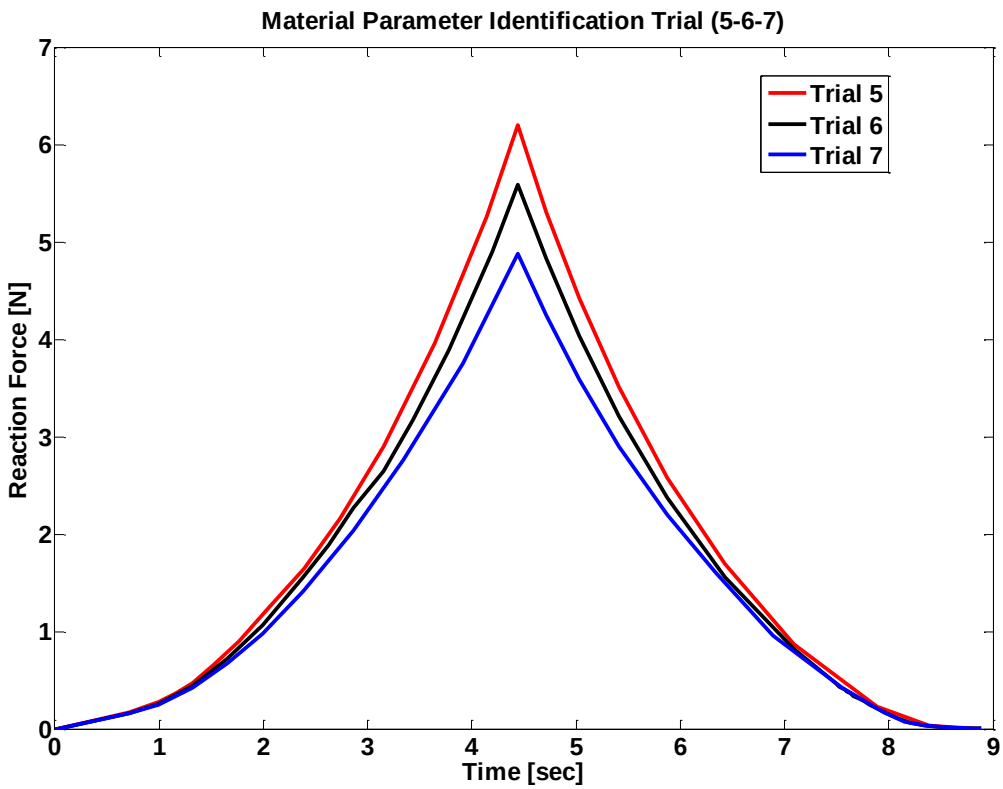

Figure 5.15 Material Parameter Investigation (Trials 5-6-7)

After investigating the behavior of material parameters, it has been observed that, the first two nonlinear elastic parameters (C_{01} and C_{10}) affects the initial linear tangent curve and they are the first order parameters. The second order parameters (C_{11} and C_{20}) affect the nonlinear part of the curve and finally the third order parameter (C_{30}) affects the whole behavior of the curve including the peak.

CHAPTER 6

AXISYMMETRIC MODELING OF SOFT TISSUE

In the previous chapter, the finite element analyses were performed with a three-dimensional, quarter model of the tissue because the experiments were performed with an ellipsoid indenter tip to detect the in-plane anisotropy of soft tissues. As for the three-dimensional model the computational time is significantly high and since tissue anisotropy is out of the scope of this thesis, an axisymmetric model of the tissue with flat tip cylindrical indenter is offered.

A manual mesh was preferred instead of adaptive mesh refinement option due to computational costs of the iterative material model parameter identification. However, local adaptivity (*node in contact* option) is turned on for only the contact elements and the level of *mesh refinement* was taken to be 3.

The axisymmetric model and mesh is created by using the software Msc.Patran 2010. The elements are full and degenerated hexahedral elements and have no mid-side nodes. The model is build-up by 4-node, type 82 *Hermann elements*. The tissue-indenter interface is modeled as complete frictionless and "delay slide off" option is turned on in order to prevent nodes sliding while deformation. 75 nodes are present just below the indenter and "node in contact" local adaptive mesh refinement option is turned on for contact elements.

6.1 Mesh Optimization

The axisymmetric tissue model and the rigid indenter model with applied boundary conditions are presented in Figure 6.1. Axisymmetric and fixed boundary conditions are applied to the tissue model. Tissue model dimensions were 200×40 *mm* in $x-y$ domain. Mesh is refined under the contact region and mesh optimization is done by decreasing the number of the elements in the mesh and comparing the wall

time of the solution and tissue reaction force obtained from the finite element simulations.

The number of elements in the mesh was decreased until the solution diverges approximately 1-2% from the previous result. The material parameters were taken as unity for mesh convergence analysis. The indenter indents the tissue model with 1mm/s velocity for 10 seconds and retracts back with the same velocity. Adaptive time stepping option was employed. The axisymmetric mesh is presented in Figure 6.1 and the refined mesh under the contact region is presented in Figure 6.2.

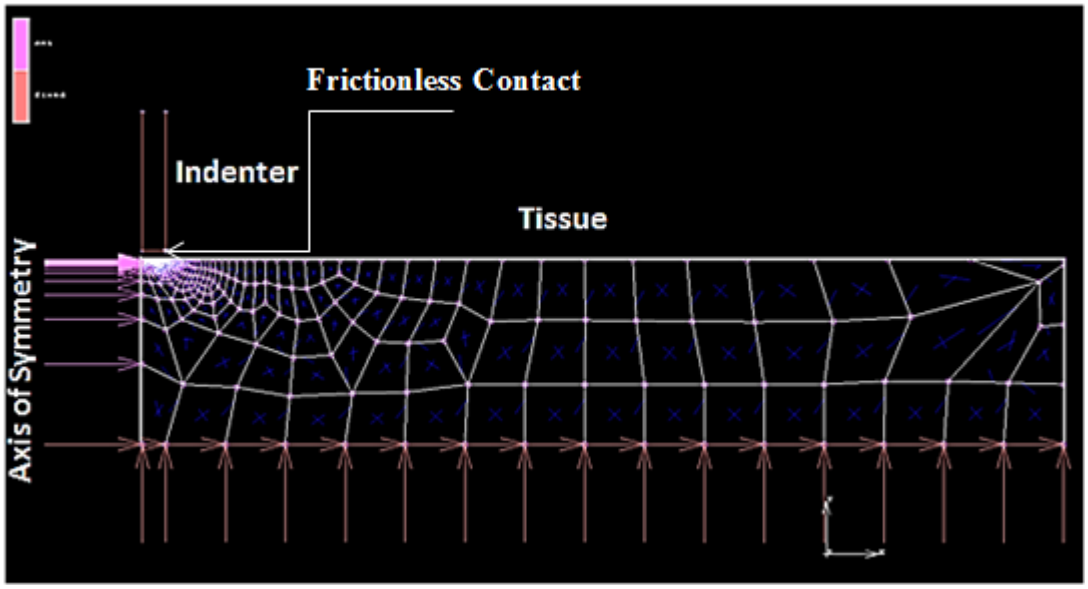

Figure 6.1 Axisymmetric FEM of Soft Tissue and Rigid Body Indenter

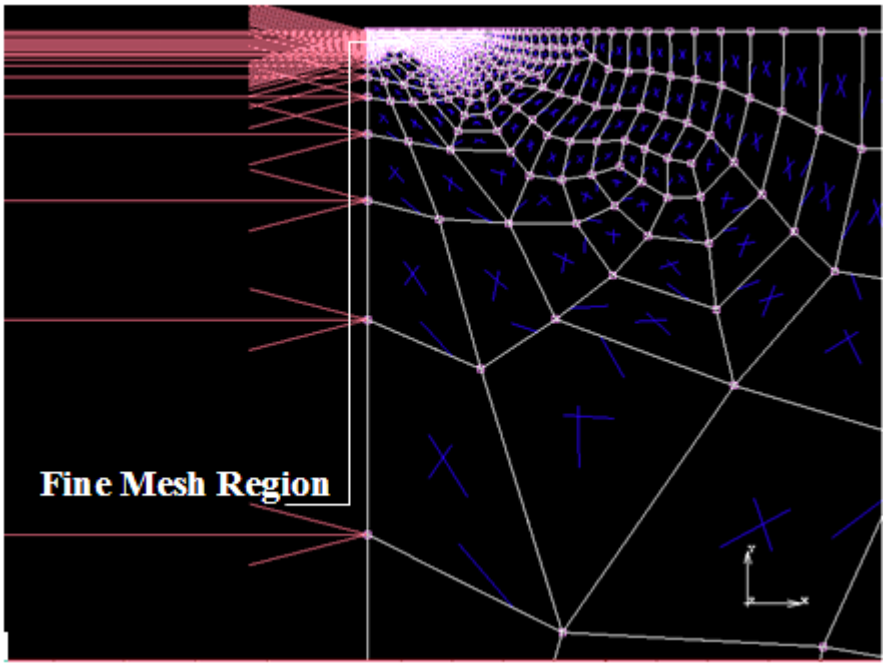

Figure 6.2 A Closer View of the Fine Mesh Region under the Indenter Tip

A refined mesh is needed to handle the severe stress gradients near the indenter edge where a stress/strain singularity may exist (Figure 6.3).

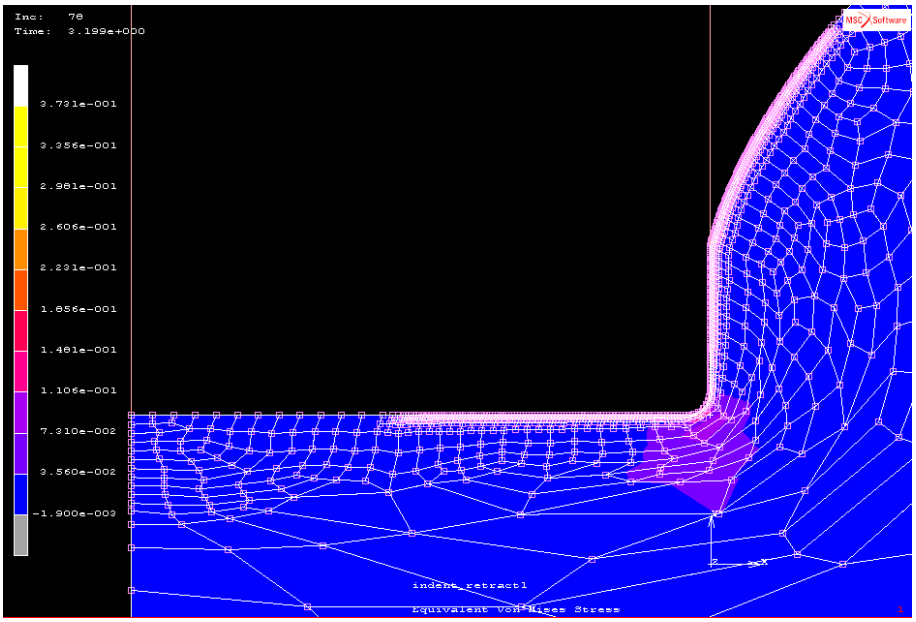

Figure 6.3 High Stress Concentration at the Edge of the Indenter Tip

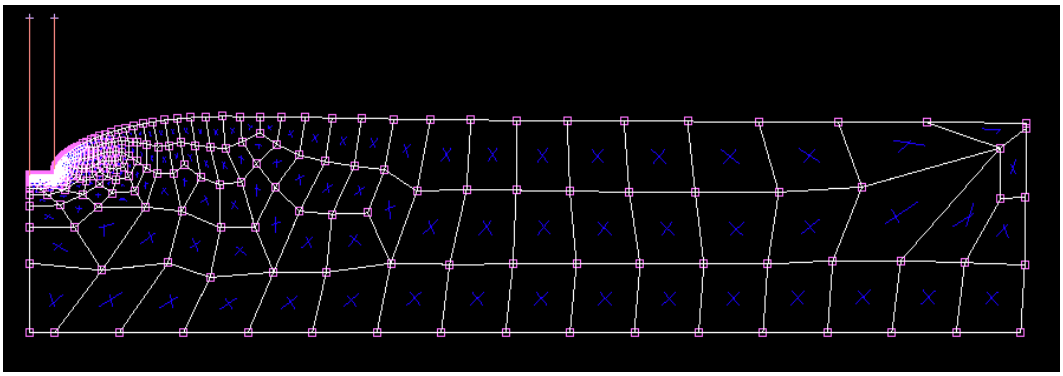

Figure 6.4 View of the Whole Tissue Model after Indentation

Mesh optimization routine is employed to work with a better model mesh. To do this, number of elements in the mesh is gradually decreased and wall time of the solution and the accuracy of the result are observed.

Table 6.1 Mesh Optimization Results (Axisymmetric Model)

Number of Elements in the Mesh	Wall Time [sec]	Peak Reaction Force [N]
3679	3103	44329
3155	3633	44790
2103	2480	44847
1435	1670	43521
829	**341**	**45512**
533	194	48209
236	64	48821
88	20	49161

According to the mesh optimization results (Table 6.1), the soft tissue mesh with 829 elements is selected as the wall time of the solution is only 341 seconds and the peak force deviates from the first result only 2.5%. Although 2.5% may seem to be large,

considering material parameter identification to be an iterative process, solution time has a priority over convergence.

In Figure 6.5, the accuracy related to the mesh can be clearly seen.

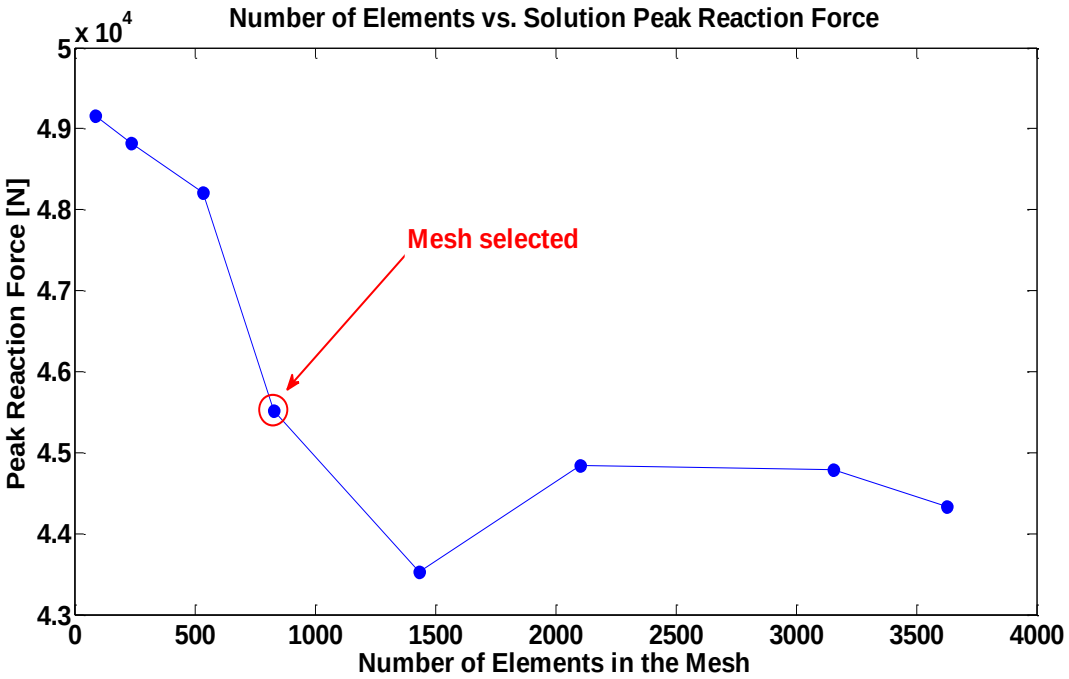

Figure 6.5 Axisymmetric Mesh Optimization Result

6.2 Analyzing Experimental Data

Parameter identification trials begin by analyzing the experimental data of (Petekkaya, 2008). In these soft biological tissue experiments several different indenter tips have been used. However, as our model is an axisymmetric model experiments performed with cylindrical indenter tips are analyzed only.

Cyclic loading, stress relaxation and creep experiment protocols which were performed on the fore-arm of the human body were analyzed. One of the experiment data regarding the cyclic loading protocol is shown in Figure 6.6. In this experiment

4 mm/s indentation rate is applied with approximately 14 mm of indentation for ten cycles. Here only the first cycle of the experiment is analyzed to identify the material parameters by fitting the material model to the experimental data.

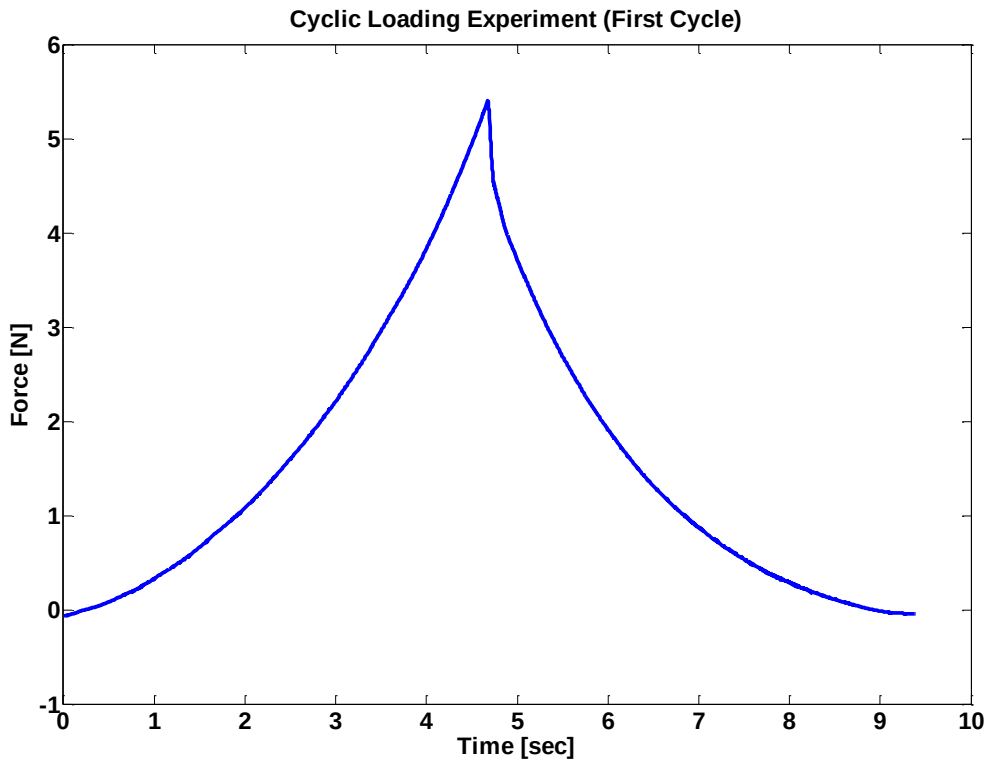

Figure 6.6 First Cycle of the Cyclic Loading Experiment

During experiments it is necessary to determine the contact of indenter tip to soft tissue. This was done by an automated protocol proposed by Petekkaya (2008). The same protocol was used to determine the instant when the indenter tip loses contact with the soft tissue during retraction (Figure 6.7).

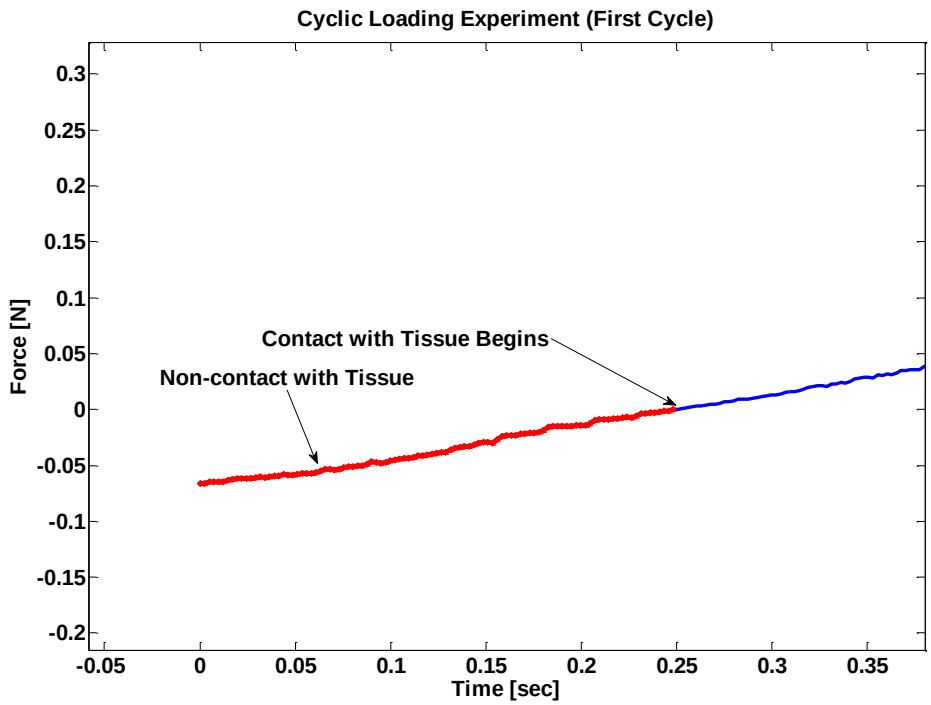

Figure 6.7 Contact Start of the Indenter Tip with the Tissue

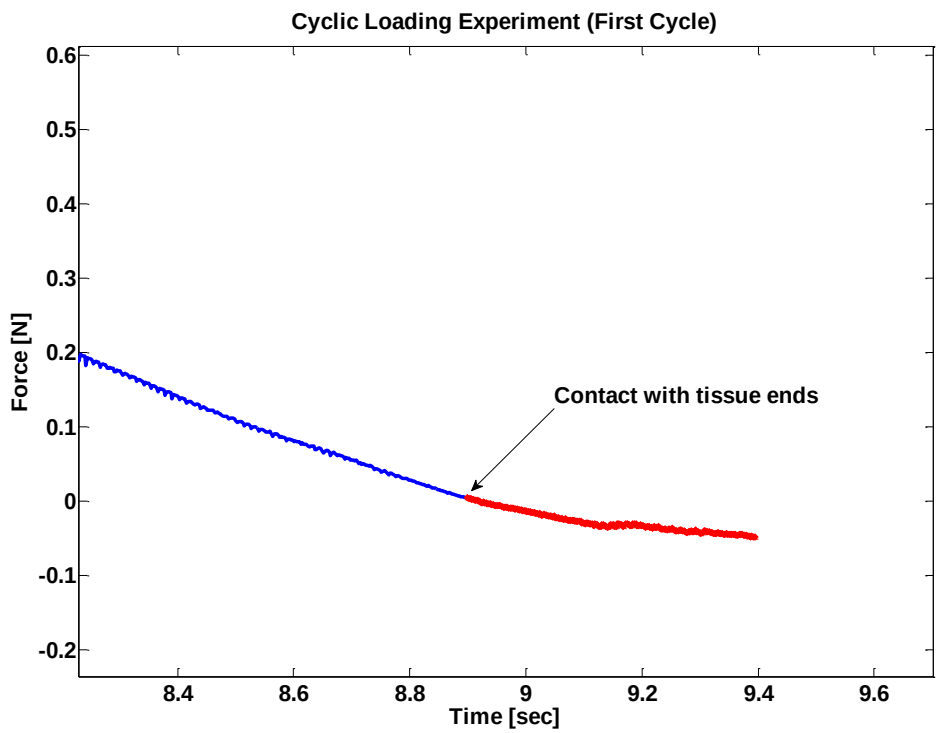

Figure 6.8 Contact End of the Indenter Tip with the Tissue

The indenter pauses for a short interval of time at the end of indentation and just before retraction begins. During this very short interval of time the tissue, being a viscoelastic material, relaxes as presented in Figure 6.9.

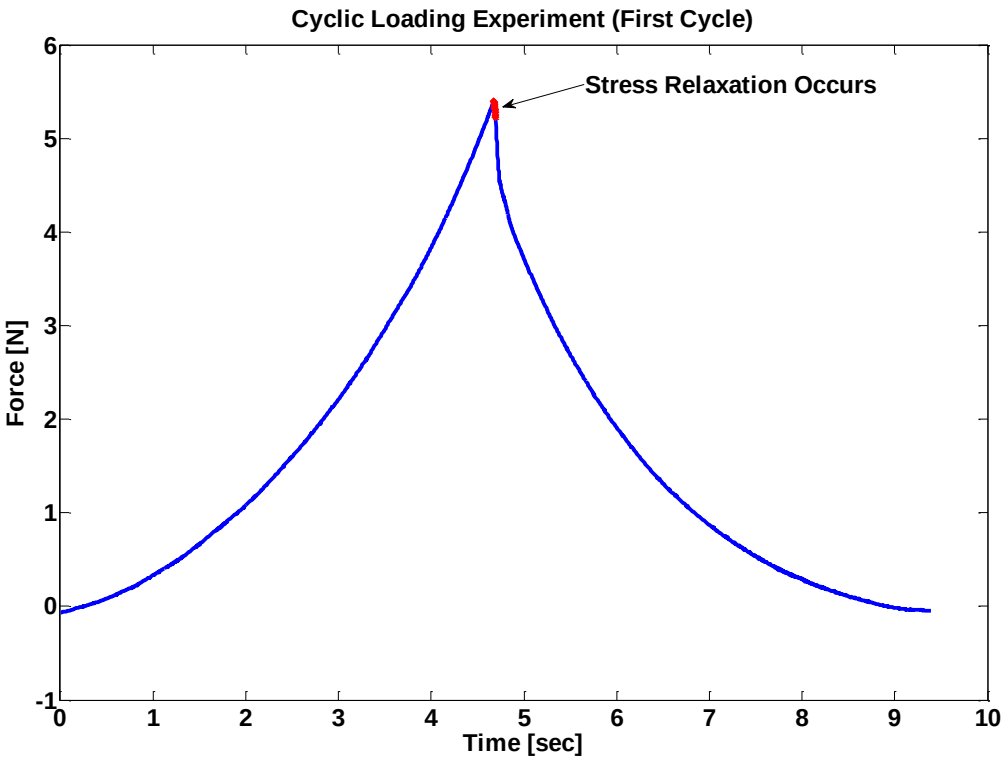

Figure 6.9 Stress Relaxation on Tissue During Cyclic Loading

Specifically for this data, the indenter pauses for about 0.022 seconds after indenting and just before retracting and for this small period of time, the peak reaction force decreases from 5.39 N to 5.22 N. The relative error becomes 3.25% when this relaxation is underestimated. The stress relaxation of the tissue between indenting and retracting is underestimated within this parameter fit, as the waiting time of the indenter after indenting and just before retracting back is significantly small.

6.3 Material Parameter Identification

6.3.1 Parameter Extraction for Experimental Relaxation Data

The in-vivo experimental relaxation experiment data is obtained from (Petekkaya, 2008) and presented in Figure 6.10. The indentation rate for the finite element simulation of the ramp portion of the relaxation test is 5 $\% mm/s$.

Pioletti, Rakotomanana & Leyvraz (1998), have demonstrated that the indentation rate affects mainly the toe-region of the stress strain relationship while it leaves the tangent modulus of the linear region almost unaffected which will also be analyzed at the end of this part.

Nonlinearities present in the finite element simulation are,

- Material nonlinearities (nonlinear properties of the soft tissue, *i.e.* stiffening of the tissue with increasing strain)
- Geometrical and contact nonlinearities

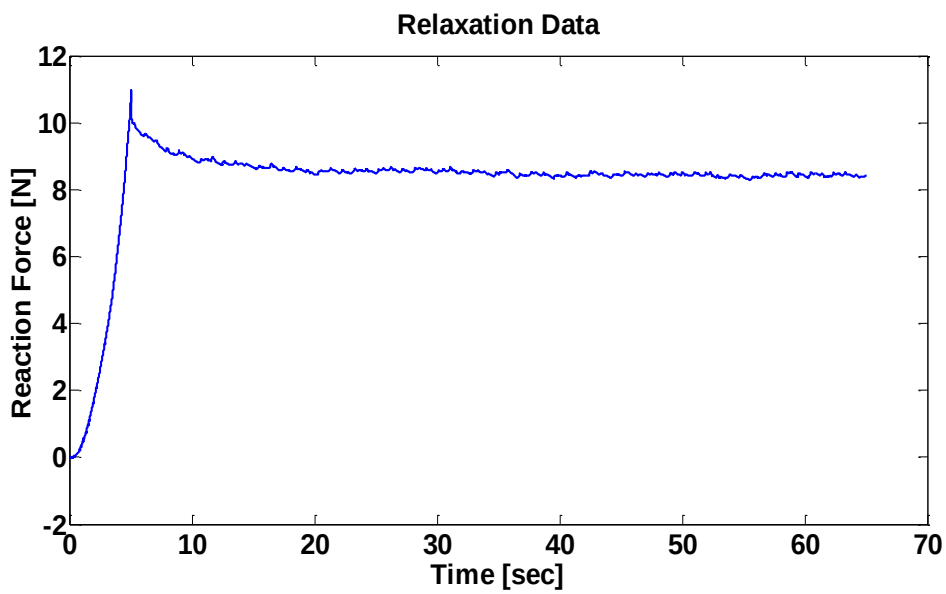

Figure 6.10 Raw Relaxation Experiment Data

Initial arbitrary estimates to nonlinear elastic and viscoelastic (by regression to tissue reaction force-time for the one dimensional model) parameter set determined is presented in Table 6.2.

Table 6.2 Parameter Set #1

Nonlinear Elastic Parameters	C_{01} $[MPa]$	C_{10} $[MPa]$	C_{11} $[MPa]$	C_{20} $[MPa]$	C_{30} $[MPa]$
	$1e-4$	$1e-4$	$5e-5$	$5e-5$	$3e-4$
Viscoelastic Parameters	τ $[s]$	δ	β		
	5.857	0.2503	0.58		
NSSE $(\%)$	8.64				

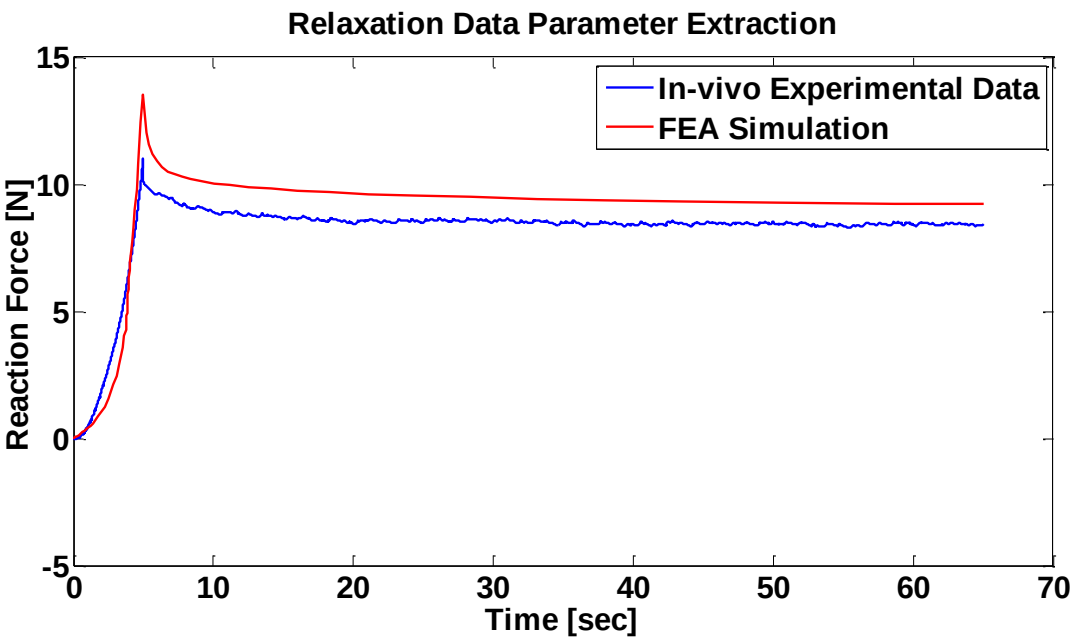

Figure 6.11 Relaxation Data Fit (Parameter Set 1)

The simulation with the estimated material parameters resulted the tissue reaction force time data presented in the Figure 6.11. Because the simulated force was not very close to the experimental data (NSSE being larger than 8 %), it can be deduced that the initial estimate material parameters were not representing the soft tissue behavior with desired accuracy and needs to be modified to match the experimental reaction force time data. The simulation was repeated with parameters presented in Table 6.3 and the simulated tissue reaction force is presented in Figure 6.12. After six trials the simulated reaction force was close enough to experimental reaction force and it was decided that the material parameters which represent the soft tissue material behavior were extracted (Figures 6.13 to 6.16 and Tables 6.4 to 6.7).

Table 6.3 Parameter Set #2

Nonlinear Elastic Parameters	C_{01} $[MPa]$	C_{10} $[MPa]$	C_{11} $[MPa]$	C_{20} $[MPa]$	C_{30} $[MPa]$
	$3e-4$	$2e-4$	$5e-5$	$5e-5$	$5e-5$
Viscoelastic Parameters	τ $[s]$	δ	β		
	1.857	0.2503	0.58		
NSSE $(\%)$	23.03				

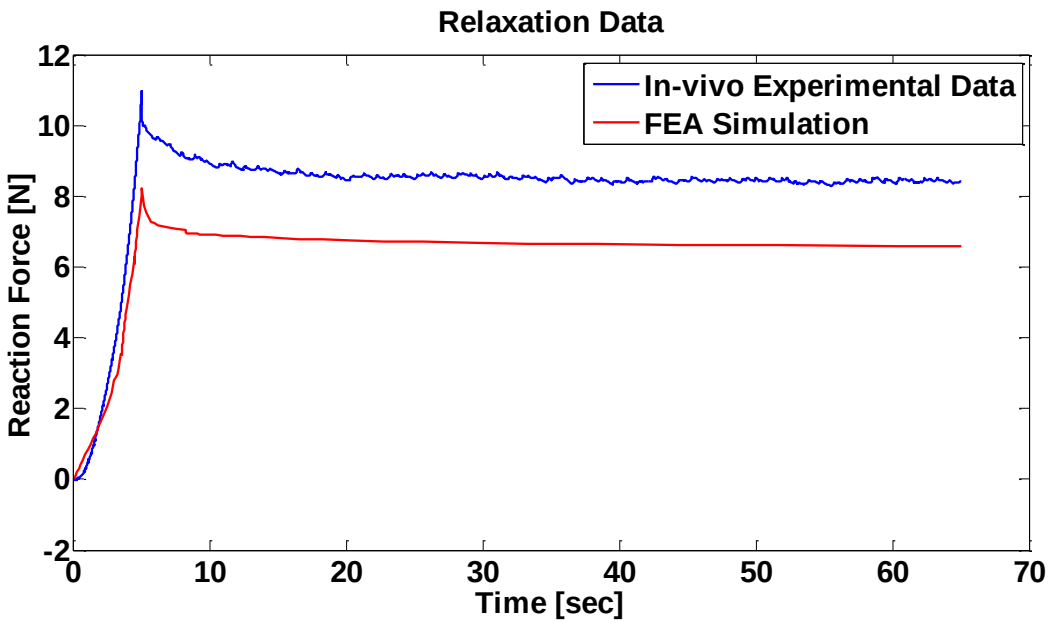

Figure 6.12 Relaxation Data Fit (Parameter Set 2)

Table 6.4 Parameter Set #3

Nonlinear Elastic Parameters	C_{01} $[MPa]$	C_{10} $[MPa]$	C_{11} $[MPa]$	C_{20} $[MPa]$	C_{30} $[MPa]$
	$1e-4$	$1e-4$	$5e-5$	$5e-5$	$1e-4$
Viscoelastic Parameters	τ $[s]$	δ	β		
	1.857	0.2503	0.58		
NSSE $(\%)$	56.18				

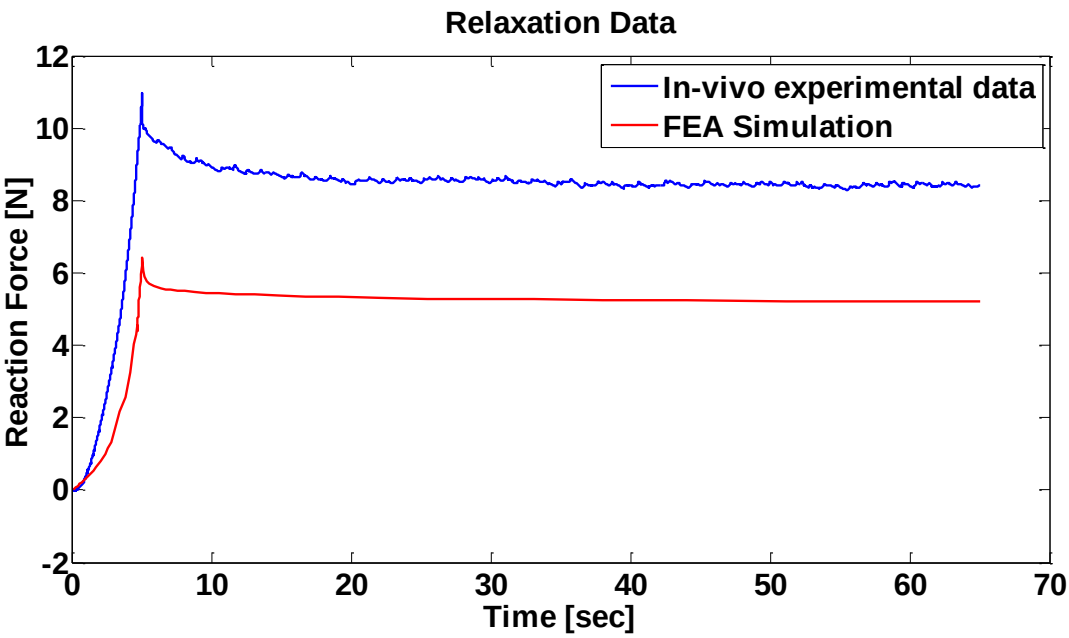

Figure 6.13 Relaxation Data Fit (Parameter Set 3)

Table 6.5 Parameter Set #4

Nonlinear Elastic Parameters	C_{01} $[MPa]$	C_{10} $[MPa]$	C_{11} $[MPa]$	C_{20} $[MPa]$	C_{30} $[MPa]$
	$1e-4$	$4e-4$	$5e-5$	$5e-5$	$1e-4$
Viscoelastic Parameters	τ $[s]$	δ	β		
	1.857	0.2503	0.58		
NSSE $(\%)$	6.45				

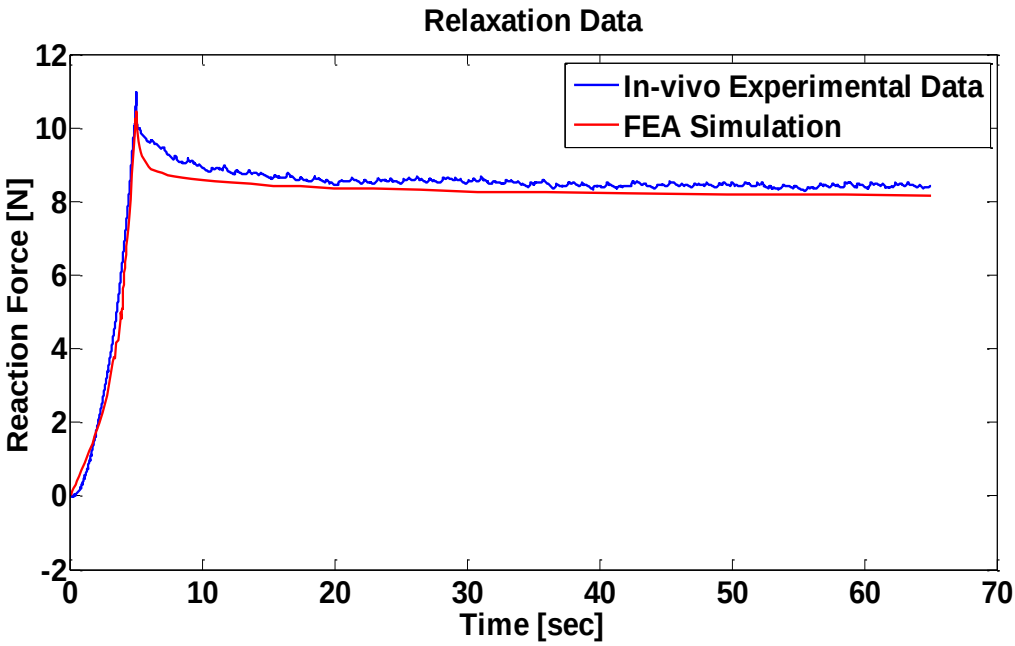

Figure 6.14 Relaxation Data Fit (Parameter Set 4)

Table 6.6 Parameter Set #5

Nonlinear Elastic Parameters	C_{01} $[MPa]$	C_{10} $[MPa]$	C_{11} $[MPa]$	C_{20} $[MPa]$	C_{30} $[MPa]$
	$1.1e-4$	$4.4e-4$	$5e-5$	$5e-5$	$1e-4$
Viscoelastic Parameters	τ $[s]$	δ	β		
	1.857	0.2503	0.58		
NSSE $(\%)$	4.57				

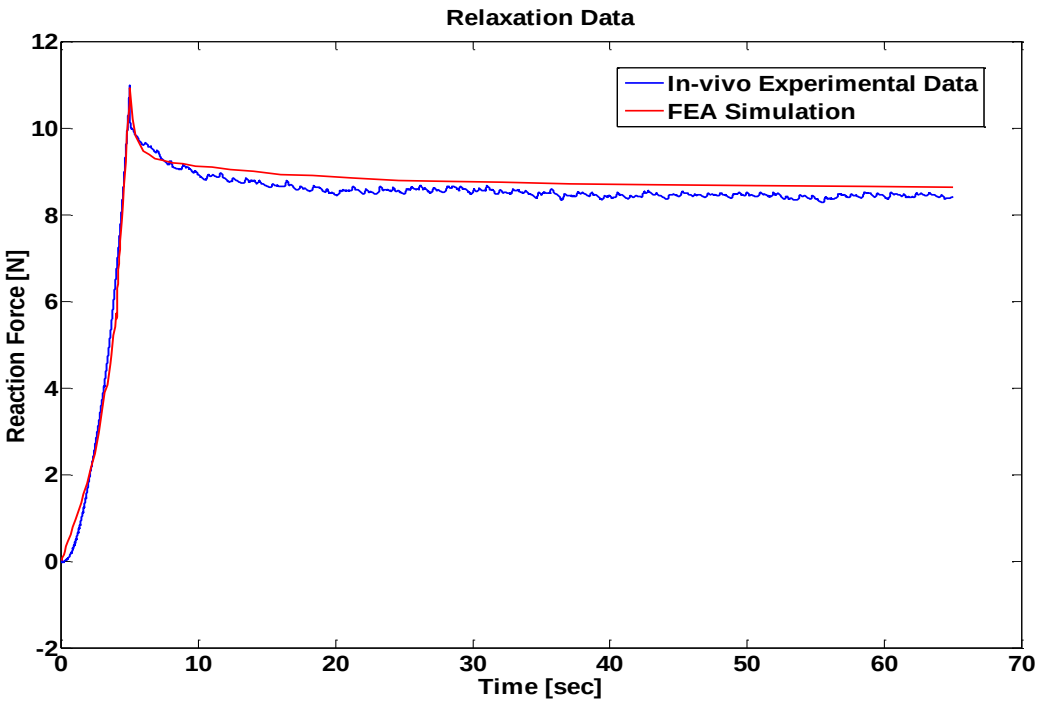

Figure 6.15 Relaxation Data Fit (Parameter Set 5)

Table 6.7 Parameter Set #6

Nonlinear Elastic Parameters	C_{01} $[MPa]$	C_{10} $[MPa]$	C_{11} $[MPa]$	C_{20} $[MPa]$	C_{30} $[MPa]$
	$1.1e-4$	$4.4e-4$	$5e-5$	$5e-5$	$1e-4$
Viscoelastic Parameters	τ $[s]$	δ	β		
	1.857	0.2503	0.70		
NSSE $(\%)$	1.15				

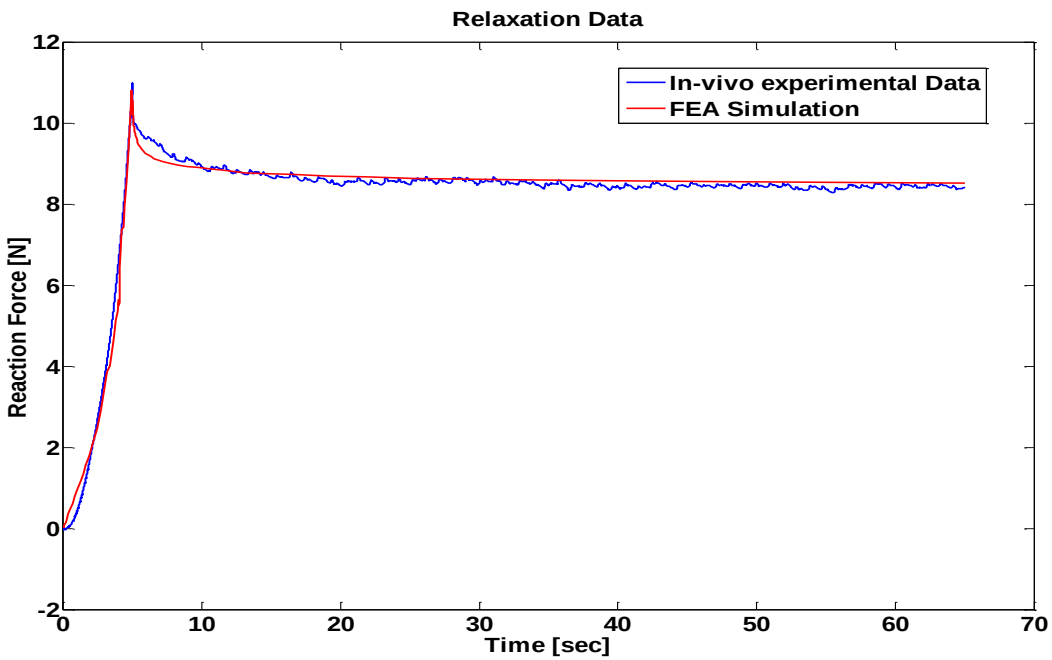

Figure 6.16 Relaxation Data Fit (Parameter Set 6)

6.3.2 Parameter Extraction for Cyclic Loading Experiment Data

Before beginning the identification of material parameters for the cyclic loading experiment data, it is required to check if the solutions obtained from "*adaptive time stepping*" and "*fixed time stepping*" solution schemes yield the same results. Figure 6.17 demonstrates the results obtained when time step is selected to be 0.01 for fixed

time stepping scheme and initial fraction of the time step is determined to be10^{-4} for the adaptive time stepping scheme. It was clearly observed that, the two solutions yield the same result (Figure 6.17).

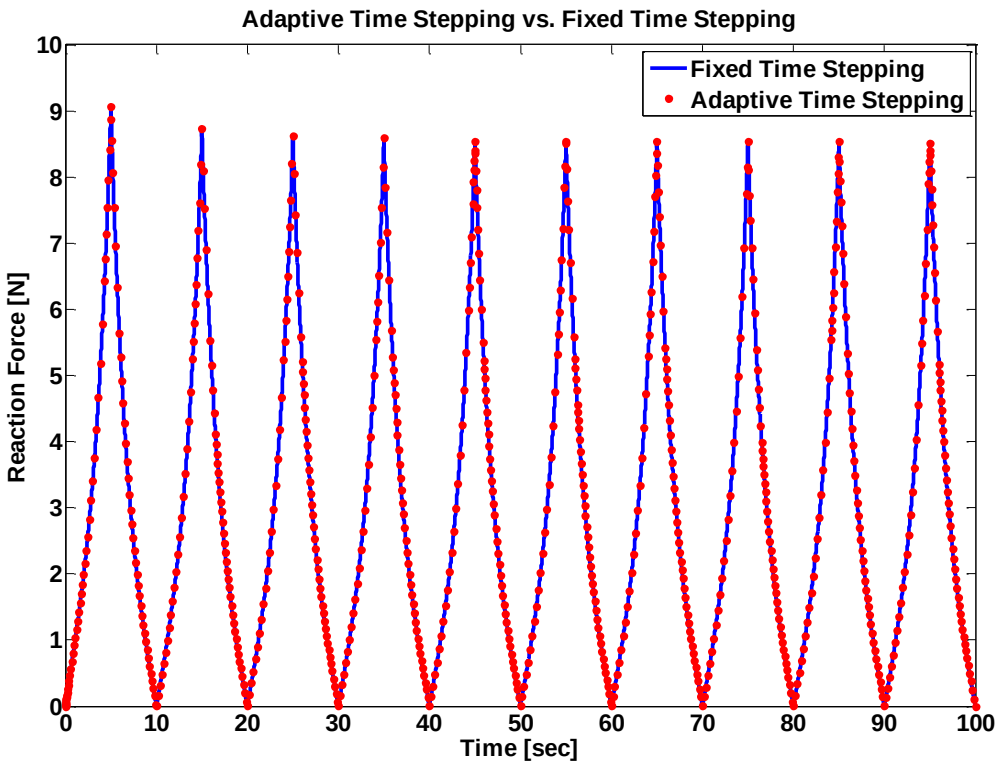

Figure 6.17 Comparison of FE Results
for "*Adaptive*" and "*Fixed*" Time Stepping Schemes

Cyclic loading (ten cycles) experiment data is taken from (Petekkaya, 2008). These experiments were performed with 10 *mm* diameter, cylindrical indenter tips. The raw cyclic loading data is shown in Figure 6.18 and only the first cycle is shown in Figure 6.19. From the ten cycles, cyclic loading experiment data, it can be deduced that the tissue is obviously preconditioned (Figure 6.18).

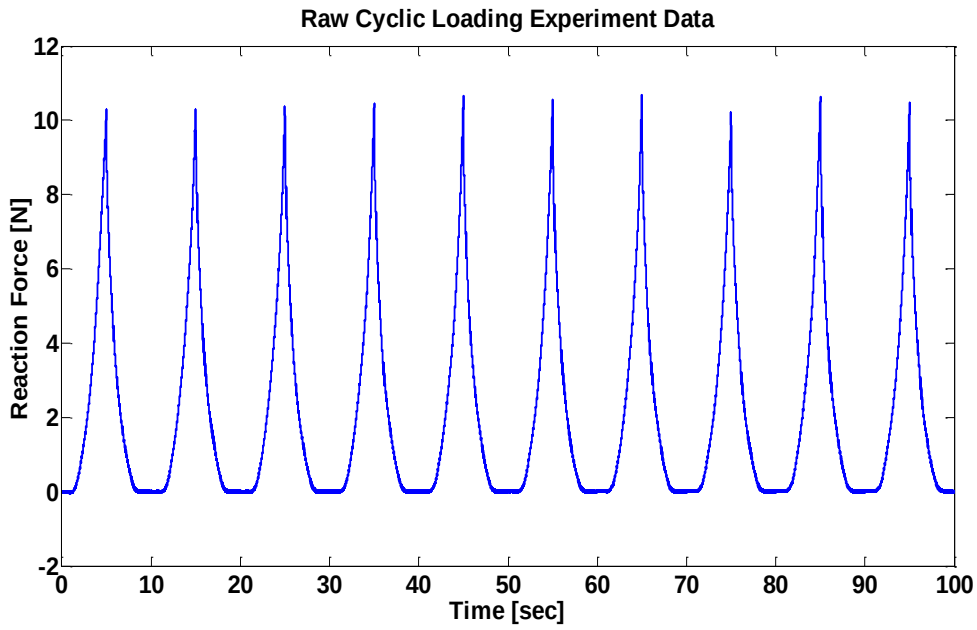

Figure 6.18 Raw Cyclic Loading Experiment Data

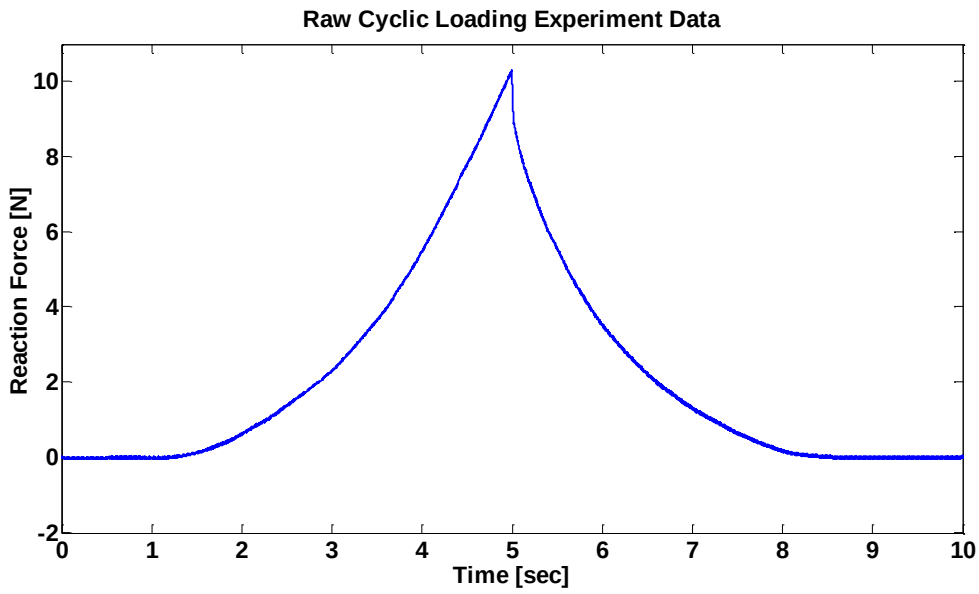

Figure 6.19 Raw Cyclic Loading Experiment Data (First Cycle)

The parameters identified by the relaxation experiment data (Table 6.7) are employed for the cyclic loading experiment data curve-fit (Table 6.8). The experiment curve is fitted with an LSE value being greater than 30% (Figure 6.20).

Table 6.8 Parameter Set #7

Nonlinear Elastic Parameters	C_{01} $[MPa]$	C_{10} $[MPa]$	C_{11} $[MPa]$	C_{20} $[MPa]$	C_{30} $[MPa]$
	$1.1e-4$	$4.4e-4$	$5e-5$	$5e-5$	$1e-4$
Viscoelastic Parameters	τ $[s]$	δ	β		
	1.857	0.2503	0.70		
NSSE $(\%)$	43.88				

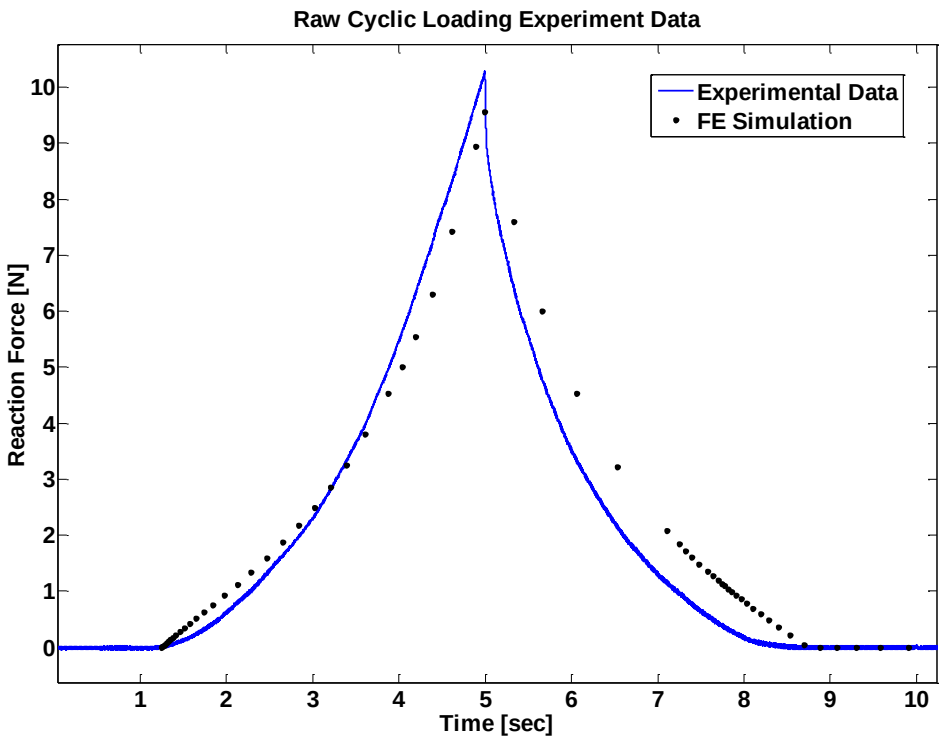

Figure 6.20 Cyclic Loading Data Fit (Parameter Set 7)

Since the fit was not satisfactory (NSSE being higher than 40 %) (tangent modulus at initial loading, and unloading portion of the curve) the material parameter set was modified to obtain a better fit as presented in Table 6.9.

Table 6.9 Parameter Set #8

Nonlinear Elastic Parameters	C_{01} $[MPa]$	C_{10} $[MPa]$	C_{11} $[MPa]$	C_{20} $[MPa]$	C_{30} $[MPa]$
	$1.3e-4$	$5.2e-4$	$5e-5$	$5e-5$	$1e-4$
Viscoelastic Parameters	τ $[s]$	δ	β		
	10.857	0.1503	0.70		
NSSE $(\%)$	55.54				

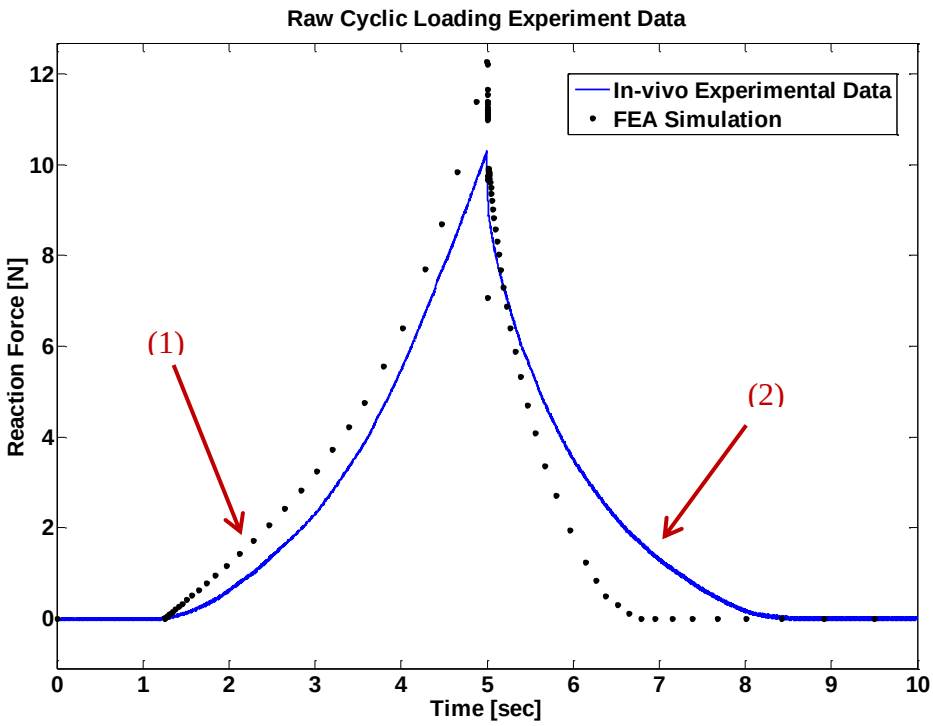

Figure 6.21 Cyclic Loading Data Fit (Parameter Set 8)

It is observed from Figure 6.21 that increasing the time constant τ yields a faster decay of the unloading curve (1) and increasing the first two nonlinear elastic parameters increases the slope of the initial linear elastic part of the curve (2). Next, the effect of increasing the parameter δ (Table 6.10) is presented in Figure 6.22.

Table 6.10 Parameter Set #9

Nonlinear Elastic Parameters	C_{01} $[MPa]$	C_{10} $[MPa]$	C_{11} $[MPa]$	C_{20} $[MPa]$	C_{30} $[MPa]$
	$1e-4$	$1e-4$	$5e-5$	$5e-5$	$1e-4$
Viscoelastic Parameters	τ $[s]$	δ	β		
	1.857	0.8503	0.70		
NSSE $(\%)$	23.58				

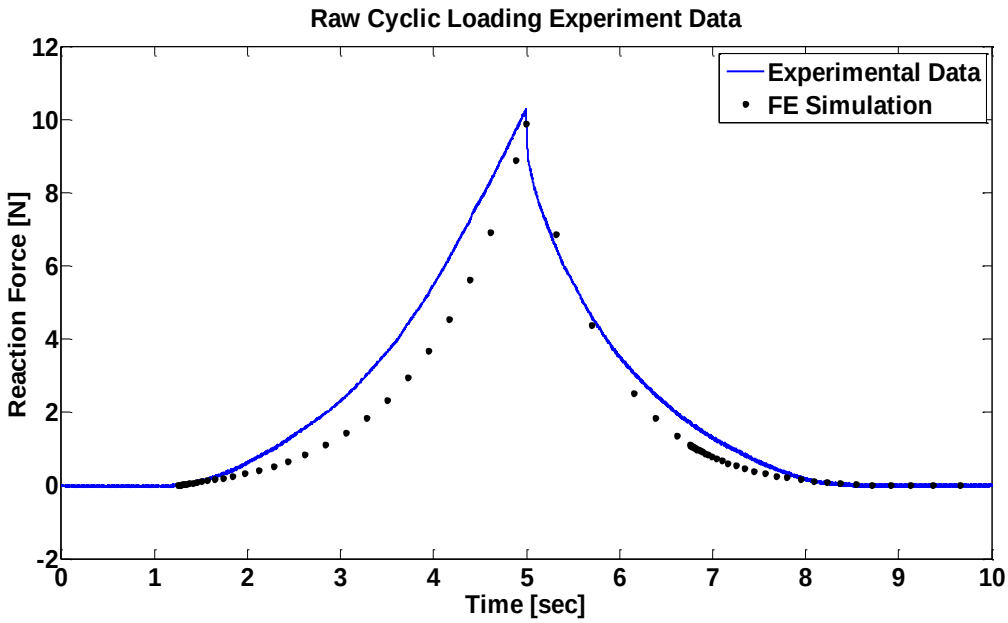

Figure 6.22 Cyclic Loading Data Fit (Parameter Set 9)

It can be concluded that, increasing the viscoelastic parameter δ results in an un-symmetry of the loading and the unloading curve which is the desired result for cyclic loading experiments.

In order to fit the loading curve with higher sensitivity, a new nonlinear elastic parameter set is tried (Table 6.11) and the curve-fit is shown in Figure 6.23.

Table 6.11 Parameter Set #10

Nonlinear Elastic Parameters	C_{01} $[MPa]$	C_{10} $[MPa]$	C_{11} $[MPa]$	C_{20} $[MPa]$	C_{30} $[MPa]$
	$2e-4$	$2e-4$	$9e-4$	0	$1e-4$
Viscoelastic Parameters	τ $[s]$	δ	β		
	2.857	0.8503	0.70		
NSSE $(\%)$	13.71				

Here C_{20} is taken as zero and the parameters C_{01} and C_{10} are taken as equal while Miller & Chinzei (1997), have taken $C_{10}/C_{01}=1$ due to equality of the energy of reciprocal deformation to that of the original one.

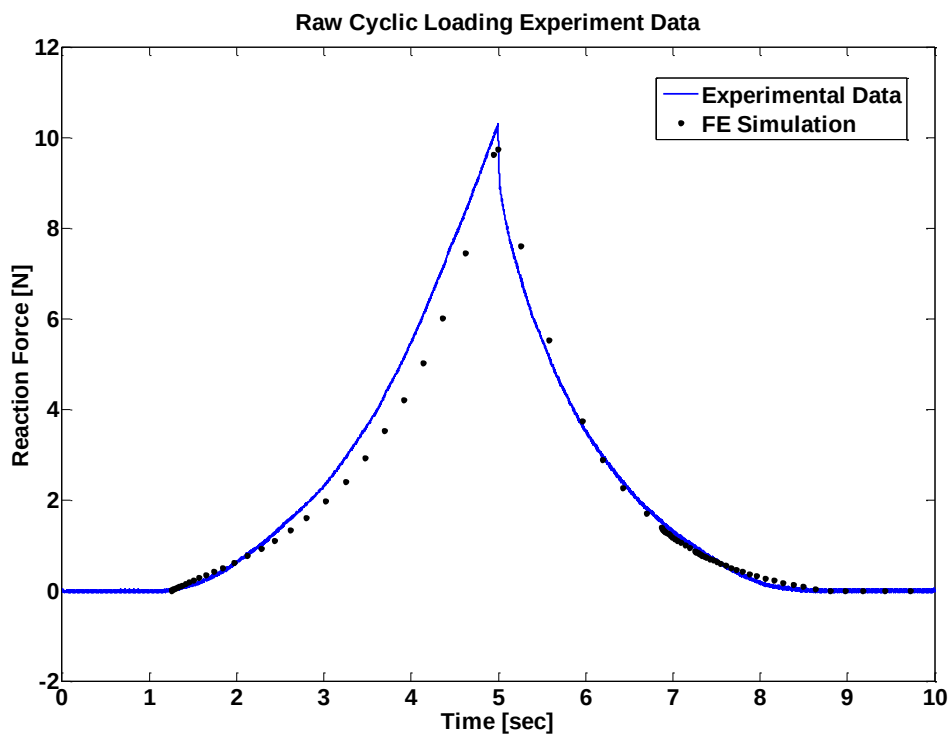

Figure 6.23 Cyclic Loading Data Fit (Parameter Set 10)

Finally the parameter C_{30} is slightly increased for a better curve-fit as presented in Table 6.12, resulting the plot in Figure 6.24.

Table 6.12 Parameter Set #11

Nonlinear Elastic Parameters	C_{01} $[MPa]$	C_{10} $[MPa]$	C_{11} $[MPa]$	C_{20} $[MPa]$	C_{30} $[MPa]$
	$2e-4$	$2e-4$	$9e-4$	0	$1.5e-4$
Viscoelastic Parameters	τ $[s]$	δ	β		
	2.857	0.8503	0.70		
NSSE $(\%)$	7.17				

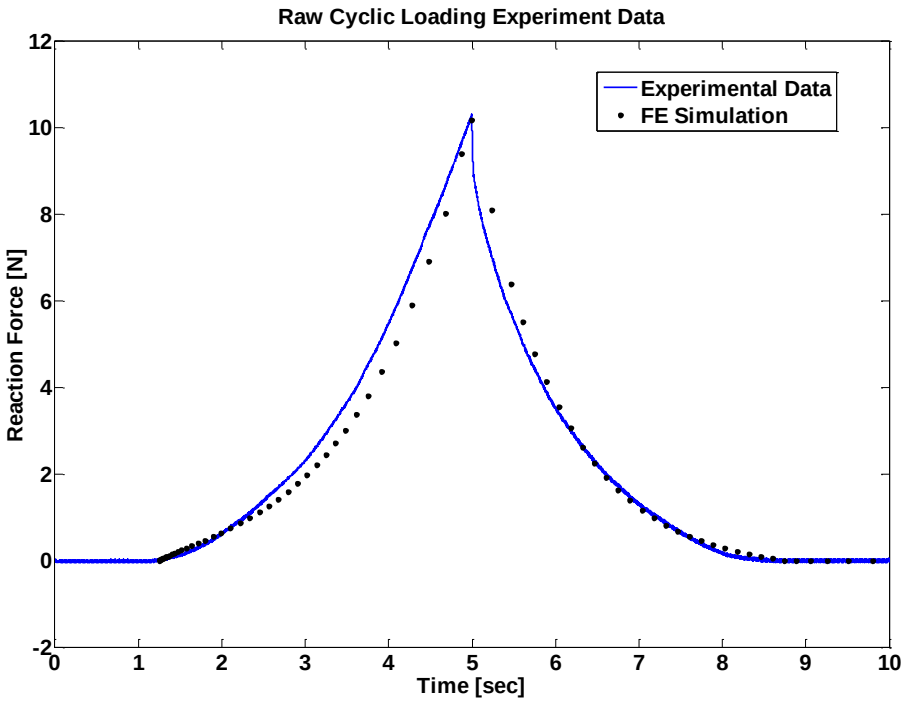

Figure 6.24 Cyclic Loading Data Fit (Parameter Set 11)

6.3.3 Simulation of Relaxation Experiment with Parameters Derived for Cyclic Loading Test

The parameters identified for the cyclic loading data (parameter set #11) are tried with the relaxation experiment data without taking the preconditioning (Mullin's effect) effect into consideration.

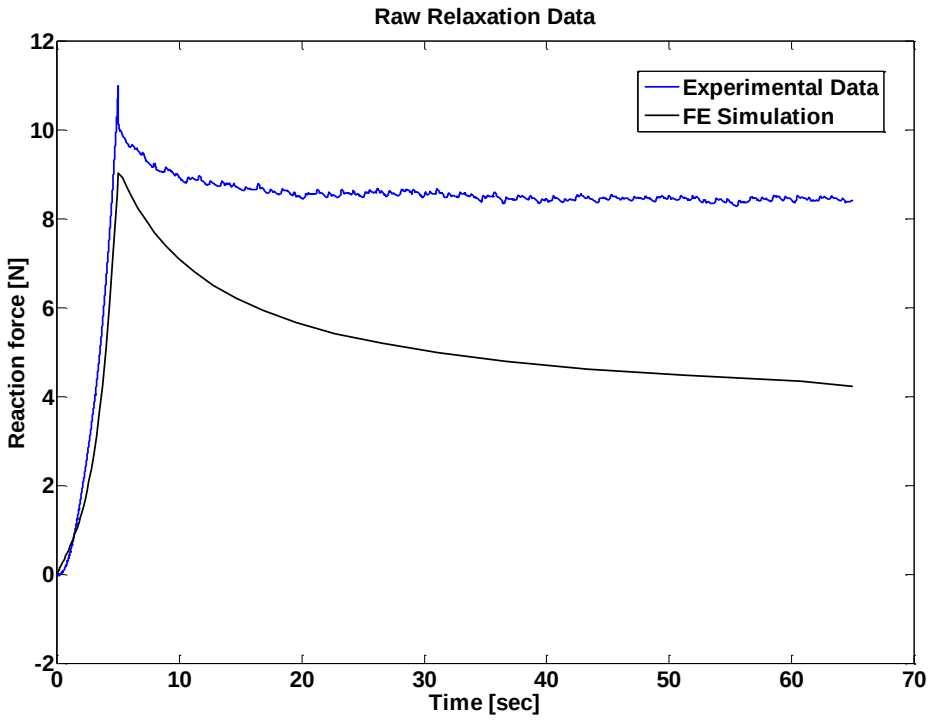

Figure 6.25 Relaxation Data Fit (Parameter Set #11)

It can be concluded that the final parameter set (#11) identified for the cyclic loading experimental data fits well however; when the parameters are tried with the relaxation data, the simulated result becomes highly different from the experiment curve. Finally it is thought that, by changing the fractional order β, a more sensitive curve-fit could be obtained. However every material identification trial remains barely a curve fit to a specific experiment which is not a material model that can simulate various loading conditions at least for a limited range.

Table 6.13 Parameter Set #12

Nonlinear Elastic Parameters	C_{01} $[MPa]$	C_{10} $[MPa]$	C_{11} $[MPa]$	C_{20} $[MPa]$	C_{30} $[MPa]$
	$2e-4$	$2e-4$	$9e-4$	0	$1.5e-4$
Viscoelastic Parameters	τ $[s]$	δ	β		
	2.857	0.8503	0.20		

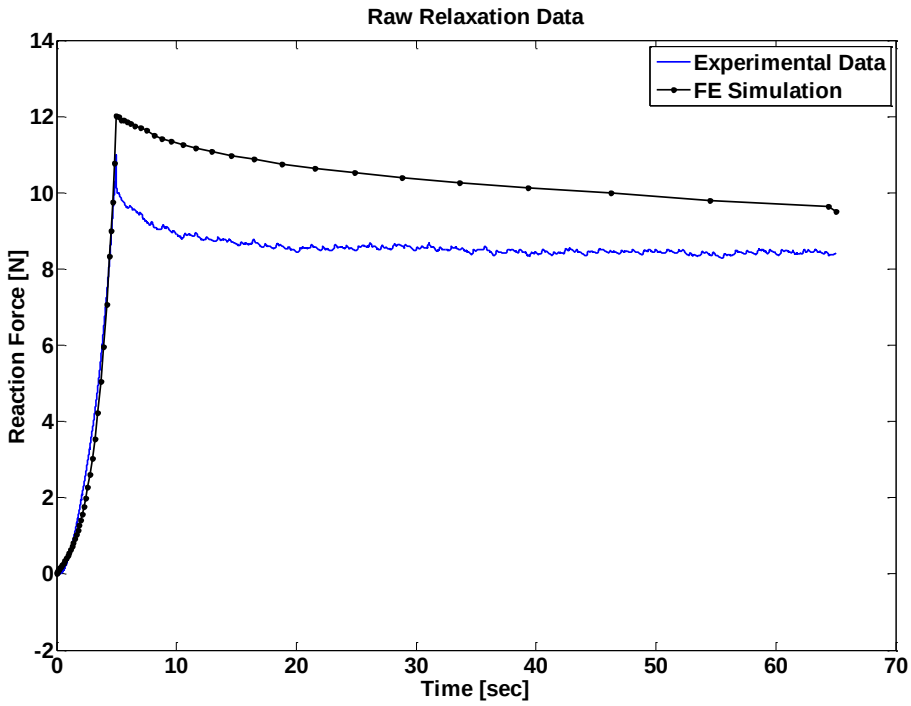

Figure 6.26 Relaxation Data Fit (Parameter Set 12)

Decreasing the viscoelastic parameter β shifts the relaxation curve upwards as the elastic behavior of the material is more significant when the parameter β is lower.

Table 6.14 Parameter Set #13

Nonlinear Elastic Parameters	C_{01} $[MPa]$	C_{10} $[MPa]$	C_{11} $[MPa]$	C_{20} $[MPa]$	C_{30} $[MPa]$
	$2e-4$	$2e-4$	$9e-4$	0	$1.5e-4$
Viscoelastic Parameters	τ $[s]$	δ	β		
	2.857	0.8503	0.30		

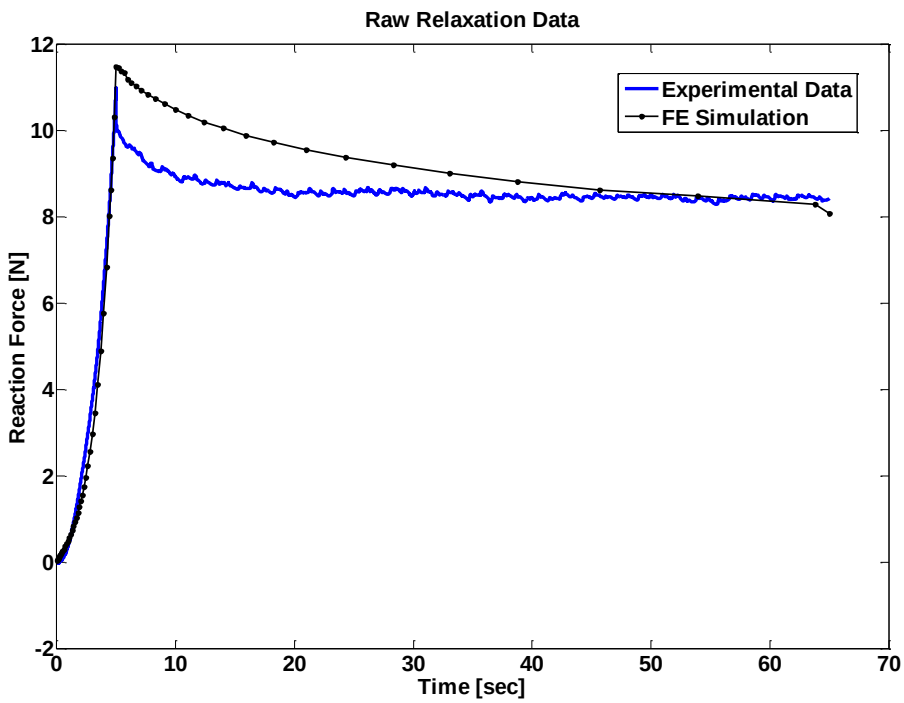

Figure 6.27 Relaxation Data Fit (Parameter Set 13)

Analyzing the figure 6.27 yields that, the time constant τ should be decreased in order to obtain a better curve-fit.

Table 6.15 Parameter Set #14

Nonlinear Elastic Parameters	C_{01} $[MPa]$	C_{10} $[MPa]$	C_{11} $[MPa]$	C_{20} $[MPa]$	C_{30} $[MPa]$
	$2e-4$	$2e-4$	$9e-4$	0	$1.5e-4$
Viscoelastic Parameters	τ $[s]$	δ	β		
	1.857	0.8503	0.30		
NSSE $(\%)$	19.79				

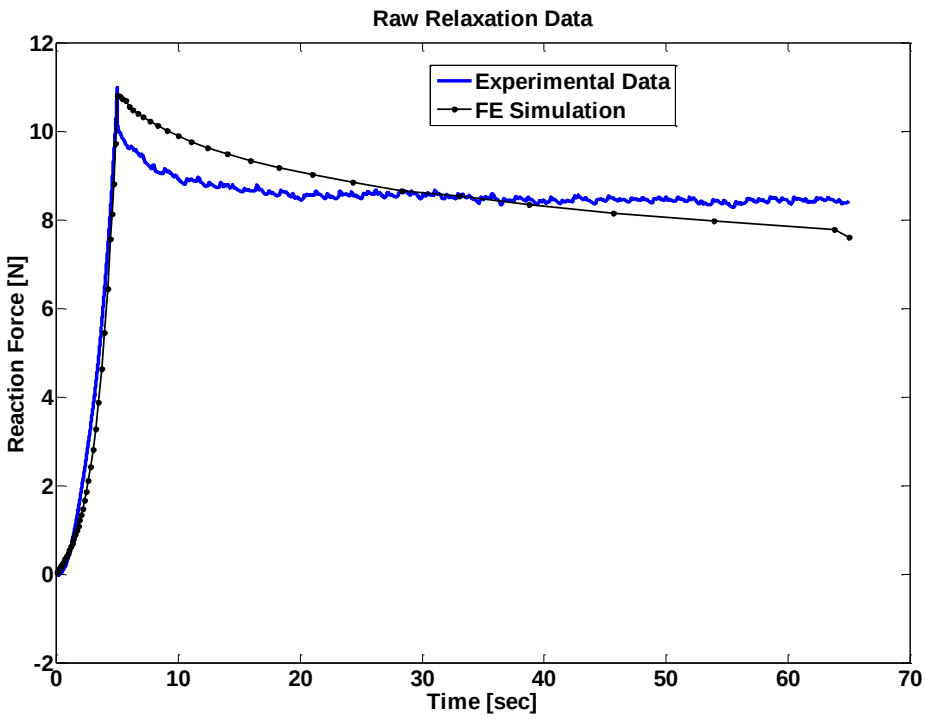

Figure 6.28 Relaxation Data Fit (Parameter Set 14)
(NSSE: 19.79 %)

Another curve is plotted for the loading and unloading data with the final parameter set (parameter set #14) obtained for the relaxation data to see the result (Figure 6.29).

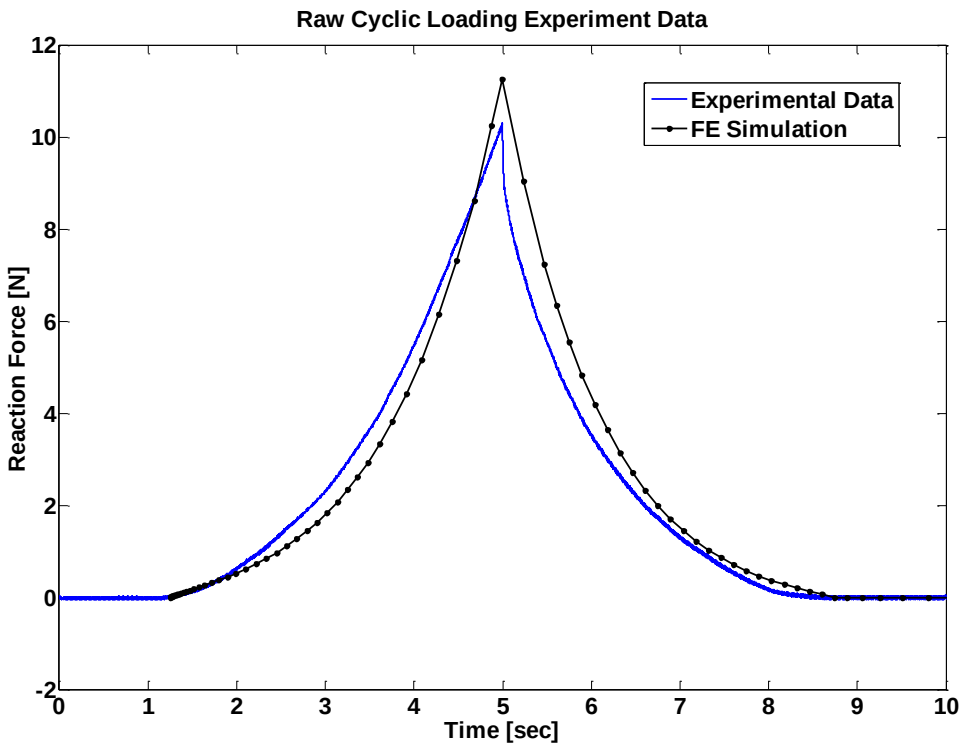

Figure 6.29 Cyclic Loading Data Fit (Parameter Set 14)
(NSSE: 25.72%)

It can be concluded that, one parameter set fits the two experiment data with an amount of accuracy. The set of parameter extracted simulates the two experiment set with a normalized sum of square error of approximately 25% however for these curve-fits; the physical limit of the viscoelastic parameter δ is exceeded. The δ parameter, which represents the relaxation magnitude, should lay between the limits, 0.2 to 0.4 for the curve-fit to be physically meaningful.

The same shift of the relaxation curve can be obtained by preconditioning the tissue prior to relaxation (Refer to Figure 2.14 in Chapter 2). The material model with the parameter set #11 is fitted to the relaxation test data after three cycles of loading and unloading of the tissue.

Finally by preconditioning the tissue and then applying ramp-and-hold displacement (relaxation) to the tissue model, the result obtained is presented in Figure 6.30.

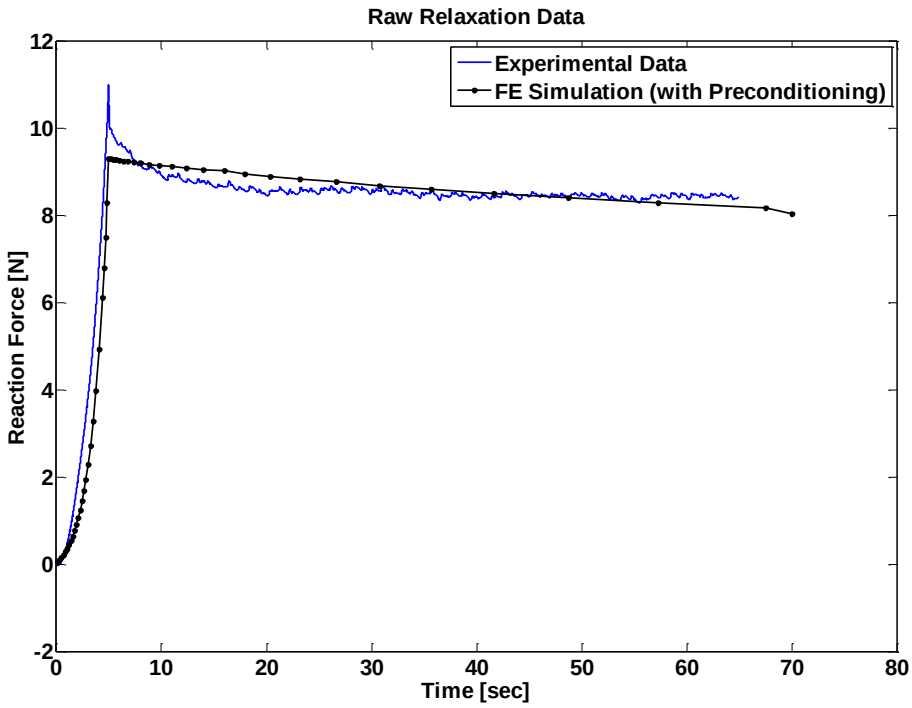

Figure 6.30 Relaxation Data Fit After Three Cycles of Loading and Unloading (Parameter Set #11)

According to the Figure 6.30, preconditioning (Mullin's effect) clearly affects the relaxation behavior of the tissue model, while the relaxation curve is shifted upwards after three cycles of loading and unloading where the tissue is preconditioned (compared with the Figure 6.25). Therefore, it can be concluded that, the finite element simulations correlates with the experimental data well, while the tissue was preconditioned when the experiment was performed. The same reasoning for the viscoelastic parameter δ applies for this curve-fit as well while, although the mathematical limits for the δ parameter is $[0,1)$, it is out of its physical, meaningful limits while $\delta = 0.8503$.

Therefore, the δ parameter was set to its previous value $(\delta = 0.2503)$.

Table 6.16 Parameter Set #15

Nonlinear Elastic Parameters	C_{01} $[MPa]$	C_{10} $[MPa]$	C_{11} $[MPa]$	C_{20} $[MPa]$	C_{30} $[MPa]$
	$2e-4$	$2e-4$	$3e-4$	0	$1e-4$
Viscoelastic Parameters	τ $[s]$	δ	β		
	1.857	0.2503	0.70		
NSSE (cyclic) $(\%)$	21.97				
NSSE (relaxation) $(\%)$	24.74				

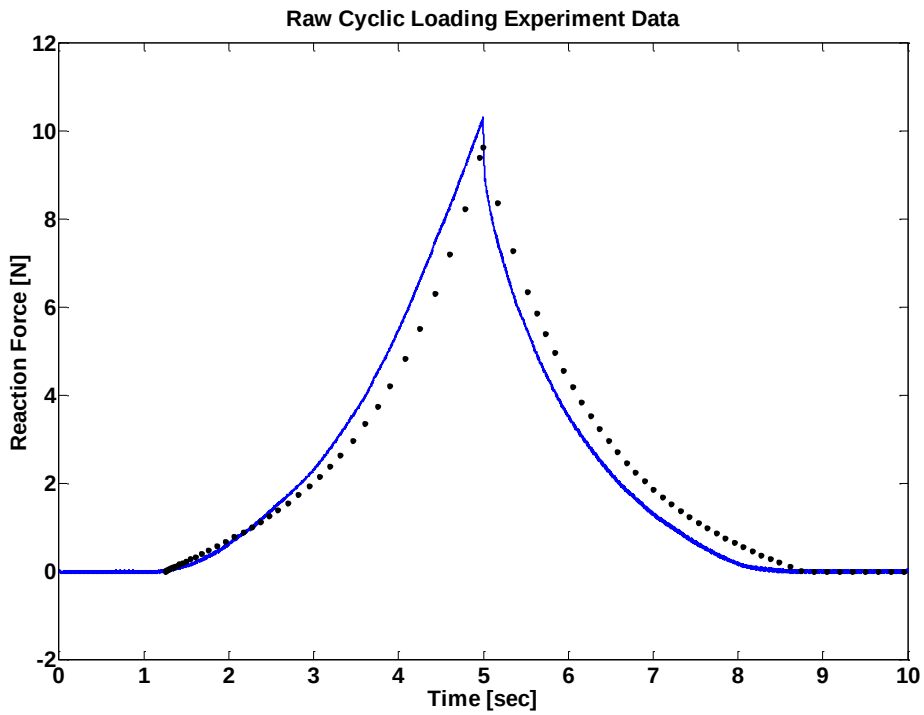

Figure 6.31 Cyclic Loading Response (Set of Parameters #15)

Relaxation response with the set of parameter #15 is,

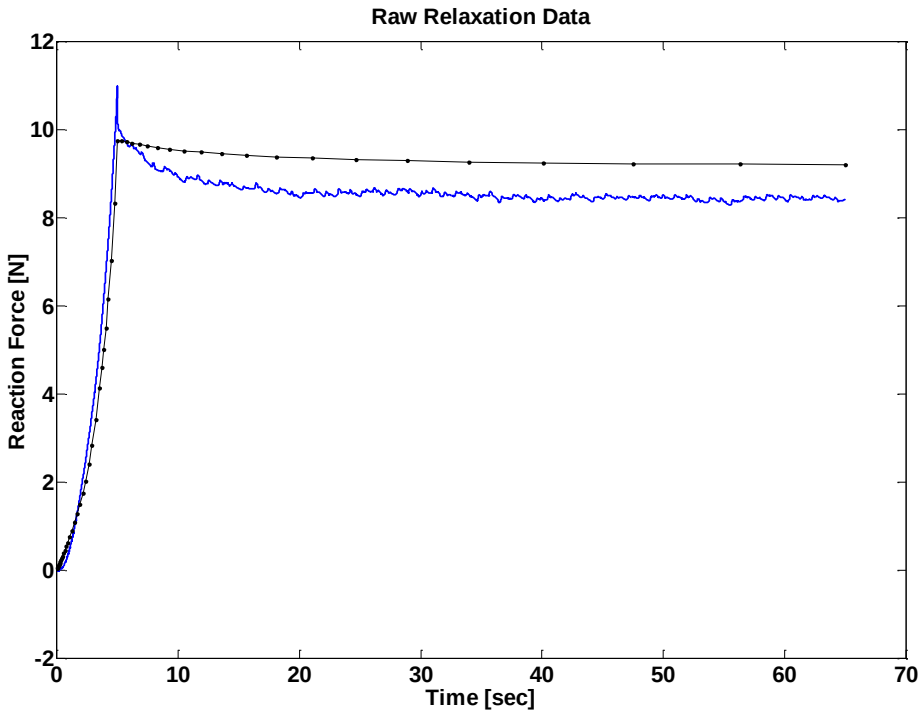

Figure 6.32 Relaxation Response (Set of Parameters #15)

Therefore, the two set of experiments performed on the same test location on the tissue can only be simulated with a sensitivity of NSSE being approximately 20%.

The set of material parameters to be identified is unique to each experiment data. Therefore, the complete material model with the parameters identified is unique to the test location, test condition and the test subject. To demonstrate the efficacy of the fractional material model in representing the experiment data, two more in-vivo relaxation data are chosen and the material model is curve-fitted to the experimental data. For the first experiment data six trials were performed and finally a set of material parameters was identified with NSSE being less than 1.2 % (Figure 6.33 & Table 6.17). For the other relaxation data, three trials were performed and the best curve-fit was obtained with NSSE being less than 7 % (Figure 6.35 & Table 6.19).

Table 6.17 Parameter Set #1-6

Material Parameters	Set 1	Set 2	Set 3	Set 4	Set 5	Set 6
$C_{01}\,[MPa]$	$2e-4$	$2e-4$	$2e-4$	$2e-4$	$2e-4$	$2e-4$
$C_{10}\,[MPa]$	$2e-4$	$2e-4$	$2e-4$	$2e-4$	$2e-4$	$2e-4$
$C_{11}\,[MPa]$	$3e-4$	$3e-4$	$3e-4$	$3e-4$	$3e-4$	$3e-4$
$C_{20}\,[MPa]$	0	0	0	0	0	0
$C_{30}\,[MPa]$	$4e-4$	$4.5e-4$	$5e-4$	$5e-4$	$4.5e-4$	$4.5e-4$
$\tau\ [s]$	2	2	2	2	2	2
δ	0.35	0.35	0.35	0.35	0.35	0.4
β	0.7	0.7	0.8	0.5	0.5	0.5

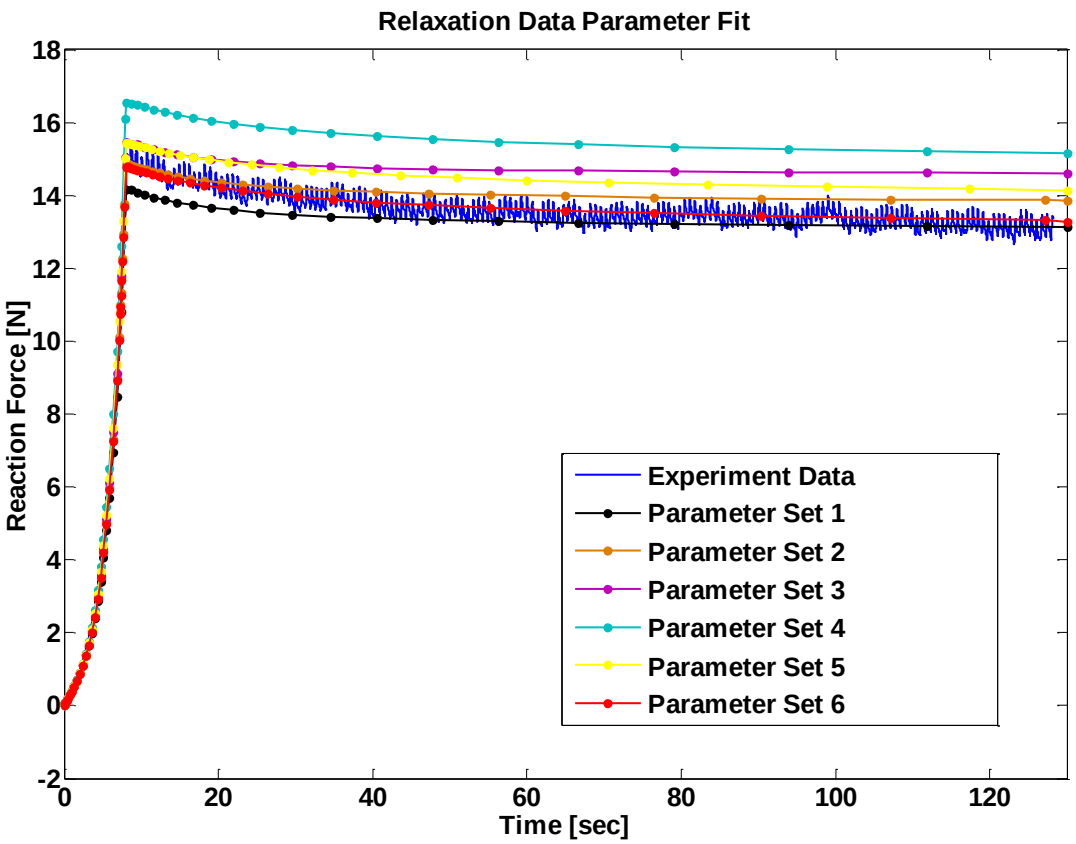

Figure 6.33 Relaxation Response (Set of Parameters #1-6)

Table 6.18 NSSE (%) Values

Parameter Set #	NSSE [%]
1	3.53
2	2.21
3	8.21
4	11.64
5	7.39
6	**1.19**

The best curve-fit is presented in Figure 6.34.

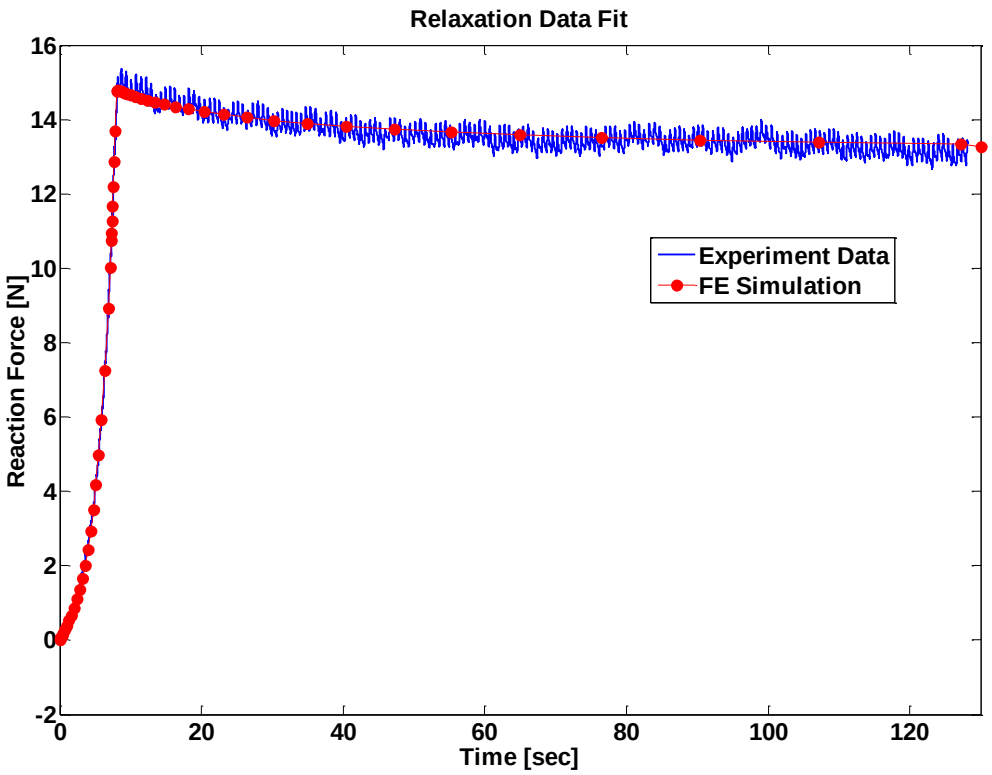

Figure 6.34 Relaxation Response (Set of Parameter #6)

Table 6.19 Parameter Set #1-3

Material Parameters	Set 1	Set 2	Set 3
$C_{01}\,[MPa]$	$2e-4$	$2e-4$	$2e-4$
$C_{10}\,[MPa]$	$2e-4$	$2e-4$	$2e-4$
$C_{11}\,[MPa]$	$3e-4$	$3e-4$	$3e-4$
$C_{20}\,[MPa]$	0	0	0
$C_{30}\,[MPa]$	$3.5e-4$	$3.5e-4$	$4e-4$
$\tau\ [s]$	2	2	2
δ	0.25	0.35	0.35
β	0.7	0.7	0.8

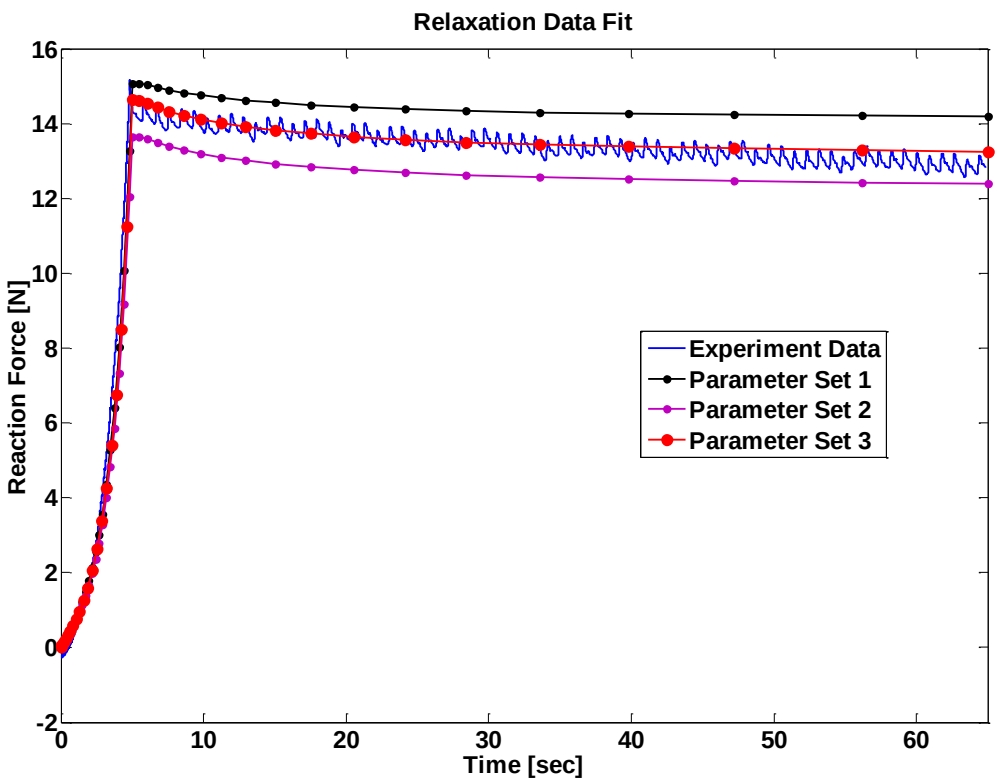

Figure 6.35 Relaxation Response (Set of Parameter #1-3)

Table 6.20 NSSE (%) Values

Parameter Set #	NSSE [%]
1	10.21
2	17.48
3	6.4

The set of parameters identified for the relaxation data (parameter set # 6) is employed for the cyclic loading (ten cycles) experiment data (Figure 6.36). The preconditioning behavior is clearly observed in correlation with the experiment data.

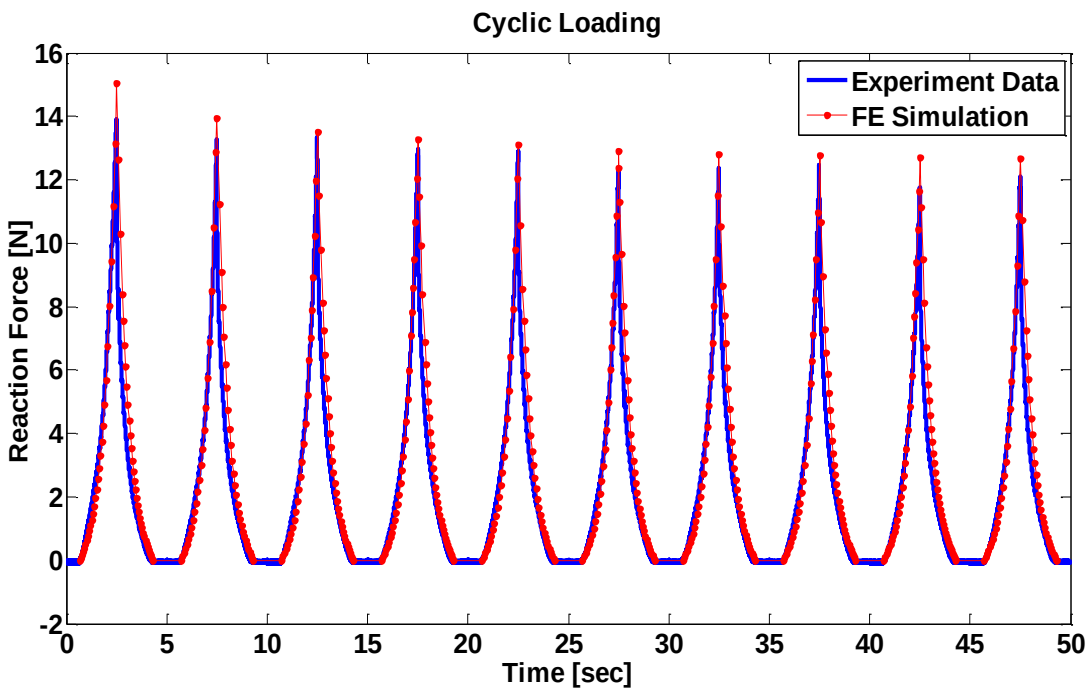

Figure 6.36 Cyclic Loading Response (Set of Parameter #6)

When only the first cycle is analyzed, the curve-fit involves an approximately 38 % NSSE.

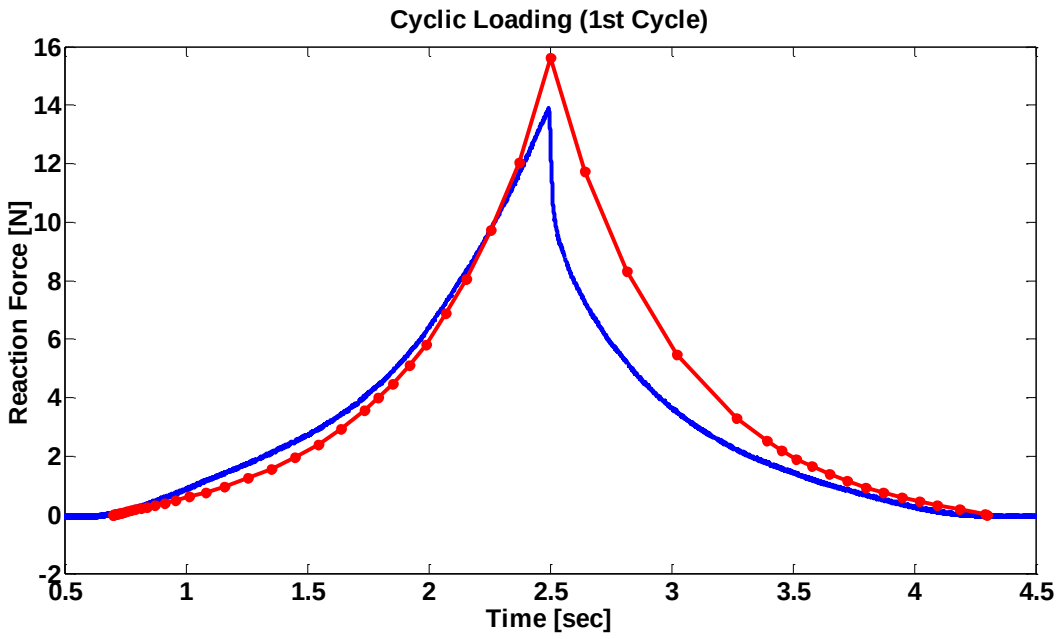

Figure 6.37 Parameter Set # 6
NSSE: 0.3773 (37.73%)

In order to compare the curve-fitting capabilities of the fractional order material model with integer order material model, a curve-fit to relaxation and cyclic loading test data was performed by employing the integer order James-Green-Simpson (J-G-S) material model with two viscoelastic exponential terms. The J-G-S material model is built-in in Marc 2010® finite element software. The nine parameters of the material model in total are identified which yields the best curve-fit to the relaxation test data with NSSE being less than 1.5 % (Figure 6.38).

Table 6.21 Parameters for the J-G-S Material Model

Material Parameters	Set 1
$C_{01}\left[MPa\right]$	$2e-4$
$C_{10}\left[MPa\right]$	$2e-4$
$C_{11}\left[MPa\right]$	$3e-4$
$C_{20}\left[MPa\right]$	0
$C_{30}\left[MPa\right]$	$1.2e-4$
$\tau_1\left[s\right]$	10
δ_1	0.012
$\tau_2\left[s\right]$	20
δ_2	0.12

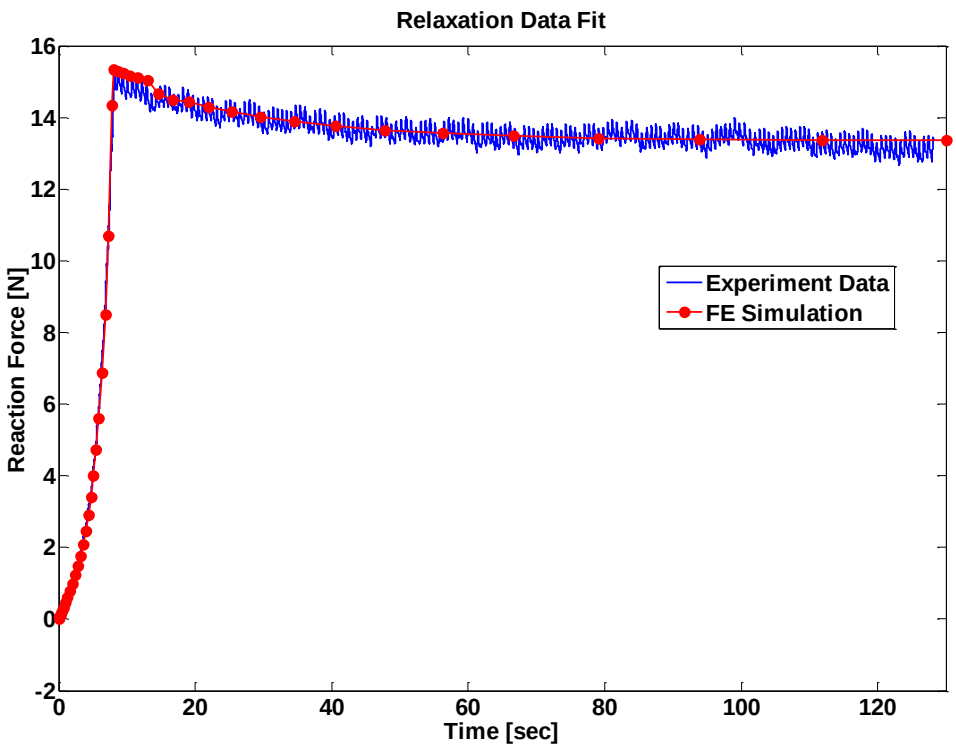

Figure 6.38 Relaxation data fit (NSSE: 0.0145 (1.45%))

The parameter set identified for the relaxation response was employed to the material model and a cyclic loading finite element simulation was performed. According to the result obtained (see Figure 6.39), the NSSE value calculated was less than the NSSE value obtained for the fractional order material model curve-fit.

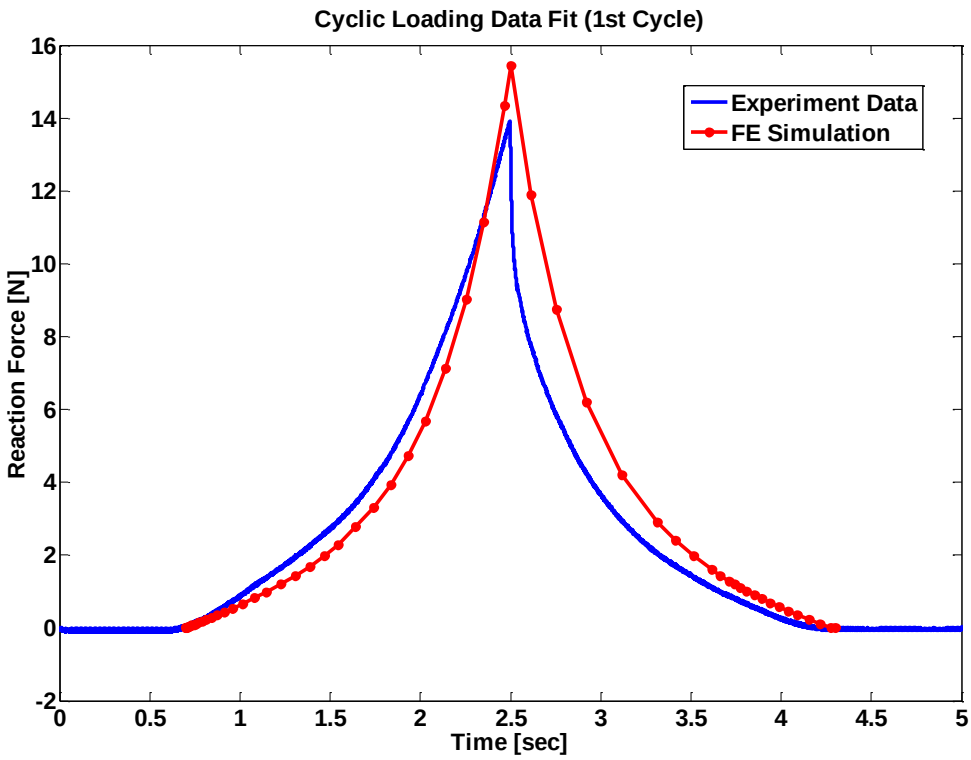

Figure 6.39 Loading and unloading for J-G-S Material Model
(NSSE: 0.2655 (26.55%))

When comparing the figures 6.39 and 6.37 it is clear that, both of the material models (fractional order and integer order) are capable of representing the nonlinear and viscoelastic behavior of soft tissues. Although, the amount of error present for the J-G-S integer order material model is low compared to the fractional order material model, the integer order material model involves nine parameters to be extracted, while the fractional order material model has only eight parameters to be identified. Further, due to axisymmetry of the soft tissue model, the number of

parameters can be further reduced to six by taking $C_{01} = C_{10}$ and $C_{11} = C_{20}$. In addition, this result can be a consequence of one unique experiment data. A vast number of experiment data should be analyzed and curve-fitted to obtain an accurate and a reliable outcome. By looking at this one result, it is quite tough to say that one of the material models is superior to the other unless the fact that the fractional order material model has less number of parameters compared to the integer order material model.

6.4 Effect of Indentation Rate on Preconditioning Behavior

As it is mentioned at the beginning of this chapter, the indentation rate affects the toe region mostly, leaving the tangent modulus of the linear part almost unaffected. Also, indentation rate affects the stiffness of the tissue model. In order to test this, two cyclic loading (ten - cycles) simulations were performed with different indentation rates by employing the parameter set #15. It should be noted that, the Mullin's effect is only noticeable when strains are greater than 10 %.

Table 6.22 Parameter Set #15

Nonlinear Elastic Parameters	C_{01} $[MPa]$	C_{10} $[MPa]$	C_{11} $[MPa]$	C_{20} $[MPa]$	C_{30} $[MPa]$
	$2e-4$	$2e-4$	$9e-4$	0	$3e-4$
Viscoelastic Parameters	τ $[s]$	δ	β		
	2.857	0.8503	0.30		

Indentation Rate $[\%mm/s]$	6.67

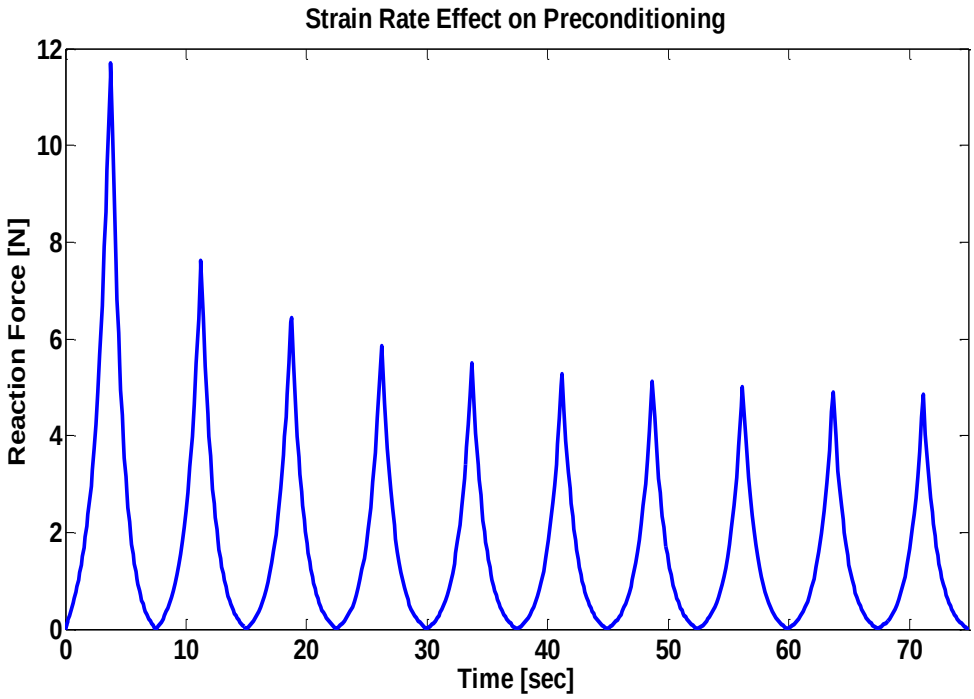

Figure 6.40 Preconditioning (Mullin's) Effect (Parameter Set 15)

Indentation Rate $[\%mm/s]$	2.5

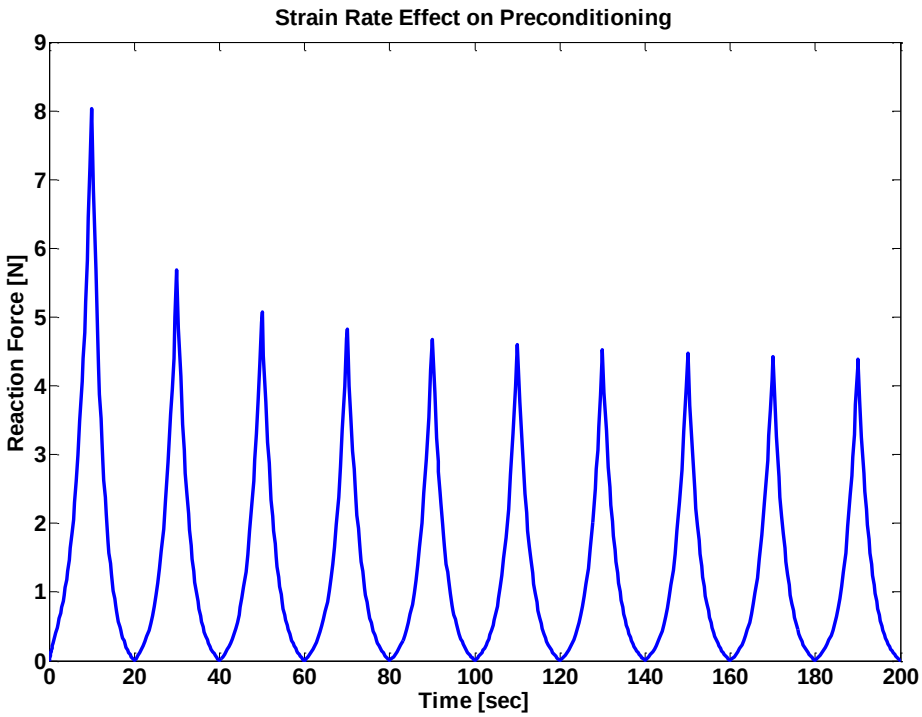

Figure 6.41 Preconditioning (Mullin's) Effect (Parameter Set 15)

It can be concluded that, indentation rate affects the stiffness of the tissue slightly before preconditioning due to the viscoelastic nature of the tissue, however after some cycles of loading and unloading (3 or 4), the tissue becomes totally preconditioned and the stress becomes no more rate dependent. Despite the independence of rate, preconditioned soft tissues still present hysteresis, so the mechanical response can be modeled as hyperelastic with different material constants at loading and unloading. It is important to note that, many soft tissues are preconditioned in their normal state, and some of them are not (*e.g.* brain).

6.5 Parameter Extraction for Creep Experiment Data

Fung (1993) states that creep is fundamentally more nonlinear. The microstructural process taking place in a material undergoing creep could be quite different from that undergoing relaxation or oscillation. Analogous situation is known for metals at elevated temperature.

For finite element simulation of creep behavior, a control node is developed at the center of rotation of the rigid body (indenter) and displacement and force boundary conditions are applied on this node consecutively by defining different load-cases.

Creep test data is obtained from the study of Petekkaya (2008). Creep test is done with 1 mm/s indentation velocity and creep time is approximately 120 seconds. The target force is determined to be 80 % of the relaxation peak force which is approximately 8 N. The raw creep test data is shown in Figure 6.42.

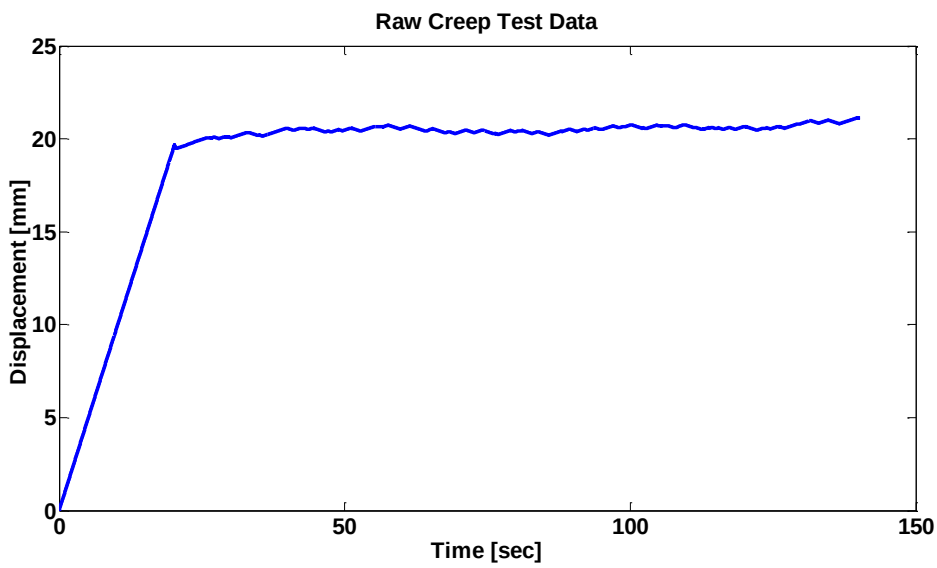

Figure 6.42 Raw Creep Experiment Data

Two simulations are performed with two different indentation rates.

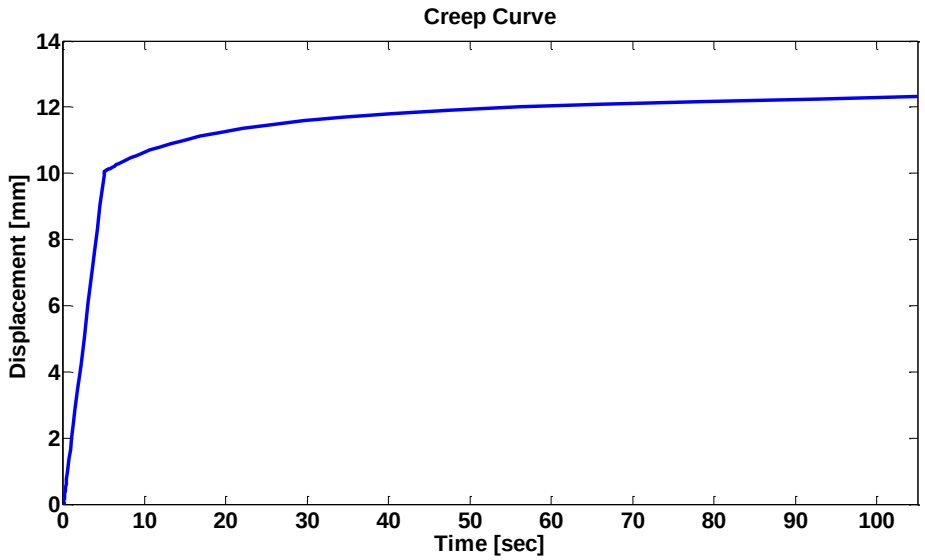

Figure 6.43 Creep Behavior Simulation (1)

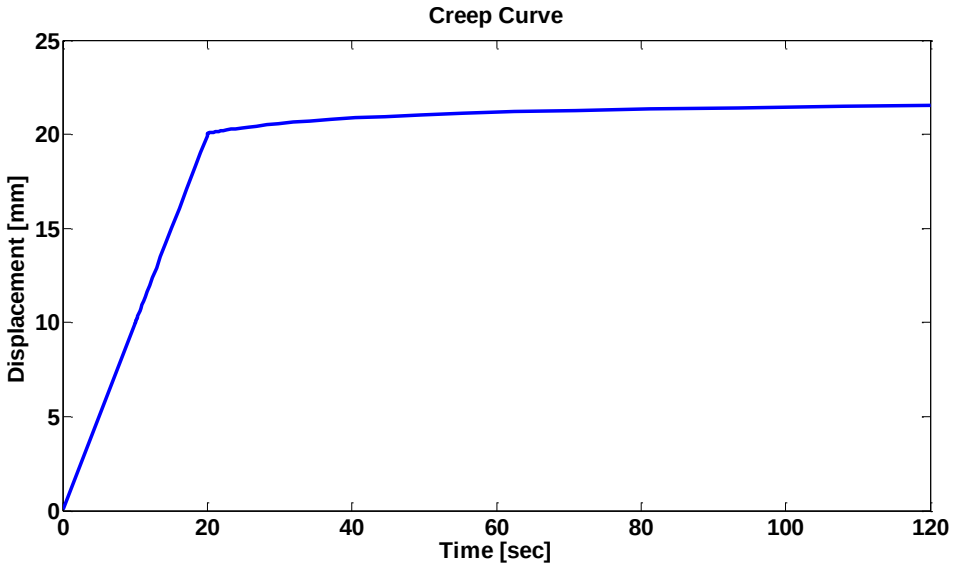

Figure 6.44 Creep Behavior Simulation (2)

Finally the material parameters identified from the relaxation curve-fit is employed for the creep data fit.

Table 6.23 Parameter Set #16

Nonlinear Elastic Parameters	C_{01} $[MPa]$	C_{10} $[MPa]$	C_{11} $[MPa]$	C_{20} $[MPa]$	C_{30} $[MPa]$
	$2e-4$	$2e-4$	$9e-4$	0	$3e-4$
Viscoelastic Parameters	τ $[s]$	δ	β		
	1.857	0.2503	0.70		

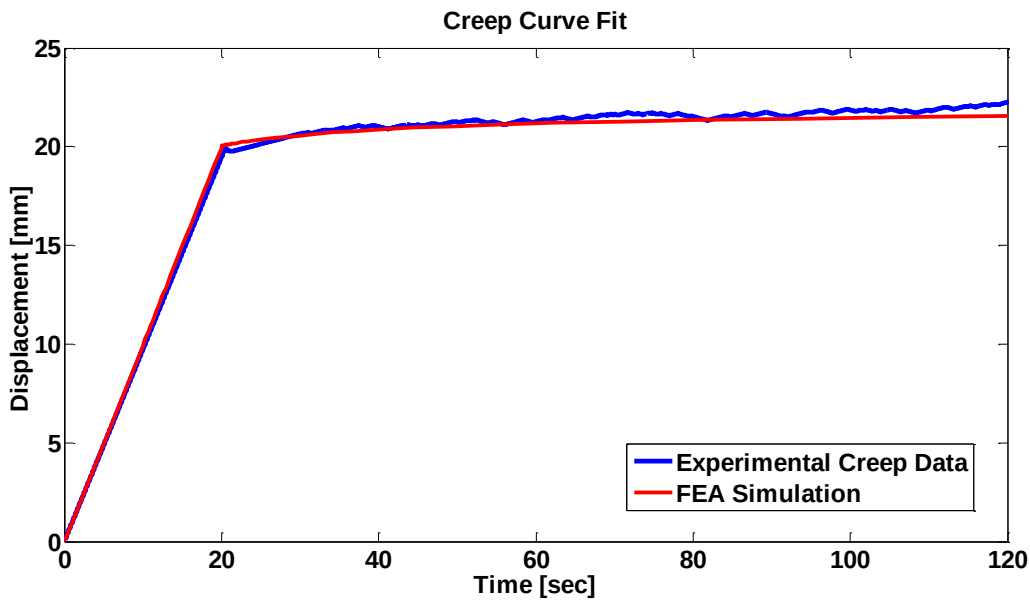

Figure 6.45 Creep Data Fit (Parameter Set 16)

As a conclusion, the parameter set identified fits well to the relaxation and creep test data; however it does not fit well to the cyclic loading test data. In other words, the parameter set identified fits to both relaxation and creep experiment results with an NSSE less than 2 %, however it does not fit well to cyclic loading data at least with that amount of NSSE value.

CHAPTER 7

CONCLUSION AND RECOMMENDATIONS FOR FUTURE WORK

7.1 Summary

This study consists of mainly two phases. The first phase is the formulation of a soft tissue material model which involves fractional (non-integer) differential operators. It has been hypothesized that, fractional order constitutive relations inherently possess some of the soft tissue complicated mechanical behavior, such as the viscoelastic behavior. Solution of fractional order constitutive equations (fractional orders of stress and/or strain), leads to solutions involving the generalized exponential function which is called the *Mittag-Leffler function*. The value of the one parameter *Mittag-Leffler function* depends on the fractional order of the constitutive equation β $\left(0 < \beta \leq 1\right)$, which is thought of an indicator of the tissue viscoelasticity.

At this first phase of the study, the one dimensional fractional order material model of the soft tissue has been compared with other traditional integer order material models (one-term and two-term Prony series) and shown that, fractional order material model fits better to the relaxation and creep experiment data than the integer order models. This initial conclusion gave the idea that, fractional order material models may represent the real tissue behavior instead of being a simple curve-fitting mathematical equation.

To test this hypothesis, this one dimensional viscoelastic fractional order material model (Zener model) is generalized to include the nonlinear behavior for finite deformations in three dimensions and implemented into the finite element software Msc.Marc 2010. The nonlinear elastic part of the material is modeled by 5-parameters James-Green-Simpson strain energy density function and the viscoelastic part of the material is modeled by the fractional order three-element Zener

viscoelastic model. Therefore the complete model assumes the tissue as, homogeneous, isotropic, incompressible, nonlinear and viscoelastic.

A user-subroutine is developed for the implementation of the material model formulated in Fortran 95 language. The user-subroutine is verified by performing a small strain finite element analysis on finite element software and comparing the results obtained with analytical linear viscoelastic solutions which disregards the nonlinear part by employing the same arbitrary material parameters. The “creep” and “relaxation” analyses have been performed and step input of displacement and force has been applied to the tissue. Small displacement and small strain analyses have yielded the relaxation and creep response and under these conditions the model reduces to a linear viscoelastic model instead of a nonlinear viscoelastic model.

After the verification of the user-subroutine developed for creep and relaxation behavior, the unknown parameters of the material model have been extracted. This comprises the second phase of the study. In this phase, by employing the inverse finite element method, the unknown material parameters have been extracted by curve-fitting to human forearm bulk soft tissue indentation experiment data.

This part of the study also includes the simulation of several relaxation, cyclic loading and creep protocols for different strain rates and nonlinear elastic and viscoelastic material parameters. Analyzing the fractional parameter β reveals that, a faster decay is observed when β is closer to 1 and a slower decay is observed when β is closer to 0.

7.2 Results and Discussion

Viscoelastic models based on fractional operators are recognized in the literature for accurately modeling the experimental behavior with fewer parameters. In this thesis, a fractional order nonlinear, viscoelastic material model is formulated and via the user-subroutine developed the material model is implemented into the finite element software Msc.Marc 2010.

Viscoelastic behavior of soft tissues, such as “relaxation”, “creep” and “hysteresis are simulated by creating a 3-D and axisymmetric finite element model of the soft tissue. The unknown parameters of the material model are identified by employing the inverse finite element methodology.

The aim through this routine was to extract a set of nonlinear elastic and viscoelastic parameters which would be able to simulate the three different experiment results performed on the same location on tissue.

It has been found out that, the set of parameters simulating the relaxation experiment with approximately 1% normalized sum of square error, simulates the cyclic loading experiment with an approximately 25% error. By the same way, the set of parameters simulating the cyclic loading test with an approximately 1% least square error, simulates the relaxation test data with approximately 99% normalized sum of square error.

Therefore a new set of parameter is sought to simulate the two set of experiment results with a close sensitivity. For this aim, the fractional order parameter β works well and by changing the parameter β the two experiment sets are simulated with a close sensitivity and a normalized sum of square error being approximately 25 %. However for this set of parameters, the physical limits of the δ parameter has been exceed therefore a new set of parameters are identified which simulates the two experiments with approximately 20% normalized sum of square error.

Finally, “creep” experiment has been simulated with the final set of parameters identified and it has been shown that, the set of parameters identified fits the creep data well.

In addition, the fractional order material model formulated is compared to the integer order James-Green-Simpson material model. It has been shown that both material models are capable of representing the soft tissue material behavior however, one set of material parameters identified for one type of data does not yield a perfect fit for

the other type of data. Therefore, the experiment protocols may be analyzed separately and different parameter sets could be extracted.

To sum-up, the fractional order material model formulated is successful in simulating the three set of experiments, namely, “relaxation”, “creep” and “cyclic loading” experiments. Also, one set of parameters can be identified with a NSSE of approximately 20 % that simulates the three experiments performed on the same location on the tissue.

7.3 Future Work

There is a bunch of future work to be done with the material model and user-subroutine developed for the material model, at hand. The future work which can be done are explained below.

First of all, more sensitive experimental data are needed to fit the material model developed to the test data. To accomplish this, a more sensitive and up-to-date experimental set-up is desired. With this set-up at hand, creep experiments cannot be done with higher indentation rates. Also, the study has been completed with limited test data available which restrains the results to certain set of test data performed on the tissue.

Secondly, estimation of quasi-static material constants requires much slower indentation tests. Therefore much slower and as a consequence long time duration experiments are necessary to be done, especially to observe the long time relaxation and creep behaviors.

Thirdly, the anisotropy of the tissue behavior is underestimated in this work and the tissue is assumed to be isotropic. However an orthotropic anisotropic model can be constructed by further modifying the ready material model and a ellipsoid indenter tip testing finite element simulation can be performed in order to capture the anisotropic behaviors of soft tissues in-plane (Bischoff, 2004) anisotropy, while bulk soft tissues are known to be highly anisotropic.

Finally, several different *in-vivo* and *in-vitro* soft tissues can be tested in the future to extract the material parameters and especially to identify the fractional order parameter which could be an indicator of the tissue differences and/or tissue pathologies as well.

REFERENCES

Abel, N. H. (1881). Solution de quelques problemes à l'aide d'intégrales définies. *Oeuvres Completes, Cristiania (Grondhal & Son) 1*, 16-18.

Adolfsson, K. (2003). *Models and numerical procedures for fractional order viscoelasticity.* Göteborg, Sweden: PhD Thesis, Chalmers University Tech.

Adolfsson, K., & Enelund, M. (2003). Fractional derivative viscoelasticity at large deformations. *Nonlinear Dynamics No:33*, 301-321.

Adolfsson, K., Enelund, M., & Olsson, P. (2005). On the fractional order model of viscoelasticity. *Mechanics of Time-Dependent Materials Vol.9*, 15-34.

Ahn, B., & Kim, J. (2009). Efficient soft tissue characterization under large deformations in medical simulations. *International Journal of Precision Eng. and Manufacturing Vol. 10, No.4* , 115-121.

Annin, B. (1961). Asymptotic expansion of an exponential function of fractional order. *Journal of Applied Mathematics and Mechanics Vol. 25 No.4*, 1192-1195.

Arıtan, S., Oyadiji, S. O., & Bartlett, S. M. (2008). A mechanical representation of the in-vivo creep behavior of muscular bulk tissue. *Joural of Biomechanics Vol. 41*, 2760-2765.

Bagley, L., & Torvik, J. (1983). A theoretical basis for the application of fractional calculus to viscoelasticity. *Journal of Rheology, Vol: 27, No:3*, 201-210.

Bagley, R. (1979). *Applications of Generalized Derivatives to Viscoelasticity.* Ph.D. Dissertation: Air Force Institute of Technology, Air Force Materials Laboratory TR-79-4103.

Bagley, R. L. (1979). *Applications of Generalized Derivatives to Viscoelasticity.* Ph. D. Dissertation: Air Force Institute of Technology, Air Force Materials Laboratory TR-79-4103.

Bagley, R. L. (1989). Power Law and Fractional Calculus Model of Viscoelasticity. *AIAA Journal, Vol. 27, No. 10*, 1412-1417.

Bagley, R. L., & Torvik, P. J. (1979). A generalized derivative model for an elastomer damper. *The Schock and Vibration Bull Part 2*, 135-143.

Bagley, R., & Torvik, P. (1984). On the appearance of the fractional derivative in the behavior of real materials. *J. Appl. Mech. Vol. 51 No. 2*, 294-298.

Bagley, R., & Torvik, P. (1986). On the fractional calculus model of viscoelastic behavior. *Journal of Rheology Vol: 3 No: 1*, 133-155.

Bateman, H. (1955). *Higher Transcendental Functions Vol.3 Bateman, Manuscript Project, California Institute of Technology.* New York: McGraw-Hill.

Bayin, S. (2010). Chapter 14: Fractional Derivatives and Integrals: Differintegrals. S. Bayin, *Supplements to Mathematical Methods in Science and Engineering.* Wiley.

Bayin, S. (2010, December 21). Fractional calculus and its applications to science and engineering. Middle East Technical University Institute of Applied Mathematics.

Bayin, S. (2010, December 21). *Fractional Calculus IAM Seminar*. http://www.metu.edu.tr/~bayin/

Bayin, S. (2010, December 21). *Middle East Technical University Institute of Applied Mathematics.* Fractional Calculus IAM-Seminar: http://www.metu.edu.tr/~bayin/

Belytschko, T., Liu, W. K., & Moran, B. (2001). *Nonlinear Finite Elements for Continua and Structures.* West Sussex, England: John Wiley & Sons Ltd.

Bernstein, B., A, K. E., & Zapas, L. J. (1963). A study of stress relaxation with finite strain. *Trans. Soc. Rheol. Vol.7*, 391-410.

Bischoff, J. E. (2004). Static indentation of anisotropic biomaterials using axially asymmetric indenters - a computational study. *Transactions of the ASME*, 498-505.

Bland, D. R. (1960). *Theory of Linear Viscoelasticity.* Oxford, New York: Pergamon Press.

Butchal, F., & Kaiser, E. (1951). The rheology of the cross-striated muscle fiber with particular reference to isotonic conditions. *Dan. Biol. Med. Vol. 21, 7,* 233-291.

Caputo, M. (1967). Linear models of dissipation whose Q is almost frequency independent-II. *Geophysical Journal of the Royal Astronomical Society Vol.13 No.5,* 529-539.

Caputo, M., & Mainardi, F. (1971a). A new dissipation model based on memory mechanism. *Pure and Applied Goephysics Vol. 91,* s. 134-147.

Caputo, M., & Mainardi, F. (1971b). Linear models of dissipation in anelastic solids. *Rivista del Nuovo Cimento Vol.1,* 161-198.

Chang, T. K., Rossikhin, Y. A., Shitikova, M. V., & Chao, C. K. (2011). Application of fractional-derivative standard linear solid model to impact response of human frontal bone. *Theoretical and Applied Fracture Solid Mechanics,* 148-153.

Choi, A. P., & Zheng, Y. P. (2005). Estimation of Young's modulus and Poisson's ratio of soft tissue from indentation using two different-sized indenters: finite element analysis of the finite deformation effect. *Medical & Biological Engineering & Computing Vol. 43,* 258-264.

Craiem, D. O., Rojo, F. J., Atienza, J. M., Guinea, G. V., & Armentano, R. L. (2008). Fractional Calculus Applied to Model Arterial Viscoelasticity. *Latin American Applied Research Vol: 38,* 141-145.

Craiem, D., & Magin, R. L. (2010). Fractional order models of viscoelasticity as an alternative in the analysis of red blood cell (RBC) mechanics. *Phys. Biol. 7,* 1-3.

Craiem, D., Rojo, F. J., Atienza, J. M., Armentano, R. L., & Guinea, G. V. (2008). Fractional-order viscoelasticity applied to describe uniaxial stress relaxation of human arteries. *Phys. Med. Biol Vol:53,* 4543-4554.

Craiem, O. D., & Armentano, L. R. (2006). Arterial Viscoelasticity: A Fractional Derivative Model. *Proceedings of the 28th IEEE EMBS Annual International Conference* (pp. 1098-1101). New York City: USA.

Dalir, M., & Bashour, M. (2010). Applications of Fractional Calculus. *Applied Mathematical Sciences*, 1021-1032.

Davis, G. B., Kohandel, M., Sivaloganathan, S., & Tenti, G. (2006). The Constitutive Properties of the Brain Paraenchyma Part.2 Fractional Derivative Approach. *Mechanical Engineering & Physics*, 455-459.

Davis, H. T. (1936). *The Theory of Linear Operators.* Bloomington, Indiana: Principia Press.

Debnath, L. (2003). Recent Applications of Fractional Calculus to Science and Engineering. *International Journal of Mathematics and Mathematical Sciences*, 3413-3442.

Dhar, P., & Zu, J. W. (2007). Design of a resonator device for in vivo measurement of regional tissue viscelasticity. *Sensors and Actuators A Vol. 133*, 45-54.

Diethelm, K., Ford, N. J., Freed, A. D., & Luchko, Y. (2005). Algortihms for the fractional calculus: A selection of numerical methods. *Computs. Methods appl. Mech. Engrg Vol. 194*, 743-773.

Djordjevic, D. V., Jaric, J., Fabry, B., Fredberg, J. J., & Stamenojic, D. (2003). Fractional derivatives embody essential features of cell rheological behavior. *Annals of Biomedical Engineering Vol: 31*, 692-699.

Doehring, C. T., Freed, D. A., Carew, O. E., & Vesely, I. (2005). Fractional order viscoelasticity of the aortic valve cusp: An alternative to quasilinear viscoelasticity. *Transactions of the ASME Vol. 127*, 700-708.

Drozdov, A. D. (1996). *Finite Elasticity and Viscoelasticity: A Course in the Nonlinear Mechanics of Solids.* Singapore: World Scientific.

Drozdov, A. D. (1997). Fractional differential models in finite viscoelasticity. *Acta Mechanica Vol. 124*, 155-180.

Enelund, M., Maehler, L., Runesson, K., & Joseffson, B. L. (1999). Formulation and integration of the standard linear viscoelastic solid with fractional order rate laws. *International Journal of Solids and Structures Vol.36*, 2417-2442.

Erdelyi, A., Magnus, W., Oberheltinger, F., & Tricomi, F. G. (1954). Higher transcendental functions, Vol. 3. New-York: Mc-Graw Hill.

Flügge, W. (1967). *Viscoelasticity* . Massachusetts: Blaisdell Publishing Company.

Freed, A. D., & Diethelm, K. (2006). Fractional calculus in biomechanics: a 3D viscoelastic model using regularized fractional derivative kernels with application to the human calcaneal fat pad. *Biomechan Model Mechanobiol Vol.5*, 203-215.

Freed, A. D., & Diethelm, K. (2007). Caputo derivatives in viscoelasticity: a non-linear finite deformation theory for tissue. *Fractional Calculus & Applied Analysis Vol.10 No.3*, 219-248.

Freed, A. D., & Diethelm, K. (2007). Caputo derivatives in viscoelasticity: a non-linear finite-deformation theory for tissue. *Fractional Calculus & Applied Analysis Vol. 10 No.3*, 219-248.

Freed, A., & Diethelm, K. (2006). Fractional calculus in biomechanics: a 3D viscoelastic model using regularized fractional derivative kernels with application to the human calcaneal fat pad. *Biomechan Model Mechanobiol Vol.5*, 203-215.

Freed, A., Diethelm, K., & Luchko, Y. (2002). *Fractional-Order Viscoelasticity (FOV): Constitutive Development Using the Fractional Calculus: First Annual Report.* Cleveland: NASA/TM - 2002-211914.

Freed, A., Diethelm, K., & Luchko, Y. (2002). *Fractional-Order Viscoelasticity (FOV): Constitutive Development Using the Fractional Calculus: First Annual Report.* NASA Glenn Research Center: NASA/TM-2002-211914.

Freed, A., Diethelm, K., & Luchko, Y. (2002). *Fractional-Order Viscoelasticity (FOV): Constitutive Development Using the Fractional Calculus: First Annual Report.* NASA Glenn Research Center: NASA/TM-2002-211914.

Friedrich, C. (1991). Relaxation and Retardation Functions of the Maxwell Model with Fractional Derivatives. *Rheologica Acta Vol.30*, 151-158.

Fung, Y. C. (1993). *Biomechanics: Mechanical Properties of Living Tissues.* Berlin: Springer-Verlag.

Gefen, A., & Margulies, S. (2008). Are in-vivo and in-situ brain tissues mechanically similar? *Journal of Biomechanics Vol. 37*, 1339-1352.

Gemant, A. (1936). A Method of Analyzing Experimental Results Obtained From Elasto-Viscous Bodies. *Physics Vol:7*, 311-317.

Gerasimov, A. N. (1948). A generalization of linear laws of deformation and its application to inner friction problems. *Prikl. Math. Mekh. Vol. 12*, 251-259.

Gorenflo, R., & Mainardi, F. (1997). Fractional Calculus: Integral and Differential Equations of Fractional Order. A. Carpinteri, & F. Mainardi, *Fractals and Fractional Calculus in Continuum Mechanics* (s. 223-276). Springer.

Grahovac, N. M., & Zigic, M. M. (2010). Modeling of the hamstring muscle group by use of fractional derivatives . *Computers and Mathematics with Applications*, 1695-1700.

Greenberg, M. D. (1998). *Advanced Engineering Mathematics.* New Jersey: Prentice-Hall Inc.

Gross, B. (1947). On creep and relaxation. *Journal of Applied Physics Vol. 18 No.2*, 212-221.

Han, L., Burcher, M., & Noble, J. A. (2002). Non-invasive measurement of biomechanical properties of in-vivo soft tissues. *Lecture Notes in Compute Science 2488*, 208-215.

Hanneken, J. W., Vaught, D. M., & Achar, B. N. (2007). Enumeration of the real zeros of the Mittag-Leffler function E (z), 1 < < 2. J. Sabatier, O. P. Agrawal, & J. A. Machada, *Advances in Fractional Calculus: Theoretical Developments and Applications in Physics and Engineering* (s. 15-26). Dordrecht, The Netherlands: Springer.

Haubold, H. J., Mathai, A. M., & Saxena, R. K. (2009). Mittag-Leffler functions and their applications. *Journal of Applied Mathematics*, 1-51.

Heymans, N., & Bauwens, J. C. (1994). Fractal rheological models and fractional differential equations for viscoelastic behavior. *Rheologica Acta, Vol. 33*, 210-219.

Holzapfel, G. A. (2000). *Nonlinear Solid Mechanics. A Continuum Approach for Engineering.* Chichester: John Wiley & Sons Ltd.

James, A. G., Green, A., & Simpson, G. M. (1975). Strain energy functions of rubber. I. Characterization of gum vulcanizates. *Journal of Applied Polymer Science Vol. 19*, 2033-2058.

Kawchuk, G., Liddle, T., Fauvel, O., & Johnston, J. (2006). The accuracy of ultrasonic indentation in detecting simulated bone displacement: A comparison of three techniques. *Journal of Manipulative and Physiological Therapeutics Vol. 29, No.2*, 126-133.

Kelly, F. J., & McGough, J. R. (2009, October). Fractal Ladder Models and Power Law Wave Equations. *J. Acoust. Soc. Am Vol:126 No:4*, pp. 2072-2081.

Koeller, R. (1984). Applications of Fractional Calculus to the Theory of Viscoelasticity. *Journal of Applied Mechanics Vol: 51*, 299-307.

Kohandel, M., Sivaloganathan, S., Tenti, G., & Drake, J. (2006). The Constitutive Properties of the Brain Parenchyma Part 1. Strain Energy Approach. *Medical Engineering & Physics Vol.28*, 449-454.

Korhonen, R. K., Saarakkala, S., Töyras, J., Laasanen, M. S., Kiviranta, I., & Jurvelin, J. S. (2003). Experimental and numerical validation for the novel configuration of an arthroscopic indentation instrument. *Physics in Medicine and Biology Vol. 48*, 1565-1576.

Lakes, R. S. (1999). *Viscoelastic Solids.* Boca Raton: CRC Press LLC.

Lei, F., & Szeri, A. (2007). Inverse analysis of constitutive models: Biological soft tissues. *Journal of Biomechanics Vol. 40*, 936-940.

Lion, A. (1997). On the thermodynamics of fractional damping elements. *Continuum Mech. Thermodyn. Vol.9*, 83-96.

Liu, C., & Choudhry, S. (2004). Finite element analysis of hyperelastic materials with MSC.Marc. *WCCM VI in conjuction with APCOM'04* (s. 5-10). Beijing,China: Tsinghua University Press & Springer-Verlag.

Liu, Y., Kerdok, A. E., & Howe, R. D. (2004). A nonlinear finite element model of soft tissue indentation. *Proceedings of Medical Simulation: Internal Symposium* (s. 1-10). Cambridge: Springer-Verlag.

Lorenzo, C. F., & Hartley, T. T. (1998). *Initialization, Conceptualization, and Application in the Generalized Fractional Calculus.* Lewis Research Center: NASA STI Report Series NASA/TP-1998-208415.

Loverro, A. (2004, May 8). Fractional Calculus: History, Definitions and Applications for the Engineer. Department of Aerospace and Mechanical Engineering University of Notre Dame, Notre Dame: University of Notre Dame.

Lu, M.-H., Yu, W., Huang, Q., Huang, Y., & Zheng, Y. (2009). Hand-held indentation system for the assesment of mechanical properties of soft tissues in-vivo. *IEEE Transactions on Instrumentation and Measurement Vol. 58, No. 9*, 3079-3085.

Magin, R. (2004). Fractional calculus in bioengineering. *Critical Reviews in Biomedical Engineering Vol. 32 No.1*, s. 105-193.

Magin, R. L. (2006). *Fractional Calculus in Bioengineering.* Redding, CT: Begell House.

Magin, R. L., Li, W., P, V. M., Trujillo, J., A, R. D., A, M., et al. (2011). Anomalous NMR relaxation in cartilage matrix components and native cartilage: Fractional-order models. *Journal of Magnetic Resonance*, 184-191.

Mainardi, F. (2010). A historical perspective on fractional calculus in linear viscoelasticity. (Sect 3.5 of the book). In F. Mainardi, *Fractional Calculus*

and Waves in Linear Viscoelasticity (pp. 74-76). London: Imperial College Press.

Mainardi, F. (2010). *Fractional Calculus and Waves in Linear Viscoelasticity.* London: Imperial College Press.

Malvern, L. E. (1969). *Introduction to the Mechanics of a Continuous Medium.* Englewood Cliffs, New Jersey: Prentice-Hall, Inc.

Maurel, W., Wu, Y., Thalmann, N. M., & Thalmann, D. (1998). *Biomechanical Models for Soft Tissue Simulation.* Berlin: Springer.

Mazza, E., Nava, A., Bauer, M., Winter, R., Bajka, M., & Holzpfel, G. (2006). Mechanical properties of the human uterine cervix. *Medical Image Analysis Vol.10,* 125-136.

Miller, K., & Chinzei, K. (1997). Constitutive modelling of brain tissue. *Journal of Biomechanics, Vol. 30,* 1115-1121.

Miller, K., Chinzei, K., Orssengo, G., & Bednarz, P. (2000). Mechanical properties of brain tissue in-vivo: Experiment and computer simulation. *Journal of Biomechanics, Vo. 33,* 1369-1376.

Mooney, M. (1940). A theory of large elastic deformation. *J. Appl. Phys. Vol. 11*, 582-592.

Nan, Y. (2009). *Fish at LTHE*. Fortran Library: http://www.lthe.fr/PagePerso/yu/program/incomplegamma.f

Nava, A., Mazza, E., Kleinermann, F., Avis, N., & McClure, J. (2003). Determination of mechanical properties of soft human tissues through aspiration experiments. *Lecture Notes in Computer Science, 2878,* 222-229.

Nonnenmacher, T. F. (1991). Fractional relaxation equations for viscoelasticity and related phenomena. *Lect. Notes in Physics, Vol. 381* (s. 309-320). Berlin: Springer-Verlag.

Nutting, P. (1921). A new general law of deformation. *J. Franklin Inst. 191*, 679-685.

Ogden, R. W. (1972, February 1). Large deformation isotropic elasticity - On the correlation of theory and experiment for incompressible rubberlike solids. *Proceedings of the Royal Society of London. Series A, Mathematical and Physical Sciences, Vol.326, No.1567,* s. 565-584.

Ogden, R. W. (1984). *Non-Linear Elastic Deformations.* New York: Dover Publications, Inc.

Oldham, K. B., & Spanier, J. (1974). *The Fractional Calculus Theory and Applications of Differentiation and Integration to Arbitrary Order.* California: Academic Press Inc.

Osborne, W. A., & Sutherland, W. (1909, November 23). The elasticity of rubber balloons and hollow viscera. *Proceedings of the Royal Society of London. Series B, Containing Papers of a Biological Character, Vol. 81, No. 551,* s. 485-499.

Ottensmeyer, M. P., Kerdok, A., Howe, R., & Dawson, S. (2004). The effects of testing environment on the viscoelastic properties of soft tissues. *Proceedings of the International Symposium on Medical Simulation,* (s. 9-18).

Padovan, J. (1987). Computational Algorithms for FE Formulations Involving Fractional Operators. *Computational Mechanics Vol:2,* 271-287.

Petekkaya, A. T. (2008). *In vivo indenter experiments on soft biological tissues for identification of material models and corresponding parameters.* Ankara: Thesis submitted to the Graduate School of Natural and Applied Sciences of Middle East Technical University.

Petekkaya, A. T. & Tönük, E. (2010).Yumuşak doku mekanik davranışının modellenebilmesi için yerinde (in-vivo) indentör deneyleri. *Makina Tasarım ve İmalat Dergisi, 10,* 19-31.

Pioletti, D. P., Rakotomanana, L. R., & Leyvraz, P. K. (1998). Viscoelastic constitutive law in large deformations: Application to human knee ligaments and tendons . *Journal of Biomechanics, Vol. 31,* 753-757.

Podlubny, I. (1999). *Fractional Differential Equations: An Introduction to Fractional Derivatives, Fractional Differential Equations, to Methods of Their Solution and some of their Applications.* California: Academic Press.

Podlubny, I. (2009, March 25). *Matlab Central*. Retrieved March 25, 2009. http://www.mathworks.com/matlabcentral/fileexchange/8738-mittag-leffler-function

Potvin, M.-J. (2001). Comparison of Time-Domain Finite Element Modelling of Viscoelastic Structures Using an Efficient Fractional Voigt-Kelvin Model or Prony Series. McGill University, Montreal: Department of Mechanical Engineering, McGill University, Doctor of Philosophy Thesis.

Rabotnov, Y. N. (1948). Equilibrium of an elastic medium with after-effect. *Prikl. Math. Mekh., Vol. 12, No. 1*, 53-62.

Rabotnov, Y. N. (1980). *Elements of Hereditary Solid Mechanics.* Moscow: Mir Publishers.

Reddy, J. N. (1985). *An Introduction to the Finite Element Method.* Singapore: McGraw-Hill Inc.

Rivlin, R. (1948, January 13). Large elastic deformations of isotropic materials IV. further developments of the general theory. *Philosophical Transactions of the Royal Society of London. Series A, Mathematical and Physical Sciences, Vol. 240, No. 822,* pp. 379-397.

Rivlin, R. S. (1947). Torsion of a rubber cylinder. *J. Appl. Phys. Vol.18*, 444-449.

Rivlin, R. S. (1948, January 13). Large elastic deformations of isotropic materials II. some uniqueness theorems for pure homogeneous deformation. *Philosophical Transactions of the Royal Society of London. Series A, Mathematical and Physical Sciences, Vol. 240, No. 822*, pp. 491-508.

Rivlin, R. S. (1965, July). Nonlinear Viscoelastic Solids. *SIAM Review, Vol. 7, No. 3*, pp. 323-340.

Ross, B. (1977, May). Fractional Calculus. *Mathematics Magazine Vol.50 No.3*, s. 115-122.

Rouse, P. E. (1953). The theory of linear viscoelastic properties of dilute solutions of coiling polymers . *J. Chem. Phys Vol. 21* , 1272-1280.

Sahay, K. B. (1984). On the choice of strain energy function for mechanical characterization of soft biological tissues. *Engineering in Medicine Vol.13 No.1*, 11-14.

Samur, E., Sedef, M., Basdogan, C., Avtan, L., & Duzgun, O. (2007). A robotic indenter for minimally invasive measurement and characterization of soft tissue response. *Medical Image Analysis Vol. 11*, 361-373.

Scherer, R., Kalla, S. L., Tang, Y., & Huang, J. (2011). The Grünwald-Letkinov method for fractional differential equations. *Computers and Mathematics with Applications*, 902-917.

Schiessel, H., & Blumen, A. (1993). Hierarchical analogues to fractional relaxation equations. *J. Phys. A: Math. Gen. Vol.26*, 5057-5069.

Schiessel, H., & Blumen, A. (1993). Hierarchical Analogues to Fractional Relaxation Equations. *J. Phys. A: Math. Gen. 26*, 5057-5069.

Schiessel, H., & Blumen, A. (1995). Mesoscopic pictures of the sol-gel transition: ladder models and fractal networks. *Macromolecules Vol: 28 No:11*, 4013-4019.

Schiessel, H., Metzler, R., Blumen, A., & Nonnenmacher, T. F. (1995). Generalized Viscoelastic Models: Their Fractional Equations with Solutions. *J. Phys. A: Math. Gen. 28*, 6567-6584.

Schiessel, H., Metzler, R., Blumen, A., & Nonnenmacher, T. F. (1995). Generalized Viscoelastic Models: Their Fractional Equations with Solutions. *J. Phys. A: Math. Gen. 28*, 6567-84.

Schmidt, A., & Gaul, L. (2002). Finite element formulation of viscoelastic constitutive equations using fractional time derivatives. *Nonlinear Dynamics 29*, 37-55.

Scilingo, E. P., Sgambelluri, N., & Bicchi, A. Haptic interfaces for biomedical applications. University of Pisa, Italy.

Scott Blair, G., & Coppen, F. M. (1939). The subjective judgement of the elastic and plastic properties of soft bodies, "the differential thresholds" for viscosities and compression moduli. *Proc. Roy. Soc. B 128*, 109-125.

Scott-Blair, G. (1944). Analytical and integrative aspects of the stress-strain-time problem. *J. Scientific Instruments 21*, 80-84.

Scott-Blair, G. W. (1974). *An Introduction to Biorheology.* Amsterdam: Elsevier.

Scott-Blair, G. W., M.A., Sc., D., & C., F. I. (1944). A study of the firmness of soft materials based on Nutting's equation. *Journal of Scientific Instruments*, 149-154.

Silver-Thorn, & M.B. (1999). In-vivo indentation of lower extremity soft tissues. *IEEE Transactions on Rehabilitation Engineering Vol. 7, No. 3*, 268-276.

Simo, J. C., & Hughes, T. J. (1989). *Computational Inelasticit, Interdisciplinary Applied Mathematics.* New-York: Springer-Verlag.

Spilker, R. L.-K. (1992). A finite element analysis of the indentation stress-relaxation response of linear biphasic articular cartilage. *Journal of Biomechanical Engineering Vol. 114*, 191-201.

Suki, B., Barabasi, A. L., & Lutchen, K. L. (1994). Lung Tissue Viscoelasticity: A Mathematical Framework and its Molecular Basis. *J. Appl. Physio. Vol: 76 No: 6*, 2749-2759.

Sun, W., & Sacks, M. S. (2005). Finite element implementation of a generalized Fung-elastic constiutive model for planar soft tissues. *Biomech Model Mechanobiol Vol.4* , 190-199.

Tay, B. K., Kim, J., & Srinivasan, M. A. (2006). In-vivo mechanical behavior of Intra-Abdominal organs. *IEEE Transactions on Biomedical Engineering, Vol. 53, No. 11*, 2129-2138.

Tönük, E., & Silver-Thorn, M. (2004). Nonlinear viscoelastic material property estimation of lower extremity residual limb tissues. *Journal of Biomechanical Engineering Vol.126*, 289-300.

Treloar, L. G. (1949). *The Physics of Rubber Elasticity.* Oxford University Press.

Üsü, K. (2008). *Identification of Soft Tissue Mechanical Material Model and Corresponding Parameters from In-Vivo Experimental Data by Using Inverse Finite Element Method.* Ankara: Graduate School of Natural and Applied Sciences of Middle East Technical University.

Vannah, W. M., S., P. a., & PhD. (1996, July). Indenter tests and finite element modelling of bulk muscular tissue in vivo. *Journal of Rehabilitation Research and Development Vol.33 No.3*, pp. 239-252.

Wei, Z., & Shimizu, N. (2001). FE Formulation for the Viscoelastic Body Modeled by Fractional Constitutive Law. *Acta Mechanica Sinica (English Series) Vol: 17 No: 4*, 354-361.

Welch, S. W., Rorrer, R. A., Duren, R. G., & JR. (1999). Application of time-based fractional calculus methods to viscoelastic creep and stress relaxation of materials. *Mechanics of Time-Dependent Materials Vol. 3*, 279-303.

Wilkie, K. P., Drapaca, C. S., & Sivaloganathan, S. (2011). A nonlinear viscoelastic fractional derivative model of infant hydrocephalus. *Applied Mathematics and Computation*, 8693-8704.

Xuru. (2008, September 7). *Fractional Calculus*. August 2005 http://www.xuru.org/fc/TOC.asp

Zheng, Y., & Mak, A. F. (1996). An ultrasound indentation system for biomechanical properties assesment of soft tissues in-vivo. *IEEE Transactions in Biomedical Engineering Vol. 43 No. 9*, 912-917.

APPENDIX A

FRACTIONAL DERIVATIVE OF SOME SIMPLE FUNCTIONS

Table A.1 Fractional Derivative of Some Simple Functions

$F(x)$	${}_0D_x^{\pm\beta}F(x)$
$f(x)=x^{\alpha}$	$${}_0D_x^{-\beta}=\frac{1}{\Gamma(\beta)}\int_0^x (x-t)^{\beta-1}t^{\alpha}dt=\frac{\Gamma(\alpha+1)}{\Gamma(\alpha+\beta+1)}x^{\alpha+\beta}$$ (Ross, 1977)
$f(x)=x^{-\alpha}$	$${}_{-\infty}D_x^{-\beta}x^{-\alpha}=\frac{1}{\Gamma(\beta)}\int_{-\infty}^x (x-t)^{\beta-1}t^{-\alpha}dt=\frac{(-1)^{\beta}\Gamma(\alpha-\beta)}{\Gamma(\alpha)}x^{-\alpha-\beta}$$ (Ross, 1977)
$f(x)=k$	$${}_0D_x^{\beta}=\frac{d^m}{dx^m}\left[\frac{1}{\Gamma(p)}\int_0^x (x-t)^{p-1}kdt\right]=\frac{d^m}{dx^m}\left[\frac{k}{\Gamma(p)}\cdot\frac{x^p}{p}\right]$$ $$=\frac{kp!x^{p-m}}{(p-m)!p\Gamma(p)}=\frac{k}{\Gamma(1-\beta)}x^{-\beta}$$ (Ross, 1977)
$f(x)=\cos(0.4\pi x)$	$$\frac{d^{-\beta}}{\left[d(t-a)^{-\beta}\right]}f(x)=\frac{1}{\Gamma(\beta)}\int_a^x (x-\tau)^{\beta-1}f(\tau)d\tau,\ \beta\geq 0$$ (Lorenzo & Hartley, 1998) $$\frac{d^{-1/2}f(x)}{\left[d(x)\right]^{-1/2}}=\frac{1}{\Gamma(1/2)}\int_0^x \frac{\cos(0.4\pi\tau)}{(x-\nu)^{1/2}}d\tau$$ (Lorenzo & Hartley, 1998)
$f(x)=\cos(0.4\pi x)$	$$\frac{d^{m-\beta}}{\left[d(x-a)^{m-\beta}\right]}f(x)=\frac{1}{\Gamma(\beta)}\frac{d^m}{dx^m}\int_a^x (x-\tau)^{\beta-1}f(\tau)d\tau,\ \beta\geq 0,\ m>\beta$$ (Lorenzo & Hartley, 1998) $$\frac{d^{-1/2}f(x)}{\left[d(x)\right]^{-1/2}}=\frac{1}{\Gamma(1/2)}\int_0^x \frac{\cos(0.4\pi\tau)}{(x-\nu)^{1/2}}d\tau$$ (Lorenzo & Hartley, 1998)

$f(x)=e^{ax}$	$D^{\beta}e^{ax}=\lim_{h\to 0}h^{-\beta}\sum_{n=0}^{\beta}(-1)^{n}\binom{\beta}{n}e^{a(x+(\beta-n)h)}$ $=e^{ax}\lim_{h\to 0}h^{-\beta}\sum_{n=0}^{\beta}(-1)^{n}\binom{\beta}{n}\left(e^{ah}\right)^{\beta-n}$ $=e^{ax}\lim_{h\to 0}h^{-\beta}\left(e^{ah}-1\right)^{\beta}$ $=a^{\beta}e^{ax}$ (Xuru, 2008)
$f(x)=e^{ax}$	${}_{0}D_{x}^{-1}e^{ax}=\int_{0}^{x}e^{a\tau}d\tau=\left(e^{ax}-1\right)$ (Magin R. , 2004)
$f(x)=1$	$\frac{d^{\beta}1}{dx^{\beta}}=\frac{x^{-\beta}}{\Gamma(1-\beta)}$ (Dalir & Bashour, 2010)
$f(x)=x$	$\frac{d^{\beta}x}{dx^{\beta}}=\frac{x^{1-\beta}}{\Gamma(2-\beta)}$ (Dalir & Bashour, 2010)
$f(x)=e^{x}$	$\frac{d^{q}e^{\pm x}}{dx^{q}}=\sum_{k=0}^{\infty}\frac{x^{k-q}}{\Gamma(k-q+1)}$ (Dalir & Bashour, 2010)
$f(x)=\sin(x)$	$\frac{d^{q}\sin(x)}{dx^{q}}=\sin\left(x+\frac{q\pi}{2}\right)$ (Dalir & Bashour, 2010)
$f(x)=\cos(x)$	$\frac{d^{q}\cos(x)}{dx^{q}}=\cos\left(x+\frac{q\pi}{2}\right)$ (Dalir & Bashour, 2010)

APPENDIX B

INDENTATION EXPERIMENTS

B.1 Indentation Experiments

In indentation experiments, the tip of the indenter is moved forward and backward towards the tissue perpendicularly and the force, displacement and time data are collected instantaneously.

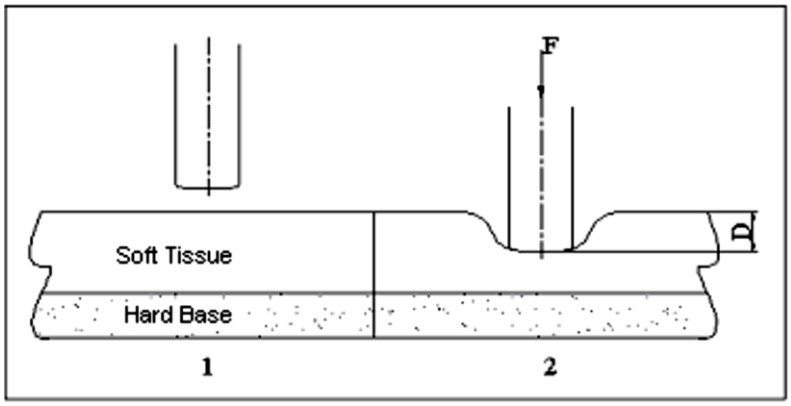

Figure B.1 Just before the tissue is indented (1), after the tissue is indented (2) (Adopted from (Petekkaya, 2008))

The indenter device which is designed specifically for soft tissue experiments is found at the Biomechanics Laboratory of the Mechanical Engineering Department of METU. The indenter device is produced with the support of TÜBİTAK-MİSAG 183 project at 2001. It is capable of performing “cyclic loading”, “creep” and relaxation experiments for soft tissues that can be reached from outside of the body. The indenter device is composed of three important units, which are,

- Control box
  - NI 6020E Data Acquisition Card
  - 12 and 15 VDC Power Source
  - LM-331 Voltage / Frequency (V/F) Converter
- Test unit
- HaydonKerk Instrument 43000 series Linear Actuator Step Motor
- ENTRAN-ELW-50N Load Cell
- Portable computer
- HP Omnibook XE3 lap-top

Figure B.2 Indenter device. Control box (1), test unit (2), portable computer (3)

The working principle of the indenter device can be summarized as,

After the determination of the necessary parameters (displacement and velocity of the indenter, the creep and relaxation time, target force for creep protocol) for the experiment protocol, the parameters are entered through the Matlab user-interface. Experiment data are collected via the data acquisition card and send to the motor drive. The motion of the step motor is induced by the commands send to the motor drive. Parallel to this, with the start of the experiment, the force data is collected by

the computer via the load cell and data acquisition card. The main purpose of the computer is the collection and processing of the data. The computer communicates with the control box via the USB terminal and sends and receives data. The control box is composed of, data acquisition card, motor, motor drive, voltage/frequency converter and load cell. Test unit is on the other hand is composed of the step motor and the load cell which is serially connected to the step motor.

Secondary parts of the indenter device are the indenter tips, mounting table, alignment element, indenter device positioners and arm rests. Apart from cylindrical tips, there are elliptical tips as well. Those tips are mounted in front of the load cell which contact with the tissue during the experiment.

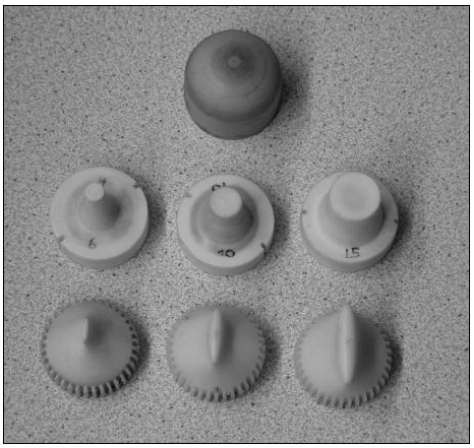

Figure B.3 Different types of indenter tips (Petekkaya, 2008)

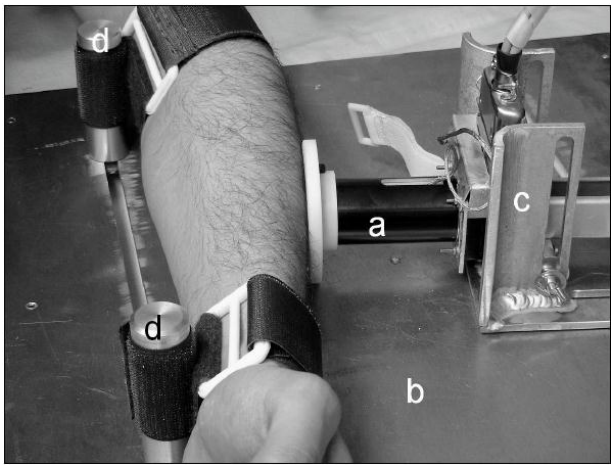

Figure B.4 Indenter test device (a), table (b), indenter device positioner (c), arm rests (d)

One of the indenter tips is the ellipsoidal indenter tip, where via this indenter tip in plane anisotropy property of the soft biological tissues could be analyzed. The figure below shows the ellipsoidal indenter tips manufactured with different dimensions.

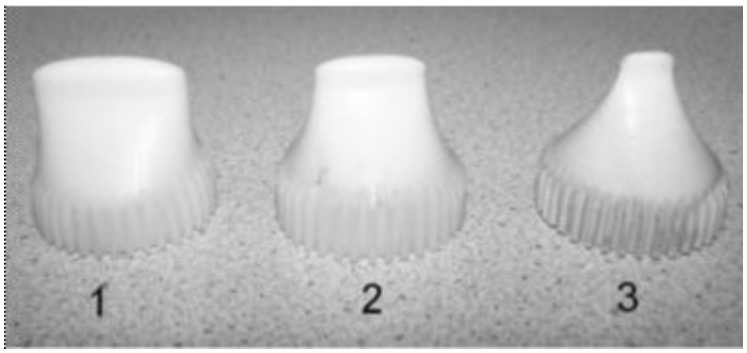

Figure B.5 Ellipsoidal tips with different dimensions.
1) 24x6 mm 2) 16x4 mm 3) 8x2 mm

It has been known that, soft tissues display anisotropic behavior, which means that their stress-strain relation depends on the orientation of the tissue. For this reason,

ellipsoidal indenter tips have been manufactured early for analyzing the orientation dependent behavior of the tissue.

Figure B.6 Alignment Element

Aligning element is used to make experiments by 10° angle intervals. By the help of the aligning element, several experiments on the fore-arm of the human body with different orientation angles are performed (Petekkaya, 2008).

B.2 Experiment Protocols:

- Rate-controlled cyclic loading: Gives idea about the nonlinear, hysteresis and preconditioning behavior of the tissue.

- Load-controlled cyclic loading: This protocol has not been applied yet however it is thought that this protocol would yield further evidence to the nonlinearity of the tissue.

- Rate-controlled relaxation: The tissue is indented to a prescribed displacement and waited until the relaxation time is over to observe the relaxation behavior of the tissue.

- Load-controlled relaxation: The tissue will be indented until a prescribed force is reached and then the relaxation behavior will be observed.

- Rate-controlled creep: The tissue is indented with a prescribed velocity until the target force is reached and the indenter is aimed to hold the target force on the tissue the same until the creep period is over.

- Load-controlled creep

This indenter device requires update to its configuration while some of the components are technologically old now and involves some deficiencies which occasionally cause some problems in different experiment protocols listed above. The deficiencies or insufficiencies of the indenter device are,

- The noisy, unsmooth motion of the step motor: The indenter device is run by a square wave which incurs discontinuities and noisy data.

- The open-loop control of the step motor: The restrictions and limitations of the data acquisition card create problems in the motion of the step motor and the instantaneous position of the indenter cannot be followed.

- The permanent deformation of the load cell due to 5 years of usage and a need for higher sensitivity load cell: The deformation on the load cell effects the measurement sensitivity of the load cell.

- The inadequacy of the data acquisition card in creep test protocol due to limitations of the digital and analog output channels which commands the step motor.

Because of the deficiencies listed above, the indenter device is insufficient to provide healthy experiment data.

Suggested improvements for the indenter device are,

- The soft tissue reaction force data to be cleared from noise by running the

step motor continuously (with a high resolution step motor and micro stepping technology),

- The closed-loop control of step motor position,
- The renewal of the load cell which was damaged and the sensitivity is reduced during use,
- The upgrade of data acquisition card which has insufficient capacity especially in closed-loop experimental protocols,
- The upgrade of indenter device software and experimental protocols and addition of newer protocols.

APPENDIX C

MATLAB CODES

C.1 Matlab Code for 1-D Fractional Viscoelastic Material Model

```
function [  ] = three_elem_model(  )
clear all;
close all;
clc;
% FOV_SLS: Fractional order standar linear solid
% Maxwell element is parallel to the spring element.
% Relaxation Modulus
syms E1 E2 eta beta tau
E1 = 1;
E2 = 1;
eta = 1;
figure;
for beta = 0.1:0.1:1
t = 0:0.001:5;
tau = (eta/E2)^(1/beta);
Z = -t.^beta./tau;
G_SLS = E1.*heaviside(t) + E2.*mlf(beta,1,Z).*heaviside(t);
plot(t,G_SLS);
hold on
end
% Creep Compliance
figure;
syms E1 E2 eta beta tau
E1 = 1;
E2 = 1;
eta = 1;
for beta = 1
Ezero = E1 + E2;
Einf = E1;
t = 0:0.001:5;
tau = (eta/E2)^(1/beta);
```

```
Z = -Einf/Ezero.*(t./tau).^beta;
J = (1/Einf + (1/Ezero-1/Einf).*mlf(beta,1,Z)).*heaviside(t);
plot(t,J);
hold on
end
% Three element model creep compliance and relaxation modulus
% Spring element is in series with the Kelvin-Voigt element.
% Creep Compliance
syms beta Ezero Eone tau1 t1
Ezero = 1;
Eone = 1;
tau1 = 1;
figure;
for beta = 0.1:0.1:1
t = 0:0.001:5;
Z = -(t./tau1).^beta;
A = mlf(beta,1,Z);
J = 1/Ezero.*(1+Ezero/Eone.*(1-A)).*heaviside(t);
plot(t,J);
hold on
end
% Relaxation Modulus
figure;
for beta = 1
t = 0:0.001:5;
t1 = tau1/((1+Ezero/Eone)^(1/beta));
Z = -(t./t1).^beta;
A = mlf(beta,1,Z);
G = Ezero.*(1-(Ezero/Eone)./(1+Ezero/Eone).*(1-A)).*heaviside(t);
plot(t,G);
hold on
end
```

M-file related to the creep compliance and relaxation modulus of the spring-pot is provided below.

```
function [  ] = springpot(  )
% Relaxation Modulus
clear all;
clc;
close all;
syms E G beta eta t
eta = 1;
```

```
E = 1;
for beta=0:0.1:1
t=0:0.01:1;
A = 1/gamma(1 - beta);
G = (A.*((t./eta).^-beta).*heaviside(t))/E;
plot(t/eta,E*G);
hold on
end
% Creep Compliance
figure;
syms E J beta eta t
eta = 1;
E = 1;
for beta=0:0.1:1
t=0:0.01:5;
A = 1/gamma(1 + beta);
J = (A.*((t./eta).^beta).*heaviside(t))/E;
plot(t/eta,E*J);
hold on
end
end
```

C.2 Matlab Code for 1-D Parameter Extraction

```
% Three-element model with extracted parameters.
global xdata ydata
% Three-element fractional order model where the spring element is parallel
% with the Maxwell element.
% The parameters were extracted by using MATLAB optimization toolbox.
E1 = 8.2623;
E2 = 2.6777;
eta = 3.4435;
beta = 0.6186;
t = xdata;
tau = (eta/E2)^(1/beta);
Z = -t.^beta./tau;
G_SLS = E1.*heaviside(t) + E2.*mlf(beta,1,Z).*heaviside(t);
% plot(t,G_SLS,'k');
% The experimental data (relaxation).
hold on
plot(xdata,ydata)
% The three-element fractional model where spring is in series with the
% Kelvin-Voigt element
% E11 = 10.9634;
E11 = 1; % Normalized to one
% The parameters are extracted by manual search.
delta = 0.2503;
tau = 1.857;
beta = 0.58;
Z = -(xdata./tau).^beta;
F =  E11.*(1-delta.*(1-mlf(beta,1,Z))).*heaviside(xdata);
hold on
plot(xdata,F,'r')
```

C.3 Matlab Code for Parameter Identification for Fung's QLV Theory

```
function stress_vec = fovqlv6()
global xdata ydata
clc
A = 1;
B = 2;
E = 1.1;
F = 1.05;
beta = 0.24;
gam = 0.47;
% numint = 0;
stress_vec = zeros(1,184);
for t = 1:83
y = @(tau) ((E + F.*((xdata(t+1)-tau).^(-beta))./gamma(1-beta)).*A.*B.*(gam.*tau).^(B-1).*gam);
stress_vec(t) = quad(y,10^-9,xdata(t+1));
% numint = stress_new;
% stress_vec(t) = stress_new;
end
for t = 84:184
y = @(tau) ((E + F.*((xdata(t)-tau).^(-beta))./gamma(1-beta)).*A.*B.*(gam.*tau).^(B-1).*gam);
stress_vec(t) = quad(y,10^-9,xdata(84));
% numint = stress_new;
% stress_vec(t) = stress_new;
end
plot(xdata,stress_vec,'r');
hold on
plot(xdata,ydata);
```

C.4 Matlab Code for Evaluation Approximate Mittag-Leffler Function

```
% Approximate ML function between interval [0,0.1]
x1=0:0.001:0.1; % First interval
beta = 0.58;
fmlnew = 0;
mlf1 = mlf(0.5,1,-x1.^beta);
for k=0:4
   fml = -fmlnew - (-(x1).^(beta*k)/gamma(1+beta*k));
   fmlnew = fml;
end
fml = fmlnew;
plot(x1,mlf1,x1,fml,'r')
xlabel('[x]')
ylabel('ML function value')
title('Approximate vs. Exact Mittag-Leffler Function Value')
% Approximate ML function between interval (0.1,15)
x=0.1:0.1:15;
beta = 0.5;
mlf=mlf(0.5,1,-x.^beta);
a0=-188.8;
a1=-13537;
a2=-3836.75;
b1=-19822.3;
b2=-20276.8;
b3=-797.517;
fml=(a0+a1*x+a2*x.^2)./(1+b1*x+b2*x.^2+b3*x.^3);
plot(x,mlf,'r',x,fml)
xlabel('[x]')
ylabel('ML function value')
title('Approximate vs. Exact Mittag-Leffler Function Value')
% Approximate ML Function between interval [15,100]
x2=15:100; % Second interval
beta = 0.5;
% mlf = mlf(0.5,1,-x2.^beta);
fmlnew = 0;
for k=1:4
   fml = -fmlnew -((x2).^(-beta*k))/(gamma(1-beta*k));
   fmlnew = fml;
end
```

```
fml = fmlnew;
figure(2);
mlf2 = mlf(0.5,1,-x2.^beta);
plot(x2,mlf2,x2,fml,'r')
xlabel('[x]')
ylabel('ML function value')
title('Approximate vs. Exact Mittag-Leffler Function Value')
```

C.5 Matlab Code for FOV Model with Exact and Approximate M-L Function

```
% 1-D Fractional Order Three Element Viscoelastic Model
% with approximate and exact Mittag-Leffler function
global xdata
E11 = 1;
delta = 0.2;
tau = 2;
beta = 0.5;
a0 = -0.188800e3;
a1 = -.135370e5;
a2 = -.383675e4;
b1 = -.198223e5;
b2 = -.202768e5;
b3 = -.797517e3;
xdata = marc(2,:);
Z = -(xdata./tau).^beta;
F_exact =  E11.*(1-delta.*(1-mlf(beta,1,Z))).*heaviside(xdata);
hold on
% plot(xdata,F_exact,'r')
for i=1:numel(xdata);
   if xdata(i)/tau >= 0 && xdata(i)/tau <= 0.1
      fmlnew = 0;
      for k=0:4
         fml = -fmlnew - (-(xdata(i)/tau)^(beta*k))/gamma(1 + beta*k);
         fmlnew = fml;
      end
      fml_approx(i) = fmlnew;
   elseif xdata(i)/tau > 0.1 && xdata(i)/tau < 15
      fml_approx(i) = (a0 + a1*(xdata(i)/tau)+ a2*(xdata(i)/tau)^2)/(1 +        b1* (xdata(i)/tau)...
            + b2*(xdata(i)/tau)^2 + b3*(xdata(i)/tau)^3);
   elseif xdata(i)/tau >= 15
      fmlnew = 0;
      for k = 1:4;
         fml = -fmlnew - ((xdata(i)/tau)^(-beta*k))/gamma(1 - beta*k);
         fmlnew = fml;
      end
      fml_approx(i) = fmlnew;
   end
end
```

```
F_approx =  E11.*(1-delta.*(1-fml_approx)).*heaviside(xdata);
hold on
plot(xdata,F_approx)
hold on
plot(xdata,marc(1,:),'r')
```

C.6 UElastomer User-Subroutine Inputs and Outputs

```
      subroutine uelastomer(iflag,m,nn,matus,be,x1,x2,x3,detft,
     $              enerd,w1,w2,w3,w11,w22,w33,w12,w23,w31,
     $              dudj,du2dj,dt,dtdl,iarray,array)
c user defined, generalized strain energy function
c implemented in the framework of updated Lagrange
c  Input:
c   iflag
c          Activated by FOAM model definition option:
c            =1 energy function in terms of invariants
c            =2 energy function in terms of principal stretches
c            =3 energy function in terms of invariants
c               with deviatoric split
c            =4 energy function in terms of principal stretches
c               with deviatoric split
c          Activated by MOONEY, ARRUDBOY or GENT model definition option:
c            =5 energy function in terms of invariants (deviatoric part only)
c               correct bulk modulus MUST be defined with either MOONEY,
c               or ARRUDBOY, or GENT model definition option
c          Activated by OGDEN model definition option:
c            =6 energy function in terms of principal stretches (deviatoric part only)
c               correct bulk modulus MUST be defined with OGDEN option
c          Activated by MOONEY, OGDEN, ARRUDBOY or GENT model definition option
c            =7 volumetric part of the strain energy
c   m(1)     user element number
c   m(2)     internal element number
c   nn       integration point number
c   matus(1) user material identification number
c   matus(2) internal material identification number
c   be       left Cauchy Green deformation tensor
c   x1,x2,x3 if iflag=1: invariants of be
c          if iflag=2: principal stretches
c          if iflag=3: deviatoric part of invariants of be
c          if iflag=4: deviatoric principal stretches
c          if iflag=5: deviatoric part of invariants of be
c          if iflag=6: deviatoric principal stretches
c   detft
c          For foam models : determinant of deformation gradient
c          For rubber models : averaged Jacobian
```

```
c    dt       array of state variables (temperature at first) at t=n
c    dtdl     incremental state variables
c    iarray   not used
c    array    not used
c  Output
c    the following must be output by you when iflag=1 to 6
c    note for iflag=5 and 6 the quantities below are deviatoric part only
c    enerd    energy density at t_n+1
c    w1       dw / dx1
c    w2       dw / dx2
c    w3       dw / dx3
c    w11      d2w / dx1 dx1
c    w22      d2w / dx2 dx2
c    w33      d2w / dx3 dx3
c    w12      d2w / dx1 dx2
c    w23      d2w / dx2 dx3
c    w31      d2w / dx3 dx1
c    the following must be output by you when iflag=7
c    enerd    energy density at t_n+1 (volumetric part only)
c    dudj     du / dj
c    du2dj    d2u / dj dj
#ifdef _IMPLICITNONE
      implicit none
#else
      implicit logical (a-z)
#endif
c     ** Start of generated type statements **
      real*8 array, be, detft, dt, dtdl, du2dj, dudj, enerd
      integer iarray, iflag, m, matus, nn
      real*8 w1, w11, w12, w2, w22, w23, w3, w31, w33, x1, x2, x3
c     ** End of generated type statements **
      dimension m(2),be(6),dt(*),dtdl(*),iarray(*),array(*),matus(2)
      return
      end
```

C.7 User-Subroutine Developed for Implementation of the Material Model

```
      subroutine uelastomer(iflag,m,nn,matus,be,x1,x2,x3,detft,
     $              enerd,w1,w2,w3,w11,w22,w33,w12,w23,w31,
     $              dudj,du2dj,dt,dtdl,iarray,array)
c user defined, generalized strain energy function
c implemented in the framework of updated Lagrange
c  Input:
c   iflag
c          Activated by FOAM model definition option:
c            =1 energy function in terms of invariants
c            =2 energy function in terms of principal stretches
c            =3 energy function in terms of invariants
c               with deviatoric split
c            =4 energy function in terms of principal stretches
c               with deviatoric split
c          Activated by MOONEY, ARRUDBOY or GENT model definition option:
c            =5 energy function in terms of invariants (deviatoric part only)
c               correct bulk modulus MUST be defined with either MOONEY,
c               or ARRUDBOY, or GENT model definition option
c          Activated by OGDEN model definition option:
c            =6 energy function in terms of principal stretches (deviatoric part only)
c               correct bulk modulus MUST be defined with OGDEN option
c          Activated by MOONEY, OGDEN, ARRUDBOY or GENT model definition option
c            =7 volumetric part of the strain energy
c   m(1)     user element number
c   m(2)     internal element number
c   nn       integration point number
c   matus(1) user material identification number
c   matus(2) internal material identification number
c   be       left Cauchy Green deformation tensor
c   x1,x2,x3 if iflag=1: invariants of be
c          if iflag=2: principal stretches
c          if iflag=3: deviatoric part of invariants of be
c          if iflag=4: deviatoric principal stretches
c          if iflag=5: deviatoric part of invariants of be
c          if iflag=6: deviatoric principal stretches
c   detft
c          For foam models : determinant of deformation gradient
c          For rubber models : averaged Jacobian
```

```
c    dt       array of state variables (temperature at first) at t=n
c    dtdl     incremental state variables
c    iarray   not used
c    array    not used
c  Output
c    the following must be output by you when iflag=1 to 6
c    note for iflag=5 and 6 the quantities below are deviatoric part only
c    enerd    energy density at t_n+1
c    w1       dw / dx1
c    w2       dw / dx2
c    w3       dw / dx3
c    w11      d2w / dx1 dx1
c    w22      d2w / dx2 dx2
c    w33      d2w / dx3 dx3
c    w12      d2w / dx1 dx2
c    w23      d2w / dx2 dx3
c    w31      d2w / dx3 dx1
c    the following must be output by you when iflag=7
c    enerd    energy density at t_n+1 (volumetric part only)
c    dudj     du / dj
c    du2dj    d2u / dj dj
#ifdef _IMPLICITNONE
      implicit none
#else
      implicit logical (a-z)
#endif
c     ** Start of generated type statements **
      real*8 array, be, detft, dt, dtdl, du2dj, dudj, enerd
      integer iarray, iflag, m, matus, nn, k
      real*8 w1, w11, w12, w2, w22, w23, w3, w31, w33, x1, x2, x3
      real*8 h1,h2
      real*8 tau, delta, c01, c10, c11, c20, c30, e1
      real*8 beta, a0, a1, a2, b1, b2, b3
      real*8 w0, gt, fml, fmlnew, ga
c     ** End of generated type statements **
      dimension m(2),be(6),dt(*),dtdl(*),iarray(*),array(*),matus(2)
      include 'creeps'
      include 'concom'
      open(1, file='data1.dat')
c      open(2, file='datanew.dat', access='append', status='unknown')
```

```
      read(1,60) beta, a0, a1, a2, b1, b2, b3
 60   format(f4.2,2x,d10.6,2x,d10.6,2x,d10.6,2x,d10.6,2x,d10.6,2x,d10.6)
      e1=1
      tau=5.d-1
      delta=5.d-1
      c01=1
      c10=1
      c11=1
      c20=1
      c30=1
c      write(2,*) beta, a0, a1, a2, b1, b2, b3
c      write(2,*) timinc, cptim, inc
      if ((cptim/tau) .ge. 0.d0 .and. (cptim/tau) .le. 1d-1) then
      fml = 0.d0
          do 10 k=0,4
          call gamma ((1.d0+beta*k),ga)
          fml = -fml - ((cptim/tau)**(beta*k))/ga
c          write(2,*) ga
 10       continue
      elseif ((cptim/tau) .gt. 1d-1 .and. (cptim/tau) .lt. 15.d0) then
      fml=(a0+a1*(cptim/tau)+a2*(cptim/tau)**2)/(1.d0+b1*(cptim/tau)
     $     +b2*(cptim/tau)**2+b3*(cptim/tau)**3)
      elseif ((cptim/tau) .ge. 15.d0) then
      fml = 0.d0
          do 20 k=1,4
          call gamma((1.d0-beta*k),ga)
          fml = -fml - ((-cptim/tau)**(-beta*k))/ga
 20       continue
      endif
      w0=c10*(h1-3.d0)+c01*(h2-3.d0)+c11*(h1-3.d0)*(h2-3.d0)
     $     +c20*(h1-3.d0)**2+c30*(h1-3.d0)**3
      gt=e1*(1.d0-delta*(1.d0-fml))
c      write(2,*) fml, gt
      h1=(x1**2+x2**2+x3**2)/(detft**(-2/3))
      h2=(x1**2*x2**2+x2**2*x3**2+x1**2*x3**2)/(detft**(-4/3))
      enerd = w0*gt
      w1 = (2*c10*x1 + c01*(2*x1*x2**2+2*x1*x3**2) + 4*c20*x1*(h1-3)
     $     + 4*c30*x1*(h1-3) + c11*(2*x1*x2**2+2*x1*x3**2)*(h1-3)
     $     + 2*c11*x1*(h2-3))*gt
      w2 = (2*c10*x2 + c01*(2*x2*x1**2+2*x2*x3**2) + 4*c20*x2*(h1-3)
```

```
$     + 4*c30*x2*(h1-3) + c11*(2*x2*x1**2+2*x2*x3**2)*(h1-3)
$     + 2*c11*x2*(h2-3))*gt
      w3 = (2*c10*x3 + c01*(2*x3*x1**2+2*x3*x2**2) + 4*c20*x3*(h1-3)
$     + 4*c30*x3*(h1-3) + c11*(2*x3*x1**2+2*x3*x2**2)*(h1-3)
$     + 2*c11*x3*(h2-3))*gt
      w11 = (2*c10 + 2*c11*(h2-3) + c01*(2*x2**2+2*x3**2) + 8*c20*x1**2
$     + 8*c30*x1**2 + 4*c20*(h1-3) + 4*c30*(h1-3)
$ +c11*2*(x2**2+x3**2)*(h1-3)+4*c11*x1*(2*x1*x2**2+2*x1*x3**2))*gt
      w22 = (2*c10 + 2*c11*(h2-3) + c01*(2*x1**2+2*x3**2) + 8*c20*x2**2
$     + 8*c30*x2**2 + 4*c20*(h1-3) + 4*c30*(h1-3)
$ +c11*2*(x1**2+x3**2)*(h1-3)+4*c11*x2*(2*x2*x1**2+2*x2*x3**2))*gt
      w33 = (2*c10 + 2*c11*(h2-3) + c01*(2*x1**2+2*x2**2) + 8*c20*x3**2
$     + 8*c30*x3**2 + 4*c20*(h1-3) + 4*c30*(h1-3)
$ +c11*2*(x1**2+x2**2)*(h1-3)+4*c11*x3*(2*x3*x1**2+2*x3*x2**2))*gt
      w31 = (4*c01*x1*x3 + 8*c20*x1*x3 + 8*c30*x1*x3
$    + 2*c11*x1*(2*x3*x1**2+2*x3*x2**2)
$    + 2*c11*x3*(2*x1*x2**2+2*x1*x3**2) + 4*c11*x1*x3*(h1-3))*gt
      w23 = (4*c01*x2*x3 + 8*c20*x2*x3 + 8*c30*x2*x3
$    + 2*c11*x2*(2*x3*x1**2+2*x3*x2**2)
$    + 2*c11*x3*(2*x2*x1**2+2*x2*x3**2) + 4*c11*x2*x3*(h1-3))*gt
      w12 = (4*c01*x1*x2 + 8*c20*x1*x2 + 8*c30*x1*x2
$    + 2*c11*x1*(2*x2*x1**2+2*x2*x3**2)
$    + 2*c11*x2*(2*x1*x2**2+2*x1*x3**2) + 4*c11*x1*x2*(h1-3))*gt
      close(1)
c     close(2)
      return
      end
       SUBROUTINE GAMMA(X,GA)
C       ==================================================
C       Purpose: Compute the gamma function â(x)
C       Input :  x  --- Argument of â(x)
C                       ( x is not equal to 0,-1,-2,úúú )
C       Output:  GA --- â(x)
C       ==================================================
        implicit double precision (a-h,o-z)
        dimension g(26)
        pi=3.141592653589793d0
        if (x.eq.int(x)) then
          if (x.gt.0.0d0) then
            ga=1.0d0
```

```
          m1=x-1
          do 10 k=2,m1
10            ga=ga*k
        else
          ga=1.0d+300
        endif
      else
        if (dabs(x).gt.1.0d0) then
          z=dabs(x)
          m=int(z)
          r=1.0d0
          do 15 k=1,m
15            r=r*(z-k)
          z=z-m
        else
          z=x
        endif
        data g/1.0d0,0.5772156649015329d0,
     &        -0.6558780715202538d0, -0.420026350340952d-1,
     &        0.1665386113822915d0,-.421977345555443d-1,
     &        -.96219715278770d-2, .72189432466630d-2,
     &        -.11651675918591d-2, -.2152416741149d-3,
     &        .1280502823882d-3, -.201348547807d-4,
     &        -.12504934821d-5, .11330272320d-5,
     &        -.2056338417d-6, .61160950d-8,
     &        .50020075d-8, -.11812746d-8,
     &        .1043427d-9, .77823d-11,
     &        -.36968d-11, .51d-12,
     &        -.206d-13, -.54d-14, .14d-14, .1d-15/
        gr=g(26)
        do 20 k=25,1,-1
20         gr=gr*z+g(k)
        ga=1.0d0/(gr*z)
        if (dabs(x).gt.1.0d0) then
          ga=ga*r
          if (x.lt.0.0d0) ga=-pi/(x*ga*dsin(pi*x))
        endif
      ENDIF
      RETURN
      END
```